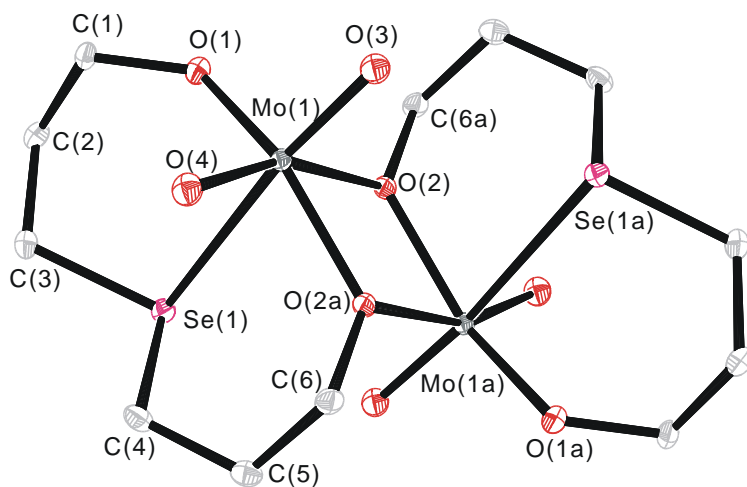
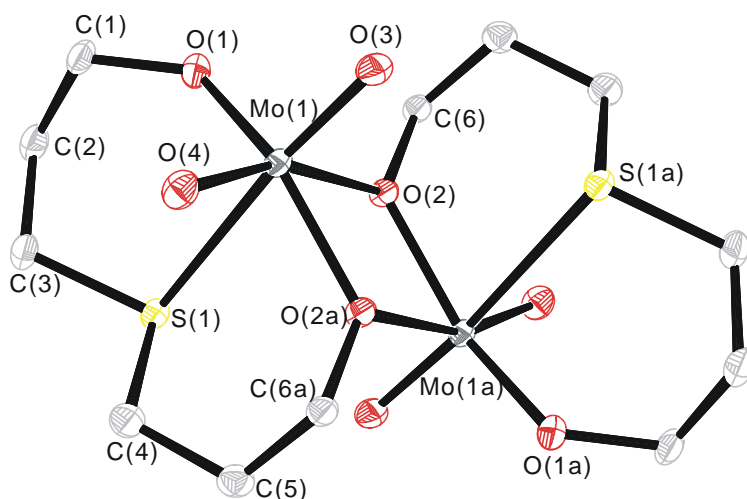


**Xiaoli Ma**

---

**Syntheses, Structures, Electrochemical and Oxygen Atom  
Transfer Properties of Molybdenum and Tungsten Complexes  
with Sulfur and Selenium Containing Ligands**

---



**Syntheses, Structures, Electrochemical and Oxygen Atom  
Transfer Properties of Molybdenum and Tungsten Complexes  
with Sulfur and Selenium Containing Ligands**

Dissertation

zur Erlangung des Doktorgrades

der Mathematisch-Naturwissenschaftlichen Fakultäten

der Georg-August-Universität zu Göttingen

vorgelegt von

Xiaoli Ma

aus Shanxi

(V. R. China)

Göttingen 2007

**D7**

**Referent:**

**Jun.-Prof. Dr. C. Schulzke**

**Korreferent:**

**Prof. Dr. F. Meyer**

**Tag der mündlichen Prüfung:**

**02.05.2007**

## Acknowledgement

The work described in this doctoral dissertation has been carried out under the guidance and supervision of Juniorprofessorin Dr. rer. nat. C. Schulzke at the Institute of Inorganic Chemistry of the Georg-August-University Göttingen between October 2004 and January 2007.

My sincere thanks and gratitude are to

### **Jun.-Prof. Dr. rer. nat. Carola Schulzke**

for her constant guidance, motivation, suggestions, and discussions throughout this work.

I would like to express my special thanks to my colleague Kerstin Starke for numerous discussions, her kind help during this work and the theoretical calculations. I thank Dr. Mathias Noltemeyer, Mr. Hans-Georg Schmidt, Prof. Jörg Magull, Arne Ringe, Anja Hofmeister, and Aritra Pal for their help in the X-ray crystal structural investigations and their friendship. I thank Dr. Fengmei Nie and Angelina Prokofieva (UV-vis measurements), Dr. Serhiy Demeshko (magnetic susceptibility measurements), Mr. Alexander Döring (electrochemistry measurements), Mr. Wolfgang Zolke, Mr. Ralf Schöne and Dr. Gernot Elter (NMR spectra measurements), Dr. Dieter Böhler, Mr. Thomas Schuchardt and Jörg Schöne (mass spectra measurements), Mr. Mathias Hesse (IR spectra measurements), and the staff of the Analytical Laboratories and Werkstatt for their timely support during this research work.

I thank all my colleagues in our research group for the good and motivating working atmosphere. I thank Dr. A. Claudia Stückl, Dr. Huaxin Zhang, Zhensheng Zhang, Ying Yang, Gurubasavaraja Prabhvodeyara Matada and Dr. Anupama Ranganathan for their friendliness.

I am grateful to my former supervisors Prof. Lisheng Wang and Prof. Junsheng Wu in Beijing Institute of Technology from whom I learnt my early lessons of research.

The full support and encouragement from my parents and my husband ZhiYang made this work possible.

The financial support by the Institut für Anorganische Chemie University of Göttingen and the Deutsche Forschungsgemeinschaft is gratefully acknowledged.

**Table of Contents**

<b>1. Introduction</b> .....	1
1.1. Molybdoenzymes and tungstoenzymes .....	2
1.2. The diversity of the enzymes .....	4
1.3. Synthetic analogues .....	5
1.4. Oxygen atom transfer properties .....	8
1.5. The selected ligand systems .....	9
1.6. Scope and objectives of this dissertation .....	10
<b>2. Results and discussion</b> .....	12
2.1. Tungsten complexes with neutral sulfur and oxygen donor ligands .....	12
2.1.1. Syntheses of $\text{WO}_2\text{Cl}_2[\text{MeS}(\text{CH}_2)_2\text{SMe}]$ ( <b>1</b> ) and $[\text{WO}_2\text{Cl}_2(\text{THF})_4]$ ( <b>2</b> ) .....	12
2.1.2. Structural investigation of <b>1</b> .....	14
2.1.3. Electrochemical investigation of <b>1</b> .....	17
2.1.4. Crystal structure description of <b>2</b> .....	20
2.2. Molybdenum and tungsten complexes with tridentate bisanionic thioether and selenoether ligands .....	24
2.2.1. syntheses of $[\{\text{MoO}_2[\text{O}(\text{CH}_2)_2\text{S}(\text{CH}_2)_2\text{O}]\}_2]$ ( <b>3</b> ), $[\{\text{WO}_2[\text{O}(\text{CH}_2)_2\text{S}(\text{CH}_2)_2\text{O}]\}_3]$ ( <b>4</b> ) and $[\{\text{MO}_2[\text{O}(\text{CH}_2)_2\text{Se}(\text{CH}_2)_2\text{O}]\}_n]$ (M = W ( <b>5</b> ), Mo ( <b>6</b> )) .....	25
2.2.2. Structures and DFT calculations of <b>3</b> and <b>4</b> .....	27
2.2.3. Electrochemical results for <b>3</b> , <b>4</b> , <b>5</b> .....	34
2.2.4. Syntheses of $[\{\text{MoO}_2[\text{O}(\text{CH}_2)_3\text{X}(\text{CH}_2)_3\text{O}]\}_2]$ (X = S ( <b>7</b> ), Se ( <b>8</b> )) and $[\{\text{WO}_2[\text{O}(\text{CH}_2)_3\text{Se}(\text{CH}_2)_3\text{O}]\}_n]$ ( <b>9</b> ) .....	37

---

2.2.5. Structures of <b>7</b> and <b>8</b> .....	39
2.2.6. Electrochemical results for <b>7</b> and <b>8</b> .....	42
2.2.7. Conclusions .....	45
2.3. The monomerization of a binuclear molybdenum(VI) dioxo complex .....	47
2.3.1. Synthesis of mononuclear molybdenum(VI) dioxo complex, [MoO <sub>2</sub> (O(CH <sub>2</sub> ) <sub>2</sub> S(CH <sub>2</sub> ) <sub>2</sub> OH)(OSiBu <sup>t</sup> Ph <sub>2</sub> )] ( <b>10</b> ) .....	47
2.3.2. Crystal structure of <b>10</b> .....	51
2.4. Molybdenum and tungsten complexes with mixed O,X,O-donor ligands (X = S or Se) .....	53
2.4.1. Syntheses of [MoO <sub>2</sub> L <sup>S</sup> ] ( <b>11</b> ), [MoO <sub>2</sub> L <sup>Se</sup> ] ( <b>12</b> ), [WO <sub>2</sub> L <sup>S</sup> ] ( <b>13</b> ) and [WO <sub>2</sub> L <sup>Se</sup> ] ( <b>14</b> ) .....	53
2.5. Molybdenum complexes with heterocyclic bidentate ligands (N, X) X = S, Se ....	57
2.5.1. Syntheses of [Mo <sub>2</sub> O <sub>3</sub> (PyS) <sub>4</sub> ] ( <b>15</b> ), [Mo <sub>2</sub> O <sub>3</sub> (PySe) <sub>4</sub> ] ( <b>16</b> ) and [Mo <sub>2</sub> O <sub>3</sub> (4-CF <sub>3</sub> -PymS) <sub>4</sub> ] ( <b>17</b> ) .....	58
2.5.2. Crystal structures of <b>15</b> , <b>16</b> and <b>17</b> .....	64
2.6. Additional experiments .....	71
2.6.1. Syntheses and structures of [H:C] <sup>+</sup> <sub>2</sub> [M <sub>6</sub> O <sub>19</sub> ] <sup>2-</sup> (M = Mo ( <b>18</b> ), W ( <b>19</b> )) .....	71
2.6.2. Synthesis and crystal structure description of [W <sub>8</sub> O <sub>19</sub> (O(CH <sub>2</sub> ) <sub>3</sub> S(CH <sub>2</sub> ) <sub>3</sub> O) <sub>3</sub> (acac) <sub>4</sub> ] ( <b>20</b> ) .....	75
2.6.3. Synthesis and crystal structure of MoO <sub>2</sub> (dipic) ( <b>21</b> ) .....	82
2.7. Catalytic oxygen atom transfer reaction .....	86
2.7.1. Oxygen atom transfer properties of <b>7</b> and <b>8</b> .....	86

---

2.7.2. Catalytic oxo-transfer reactivity of <b>10</b> .....	93
2.7.3. Catalytic oxo-transfer reactivity of <b>11-14</b> .....	95
2.7.4. Catalytic oxo-transfer activities of <b>15</b> and <b>16</b> .....	101
<b>3. Summary and Outlook</b> .....	<b>105</b>
3.1. Summary .....	105
3.2. Outlook .....	112
<b>4. Experimental Section</b> .....	<b>113</b>
4.1. General Procedures .....	113
4.2. Physical Measurements .....	113
4.3. DFT calculations .....	115
4.4. Electrochemistry .....	115
4.5. Catalytic oxo-transfer reactions .....	116
4.6. Starting materials .....	117
4.7. Syntheses of compounds <b>1-21</b> .....	117
4.7.1. synthesis of $\text{WO}_2\text{Cl}_2(\text{MeSCH}_2\text{CH}_2\text{SMe})$ ( <b>1</b> ) .....	117
4.7.2. synthesis of $[\text{WO}_2\text{Cl}_2(\text{THF})]_4$ ( <b>2</b> ) .....	118
4.7.3. synthesis of $[\{\text{MoO}_2[\text{O}(\text{CH}_2)_2\text{S}(\text{CH}_2)_2\text{O}]\}_2]$ ( <b>3</b> ) .....	118
4.7.4. synthesis of $[\{\text{WO}_2[\text{O}(\text{CH}_2)_2\text{S}(\text{CH}_2)_2\text{O}]\}_3]$ ( <b>4</b> ) .....	119
4.7.5. synthesis of $[\{\text{WO}_2[\text{O}(\text{CH}_2)_2\text{Se}(\text{CH}_2)_2\text{O}]\}_n]$ ( <b>5</b> ) .....	119
4.7.6. synthesis of $[\{\text{MoO}_2[\text{O}(\text{CH}_2)_2\text{Se}(\text{CH}_2)_2\text{O}]\}_n]$ ( <b>6</b> ) .....	120
4.7.7. synthesis of $[\{\text{MoO}_2[\text{O}(\text{CH}_2)_3\text{S}(\text{CH}_2)_3\text{O}]\}_2]$ ( <b>7</b> ) .....	121
4.7.8. synthesis of $[\{\text{MoO}_2[\text{O}(\text{CH}_2)_3\text{Se}(\text{CH}_2)_3\text{O}]\}_2]$ ( <b>8</b> ) .....	121

---

4.7.9. synthesis of $[\{\text{WO}_2(\text{O}(\text{CH}_2)_3\text{Se}(\text{CH}_2)_3\text{O})\}_n]$ ( <b>9</b> ) .....	122
4.7.10. synthesis of $[\text{MoO}_2(\text{O}(\text{CH}_2)_2\text{S}(\text{CH}_2)_2\text{OH})(\text{OSiBu}^t\text{Ph}_2)]$ ( <b>10</b> ) .....	122
4.7.11. synthesis of $[\text{MoO}_2\text{L}^{\text{S}}]$ ( <b>11</b> ) .....	123
4.7.12. synthesis of $[\text{MoO}_2\text{L}^{\text{Se}}]$ ( <b>12</b> ) .....	124
4.7.13. synthesis of $[\text{WO}_2\text{L}^{\text{S}}]$ ( <b>13</b> ) .....	124
4.7.14. synthesis of $[\text{WO}_2\text{L}^{\text{Se}}]$ ( <b>14</b> ) .....	125
4.7.15. synthesis of $[\text{Mo}_2\text{O}_3(\text{PyS})_4]$ ( <b>15</b> ) .....	126
4.7.16. synthesis of $[\text{Mo}_2\text{O}_3(\text{PySe})_4]$ ( <b>16</b> ) .....	127
4.7.17. synthesis of $[\text{Mo}_2\text{O}_3(4\text{-CF}_3\text{-PymS})_4]$ ( <b>17</b> ) .....	128
4.7.18. synthesis of $[\text{H}:\text{C}]_2[\text{Mo}_6\text{O}_{19}]$ ( <b>18</b> ) .....	129
4.7.19. synthesis of $[\text{H}:\text{C}]_2[\text{W}_6\text{O}_{19}]$ ( <b>19</b> ) .....	129
4.7.20. synthesis of $[\text{W}_8\text{O}_{19}(\text{O}(\text{CH}_2)_3\text{S}(\text{CH}_2)_3\text{O})_3(\text{acac})_4]$ ( <b>20</b> ) .....	130
4.7.21. synthesis of $\text{MoO}_2(\text{dipic})$ ( <b>21</b> ) .....	131
<b>5. Handling and Disposal of Solvents and Residual Waste</b> .....	<b>132</b>
<b>6. Crystal Data and Refinement Details</b> .....	<b>134</b>
<b>7. References</b> .....	<b>148</b>

**Lebenslauf**



**Abbreviations**

$\delta$	chemical shift
$\lambda$	wavelength
$\mu$	bridging
$\nu$	wave number
$\chi_M$	molar magnetic susceptibility
acac	acetylacetonate
av	average
B.p.	boiling point
br	broad
Bu <sup>t</sup>	<i>tert</i> -butyl (tertiary butyl)
C	3,4-dimethyl-N,N'- <i>bis</i> -isopropylimidazolyl carbene
calcd.	calculated
d	day(s), doublet
dec.	decomposition
DFT	density functional theory
DME	ethyleneglycol dimethylether
DMF	dimethyl formamide
DMS	dimethyl sulfide
DMSO	dimethyl sulfoxide
EI	electron impact ionization
equiv	equivalent(s)
Et	ethyl
eV	electron volt
g	gram(s)
h	hour(s)
HMPA	hexamethyl phosphorotriamide
<i>i</i> Pr	<i>iso</i> -propyl
IR	infrared
K	Kelvin

---

L	ligand
M	metal
m	middle, multiplet
<i>m/z</i>	mass/charge
M.p.	melting point
$M^+$	molecular ion
Me	methyl
min.	minute(s)
mL	milliliter
mmol	millimolar
MS	mass spectrometry, mass spectra
NMR	nuclear magnetic resonance
OPPh <sub>3</sub>	triphenylphosphine oxide
Ph	phenyl
PPh <sub>3</sub>	triphenylphosphine
ppm	parts per million
q	quartet
R	organic substituent
r.t.	room temperature
s	strong, singlet
sept	septet
t	time, triplet
THF	tetrahydrofuran
TMS	tetramethylsilane
UV-vis	ultraviolet-visible
<i>V</i>	volume
vs	very strong
w	weak
<i>Z</i>	number of molecules in the unit cell

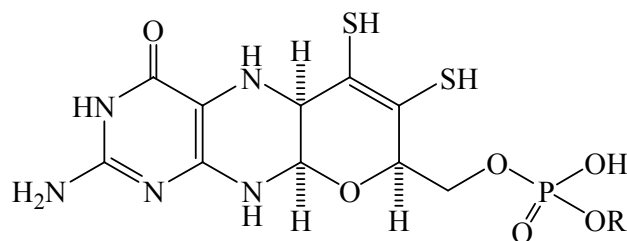
## 1. Introduction

Molybdenum and tungsten are chemically analogous elements, and both are relatively scarce in natural environments.<sup>[1-3]</sup> It is perhaps surprising that the two elements (Mo, 42 and W, 74) are required for the normal metabolism of biological systems when one considers that with the exception of iodine (53), life forms on this planet typically thrive by utilizing elements with atomic numbers below 35.<sup>[4,5]</sup> Yet, from a biological perspective, Mo and W provide a fascinating study in contrasts. Enzymes containing molybdenum and tungsten at their active sites appear to be present in all forms of life, from ancient archaea to man. These enzymes catalyze a wide range of reactions in carbon, sulfur, and nitrogen metabolism, and at least 50 enzymes are known today.<sup>[6-8]</sup>

With the exception of the molybdenum-containing nitrogenase, the main role of molybdenum and tungsten in biology is as the catalytic centre of a wide variety of enzymes, virtually all of which catalyze the oxygen atom transfer (OAT) to, or from, the substrate<sup>[7,9,10]</sup>. In general, the enzymes utilize water as the ultimate source or sink of oxygen in the overall catalytic reaction  $X + H_2O \leftrightarrow XO + 2H^+ + 2e^-$ . The reaction is coupled to electron transfer between substrate X/XO and metal.<sup>[11,12]</sup>

In all of the molybdo- and tungsto-enzymes, the metal atom is bound to the dianion(s) (ene-1,2-dithiolate) of one or two molecules of a special ligand, molybdopterin (MPT)<sup>[13-16]</sup>. It is a tricyclic pyranopterin, the pyran ring of which carries an ene-1,2-dithiol (or dithiolene) and a phosphate group as side-chain. In all of the native enzymes structurally characterized so far, the pterin is at the dihydro oxidation level and the dithiolene group acts as a bidentate ligand to bind Mo (or W); in some bacterial enzymes the phosphate group is covalently linked

to a dinucleotide.



Molybdopterin (MPT)

R = H or a dinucleotide

### 1.1. Molybdoenzymes and tungstoenzymes

Molybdenum is an essential trace element for all living systems.<sup>[7,13,17]</sup> This metal acts as an integral component of the multinuclear M center of nitrogenases<sup>[18,19]</sup> and as the mononuclear active sites of a much more diverse group of enzymes that in general function catalytically to transfer an oxygen atom either to or from a physiological acceptor or donor molecule. The vast majority of these enzymes possess a Mo=O unit in their active sites and are often referred to as oxomolybdenum enzymes.<sup>[20]</sup> The latter mononuclear molybdoenzymes constitute a fairly large class of enzymes.

Hille<sup>[7,8]</sup> has classified molybdenum enzymes into three families based upon their protein sequences, the structures of their oxidized active sites, and function: the xanthine oxidase, sulfite oxidase, and dimethyl sulfoxide reductase (DMSOR) families, respectively. The active sites of the three families of mononuclear molybdenum enzymes may be represented as indicated in Figure 1. Members of the xanthine oxidase family (*i.e.*, the true hydroxylases) have molybdenum centers consisting of a single cofactor dithiolene ligand coordinated to a *fac*MoOS(H<sub>2</sub>O) unit. Members of the sulfite oxidase family are likely to possess a single cofactor dithiolene coordinated to a *cis* MoO<sub>2</sub> unit (additional coordination positions may be

taken up by water and/or hydroxide and a cysteine residue that is conserved within the family). Members of the DMSO reductase family are distinguished by bisdithiolene coordination of the molybdenum, but this group of enzymes is likely to be more structurally diverse than the other two families. The Mo=X position may be taken up by oxygen, sulfur, or (possibly) selenium, while the sixth ligand coordination position may be occupied by serine, cysteine, selenocysteine or aspartate.

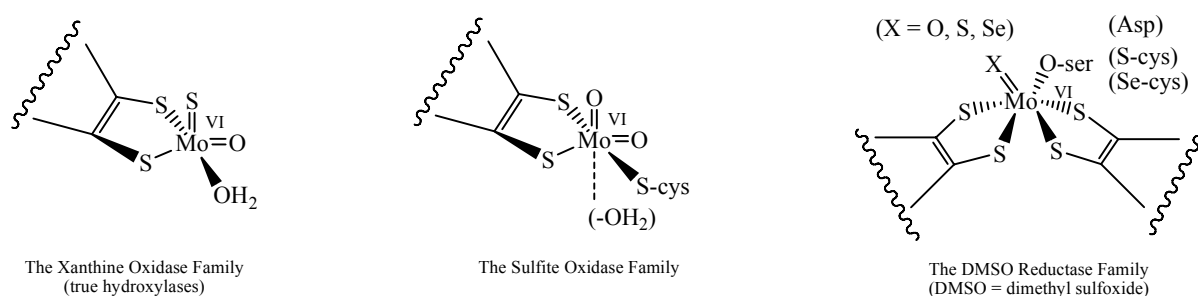


**Figure 1.** The major families of mononuclear molybdenum enzymes.

The knowledge about the positive biological role of tungsten has a very short history compared to that of Mo. The first crystal structure of a tungsten enzyme appeared in 1995.<sup>[21]</sup> Tungsten has also been shown to be present at the catalytic centre of enzymes, and it is notable that many of tungstoenzymes occur in thermophilic bacteria.<sup>[17,22]</sup> For almost all of the known tungstoenzymes there is an analogous molybdoenzyme that is present within the same organism or in a very closely related species.<sup>[23]</sup> In other words, of the vast array of life forms that utilize Mo, a very small subset are also able to use W.

The tungstoenzymes are divided into three categories by Johnson et al (Figure 2)<sup>[22]</sup>. The majority fall within the so-called AOR-type, with aldehyde ferredoxin oxidoreductase (AOR) from the hyperthermophile, *Pyrococcus furiosus* (Pf; maximum growth temperature,  $T_{max}$ , 105 °C) being the best studied example.<sup>[21,24,25]</sup> The second family of tungstoenzymes

involves two types, both of which utilize  $\text{CO}_2$  as the substrate. One is formate dehydrogenase (FDH), which was the first W-containing enzyme to be purified.<sup>[26]</sup> The other member of the second class of tungstoenzyme is *N*-formylmethanofuran dehydrogenase (FMDH). The third class of tungstoenzyme has just one member, and it is the most recently discovered and the least characterized. It is termed acetylene hydratase (AH) and was purified from the acetyleneutilizing anaerobe *Pelobacter acetylenicus* (Pa).<sup>[27]</sup> Members of the AOR and F(M)DH families catalyze redox reactions. In contrast, AH catalyzes the hydration of acetylene.

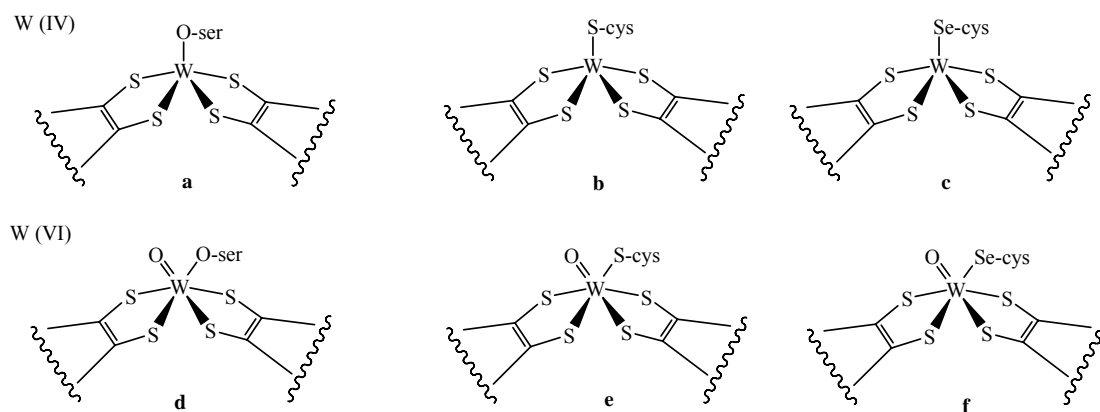


**Figure 2.** The major families of Tungstoenzymes (AOR: **a** and **d**; F(M)DH: **b**, **c**, **e** and **f**).

## 1.2. The diversity of the enzymes

Molybdenum as well as tungsten can be found at the active sites of the molybdopterin containing OAT enzymes<sup>[28]</sup> because of the chemical similarity of the two metals. However, the distribution of the metals is quite interesting; molybdenum is found mainly in mesophilic organisms while tungsten is found mainly in thermophilic and hyperthermophilic microorganisms, and it is not known until today whether this distribution was developed for reasons of supply<sup>[22,29]</sup>, stability<sup>[22,30]</sup> or reactivity<sup>[31]</sup> (i.e. redox potential). The presence of the two metals active sites causes the extensions of the types of the enzymes.

Another interesting diversity of these enzymes is that, in the DMSO reductase family<sup>[7]</sup> (molybdenum enzymes with two molybdopterin ligands) the metal is bound to the peptide moiety through either serine (O)<sup>[32]</sup>, cysteine (S)<sup>[33]</sup>, selenocysteine (Se)<sup>[34]</sup> or aspartate (O, mono- or bidentate)<sup>[35]</sup>. It is still not known whether the different types of amino acid ligands are used purposefully or merely accidentally. The amino acid ligands are supposed to play a role in stabilizing the enzyme-substrate complexes. The coordination of selenocysteine as well as the coordination of sulfur atoms to tungsten were also established although far fewer structures of tungsten-containing OAT enzymes are available.<sup>[21,36,37]</sup>

### 1.3. Synthetic analogues

In order to ascertain the role of that particular feature of the active sites of molybdenum and tungsten enzymes on the chemical reactivity and the spectroscopic properties of the centre, chemical approaches to the sites have been directed toward mimicking a portion of the structural centre.

Thus, many small-molecule complexes incorporating the high valent (Mo or W<sup>IV-VI</sup>) oxo-containing, sulfur-rich environments of these enzymes are essential as potential structural and/or functional models<sup>[12,38-41]</sup>.

So far an enormous amount of model complexes have been synthesized and characterized. They can be divided into two main types.<sup>[28]</sup> The first one contains non-dithiolene systems, which means that coordination spheres contain nonphysiological ligands. Figure 3 (**a**<sup>[42]</sup>, **b**<sup>[43,44]</sup>, **c**<sup>[45,46]</sup>, **d**<sup>[47]</sup>, **e**<sup>[48]</sup>, **f** and **g**<sup>[49]</sup>) shows some examples of non-dithiolene oxo-molybdenum complexes.

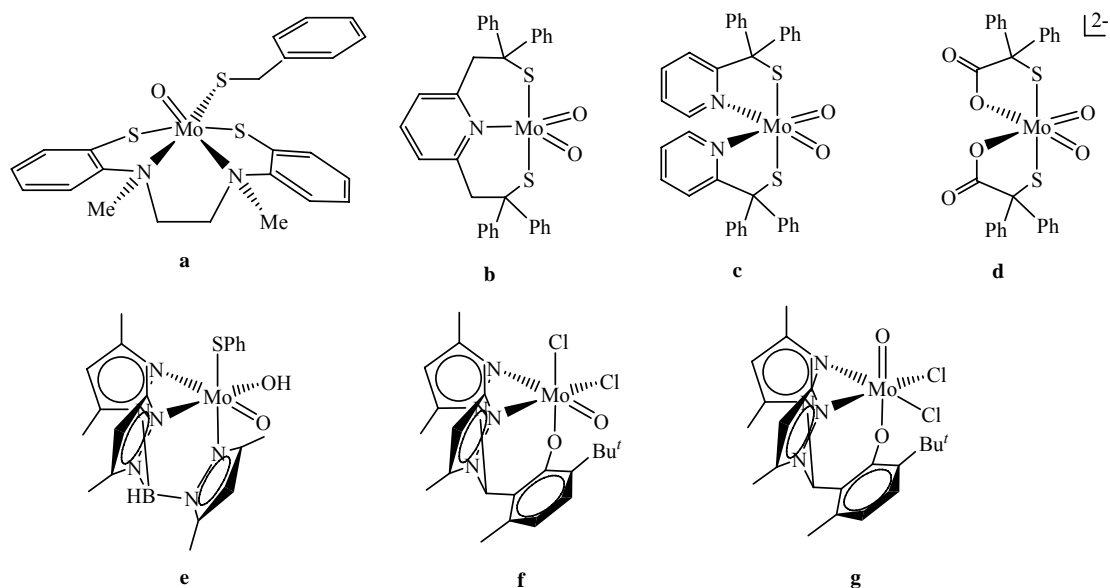


**Figure 3.** Structures of non-dithiolene oxo-molybdenum complexes.

Tungsten analogues including the *cis,trans* forms of  $[W^{VI}O_2(L-N_2S_2)]$ ,  $[W^{VI}OS(L-N_2S_2)]$ , and  $[W^{VI}S_2(L-N_2S_2)]$ , *cis,cis*- $[W^VOX(L-N_2S_2)]$ , and *cis,trans*- $[W^VOX-(L-N_2S_2)]$  ( $X = NCS^-$ ,  $Cl^-$ ,  $OPh^-$ ,  $SPh^-$ ) (all from ref [50]),  $[W^{VI}O_2(O_2CCSPh_2)_2]^{2-}$ ,<sup>[51]</sup> and  $[(Tp^*)W^{VI}OSX]$  and  $[(Tp^*)W^{VI}S_2X]$ <sup>[52,53]</sup> ( $Tp^* = \text{hydrotris(3,5-dimethylpyrazolyl)borate(1-)}$ ), and so on, have been prepared and investigated.

These hindered ligands were employed with the intention of providing biologically relevant coordination (N, S, O) and suppressing the formation of a  $\mu$ -oxo Mo(V) dimer.

The second one is called dithiolene systems, which contain one or two ene-1,2-dithiolate ligands and, where appropriate, simulated protein ligands, and are closer approaches to the active sites of enzymes. The two fundamental types of dithiolene ligands are depicted in their classical, fully reduced forms, ene-1,2-dithiolate (**a**) and benzene-1,2-dithiolate (**b**, bdt), in Figure 4. Both ligand types are available with a variety of substituents.



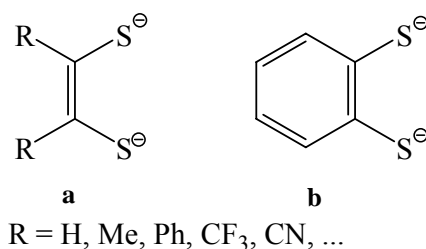


**Figure 4.** Structures of the two fundamental types of dithiolene ligands in the dithiolate oxidation state.

Since metal dithiolene complexes were first prepared in the early 1960s<sup>[54]</sup>, the investigation of molybdenum and tungsten dithiolenes have attracted considerable interest. With molybdenum, meaningful site analogues and analogue systems of the SO and DMSOR families have been achieved, but not yet in the XnO family. The sulfite oxidase family sites analogues require the preparation of monodithiolene species.<sup>[55]</sup> Active sites in DMSO reductase family require as analogues bis(dithiolene) complexes. Extensive research was performed on this kind of complexes. The principal routes and synthetic schemes were summarized by Enemark et al.<sup>[28]</sup>

Relevant tungsten dithiolene chemistry began in 1992, with the preparation of  $[\text{WO}(\text{mnt})_2]^{2-}$ <sup>[56]</sup> and the set  $[\text{WO}(\text{bdt})_2]^{-2-}$  and  $[\text{WO}_2(\text{bdt})_2]^{2-}$ .<sup>[57]</sup> In 1996,  $[\text{WO}_2(\text{mnt})_2]^{2-}$  was reported,<sup>[29]</sup> as were the naphthalene-2,3-dithiolate complexes  $[\text{WO}(\text{ndt})_2]^{2-}$  and  $[\text{WO}_2(\text{ndt})_2]^{2-}$ .<sup>[58]</sup> Two years later, a series of  $[\text{WO}(\text{S}_2\text{C}_2\text{R}_2)_2]^{2-}$  complexes was prepared.<sup>[59]</sup> (Here mnt means *cis*-1,2-dicyano-1,2-ethylenedithiolate(2-); bdt means benzene-1,2-dithiolate(2-); ndt means naphthalene-2,3-dithiolate(2-).) All tungsten complexes are isostructural and isoelectronic with their molybdenum counterparts.

#### 1.4. Oxygen atom transfer properties

As described above, with the exception of nitrogenase,<sup>[60]</sup> the known molybdenum-containing enzymes catalyze reactions that, at least formally, are oxygen atom transfer processes. These oxo-transfer reactions are of two types: oxidation, involving the addition of an oxygen atom to substrate, and reduction, involving the removal of an oxygen atom from substrate. Mononuclear tungsten enzymes are also known<sup>[22]</sup> but, in contrast to the well developed molybdenum chemistry, tungsten-mediated atom transfer reactions have been significantly less studied.<sup>[59,61-63]</sup> This is primarily a consequence of the difficulty in reducing W(VI) species to corresponding W(IV) species.<sup>[64]</sup>

Understanding the chemical mechanism of the enzymes has been greatly facilitated by studies of the chemistry of inorganic complexes that are useful mechanistic models for the enzymes. The employed ligands should be bulky to effectively prevent the thermodynamically very favorable dimerization of the mononuclear complexes to give  $\mu$ -oxo bridged  $\text{Mo}_2^{\text{V}}$  clusters.

In general, the circle process of dioxo molybdenum or tungsten complexes catalyzing oxygen atom transfer reaction from DMSO to a phosphine can be displayed as in Figure 5.

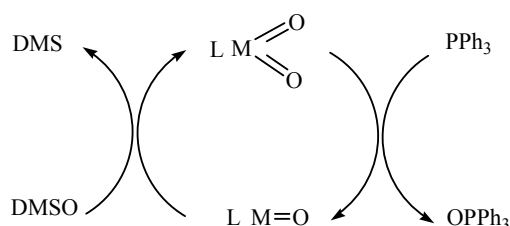


**Figure 5.** Schemes of dioxo enzymatic analogues catalyzing oxygen atom transfer reaction.

The compound  $\text{M}^{\text{VI}}$  oxidizes  $\text{PPh}_3$  stoichiometrically to give the reduced  $\text{M}^{\text{IV}}$  compound and  $\text{OPPh}_3$  and the reduced monooxo complex thus obtained can be returned to the oxidized parent compound by reaction with dimethyl sulfoxide (giving dimethyl sulfide). The

discussion about the mechanism of oxygen atom transfer reaction has been extensively reviewed.<sup>[29,43-46,65-69]</sup>

### 1.5. The selected ligand systems

In this research, the mainly used ligand system is a tridentate bianion alkoxyate containing a thio or selenoether function. (Figure 6, **a** and **b**) The coordination of thioethers or selenoethers to metal centers in high oxidation states represents hard-soft metal-ligand combinations that are usually not very stable.<sup>[70]</sup> To achieve this kind of coordination this ligand system is used to cling to the molybdenum center rather strongly and hold the ether function in a position where a metal ether interaction can be easily developed. Although in the enzymes the sulfur atom is bound as the thiolate or sulfido ligand and the selenium as the selenate ligand, the investigation of the ether variants of these ligand atoms could give some insight into their influence.

In addition, the phenol containing O,X,O (X = S, Se) donor ligands are also chosen (Figure 6, **c**). This kind of ligand has attracted considerable attention in the bioinorganic chemistry community because of the widespread occurrence of tyrosyl radicals in a variety of metalloenzymes involved in oxygen-dependent enzymatic catalysis. An interesting feature associated with the ligands containing two phenolate donor atoms is their good  $\pi$ -donor ability to stabilize higher oxidation states with highly covalent M–O(phenolate) bonds and their tendency to form phenoxy radical complexes.<sup>[71]</sup>

The two chosen ligand systems generate a coordination sphere consisting only of group 16 elements around the molybdenum and tungsten, which somehow matches well the active sites of the enzymes even though the important dithiolene function of the molybdopterin is

neglected.

In addition to the ligand systems described above, bidentate neutral (S,S) thioether (Figure 6, **d**) and heterocyclic bidentate ligands (N, X), X = S, Se (Figure 6, **e** and **f**) are used as well because of their relevance to biological systems.<sup>[72,73]</sup>

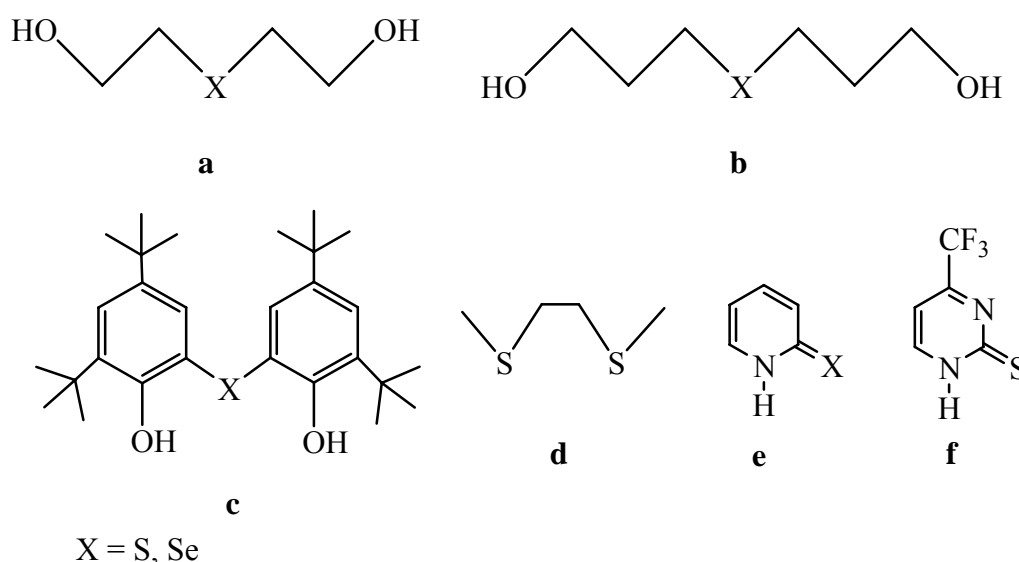


**Figure 6.** The selected ligand systems.

## 1.6. Scope and objectives of this dissertation

Based on the above introduction, the reasons for the diversity of the molybdopterin-containing OAT enzymes due to the presence of molybdenum and tungsten centers and the coordination of the different types of amino acid ligands are still a challenging problem.

In order to obtain more insight into these questions, the objectives of the present work are:

- (1) Syntheses and characterization of corresponding molybdenum and tungsten compounds that mimic the active sites of the OATs where the coordination sphere of the metal consists of oxygen and sulfur or selenium, respectively, and where at least one oxo ligand

is present.

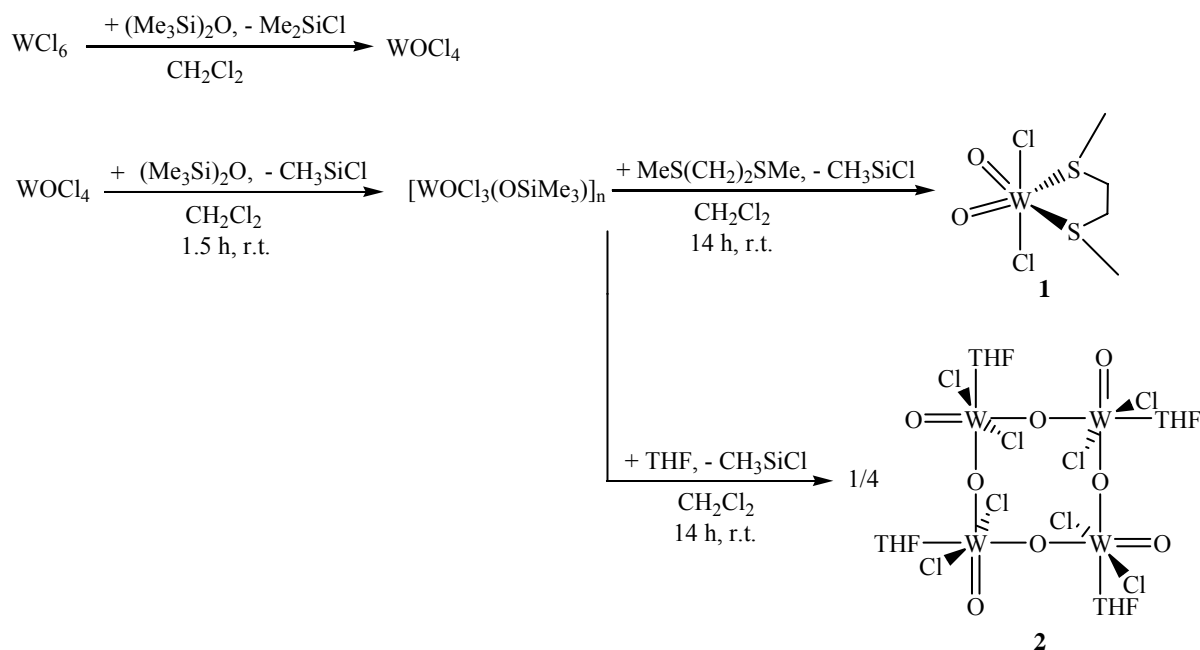
- (2) Syntheses and characterization of compounds with thio- and analogous seleno functional ligands.
- (3) Comparison of the molybdenum and tungsten analogues with sulfur and selenium containing ligands to explore the structural and electronic influences of replacing molybdenum by tungsten and of varying the ligand atoms (O/S/Se) with regard to their redox and oxygen atom transfer properties.

## 2. Results and Discussion

### 2.1. Tungsten complexes with neutral sulfur and oxygen donor ligands

#### 2.1.1. Syntheses of $\text{WO}_2\text{Cl}_2[\text{MeS}(\text{CH}_2)_2\text{SMe}]$ (**1**) and $[\text{WO}_2\text{Cl}_2(\text{THF})]_4$ (**2**)

The chemistry of medium and high oxidation state molybdenum and tungsten centres with neutral sulfur or oxygen donor ligands remains little studied.<sup>[74-76]</sup> Herein,  $\text{WO}_2\text{Cl}_2[\text{MeS}(\text{CH}_2)_2\text{SMe}]$  (**1**) and  $[\text{WO}_2\text{Cl}_2(\text{THF})]_4$  (**2**) were synthesized by an analogous method to the preparation of  $\text{WO}_2\text{Cl}_2(\text{DME})$ <sup>[76]</sup> (Scheme 1).



**Scheme 1.** Preparation of  $\text{WO}_2\text{Cl}_2[\text{MeS}(\text{CH}_2)_2\text{SMe}]$  (**1**) and  $[\text{WO}_2\text{Cl}_2(\text{THF})]_4$  (**2**).

Hexamethyl disiloxane reacted with an equimolar amount of  $\text{WOCl}_4$  which was derived from  $\text{WCl}_6$  suspended in  $\text{CH}_2\text{Cl}_2$  to give a light yellow solid. Based on IR observations a likely formation of this intermediate is a highly polymeric tungsten complex,  $[\text{WOCl}_3(\text{OSiMe}_3)]_n$ .<sup>[76]</sup> After addition of excess dithioether or THF most of the suspended solid was dissolved. Compound **1** and **2** were obtained as colorless crystals from the filtrate by keeping it at  $4^\circ\text{C}$  overnight or by the addition of diethylether and cooling to  $-30^\circ\text{C}$ , respectively. The

dissolution of the initially formed solid on addition of dithioether indicates the formation of a thioether adduct,  $[\text{WOCl}_3(\text{OSiMe}_3)(\text{MeS}(\text{CH}_2)_2\text{SMe})]$ , as the next step in the reaction sequence. Further elimination of  $\text{ClSiMe}_3$  from this intermediate to give the isolated product is probably facilitated by the presence of the second sulfur atom of the dithioether ligand in the coordination sphere of the tungsten atom.

The previous literature has described that attempts to exchange the DME ligand in the complex for two THF ligands gave a white product with bands at 1040 and 847  $\text{cm}^{-1}$  in its IR spectrum as expected for coordinated THF.<sup>[77]</sup> In addition the presence of a strong broad band at 725  $\text{cm}^{-1}$  in the IR spectrum reveals bridging oxo-groups. The analytical data (Found (Calc.) W, 50.3 (51.2); Cl, 19.2 (19.7); C, 13.9 (13.4); H, 2.4 (2.1)%) for this compound are close to the formula  $\text{WO}_2\text{Cl}_2(\text{THF})$  and this formulation is also supported by the bridging oxo group as observed by IR. Whether this oxo bridged structure exists in THF solution or if it is formed as a consequence of a loss of THF during the isolation of the complex is not known. A decreased solubility in THF after initial isolation indicates that a loss of THF with subsequent formation of oxo bridges might occur. The deduction was confirmed by the preparation of **2**, which contains four units of  $\text{WO}_2\text{Cl}_2(\text{THF})$ .

Attempted preparation of **1** and **2** *via* direct reactions of dithioether and THF with  $\text{WO}_2\text{Cl}_2$ , respectively, did not lead to any dissolution of  $\text{WO}_2\text{Cl}_2$  although the reaction was continued for several weeks. This indicates that the barrier for breaking up the polymeric network of solid  $\text{WO}_2\text{Cl}_2$  is so high that a direct synthesis is not feasible.

Other attempts to prepare the selenoether analogue,  $\text{WO}_2\text{Cl}_2[\text{MeSe}(\text{CH}_2)_2\text{SeMe}]$ , of **1** by the same method as that of **1** or by exchanging the DME or THF ligands in complex  $\text{WO}_2\text{Cl}_2$  (DME) or **2** with diselenoether ligands, respectively, were also failed. During the reaction

processes, the intense blue solution and solid formed gradually with the increase of the temperature (to r. t.) even though the initial reactions were performed at very low temperature (ca.  $-78^{\circ}\text{C}$ ). There is no evidence for W(VI) selenoether complex formation. This indicates that the diselenoether compound is thermally very unstable like its molybdenum analogue.<sup>[78]</sup>

### 2.1.2. Structural investigation of **1**

The crystal structure of **1** and selected bond distances and angles are presented in Figure 7 and Table 1, respectively.

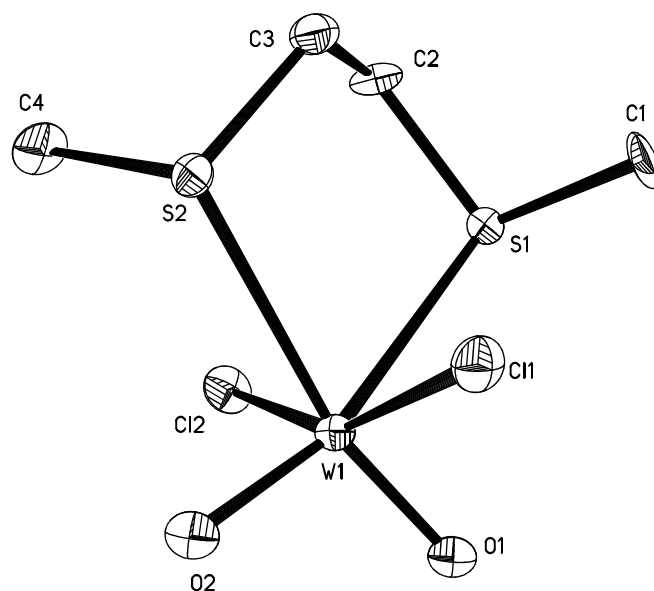


**Figure 7.** View of the structure of  $\text{WO}_2\text{Cl}_2[\text{MeS}(\text{CH}_2)_2\text{SMe}]$  (**1**) with numbering Scheme.

Hydrogen atoms are not shown. Ellipsoids are drawn at 50% probability.

The  $\text{W}^{\text{VI}}$  atom of **1** has a distorted octahedral coordination environment, derived from two *cis* oxo ligands, two *trans* chloro ligands and a chelating dithioether which occupies the coordination sites *trans* to the oxo ligands and adopts the DL configuration with the Me groups oriented on opposite sides of the  $\text{O}_2\text{S}_2$  plane. The W-S distances of 2.748(2) and 2.752(2) Å are ca. 0.4 Å longer than  $d(\text{W}-\text{Cl})$  involving the isoelectronic chloro ligand,



indicating a very weak interaction between the hard hexavalent W centre and the soft, weakly donating thioether functions. The angle S-W-S is  $77.4^\circ$ . The oxide ions are *cis* oriented, as also suggested from theoretical calculations,<sup>[79]</sup> with both W=O bond distances of  $1.716(7) \text{ \AA}$  and an angle O=W=O of  $105.3(3)^\circ$ . The W=O bond distance is close to the mean value of  $1.709 \text{ \AA}$ , calculated from other dioxo complexes.<sup>[80]</sup> Two chloride atoms at  $2.333(2)$  and  $2.337(2) \text{ \AA}$  complete the octahedron around tungsten. Both chlorine atoms are bent towards the thioether ligand resulting in a Cl-W-Cl angle of  $155.13(8)^\circ$ . The environment at W(VI) in the thioether complex may alternatively be described as distorted tetrahedral primary O<sub>2</sub>Cl<sub>2</sub> coordination, with additional weak S<sub>2</sub> coordination, giving the overall distorted 6-coordinate geometry. The slight shortening of the Mo-Cl distances and the changes in the angle around W may be evidence for increased  $\pi$ -donation from Cl to compensate for the weak S-donation. Compound **1** is analogous to a recently published molybdenum compound.<sup>[78]</sup> The compounds MO<sub>2</sub>Cl<sub>2</sub>(DME) are well-established for both metals.<sup>[75,76]</sup> Therefore, with this new compound a thorough structural investigation of these compounds and comparison between oxygen and sulfur coordination as well as a comparison between molybdenum and tungsten compounds could be undertaken.

The structures of MoO<sub>2</sub>Cl<sub>2</sub>[MeS(CH<sub>2</sub>)<sub>2</sub>SMe]<sup>[78]</sup> and WO<sub>2</sub>Cl<sub>2</sub>[MeS(CH<sub>2</sub>)<sub>2</sub>SMe] (**1**) (see Figure 7) are almost identical, and the largest differences occur for the metal–chlorine bond length ( $0.05 \text{ \AA}$ ) and the O=M=O angle ( $1^\circ$ ) (see Table 1). Both compounds crystallize in the same crystal system (hexagonal) and space group (*P6*<sub>1</sub>).

This is also true for the compounds MoO<sub>2</sub>Cl<sub>2</sub>(DME)<sup>[75]</sup> and WO<sub>2</sub>Cl<sub>2</sub>(DME)<sup>[76]</sup>, where the largest difference for a bond length is that for the M–O(ether) bond of  $0.04 \text{ \AA}$ , and the difference for the O(ether)–M–O(ether) angle is  $0.4^\circ$ , which is the largest difference for an

angle. Nevertheless, it has to be noted that the value for the Cl–Mo–Cl angle is not mentioned in the respective publication.<sup>[75]</sup> Again, both compounds crystallize in the same crystal system (monoclinic) and space group ( $P2_1/n$ ).

**Table 1.** Selected bond lengths and angles for the molybdenum and tungsten complexes with bidentate ether and thioether ligands.

	WO <sub>2</sub> Cl <sub>2</sub> (MeSC <sub>2</sub> H <sub>4</sub> SMe) ( <b>1</b> )	MoO <sub>2</sub> Cl <sub>2</sub> (Me SC <sub>2</sub> H <sub>4</sub> SMe) <sup>a</sup>	WO <sub>2</sub> Cl <sub>2</sub> (DME) <sup>b</sup>	MoO <sub>2</sub> Cl <sub>2</sub> (DME) <sup>c</sup>
M=O [Å]	1.716(7)	1.691	1.690	1.667
	1.716(7)	1.699	1.690	1.673
M-Cl [Å]	2.333(2)	2.345	2.344	2.347
	2.337(2)	2.385	2.344	2.340
M-O/S [Å]	2.748(2)	2.759	2.253	2.289
	2.752(2)	2.771	2.292	2.281
O=M=O [°]	105.3(3)	106.3	105.1	105.0
O/S-M-O/S [°]	77.37(7)	77.3	70.5	70.9
Cl-M-Cl [°]	155.13(8)	154.4	157.6	-

a Ref. [78], b Ref. [76], c Ref. [75]

The differences observed as a result of a comparison of ether and thioether ligands are of course larger, but only for those values that are derived directly from the different radii of the oxygen and sulfur atoms. The difference in the metal–ether/thioether bond is 0.49 Å for the molybdenum complexes and 0.50 Å for the tungsten complexes. The values for the O/S–M–O/S angles differ by 6.5° for the molybdenum and by 6.9° for the tungsten compound, where the angles for the thioether ligands are wider. All other distances and angles involving

the metal center are only slightly influenced; the largest difference for a bond length was 0.05 Å for the Mo–Cl bond and the largest difference for an angle was 2.5° for the Cl–W–Cl angle. This is an indication that the electronic influence of replacing oxygen ligand atoms by sulfur ligand atoms is only very small. Otherwise we would have observed larger differences, especially in the parameters for the ligand atoms that are in a *trans* position to the ether/thioether functions (oxo ligands in all four cases).

We have seen that molybdenum and tungsten form almost identical complexes with the bidentate ether and thioether ligands. The metal atom does not affect the structure of the complexes, though it has an influence on the stability of the complexes because of a difference in the strength of orbital overlap. For the oxygen-atom-transfer enzymes, where only mono- or bidentate ligands are present, a geometrical or steric influence as a result of changing the metal atom can be excluded.

Changing the ligand atoms does not result in any significant structural alterations, with the only exception of the metal-to-ether/thioether-ligand-atom bond length and angle, but these differences are merely a result of the different radii of the ligand atoms. There was no indication of a significant electronic influence of changing the ligand atoms (oxygen versus sulfur) on the metal, except that the potentials of the molybdenum and tungsten complexes were closer together with sulfur ligation than with oxygen ligation as can be seen in the following chapter.

### 2.1.3. Electrochemical investigation of **1**

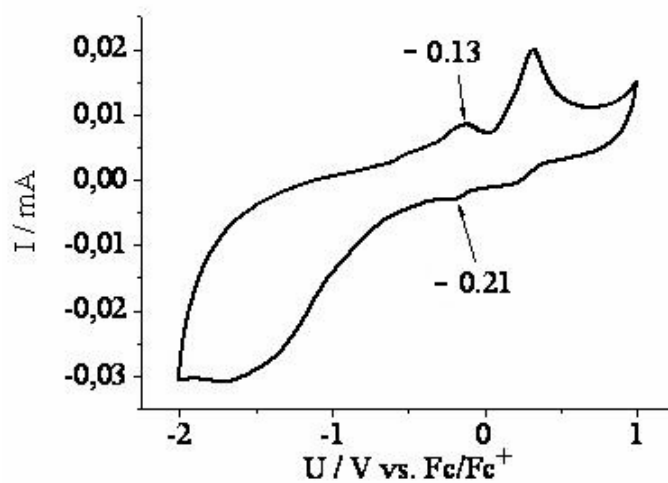
The redox potentials of compounds MoO<sub>2</sub>Cl<sub>2</sub>(DME),<sup>[75]</sup> WO<sub>2</sub>Cl<sub>2</sub>(DME),<sup>[76]</sup> MoO<sub>2</sub>Cl<sub>2</sub>[MeS(CH<sub>2</sub>)<sub>2</sub>SMe],<sup>[78]</sup> and WO<sub>2</sub>Cl<sub>2</sub>[MeS(CH<sub>2</sub>)<sub>2</sub>SMe] (**1**) were compared (see Table

2). Here, we used cyclic voltammetry and observed quasi-reversible behavior for all compounds for the  $M^V \leftrightarrow M^{VI}$  transition. In the range from  $-1.0$  to  $-1.5$  V an irreversible reduction occurs in all cases probably because of the loss of one oxo ligand accompanying the reduction to  $M^{IV}$ . The formation of this new species led to the emergence of new signals in the voltammograms. We therefore only compared the potentials of the quasi-reversible process assigned to the  $M^V \leftrightarrow M^{VI}$  transition.

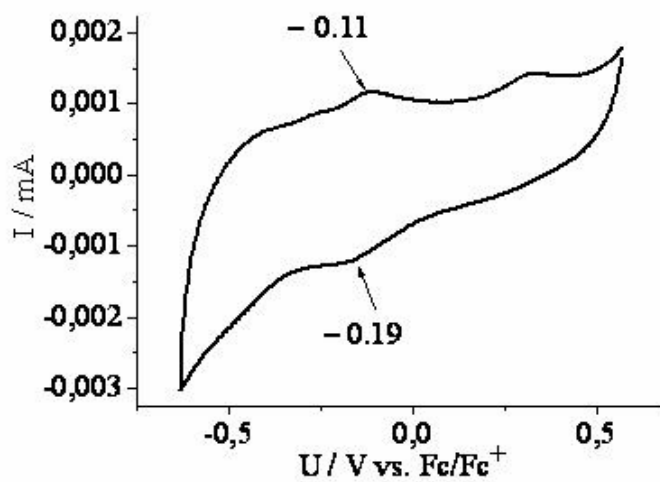
**Table 2.** Redox potentials for the molybdenum and tungsten compounds with the bidentate ether/thioether ligands for the  $M^V \leftrightarrow M^{VI}$  redox processes referenced internally vs. ferrocene/ferrocenium.

Compound	$E_{1/2} M^V \leftrightarrow M^{VI}$ vs. Fc/Fc <sup>+</sup> [V]
MoO <sub>2</sub> Cl <sub>2</sub> (dme)	-0.17
MoO <sub>2</sub> Cl <sub>2</sub> (MeSC <sub>2</sub> H <sub>4</sub> SMe)	-0.15
WO <sub>2</sub> Cl <sub>2</sub> (dme)	-0.34
WO <sub>2</sub> Cl <sub>2</sub> (MeSC <sub>2</sub> H <sub>4</sub> SMe) ( <b>1</b> )	-0.28

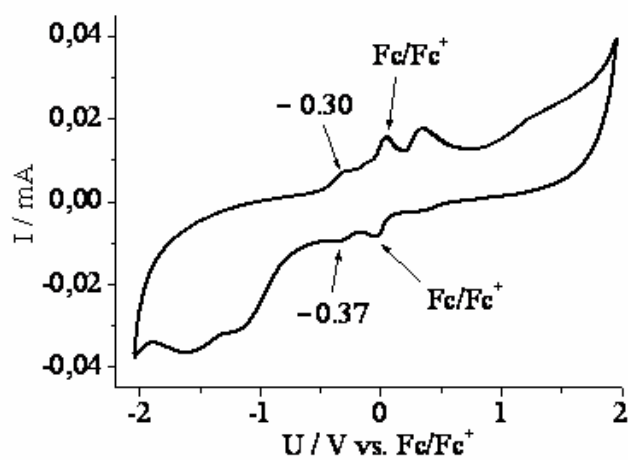
Figure 8 shows a long-range cyclic voltammogram (including the irreversible reduction and ligand-centered quasi-reversible oxidation) of MoO<sub>2</sub>Cl<sub>2</sub>(DME) (a), a short-range cyclic voltammogram of MoO<sub>2</sub>Cl<sub>2</sub>(MeS(CH<sub>2</sub>)<sub>2</sub>SMe) (b), and a long-range cyclic voltammogram of WO<sub>2</sub>Cl<sub>2</sub>(DME) (c) with the internal reference ferrocene.



(a)



(b)



(c)

**Figure 8.** Cyclic voltammogram of (a)  $\text{MoO}_2\text{Cl}_2(\text{DME})$  (long range, the 2<sup>nd</sup> scan of the measurement), (b)  $\text{MoO}_2\text{Cl}_2(\text{MeS}(\text{CH}_2)_2\text{SMe})$  (short range, the 3<sup>rd</sup> scan of the measurement) and (c)  $\text{WO}_2\text{Cl}_2(\text{DME})$  (long range, the 2<sup>nd</sup> scan of the measurement) referenced internally vs.  $\text{Fc}/\text{Fc}^+$ . The redox process that was investigated is marked with arrows.

The molybdenum compounds have potentials that are higher than their tungsten analogs and the complexes with sulfur ligand atoms have potentials that are higher than their counterparts with oxygen ligand atoms. The latter differences are again smaller (between 20 and 60 mV) than the differences between molybdenum and tungsten compounds, which are about three times larger (between 130 and 170 mV). Since the bonds between metal and sulfur atoms exhibit  $\pi$ - $\pi$ -interactions, it can be noted that the differences between the redox potentials of the molybdenum and tungsten thioether complexes are smaller than those between the complexes with the oxygen ligand atoms. Changing the metal atoms has a much more significant influence on the redox potentials than changing the ligand atoms.

#### 2.1.4. Crystal structure description of **2**

The molecular structure of compound **2** is shown in figure 9; selected bond lengths and angles are listed in Table 3.

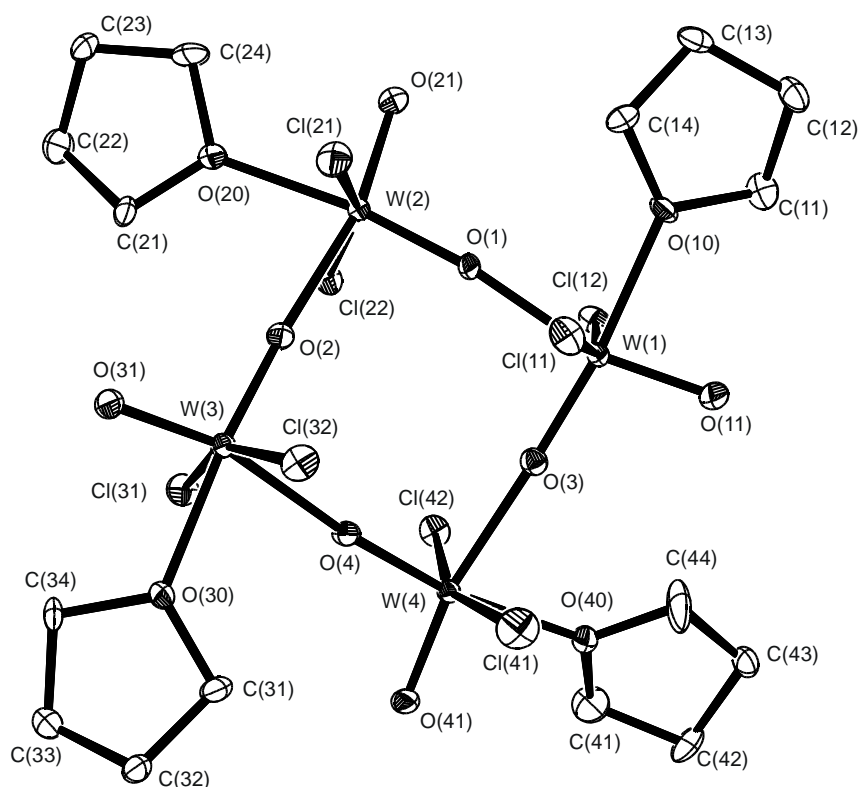


**Figure 9.** Molecular structure of **2**.

**Table 3.** Selected bond lengths (Å) and angles (°) for **2**.

<i>Bond lengths</i>			
W(1)-O(11)	1.697(5)	W(1)-O(10)	2.210(4)
W(1)-O(3)	1.744(4)	W(1)-Cl(11)	2.3083(17)
W(1)-O(1)	2.172(4)	W(1)-Cl(12)	2.3286(17)
<i>Bond angles</i>			
O(11)-W(1)-O(3)	101.4(2)	O(1)-W(1)-Cl(11)	79.93(13)
O(11)-W(1)-O(1)	164.9(2)	O(10)-W(1)-Cl(11)	83.37(13)
O(3)-W(1)-O(1)	93.52(18)	O(11)-W(1)-Cl(12)	96.44(18)
O(11)-W(1)-O(10)	85.2(2)	O(3)-W(1)-Cl(12)	94.67(15)
O(3)-W(1)-O(10)	173.38(19)	O(1)-W(1)-Cl(12)	80.38(13)
O(1)-W(1)-O(10)	79.87(17)	O(10)-W(1)-Cl(12)	84.41(13)
O(11)-W(1)-Cl(11)	100.25(18)	Cl(11)-W(1)-Cl(12)	158.36(6)
O(3)-W(1)-Cl(11)	95.41(15)	W(2)-O(1)-W(1)	172.8(3)

Compound **2** crystallizes in the monoclinic space group  $P2_1/n$ . This compound **2** has a tetrameric structure in which every two molybdenum atoms are bridged by one  $\mu$ -oxo ligand. The structure is formed by the association of four  $\text{WO}_3\text{Cl}_2(\text{THF})$  octahedral sharing corners in such a way that the W atoms are in a roughly square arrangement. All tungsten atoms are crystallographically equivalent. Each tungsten atom is coordinated to two bridging oxygens, one unshared (oxo type) oxygen, two “axial” chlorine atoms and one “equatorial” O-bonded THF ligand. The interatomic distances and bond angles show that the tungsten atom is not found at the center of the coordination octahedron, but is shifted toward the terminal unshared oxygen atom, as usual for oxo complexes of tungsten. The distances of each tungsten and two bridging  $\mu$ -oxo ligands are different, for example, W(1)-O(3) (1.744(4) Å) and W(1)-O(1) (2.172(4) Å). The shorter bond length (W(1)-O(3)) is closer to that of tungsten and the terminal oxygen atom (W(1)-O(11), 1.697(5) Å) and indicates some  $\pi$  character, whereas the longer one is closer to that of tungsten and the oxygen atom of the THF ligand (W(1)-O(10), 2.210(4) Å). These indicate the two  $\mu$ -oxo ligands are similar to the terminal oxygen atom and the coordinated oxygen atom of the THF ligand, respectively, and they are not equivalent for the tungsten atom. The two chlorine atoms are in a *trans* position and on the different sides of the roughly planar square formed by the four tungsten atoms. Each  $\{\text{WO}_3\text{Cl}_2(\text{THF})\}$  unit in **2** is similar to the configuration of **1**. The average W-O-W bridge angle ( $174.6^\circ$ ) is almost linear and the average for  $\mu$ -O-W- $\mu$ -O angle is  $92.30^\circ$  which approaches a right angle.

A valuable comparison can be made with two analogous tetrameric compounds,  $[\text{W}_4\text{O}_8\text{Cl}_8(\text{H}_2\text{O})_4]^{2-}$  [81] and  $[\text{W}_4\text{O}_8(\text{NCS})_{12}]^{6-}$  [82]. First of all, **2** is uncharged and every tungsten exhibits the oxidation state VI, while both  $[\text{W}_4\text{O}_8\text{Cl}_8(\text{H}_2\text{O})_4]^{2-}$  [81] and  $[\text{W}_4\text{O}_8$



$(\text{NCS})_{12}]^{6-}$  [82] are ions of mixed-valence compounds with 2  $\text{W}^{\text{V}}$  and  $\text{W}^{\text{VI}}$ . Both latter compounds exhibit exchange interaction properties between neighboring tungsten atoms due to the  $\pi$  character of the linear W-O-W chain. The distances of each tungsten to its two  $\mu$ -oxo ligand are almost the same which explicits that they are equivalent for the tungsten atom. The disposition of the terminal oxygen atom in the present case is different from the cases of  $[\text{W}_4\text{O}_8\text{Cl}_8(\text{H}_2\text{O})_4]^{2-}$  [81] and  $[\text{W}_4\text{O}_8(\text{NCS})_{12}]^{6-}$  [82]. In **2** they all were almost arranged on the roughly square plane, while in  $[\text{W}_4\text{O}_8\text{Cl}_8(\text{H}_2\text{O})_4]^{2-}$  [81] they were found alternately above and below the molecular plane and in  $[\text{W}_4\text{O}_8(\text{NCS})_{12}]^{6-}$  [82] they exhibit a “chair” arrangement (see Figure 10).

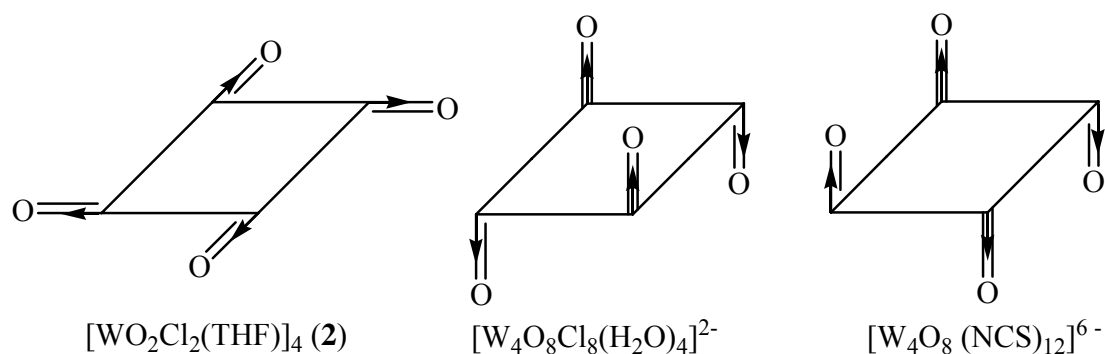


**Figure 10.** Sketch of the three possible configurations of the  $\text{W}_4\text{O}_8^{6+}$  core. The arrows show the displacements of the tungsten atoms with respect to a regular octahedral coordination.

The two chlorine atoms are arranged in *cis* positions and on the molecular plane in  $[\text{W}_4\text{O}_8\text{Cl}_8(\text{H}_2\text{O})_4]^{2-}$  [81], which is different from the present compound **2**.

On the other hand, the molybdenum analogue formed a mononuclear compound with two THF ligands,  $\text{MoO}_2\text{Cl}_2(\text{THF})_2$  [83]. The two metals are chemically similar, but they adopt different structures, which poses a challenging question for the future.

## 2.2. Molybdenum and tungsten complexes with tridentate bisanionic thioether and selenoether ligands

High-valent metal complexes with thioether or selenoether ligands that represent hard–soft metal–ligand combinations are relatively rare mainly because these compounds are rather unstable.<sup>[70]</sup> Even though molybdenum(VI) and tungsten(VI) can be considered as moderately hard, only a handful of these metals complexes with thioether or selenoether ligands are known.<sup>[78,84-86]</sup> There are known only very few examples of selenoether complexes with molybdenum, which contain molybdenum in the oxidation states VI, V and 0.<sup>[78,87]</sup> To our knowledge, none of these compounds was characterized by X-ray crystallography. Of the chemically similar tungsten on the other hand the structures of a few selenoether compounds were solved.<sup>[88]</sup> All of them contain tungsten in the oxidation state 0.

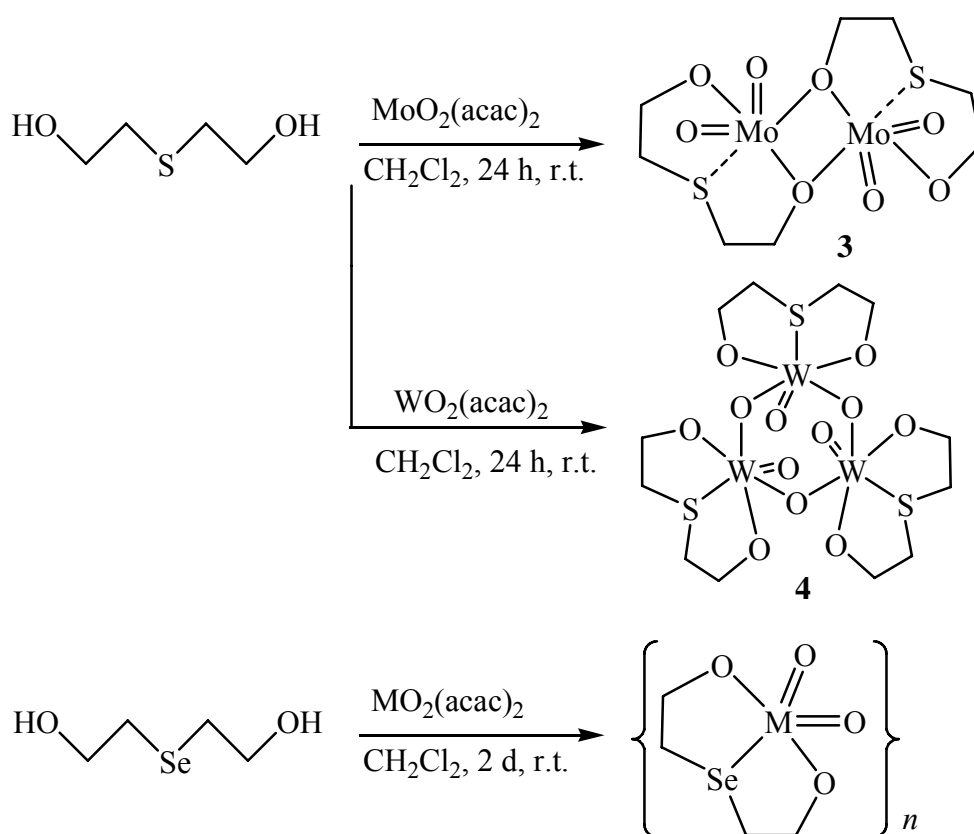
In spite of the assumption that these kinds of complexes with Mo<sup>VI</sup> and W<sup>VI</sup> may not be easy to prepare and handle, we tried to synthesize and characterize a small variety of these compounds with additional alkoxy functions at the ligands for enhanced stability. Here sulfur and selenium coordination is concentrated on due to the fact that there are rather few studies about the selenium coordination with respect to the molybdenum cofactors<sup>[68,89]</sup> and because sulfur and selenium are of the almost same size and therefore behave similarly when employed within the same kind of ligand system.

The aims of the research are: (1) To obtain complexes that mimic the active sites of the OATs where the coordination sphere of the metal consists only of oxygen and sulfur or selenium, respectively, and where one oxo ligand is present with an oxidation state of +6 for the metal. (2) To also obtain complexes that enable us to compare the influences of molybdenum versus tungsten and sulfur versus selenium with regard to their redox properties and oxygen atom

transfer properties.

**2.2.1.** syntheses of  $[\{\text{MoO}_2[\text{O}(\text{CH}_2)_2\text{S}(\text{CH}_2)_2\text{O}]\}_2]$  (**3**),  $[\{\text{WO}_2[\text{O}(\text{CH}_2)_2\text{S}(\text{CH}_2)_2\text{O}]\}_3]$  (**4**) and  $[\{\text{MO}_2[\text{O}(\text{CH}_2)_2\text{Se}(\text{CH}_2)_2\text{O}]\}_n]$  (M = W (**5**), Mo (**6**))

In the synthesis we focused on the simple replacement of acetylacetonate ligands in  $\text{MO}_2(\text{acac})_2$  (M = Mo, W) by alkali salts of alkoxyates containing a thio- or selenoether function. The compounds  $[\{\text{MoO}_2[\text{O}(\text{CH}_2)_2\text{S}(\text{CH}_2)_2\text{O}]\}_2]$  (**3**),  $[\{\text{WO}_2[\text{O}(\text{CH}_2)_2\text{S}(\text{CH}_2)_2\text{O}]\}_3]$  (**4**) and  $[\{\text{MO}_2[\text{O}(\text{CH}_2)_2\text{Se}(\text{CH}_2)_2\text{O}]\}_n]$  (M = W (**5**), Mo (**6**)) were all prepared by the same method (Scheme 2).



M = W (**5**), Mo (**6**);  $n$  is undetermined

**Scheme 2.** Preparation of  $[\{\text{MoO}_2[\text{O}(\text{CH}_2)_2\text{S}(\text{CH}_2)_2\text{O}]\}_2]$  (**3**),  $[\{\text{WO}_2[\text{O}(\text{CH}_2)_2\text{S}(\text{CH}_2)_2\text{O}]\}_3]$  (**4**) and  $[\{\text{MO}_2[\text{O}(\text{CH}_2)_2\text{Se}(\text{CH}_2)_2\text{O}]\}_n]$  (M = W (**5**), Mo (**6**)). No X-ray structural analysis was possible for **5** and **6**, and  $n$  could not be determined.

The appropriate metal precursor,  $\text{MO}_2(\text{acac})_2$ , and one equivalent of the ligand, bis(2-hydroxyethyl)sulfide or bis(2-hydroxyethyl)selenide, were combined in a  $\text{CH}_2\text{Cl}_2$  solution, stirred at room temperature for one or two days, and filtered. The compounds were isolated from the filtrate by crystallization or drying in vacuo or by the filtration. The yields range from a rather good 60% for the tungsten selenoether (**6**) compound (obtained by drying) to only 32% for the tungsten thioether compound (**4**). The complexes **3-6** are not readily soluble in common organic solvents except that **5** has good solubility in DMSO. They are stable in dry air whereas moisture leads to slow decomposition forming blue intractable solids. All compounds were characterized by elemental analysis, IR spectroscopy, EI mass spectrometry. Due to the poor solubilities, only the  $^1\text{H}$  NMR spectra of compound **3** in  $\text{CDCl}_3$  and the  $^1\text{H}$ ,  $^{13}\text{C}$ ,  $^{77}\text{Se}$  NMR of **5** in  $\text{DMSO}-d_6$  were performed. The  $^1\text{H}$  NMR spectra of **3** and **5** show resonances for two different methylene groups ( $\delta = 2.31$  and  $3.36$  ppm for **3**,  $2.60$  and  $3.56$  ppm for **5**) consistent with the solid state structure. The  $^{13}\text{C}$  NMR spectra of **5** show the signal for the  $\text{SeCH}_2$  and  $\text{OCH}_2$  ( $\delta = 26.14$  and  $61.62$  ppm). Because we were unable to obtain crystals of the tungsten selenium compound **5**,  $^{77}\text{Se}$  NMR spectroscopy on the complex ( $\delta = 100.22$  ppm) as well as on the ligand ( $\delta = 68.23$  ppm) was performed and only one signal was observed that was shifted to higher frequencies / lower field in the complex, which indicates that a metal-selenium bond was indeed formed.<sup>[90]</sup>

The IR spectra display the characteristic features: strong bands in the ranges of  $1069\text{-}1025$   $\text{cm}^{-1}$  and  $802\text{-}723$   $\text{cm}^{-1}$  for **3**,  $1091\text{-}1033$   $\text{cm}^{-1}$  and  $801\text{-}722$   $\text{cm}^{-1}$  for **4**,  $1094\text{-}1020$   $\text{cm}^{-1}$  and  $800$   $\text{cm}^{-1}$  for **5**, and  $954$ ,  $911$   $\text{cm}^{-1}$  and  $798$   $\text{cm}^{-1}$  for **6**, respectively, assigned to  $\nu \text{M}=\text{O}_t$  and  $\nu \text{M-O-M}$  ( $\text{M} = \text{Mo}, \text{W}$ ) stretching modes involving terminal and bridging oxo ligands.

### 2.2.2. Structures and DFT calculations of **3** and **4**

Suitable crystals of the molybdenum and tungsten thioether compounds were analyzed by X-ray crystallography with quite interesting results (see Figure 11 and Figure 12).

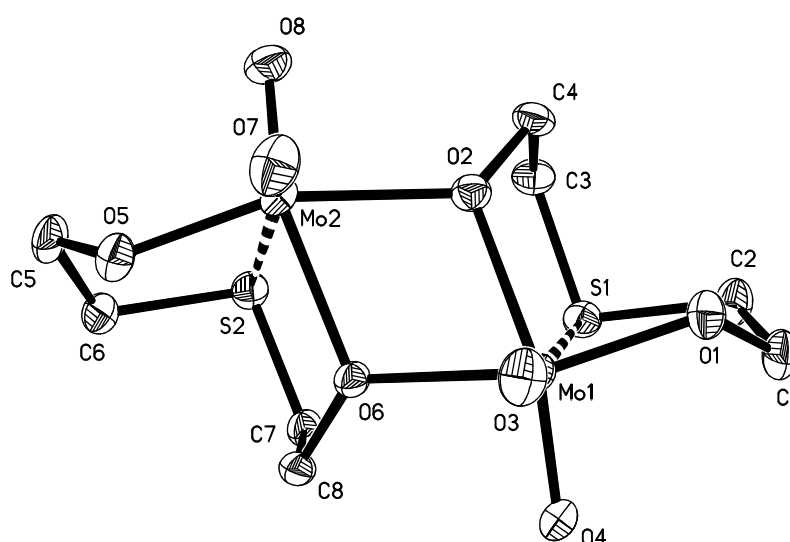


**Figure 11.** View of the structure of  $[\{\text{MoO}_2[\text{O}(\text{CH}_2)_2\text{S}(\text{CH}_2)_2\text{O}]\}_2]$  (**3**) with numbering Scheme. Hydrogen atoms are not shown. Ellipsoids are drawn at 50% probability.

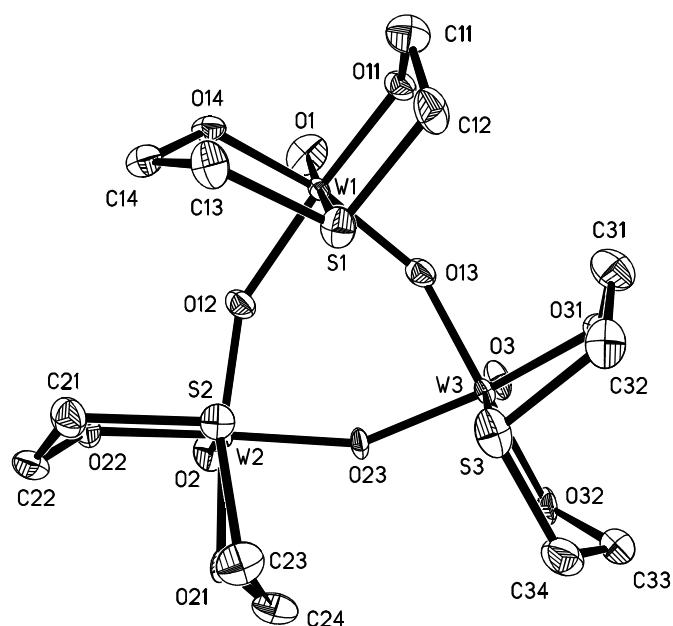


**Figure 12.** View of the structure of  $[\{\text{WO}_2[\text{O}(\text{CH}_2)_2\text{S}(\text{CH}_2)_2\text{O}]\}_3]$  (**4**) with numbering Scheme. Hydrogen atoms are not shown. Ellipsoids are drawn at 50% probability.

The molybdenum complex with the thioether ligand has a dimeric structure in which the two molybdenum atoms are bridged by one alkoxylate function of each of the two thioether ligands. The tungsten, on the other hand, forms a trimeric structure in which one of the former oxo ligands of each metal bridges two tungsten atoms, forming a six-membered ring. In both structures the metal achieves a slightly distorted octahedral coordination geometry through the two different kinds of aggregation although the molybdenum is explicitly only bound to five ligand atoms with rather long metal–sulfur distances. Instead of the usual distance between the metal (molybdenum or tungsten) and sulfur atoms of a thioether ligand, which is in the range of 2.45 to 2.77 Å,<sup>[78,91]</sup> we found distances of 2.93 and 3.00 Å, indicating only weak bonds, if bonds at all. The tungsten–sulfur distances are shorter (2.79, 2.81, and 2.83 Å) even though the central metal is slightly larger, and these interactions can be considered bonds without doubt.

In spite of the fact that five-ring complexes with thio or selenoether functions are supposed to be stable<sup>[78]</sup> the expected molybdenum–sulfur bond with this ligand is not explicitly formed. The reaction of the OSO ligand with MoO<sub>2</sub>(acac)<sub>2</sub> results in a compound that instead of forming two stable five-ring units, somehow rather resembles an eight-ring complex. In contrast a certain monomeric molybdenum complex with the analogous ligand that contains an ether function instead of the thioether function is known to exhibit an oxygen(ether)–metal bond even though the distance is longer than usual.<sup>[92]</sup> This is not completely surprising for these kinds of ligands although the analogous cobalt complexes, with ligands where the alkoxylate and the ether/thioether functions are bridged by phenyl rings, show the reverse behavior. With the ether function, no bond is formed between the metal and oxygen atoms,

whereas with the thioether function, there is a bond between the cobalt and sulfur atoms.<sup>[93]</sup>

Unfortunately, the crystals of **4** were racemic twins, and the structure could only be solved in an acentric space group. The crystallographic problem encountered was one reason for performing DFT calculations on this compound. The results of the DFT calculations confirmed those of the structural analysis with some differences especially in the bond lengths between the metal and sulfur atoms (see Table 4). In general the distances obtained from X-ray analysis are shorter than the calculated ones, with the only exception of the metal–oxo distances, which are slightly longer. With these two data sets (X-ray data and DFT data) for **4** we are now able to discuss the structural parameters of compound **4** as well as of compound **3** with some certainty, despite the crystallographic problems concerning the structure of **4**.

In compound **3** the metal is pseudo-octahedrally coordinated. The thioethers form only very weak bonds, if at all, to the molybdenum atoms (interatomic distances: 2.931, 3.002 Å obtained from X-ray). The molybdenum atoms are positioned above (0.3647 and 0.3664 Å) the plane that consists of three alkoxyate groups and one oxo *trans* to the bridging alkoxyate function. Within the Mo<sub>2</sub>O<sub>2</sub> ring, the angles at the metal atom are smaller than 90°, whereas the angles at the oxygen atom are larger. The tridentate ligands and the oxo ligands that are coordinated *trans* to the sulfur atoms are positioned on different sides of the Mo<sub>2</sub>O<sub>2</sub> ring. The two oxo functions, as well as the two tridentate ligands, are on the same side of this ring, although one could assume that the *trans* form would be sterically less demanding.

**Table 4.** Selected bond lengths and angles obtained from an X-ray structural analysis of [ $\{\text{MoO}_2[\text{O}(\text{CH}_2)_2\text{S}(\text{CH}_2)_2\text{O}]\}_2$ ] (**3**) and [ $\{\text{WO}_2[\text{O}(\text{CH}_2)_2\text{S}(\text{CH}_2)_2\text{O}]\}_3$ ] (**4**) and from DFT calculations for [ $\{\text{WO}_2[\text{O}(\text{CH}_2)_2\text{S}(\text{CH}_2)_2\text{O}]\}_3$ ] (**4**).

	[{MoO <sub>2</sub> [OSO]} <sub>2</sub> ] (3) <sup>[a]</sup>	[{WO <sub>2</sub> [OSO]} <sub>3</sub> ] (4) <sup>[a]</sup>	[{WO <sub>2</sub> [OSO]} <sub>3</sub> ] (4) <sup>[a]</sup>
	X-ray	X-ray	DFT
M=O [Å]	1.6916(19), 1.6912(19)	1.707(12)	1.7060
	1.6926(19), 1.6982(18)	1.712(11)	1.7062
		1.734(11)	1.7076
M-S [Å]	2.931(4), 3.002(5)	2.793(4), 2.812(4), 2.827(4)	3.1220, 3.1286, 3.2135
M-O <sub>alkoxy</sub> [Å]	1.8973(18)	1.865(10), 1.889(10)	1.9544, 2.0095
	1.8973(18)	1.888(10), 1.897(11)	1.9350, 1.9461
		1.862(10), 1.880(10)	1.9274, 1.9377
M-O <sub>bridge</sub> [Å]	2.0718(17), 2.1410(17)	1.870(10), 1.944(8)	1.9206, 1.9407
	2.0940(17), 2.1484(18)	1.853(8), 1.937(7)	1.9112, 1.9358
		1.885(10), 1.905(10)	1.9143, 1.9487
O=M=O [°]	106.65(9), 108.19(10)		
O <sub>bridge</sub> -M-O <sub>bridge</sub> [°]	70.04(7), 69.49(7)	85.2(4), 85.4(3), 84.9(4)	86.32, 86.11, 84.26
M-O <sub>bridge</sub> -M [°]	105.72(7), 106.24(7)	150.7(5), 153.6(4)	139.693, 150.667, 151.89
O <sub>alkoxy</sub> -M-O <sub>alkoxy</sub> [°]	90.34(7), 90.99(7)	90.5(4), 86.4(4), 94.1(4)	85.94, 86.91, 92.29
S-M=O [°]	167.52(7), 165.7(7)	172.7(4), 170.3(4)	164.76, 164.22, 167.00
C-S-C [°]	100.70(13), 101.76(13)	100.9(8), 101.1(8)	100.88, 102.20, 102.54

[a] OSO = <sup>-</sup>O(CH<sub>2</sub>)<sub>2</sub>S(CH<sub>2</sub>)<sub>2</sub>O<sup>-</sup>.

Compound **4** is analogous to a published tungsten trimer in which phenyl rings bridge the alkoxy and thioether functions instead of ethyl groups.<sup>[86]</sup> In the published complex, two of the tridentate ligands and one oxo function are positioned on one side of the W1–W2–W3 plane, whereas the remaining two oxo functions and one tridentate ligand are on the opposite



side. For compound **4**, all oxo functions are positioned on the same side of the W1–W2–W3 plane and all tridentate ligands on the opposite side. From the structural analysis, we obtained metal–oxo distances that were longer, and metal–sulfur and metal–oxygen distances that were shorter than the parameters obtained from DFT calculations. The significantly longer metal–sulfur distances in the theoretical investigations were also observed for compound **3** (compare Table 4 and Table 5). Therefore, we think that the structural analysis gives a more accurate value for this parameter than the DFT calculations which usually is difficult for long range bonds. In compound **4**, the metal is again coordinated in a pseudo-octahedral geometry that is slightly less distorted than that of compound **3**. The tungsten–sulfur distances (2.79, 2.81, and 2.83 Å) are shorter than the molybdenum–sulfur distances in compound **3**. The oxo ligand is bound *trans* to the sulfur atom with a short distance of 1.71 to 1.73 Å. In this way, the ligand that is most tightly bound to tungsten is in a *trans* position to the ligand that is most weakly bound to the metal, which is the most stable geometry. All other metal–oxygen distances to the alkoxylate functions as well as to the bridging oxygen atoms are within the usual range of 1.86 to 1.95 Å for oxygen–tungsten single bonds. The tungsten atoms are positioned slightly above the equatorial plane (two bridging oxygen atoms, two alkoxylate functions) in the direction of the oxo ligands by 0.04 to 0.36 Å.

DFT calculations were not only performed to confirm the results of the X-ray crystal structure analysis for compound **4**, but also to understand the formation of surprisingly different complexes for molybdenum and tungsten with the same ligand and by the same preparation method. The most important differences between the two structures can be summarized shortly as follows: (i) a trimeric structure for the tungsten compound versus a dimeric structure for the molybdenum compound; (ii) former oxo ligands as bridging atoms for the

tungsten compound versus alkoxylate functions of the thioether ligand for the molybdenum compound.

The important parameters obtained from DFT calculations are summarized in Table 5.

**Table 5.** Selected bond lengths and angles obtained from DFT calculations for the molybdenum dimer **3** and trimer and for the tungsten dimer and trimer **4**.

	[{MoO <sub>2</sub> [OSO]} <sub>2</sub> ] ( <b>3</b> ) <sup>[a]</sup>	[{MoO <sub>2</sub> [OSO]} <sub>3</sub> ] <sup>[a]</sup>	[{WO <sub>2</sub> [OSO]} <sub>2</sub> ] <sup>[a]</sup>	[{WO <sub>2</sub> [OSO]} <sub>3</sub> ] ( <b>4</b> ) <sup>[a]</sup>
M=O [Å]	1.7127, 1.7295	1.6988	1.7189, 1.7344	1.7060
	1.7124, 1.7294	1.7014	1.7185, 1.7343	1.7078
		1.7035		1.7098
M-S [Å]	3.3557, 3.4079	3.1567/3.2187/ 3.2778	3.2903, 3.3594	3.1220, 3.1486, 3.1235
M-O <sub>alkoxy</sub> [Å]	1.9227	1.9421, 1.9505	1.9116	1.9348, 1.9409
	1.9232	1.9411, 1.9561	1.9119	1.9333, 1.9445
		1.9299, 1.9410		1.9221, 1.9325
M-O <sub>bridge</sub> [Å]	2.1265, 2.1363	1.8872/1.9723	2.1122, 2.1390	1.8988, 1.9453
	2.1273, 2.1349	1.8876/1.9710	2.1116, 2.1346	1.9010, 1.9441
		1.9168/1.9695		1.9295, 1.9440
O=M=O [°]	108.05, 108.09		107.22, 107.36	
O <sub>bridge</sub> -M-O <sub>bridge</sub>	68.35, 68.39	86.76, 87.91, 93.68	67.87, 67.96	83.0, 85.88, 91.71
[°]				
M-O <sub>bridge</sub> -M [°]	110.26, 110.28	142.35, 150.89, 156.09	110.95, 111.10	142.99, 150.15, 155.62
S-M=O [°]	163.47, 164.36	163.79, 164.03, 166.84	163.27, 164.32	164.23, 164.76, 167.00
S-M-O <sub>equatorial</sub> [°]	76.32	77.46	68.45	77.73
C-S-C [°]	101.29, 101.33	100.75, 100.79, 102.26	101.15, 101.21	100.72, 100.95, 102.08
HOMO LUMO	0.144	0.127	0.175	0.157
gap [eV]				

[a] OSO = <sup>-</sup>O(CH<sub>2</sub>)<sub>2</sub>S(CH<sub>2</sub>)<sub>2</sub>O<sup>-</sup>.

The most significant differences between the molybdenum and the tungsten compounds are as follows: The metal-to-bridging-oxygen distances for the trimer are much more unsymmetrical for the molybdenum than for the tungsten compound. It seems that the molybdenum center is somehow reluctant to share one of its oxo ligands with another molybdenum atom and to form a single bond instead of a double bond to the respective oxygen atom. The double-bond character of the metal–oxygen interaction is certainly more conserved in the molybdenum than in the tungsten trimer. In the dimer as well as in the trimer the molybdenum–oxo bonds are shorter than the tungsten–oxo bonds. All this is an indication that the molybdenum–oxo bond is stronger than the tungsten–oxo bond as would be expected taking into account the hard–soft interactions.

The metal–sulfur distances provide a further clue to the differing behavior of the two metals in reaction with the same ligand. It has to be noted that, although these calculated parameters are the ones that differ most from the X-ray structural parameters, at least the trend seems to be represented correctly. The metal–sulfur distances for the dimer as well as for the trimer are shorter for the tungsten than for the molybdenum compound, and the metal–sulfur distances for the trimers are shorter than the distances for the dimers. The octahedral geometry is less distorted for the tungsten trimer than for the tungsten dimer, providing more space for the sixth ligand, the sulfur atom. Even though the metal–sulfur distances in all four cases are significantly longer than for a regular metal–thioether bond, the observed parameters show that the trimer provides a coordination geometry that enhances the formation of a metal–sulfur bond much more than the dimer does. We also have to keep in mind that the actual metal–sulfur distances, at least for the two compounds that were analyzed by X-ray diffraction, are much shorter than those provided by the DFT calculations. We conclude from

all of this that molybdenum forms the dimeric structure, because it is able to keep both of the doubly bonded oxo ligands, and that tungsten forms the trimeric structure because it is able to form a stronger metal–sulfur interaction. This behavior is confirmed by the fact that with similar ligand sets only a tungsten trimer,<sup>[86]</sup> where terminal oxo ligands are converted into bridging oxo ligands, and molybdenum monomers<sup>[92]</sup> and dimers,<sup>[94]</sup> where the oxo ligands are retained as doubly bonded, are obtained and structurally characterized.

Again, this shows that molybdenum forms stronger interactions with oxygen than tungsten but weaker interactions with sulfur.

### 2.2.3. Electrochemical results for **3**, **4**, **5**

In order to evaluate the influence of the metal and of the ligand atoms (S versus Se) on the redox properties, compounds **3**, **4**, and **5** were investigated by differential pulse voltammetry (DPV). This method was chosen over cyclic voltammetry because all compounds, but especially compound **5**, were only slightly soluble in acetonitrile, and the signals of the redox processes in the cyclic voltammograms were rather weak (see Figure 13), whereas in the oxidative as well as in the reductive DPVs all transitions were sharp and sufficiently intense and therefore easily detected (Figure 14). The peak positions given in Table 6 were determined from both the reductive and the oxidative DPVs as an average. For each of the compounds [**3** (MoS), **4** (WS), **5** (WSe)], two reversible transitions were observed in the differential pulse voltammograms for the redox processes  $M^{IV} \leftrightarrow M^V$  and  $M^V \leftrightarrow M^{VI}$  (see Figure 13). As expected, the redox processes  $M^{VI} \leftrightarrow M^V$  and  $M^V \leftrightarrow M^{IV}$  for the molybdenum compound are at a higher voltage than those for the respective tungsten compound, whereas it is not expected that those for the tungsten–selenium compound are at a higher voltage than

those for the tungsten–sulfur compound. A third redox process was found at a rather high voltage for all three compounds. It showed irreversible behavior in the cyclic voltammograms, but a slightly shifted transition was also observed in the reductive DPV (see Figure 14). This leads to the conclusion that the third redox process is due to a structural reorganization of the molecule, where the oxidation occurs much more readily than the reduction. Because the oxidation probably takes place at the sulfur/selenium atom, the metal–sulfur/metal–selenium bond must dissolve and therefore a reorganization of the molecule is necessary. We assume that the reduction at the sulfur/selenium atom involves a more demanding structural reorganization than the oxidation process. Therefore reduction occurs much more slowly and it could not be observed in the CV but in the much slower DPV recording. Interestingly, the third transition for compound **5** (WSe) is at a significantly lower voltage than the transition for compound **4** (WS), reversing the observed behavior for the two transitions taking place at the metal atom with more positive potentials for **5** (WSe) than for **4** (WS). This is another indication that this redox process does indeed take place at the ligand atom. Here the oxidation of selenium is easier to achieve than that of sulfur as would be expected by taking the sizes of the two atoms and the metallic character of the selenium atom into account.

**Table 6.** Redox potentials for the molybdenum and tungsten compounds with the tridentate thioether/selenoether alkoxyolate ligands for the  $M^{IV} \leftrightarrow M^V$  and  $M^V \leftrightarrow M^{VI}$  transitions and for the oxidation at the ligand atom as obtained from DPV investigations referenced internally vs. ferrocene/ferrocenium.

Compound	$E_{1/2} M^{IV} \leftrightarrow M^V$ vs. Fc/Fc <sup>+</sup> [V]	$E_{1/2} M^V \leftrightarrow M^{VI}$ vs. Fc/Fc <sup>+</sup> [V]	$E_{1/2} ([MO_2(OXO)] \leftrightarrow [MO_2(OXO)]^+)$ vs. Fc/Fc <sup>+</sup> [V]
[{MoO <sub>2</sub> [OSO]} <sub>2</sub> ] (3) <sup>[a]</sup>	-0.93	0.31	1.49
[{WO <sub>2</sub> [OSO]} <sub>3</sub> ] (4) <sup>[a]</sup>	-1.41	-0.07	1.24
[{WO <sub>2</sub> [OSeO]} <sub>n</sub> ] (5) <sup>[b]</sup>	-1.37	-0.02	0.96

[a] OSO = <sup>-</sup>O(CH<sub>2</sub>)<sub>2</sub>S(CH<sub>2</sub>)<sub>2</sub>O<sup>-</sup>. [b] OSeO = <sup>-</sup>O(CH<sub>2</sub>)<sub>2</sub>Se(CH<sub>2</sub>)<sub>2</sub>O<sup>-</sup>.

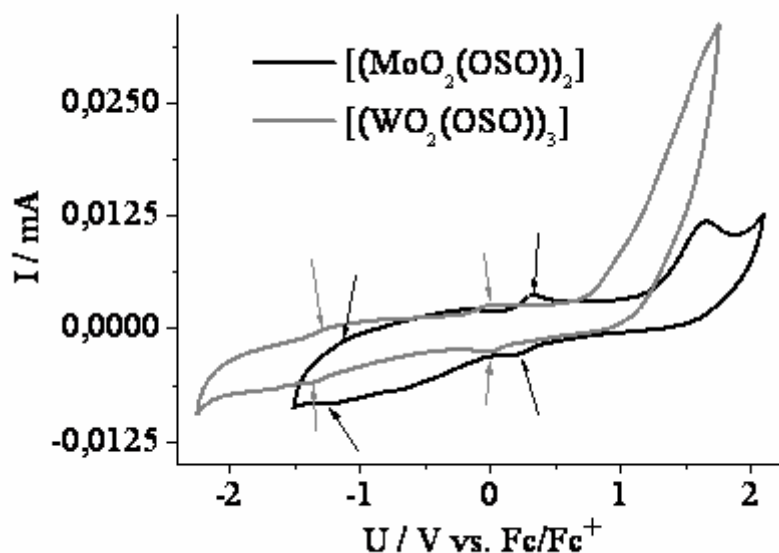


**Figure 13.** Cyclic voltammograms of compounds [ $\{MoO_2[O(CH_2)_2S(CH_2)_2O]\}_2$ ] (3) and [ $\{WO_2[O(CH_2)_2S(CH_2)_2O]\}_3$ ] (4) referenced vs. ferrocene/ferrocenium showing two reversible redox processes (indicated by arrows) and an irreversible oxidation (of very poor intensity for 4). The current values of 4 were multiplied by a factor of 4 in order to fit all the data into one graph.

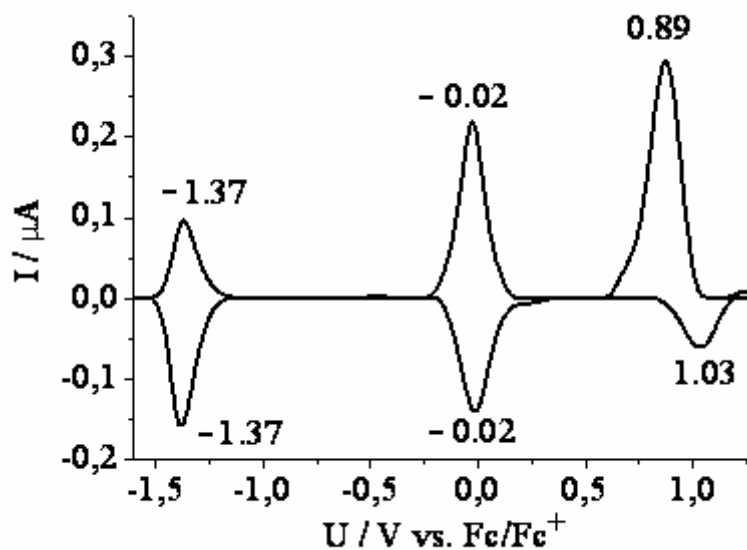
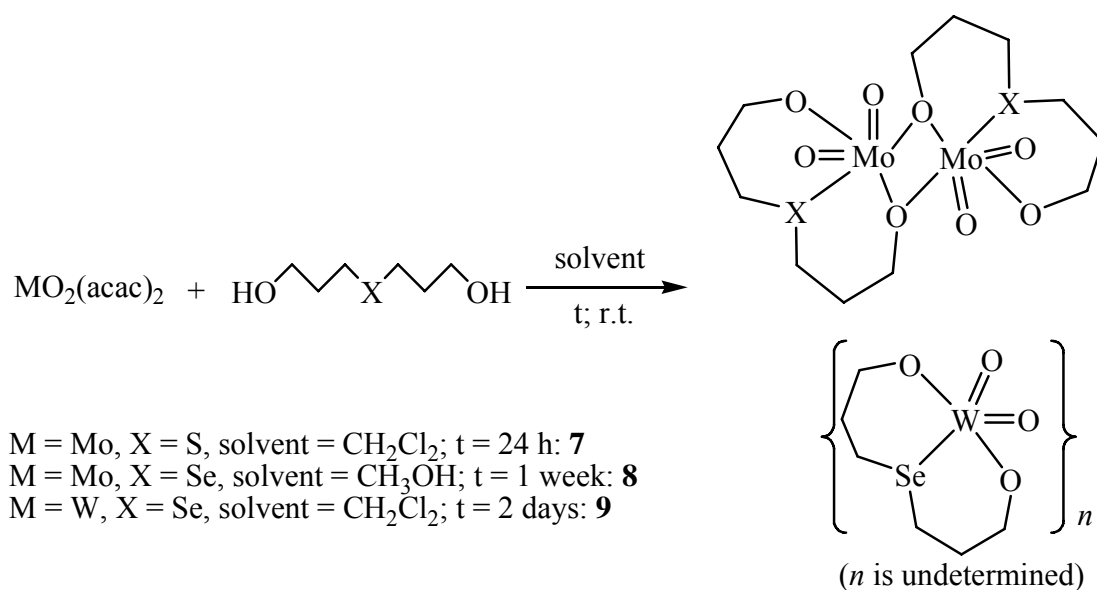


**Figure 14.** Reductive and oxidative differential pulse voltammograms of compound **5** referenced vs. ferrocene/ferrocenium. The plots were generated using the automatic baseline correction function of the GPES software.

**2.2.4.** Syntheses of  $[\{\text{MoO}_2[\text{O}(\text{CH}_2)_3\text{X}(\text{CH}_2)_3\text{O}]\}_2]$  ( $\text{X} = \text{S}$  (**7**),  $\text{Se}$  (**8**)) and  $[\{\text{WO}_2[\text{O}(\text{CH}_2)_3\text{Se}(\text{CH}_2)_3\text{O}]\}_n]$  (**9**)

Bis(3-hydroxypropyl)sulfide and bis(3-hydroxypropyl)selenide were used as ligands due to the fact that a dimeric molybdenum complex, formed with bis(2-hydroxyethyl)sulfide as ligand, only had very weak Mo-S interactions (distances = 2.931 Å, 3.002 Å).<sup>[95]</sup> By introduction of another CH<sub>2</sub> group into the ligands backbones we wanted to obtain a more flexible ligand system able to form stronger Mo-S and Mo-Se bonds and therefore to observe a stronger influence of a ligand atom exchange on the properties of the resulting complexes. The compounds  $[\{\text{MoO}_2[\text{O}(\text{CH}_2)_3\text{S}(\text{CH}_2)_3\text{O}]\}_2]$  (**7**),  $[\{\text{MoO}_2[\text{O}(\text{CH}_2)_3\text{Se}(\text{CH}_2)_3\text{O}]\}_2]$  (**8**) and  $[\{\text{WO}_2[\text{O}(\text{CH}_2)_3\text{Se}(\text{CH}_2)_3\text{O}]\}_n]$  (**9**) were prepared by similar synthetic methods (Scheme 3).



**Scheme 3.** Preparation of [ $\{\text{MoO}_2[\text{O}(\text{CH}_2)_3\text{S}(\text{CH}_2)_3\text{O}]\}_2$ ] (**7**), [ $\{\text{MoO}_2[\text{O}(\text{CH}_2)_3\text{Se}(\text{CH}_2)_3\text{O}]\}_2$ ] (**8**) and [ $\{\text{WO}_2[\text{O}(\text{CH}_2)_3\text{Se}(\text{CH}_2)_3\text{O}]\}_n$ ] (**9**).

For the preparation of **7** and **8** ligand and  $\text{MoO}_2(\text{acac})_2$  precursor were combined in a  $\text{CH}_2\text{Cl}_2$  or  $\text{CH}_3\text{OH}$  solution, stirred at room temperature for 1 or 7 days respectively and filtered. The compounds were isolated from the filtrate by removing the solvent in vacuo, extraction with toluene or dichloromethane and subsequent crystallization. The yields are 42% for the sulfur and 20% for the selenium compound. **9** was obtained by stirring the reaction mixture for 2 days and was collected by filtration. The yield (63%) is higher than those of **7** and **8**, whereas several attempts to crystallize **9** were unsuccessful. These three compounds were identified by the usual characterization methods, such as elemental analysis, IR, EI mass spectroscopy. In addition, **7** and **8** were characterized by UV-vis spectroscopy and for **8** and **9**  $^1\text{H}$ ,  $^{13}\text{C}$ ,  $^{77}\text{Se}$  NMR spectra were measured. The IR spectra in the range of 1067-686  $\text{cm}^{-1}$  for **7**, 1029-669  $\text{cm}^{-1}$  for **8** and 1079-667  $\text{cm}^{-1}$  for **9** were assigned to  $\nu\text{M-O}_t$  and  $\nu\text{M-O-M}$  stretching modes. The spectra data for **9** are similar to those of **8**, which may be an indication that **9** forms a



aggregate.

### 2.2.5. Structures of 7 and 8

The sulfur and the selenium ligand form analogous dimeric complexes with the metal (Figures 15 and 16) similar to the molybdenum bis(2-hydroxyethyl)sulfide complex. Space group and crystal system are the same for both compounds.

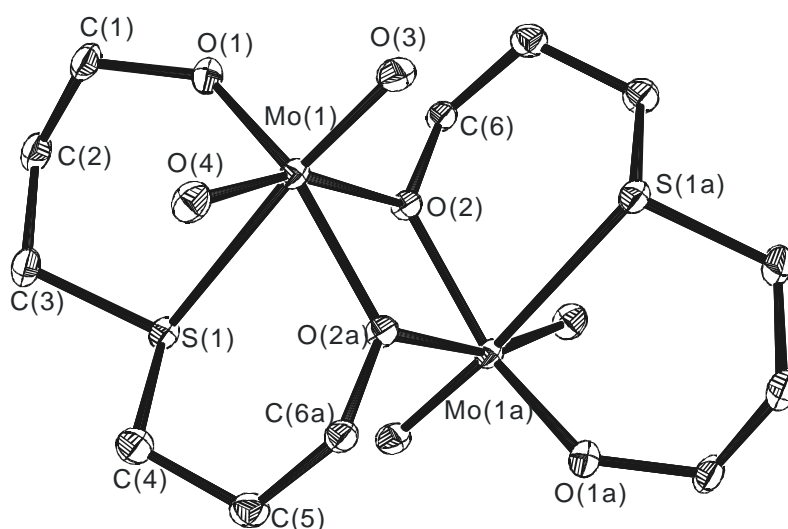


**Figure 15.** View of the structure of  $[\{\text{MoO}_2(\text{O}(\text{CH}_2)_3\text{S}(\text{CH}_2)_3\text{O})\}_2]$  (**7**) without hydrogen atoms (with numbering scheme). Ellipsoids are drawn at 50% probability.

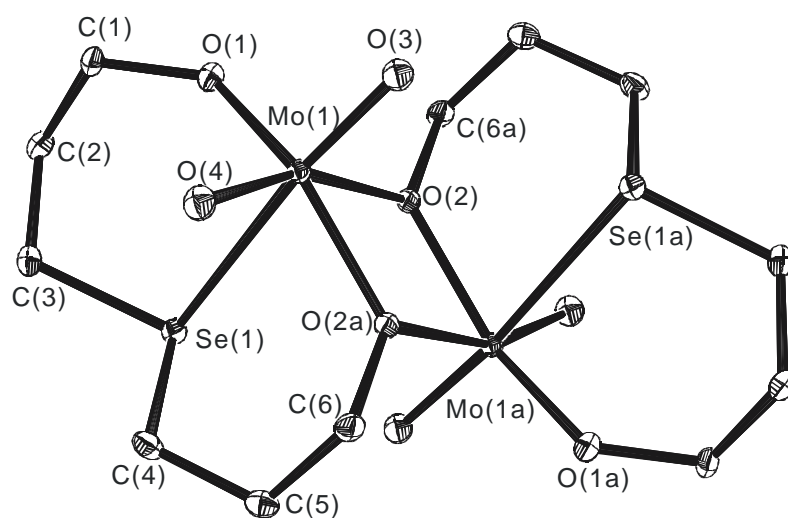


**Figure 16.** View of the structure of  $[\{\text{MoO}_2(\text{O}(\text{CH}_2)_3\text{Se}(\text{CH}_2)_3\text{O})\}_2]$  (**8**) without hydrogen

atoms (with numbering scheme). Ellipsoids are drawn at 50% probability.

The geometrical parameters for both complexes are almost identical (see Table 7) with the exception of the metal sulfur and the metal selenium bond that differ by 0.081 Å. This difference, though, can be ascribed to the different radii of both elements their van der Waals radii being 1.80 Å (S) and 1.90 Å (Se).<sup>[96]</sup> The lengths of the metal to sulfur (2.804 Å) and to selenium (2.885 Å) bond are rather long implicating only weak interactions between molybdenum and ligand atom. The bond length of tungsten(0) to the selenomether ligand atom for comparison is much shorter (in the range of 2.627 Å to 2.692 Å)<sup>[88]</sup> due to the fact that soft-soft metal-ligand combinations certainly form much stronger bonds than the hard-soft combination. Reported molybdenum-selenium distances are for terminal selenolate coordination 2.42-2.65 Å<sup>[68,72,89,97]</sup> and for bridging selenolate coordination between two molybdenum centers 2.48-2.67 Å.<sup>[98]</sup> The distance between molybdenum and the coordinated thioether sulfur (2.804 Å) is well within the usually observed range of 2.436-2.906 Å where the shorter distances are found in molybdenum complexes with lower oxidation states and the longer distances in complexes with molybdenum in higher oxidation states.<sup>[78,99]</sup>

All molybdenum-oxo distances of **7** and **8** (1.704-1.709 Å) are typical for group 6 oxo bonds.<sup>[100]</sup> The distances of the molybdenum to its oxo ligand that is located trans to the sulfur (**7**) or selenium (**8**) are roughly the same ( $\Delta = 0.002$  Å) and only about 0.003 Å longer than the distance between Mo and the oxo ligand in *cis* position to X (X = S, Se). Overall no trans influence can be observed. This indicates that there is not much electronical influence by exchanging the sulfur ligand for the selenium ligand.

**Table 7.** Important structure parameters of [ $\{\text{MoO}_2(\text{O}(\text{CH}_2)_3\text{S}(\text{CH}_2)_3\text{O})\}_2$ ] (**7**) and [ $\{\text{MoO}_2(\text{O}(\text{CH}_2)_3\text{Se}(\text{CH}_2)_3\text{O})\}_2$ ] (**8**).

	[ $\{\text{MoO}_2(\text{OSO})\}_2$ ] <b>7</b> <sup>a)</sup>	[ $\{\text{MoO}_2(\text{OSeO})\}_2$ ] <b>8</b> <sup>b)</sup>
<i>Bond lengths (Å)</i>		
Mo=O	1.704(3), 1.707(3)	1.7058(17), 1.7086(17)
Mo-X <sup>c)</sup>	2.8042(13)	2.8850(5)
Mo-O <sub>alkoxy</sub>	1.887(3)	1.8879(17)
Mo-O <sub>bridge</sub>	2.039(3), 2.229(3)	2.0494(16), 2.2172(16)
Mo-Mo	3.503	3.507
<i>Bond angles (°)</i>		
O=Mo=O	104.00(17)	104.63(8)
O <sub>bridge</sub> -Mo-O <sub>bridge</sub>	69.77(14)	69.51(7)
Mo-O <sub>bridge</sub> -Mo	110.23(14)	110.49(7)
X-Mo=O <sub>trans</sub> <sup>c)</sup>	171.76(12)	169.78(6)
X-Mo=O <sub>cis</sub> <sup>c)</sup>	83.51(12)	84.89(6)
X-Mo-O <sub>alkoxy</sub> <sup>c)</sup>	79.62(11)	79.17(5)
X-Mo-O <sub>bridge</sub> <sup>c)</sup>	80.39(9), 74.71(10)	79.15(4), 74.95(5)
C-X-C <sup>c)</sup>	100.2(2)	98.59(10)

a) (OSO) =  $^-\text{O}(\text{CH}_2)_3\text{S}(\text{CH}_2)_3\text{O}^-$ , b) (OSeO) =  $^-\text{O}(\text{CH}_2)_3\text{Se}(\text{CH}_2)_3\text{O}^-$ , c) X = S, Se

The biggest difference for the angles of compounds **7** and **8** is 2° for the angle at molybdenum of sulfur or selenium to its trans oxo ligand with the smaller angle for the selenium compound (**8**). Here the octahedral geometry is slightly more distorted. On the other hand in compound **8** the symmetry around the bridging oxygen atoms (O2) is marginally higher. The differences of the metal distances is only 0.168 Å while it is 0.190 Å for compound **7**.

In **7** and **8** the two tridentate ligands are on different sides of the Mo<sub>2</sub>O<sub>2</sub> ring, which is different from **3** discussed above where the two tridentate ligands are on the same side of the

ring.

Overall both structures are surprisingly similar (see Figure 17, superimposition of both structures) maybe due to the fact that the exchanged ligand atoms are not bound to the metal that strongly.

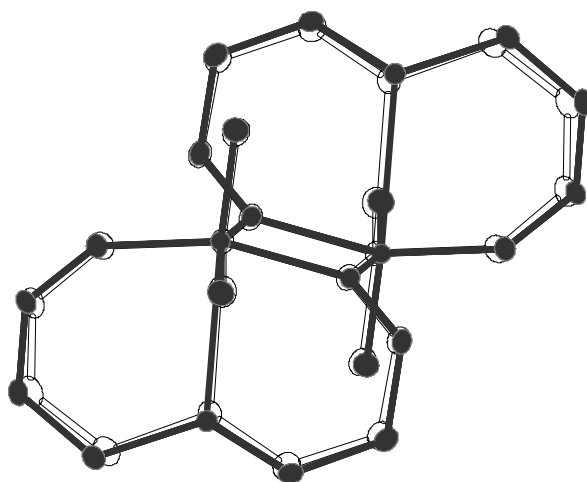


**Figure 17.** Superimposition of the structures of  $[\{\text{MoO}_2(\text{O}(\text{CH}_2)_3\text{S}(\text{CH}_2)_3\text{O})\}_2]$  (**7**) in white and  $[\{\text{MoO}_2(\text{O}(\text{CH}_2)_3\text{Se}(\text{CH}_2)_3\text{O})\}_2]$  (**8**) in gray as ball and stick models.

#### 2.2.6. Electrochemical results for **7** and **8**

To evaluate the ligand atoms influence (S vs. Se) on the redox potentials of compounds **7** and **8** they were investigated by square wave voltammetry (SWV). This method was chosen over the cyclic voltammetry because both compounds were only slightly soluble in acetonitrile and the signals of the redox processes in the cyclic voltammograms rather weak (**7**) (Figure 18) or not detectable (**8**). In the oxidative as well as in the reductive SWVs though all transitions were sufficiently intense. The peak positions were determined from both the reductive as well as the oxidative SWV as an average and referenced internally vs. Ferrocene/Ferrocenium. In Figure 19 the oxidative SWVs for both compounds are shown. The scan was started at a reductive potential and the oxidation of the first reduced species monitored.

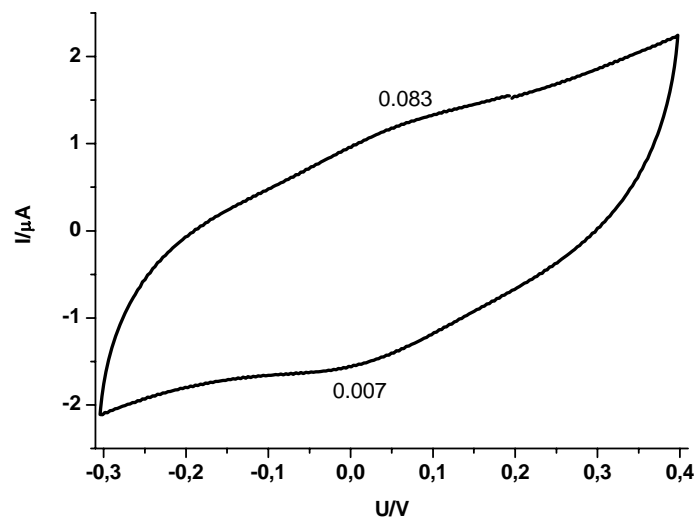


**Figure 18.** Cyclic voltammogram of **7** referenced internally vs. ferrocene/ferrocenium. The scan rate was 100 mV/s.

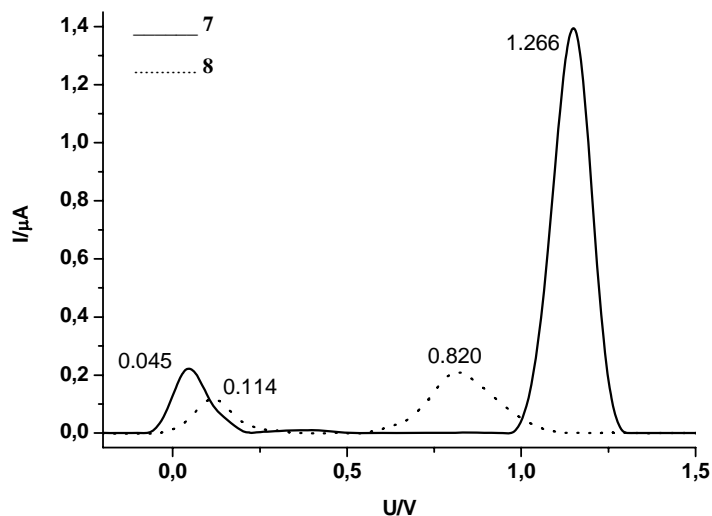


**Figure 19.** Oxidative square wave voltammograms of compounds  $[\{\text{MoO}_2(\text{O}(\text{CH}_2)_3\text{S}(\text{CH}_2)_3\text{O})\}_2]$  **7** and  $[\{\text{MoO}_2(\text{O}(\text{CH}_2)_3\text{Se}(\text{CH}_2)_3\text{O})\}_2]$  **8** referenced vs. ferrocene/ferrocenium showing one metal centered (0.045 V / 0.114 V) and one ligand centered oxidation (0.820 V / 1.266 V). To fit into one figure the current value of **7** was multiplied by 1/3.

For both, compound **7** and compound **8**, a reversible redox process was found that could be ascribed to the  $\text{Mo}^{\text{V}} \leftrightarrow \text{Mo}^{\text{VI}}$  transition. The quasi reversibility of this signal is demonstrated in the (low intensity) CV of compound **7** which can be found in Figure 18. For this process the signal for the sulfur containing compound **7** is at a lower voltage (0.045 V) than for the selenium containing compound **8** (0.114 V). Although there seems to be no general trend for the redox potentials of analogous molybdenum compounds with sulfur or selenium functional ligands<sup>[101]</sup> this is consistent with the findings of chapter 2.2.3. The difference between the redox potentials for the  $\text{Mo}^{\text{V}} \leftrightarrow \text{Mo}^{\text{VI}}$  transition for the sulfur and for the selenium compound is 0.069 V. It is therefore rather small compared to the differences that were observed for an exchange of the metal atoms Mo vs. W. This exchange was investigated due to the fact that there are analogous oxygen atom transfer enzymes, some using molybdenum and others tungsten at their active sites.<sup>[6,59,61,102]</sup> The shift of the redox potential when exchanging tungsten for molybdenum is usually not smaller than about 0.20 V (about three times the size of the here observed shift) even for those compounds that contain ligands with a strong non-innocent character and it can even rise to the range of 1 V.

At higher voltage a ligand centered quasi reversible redox process could be observed of much higher intensity for the oxidative SWV than for the reductive SWV and of much higher intensity for **7** than **8**. This signal is also slightly shifted to lower voltage in the reductive SWVs (1.134 V for **7** and 0.817 V for **8**) compared to the oxidative SWVs (1.266 V/0.820 V). It can be assumed that the oxidation of the ligand atom causes a structural reorganisation of the molecule that cannot be easily reversed when the reduction occurs. The average signal for this redox process is at significantly higher voltage for the sulfur containing compound **7** (1.200 V) than

that for the selenium containing compound **8** (0.818 V). The oxidation of the selenium is obviously easier to achieve than that of the sulfur as would be expected by taking into account the size of both atoms and the metallic character of the selenium.

Still, this feature has probably no effect on the active sites with cysteine or selenocysteine coordination to molybdenum, because redox processes there occur only at the metal or maybe at the sulfur of the dithiolene containing ligand molybdopterin but not at the sulfur or the selenium of the amino acid residues.

### 2.2.7. Conclusions

With the tridentate bisanionic ligand, bis(2-hydroxyethyl)sulfide, molybdenum and tungsten form rather different complexes, the former giving a dimeric and the latter a trimeric complex. Interestingly, the thioether function forms no explicit bond with the molybdenum, whereas the analogous ether ligand does form a bond with this metal atom (no analogous compound was published for tungsten).<sup>[92]</sup>

In addition, molybdenum compounds with bis(3-hydroxypropyl)sulfide and selenide ligands form two structurally almost identical dimeric molecules. No trans influence was observed in the crystalline forms and thus no electronical influence of the different ligand atoms. However, they have stronger Mo-S or Mo-Se interactions than the molybdenum compound with the bis(2-hydroxyethyl)sulfide ligand.

We conclude from this that the structural influence of the ligand atom plays a vital role in structurally demanding ligands (tridentate) but not in those with a simpler geometry (bidentate or monodentate).

This may be because the hard-soft interactions between the ether/thioether function of the

ligands and the metal center favor the oxygen–molybdenum combination over the sulfur–molybdenum combination. Molybdenum prefers O functional ligands although it has been said that the bond strength of ether functions to metals increases within the group of the chalcogens.<sup>[91]</sup> Interestingly, in nature the ligand–metal combinations that are less favorable than others from this point of view occur at the active sites of the OATs: for instance the coordination of thiolate (cysteine) to molybdenum at the active site of the DMSO reductase of *Desulfovibrio desulfuricans*<sup>[33]</sup> or the coordination of serine to tungsten in the aldehyde oxidoreductase of *Pyrococcus furiosus*.<sup>[21,36]</sup>

The influence of the metal on the redox potential is, as expected, such that the molybdenum complexes have more positive redox potentials than the analogous tungsten complexes in all cases. With regard to the enzymes, this means that in all cases one metal is better suited for the catalyzed reaction with the substrate, while with the other metal the active site is more easily regenerated. For a given enzyme, there is always an advantage as well as a disadvantage in using either of the two metals, molybdenum or tungsten. If the redox potential is important for the choice of the metal, the basis of this choice would be a difference in the redox behavior of the two metals at different temperatures<sup>[103]</sup> rather than their relative redox potentials at room temperature.

The influence of the ligand atoms on the redox potentials is small but of consequence; the sulfur ligands cause more positive redox potentials than the oxygen ligands, and the selenium ligands cause more positive potentials than the sulfur ligands. However, the observed differences are smaller than those that result from changing the metal atoms.

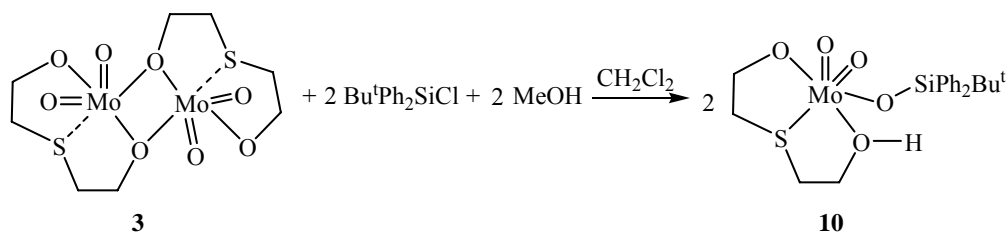


### 2.3. The monomerization of a binuclear molybdenum(VI) dioxo complex

As described above, a dimeric molybdenum(VI) dioxo complex with tridentate thioether ligands, **3**, which was employed due to the assumption that O,S-based systems are essential in the coordination sphere of molybdenum-containing enzymes<sup>[12,40,46,55,68,104]</sup>, was synthesized<sup>[95]</sup>. In order to obtain a mononuclear complex, we tried to introduce a sterically hindered silylating substituent to the dimer in the presence of methanol and successfully got a mononuclear dioxo complex with silyloxy. To the best of our knowledge, this is the first example of the monomerization of a binuclear molybdenum(VI) dioxo complex by a silylation reaction.

#### 2.3.1. Synthesis of mononuclear molybdenum(VI) dioxo complex, [MoO<sub>2</sub>(O(CH<sub>2</sub>)<sub>2</sub>S(CH<sub>2</sub>)<sub>2</sub>OH)(OSiBu<sup>t</sup>Ph<sub>2</sub>)] (**10**)

Treatment of [MoO<sub>2</sub>(O(CH<sub>2</sub>)<sub>2</sub>S(CH<sub>2</sub>)<sub>2</sub>O)]<sub>2</sub> (**3**) with two equivalents of *tert.*-Butyl-chlor-diphenylsilane (Bu<sup>t</sup>Ph<sub>2</sub>SiCl) in CH<sub>2</sub>Cl<sub>2</sub>, followed by a small amount of methanol at room temperature, afforded [MoO<sub>2</sub>(O(CH<sub>2</sub>)<sub>2</sub>S(CH<sub>2</sub>)<sub>2</sub>OH)(OSiBu<sup>t</sup>Ph<sub>2</sub>)] (**10**) in nearly quantitative yield (89%) (Scheme 4). **3** is almost insoluble in CH<sub>2</sub>Cl<sub>2</sub> and forms a white suspension. With the addition of methanol the white suspension changed gradually to a clear colorless solution within 5 min, otherwise no change occurred even though the mixture was stirred for several days. This indicated that methanol indeed participated in the monomerization of the binuclear complex by a silylation reaction. Single crystals suitable for X-ray diffraction analysis of **10** were obtained by recrystallization from acetonitrile/methanol solution.



**Scheme 4.** Preparation of  $[\text{MoO}_2(\text{O}(\text{CH}_2)_2\text{S}(\text{CH}_2)_2\text{OH})(\text{OSiBu}^t\text{Ph}_2)]$  (**10**)

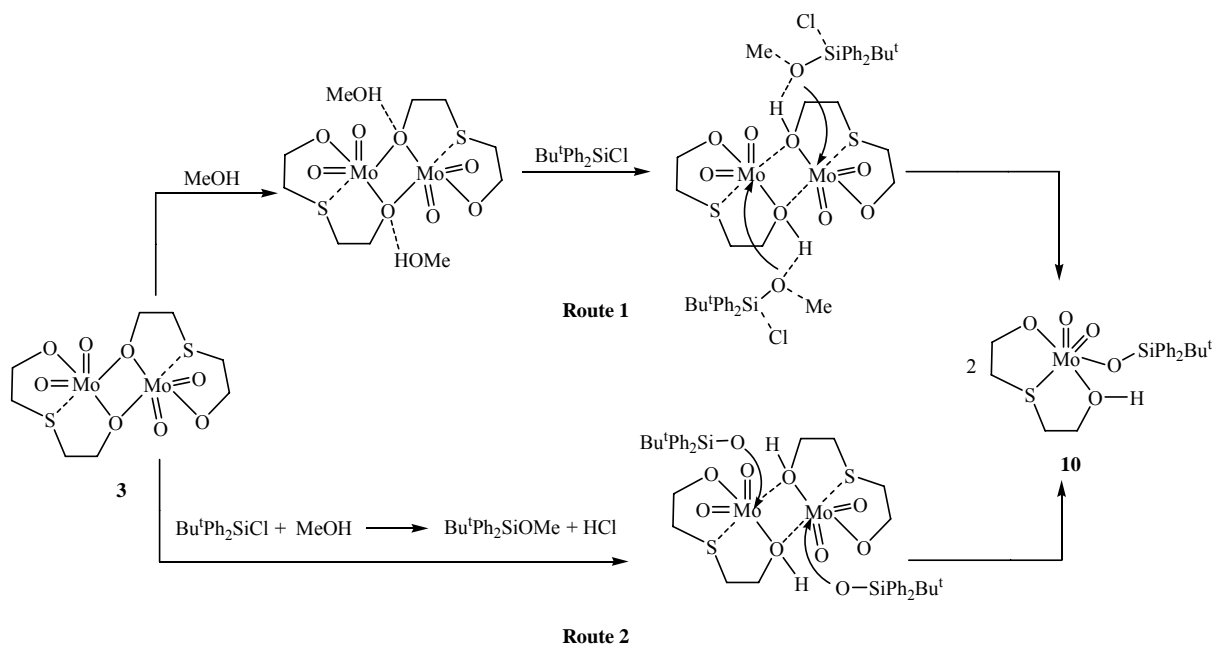
There are two kinds of silylation reaction methods. One is that the silylation of oxo ligands of complexes in corresponding oxidation states, such as  $[\text{M}^{\text{IV}}(\text{OSiR}_3)(\text{bdt})_2]^-$ ,  $[\text{M}^{\text{VI}}\text{O}(\text{OSiR}_3)(\text{bdt})_2]^-$  ( $\text{M} = \text{Mo}$ ,<sup>[105,106]</sup>  $\text{W}$ <sup>[105,107]</sup>), and  $[\text{M}^{\text{VI}}\text{O}(\text{OSiMe}_3)(\text{CN})\text{L}_2]$  ( $\text{L} =$  diethyl dithiocarbamate)<sup>[108]</sup>; the other one is that with  $[\text{Mo}^{\text{VI}}\text{O}_2(\text{OSiPh}_3)_2]$  as the starting compound, treatment with  $\text{Li}_2(\text{bdt})$  in THF afforded a monodithiolene  $\text{Mo}^{\text{VI}}\text{O}_2$  complex with silyloxy,  $[\text{M}^{\text{VI}}\text{O}(\text{OSiR}_3)(\text{bdt})_2]^-$ .<sup>[55]</sup>

In the first type treatment of  $(\text{Et}_4\text{N})_2[\text{M}^{\text{IV}}\text{O}(\text{bdt})_2]$  or  $(\text{Et}_4\text{N})_2[\text{M}^{\text{VI}}\text{O}_2(\text{bdt})_2]$  ( $\text{M} = \text{Mo}$ ,<sup>[105,106]</sup>  $\text{W}$ <sup>[105,107]</sup>) with the chlorosilanes  $\text{R}_3\text{SiCl}$  resulted in silylation of the oxo ligand and formation of the deoxo or monooxo species ( $(\text{Et}_4\text{N})[\text{M}^{\text{IV}}(\text{OSiR}_3)(\text{bdt})_2]$  or  $(\text{Et}_4\text{N})[\text{M}^{\text{VI}}\text{O}(\text{OSiR}_3)(\text{bdt})_2]$ ), respectively. In this process, the chlorine of the chlorosilane was eliminated as  $\text{Et}_4\text{NCl}$  salt. In addition, the reaction of a neutral molybdenum(VI) dioxo complex with trimethylcyanosilane which underwent cleanly a 1:1 addition yielded a rare seven coordination neutral complex.<sup>[110]</sup>

In this process, one of two oxo ligands was silylated and cyanogen in trimethylcyanosilane was coordinated to Mo center rather than eliminated to form a byproduct. The second type of reaction is different from the first one. Here the starting material already contains two silyloxides and was reacted with  $\text{Li}_2(\text{bdt})$ .<sup>[55]</sup> During this process, one of silyloxides was substituted by bdt and a stable lithium silyloxy was eliminated.

As is shown in Scheme 4, the way of the presented reaction here is different from both

methods mentioned above. The precursor **3** has a neutral dimeric structure in which the two molybdenum atoms are bridged by one alkoxylate function of each of the two thioether ligands. This prevents the silylation of one of both oxo ligands at each molybdenum atom because of the steric hindrance. On the other hand, the chloride ion can neither be eliminated because of the neutrality of the complex resulting in no cation to combine with it nor can it be coordinated to the molybdenum atom because of no vacant coordination place. Only by addition of methanol the reaction is started. Therefore two presumptions for this reaction route (see Scheme 5) are raised. In the first possible route, the acidic proton from methanol was coordinated to each of the bridging oxygen atoms between the two molybdenum centers. The silicon atom of the silylating agent attacked the oxygen atom of the coordinated methanol and formed the  $\text{Bu}^i\text{Ph}_2\text{SiOMe}$  intermediate. At the meantime, the bond between one molybdenum atom and one alkoxylate function of the thioether ligand coordinated to another molybdenum atom is weakened and finally broken. The silyloxy part of  $\text{Bu}^i\text{Ph}_2\text{SiOMe}$  now coordinates to the vacant position of the former  $\text{Mo-O}_{\text{alkoxyde}}$  bond. So this mononuclear molybdenum (VI) dioxo complex with silyloxy is formed. Another possible route is that the reaction of  $\text{Bu}^i\text{Ph}_2\text{SiCl}$  with excess methanol first probably resulted in the formation of  $\text{Bu}^i\text{Ph}_2\text{SiOMe}$  and hydrogen chloride<sup>[109]</sup>. Subsequently, the free protons of hydrogen chloride coordinated to each bridge oxygen atom between two molybdenum atoms, followed by the  $\text{Mo-O}_{\text{alkoxyde}}$  bond breaking and silyloxy coordinating to the vacant position in each molybdenum atom. Finally, the mononuclear compound **10** formed.



Scheme 5.

Complex **10** was characterized by elemental analysis, IR spectroscopy,  $^1\text{H}$ ,  $^{13}\text{C}$  and  $^{29}\text{Si}$  NMR spectroscopy, EI mass spectrometry and single-crystal X-ray crystallography. The IR spectra exhibit two strong  $\nu_{\text{Mo}=\text{O}}$  bands at  $915\text{ cm}^{-1}$  and  $904\text{ cm}^{-1}$ , the characteristic features for symmetric and asymmetric vibrational modes, respectively, of the *cis*- $[\text{MoO}_2]^{2+}$  fragment.<sup>[46,68,104]</sup> And a middle band at  $968\text{ cm}^{-1}$  for  $\nu_{\text{Si}-\text{O}}$  and a middle broad band at  $3440\text{ cm}^{-1}$  for  $\nu_{\text{O}-\text{H}}$  are also displayed. The  $^1\text{H}$  NMR spectra in methanol- $d_4$  show a resonance at  $\delta$  3.49 ppm for the proton connected with one alkoxy of the thioether ligand.  $^{29}\text{Si}$  NMR spectrometry reveals a resonance at  $\delta$  -2.37 ppm for **10**, whereas that for the pure silylating agent ( $\text{Bu}^t\text{Ph}_2\text{SiCl}$ ) is shifted to lower field ( $\delta$  13.02 ppm), which is consistent with a decreased electron density at silicon center. All the analysis data are well in accord with the complex **10**.

### 2.3.2. Crystal structure of **10**

Figure 20 shows the molecular structure of complex **10** and selected bond lengths and angles are summarized in Table 8. Complex **10** crystallizes in the triclinic space group  $P\bar{1}$ , whereas its precursor **3** belongs to the monoclinic space group  $P2_1/n$ .

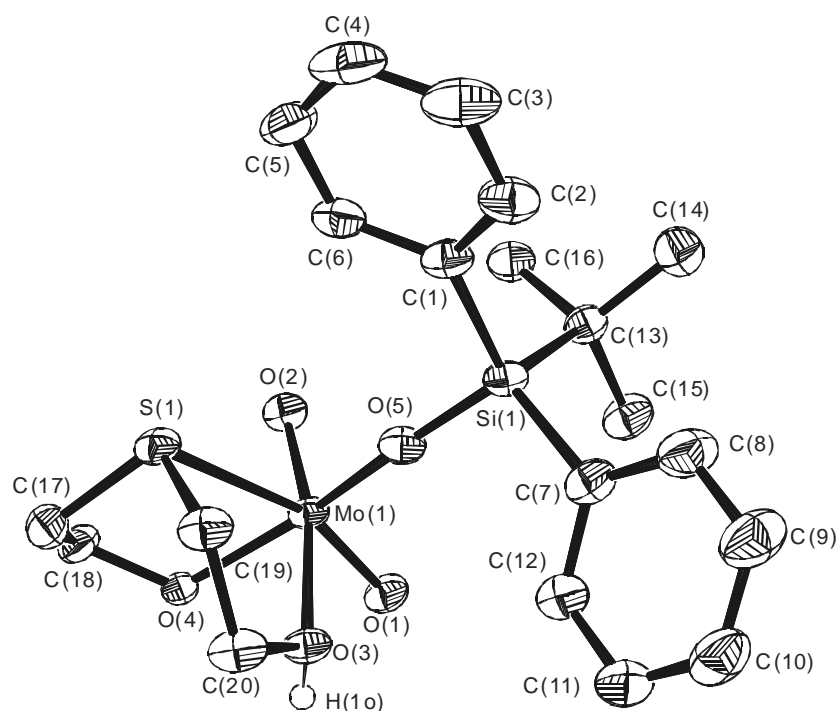


**Figure 20.** Molecular structure of **10**. H atoms except H(1o) have been omitted for clarity.

The ellipsoids are drawn at 50% probability.

**Table 8.** Selected bond lengths (Å) and angles (°) for the mononuclear silyloxy molybdenum(VI) complexes **13**.

<i>Bond lengths</i>			
Mo(1)-O(2)	170.4(2)	Mo(1)-O(1)	170.6(2)
S(1)-Mo(1)	271.0(1)	Mo(1)-O(4)	199.0(2)
Mo(1)-O(3)	230.3(2)	Mo(1)-O(5)	189.1(2)
<i>Bond angles</i>			
O(2)-Mo(1)-O(1)	106.48(12)	O(5)-Mo(1)-O(3)	81.19(9)
O(4)-Mo(1)-O(3)	79.71(9)	O(1)-Mo(1)-S(1)	158.96(9)
O(2)-Mo(1)-S(1)	92.60(9)	C(19)-S(1)-C(17)	104.28(18)

The structure of **10** exhibits a slightly distorted octahedral coordination geometry around the molybdenum atom, which is similar to **3** although the molybdenum in **3** is explicitly only bound to five ligand atoms with rather long metal-sulfur distances. The Mo-S bond length (2.710 (1) Å) in **10** is in the range (2.45-2.77 Å) of the usual distance between the metal (molybdenum or tungsten) and sulfur atoms of a thioether ligand.<sup>[78,91]</sup> The molybdenum-sulfur distance is shorter than distances found in **3** (2.93 and 3.00 Å), which indicates that the formation of the mononuclear complex enhances the interaction between molybdenum and sulfur. In **10**, the bond lengths of two Mo=O are the same (1.704(2) Å, 1.706(2) Å). Further, the distances of the Mo=O in **10** and those in **3** are indistinguishable. We can conclude that the enhanced Mo-S interaction has no trans influence on the Mo=O bonds. The bonds between molybdenum and two alkoxy of the thioether ligand (Mo(1)-O(4) and Mo(1)-O(3)) become longer by 0.093 Å and 0.158 Å, respectively, in **10** compared with the average values in **3**. The distance between molybdenum and oxygen of the silyloxy ligand (Mo(1)-O(5)) in **10** is 0.192 Å shorter than the mean value of the bond lengths between one molybdenum atom and the bridging oxygen atom of the thioether ligand coordinated to another molybdenum atom in **3** by the conversion from **3** to **10**. The angles of O=Mo=O are almost unchanged from **10** to **3**. The angles of O(5)-Mo(1)-O(3), O(3)-Mo(1)-O(4) and S(1)-Mo(1)=O(1) in **10** show about 10° differences from the corresponding angles in **3**. There are no significant differences in the other corresponding bond lengths and angles between **10** and **3**, either. The structure analysis exhibits that the structure in complex **10** has the same ligand positions as in the moiety of **3** and the silyloxy is in place of one of the former bridging oxygen atoms. This supplies more evidences for the assumption of the

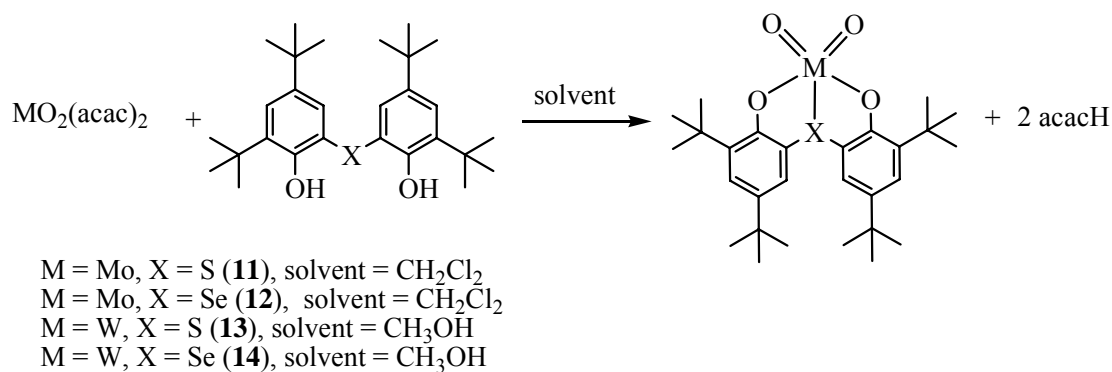
reaction process discussed above.

#### 2.4. Molybdenum and tungsten complexes with mixed O,X,O-donor ligands (X = S or Se)

In this section, tridentate bisphenol ligands containing [O,X,O]donor atoms (X = S or Se) were used to generate novel molybdenum and tungsten complexes. The roles of the phenol containing ligands have been described in the introduction. The ligands 2,2'-thiobis(4,6-di-*tert*-butylphenol)<sup>[110]</sup> H<sub>2</sub>L<sup>S</sup> and 2,2'-selenobis(4,6-di-*tert*-butylphenol)<sup>[71]</sup> H<sub>2</sub>L<sup>Se</sup> are depicted with their labels. It would be interesting to examine the effect of coordinating S or Se to the two metals.

##### 2.4.1. Syntheses of [MoO<sub>2</sub>L<sup>S</sup>] (**11**), [MoO<sub>2</sub>L<sup>Se</sup>] (**12**), [WO<sub>2</sub>L<sup>S</sup>] (**13**) and [WO<sub>2</sub>L<sup>Se</sup>] (**14**)

The general method for the syntheses of complexes **11-14** involve replacements of acetylacetonate ligands on MO<sub>2</sub>(acac)<sub>2</sub> by reaction with the ligands H<sub>2</sub>L<sup>X</sup> in dry CH<sub>2</sub>Cl<sub>2</sub> (**11** and **12**) or MeOH (**13** and **14**), which are depicted in Scheme 6. The molybdenum compounds **11** and **12** were purified by extraction with acetonitrile and toluene, respectively, and dried *in vacuo*. The tungsten compounds **13** and **14** were obtained by crystallization from the initial concentrated filtrate. Unfortunately, the formed red microcrystalline solid was not suitable for X-ray diffraction. The yields of molybdenum compounds (~ 80%) are higher than those of tungsten compounds (~ 50%).



### Scheme 6. Preparation of **11-14**.

IR data for complexes **11-14** are given in the experimental section. The presence of the ligands was confirmed by a strong peak in the region  $3000\text{-}2800 \text{ cm}^{-1}$  due to  $\nu(\text{C-H})$  of *tert*-butyl groups of the ligands together with other  $\nu(\text{C-H}, \text{C}=\text{C}, \text{C-O})$  vibrations found in the normal range for these types of linkages. The sharp  $\nu(\text{OH})$  band for the free ligands in the region  $3500\text{-}3300 \text{ cm}^{-1}$  is replaced by a broad band in the complexes indicating that the phenol character of the ligand is lost. Mass spectrometry in the EI mode has proved to be a very useful analytical tool for the characterization of the complexes and also for the identification of the metal center, and the compositions are in good agreement with the elemental analysis. The EI mass spectrum (MS) of **11** shows the molecular ion peak at  $m/z$  569 with an abundance of 14% with the expected isotope pattern. Similarly, complexes **12**, **13** and **14** show the molecular ion peak at  $m/z$  616, 657 and 703 with 76%, 29% and 46% abundances, respectively, with an isotopic distribution calculated for the complexes. As a representative example, Figure 21 shows the comparison of the experimental and theoretical isotope pattern of the  $\text{M}^+$  ion for **12**. This isotope pattern reflects the natural abundance of metal and ligand atom isotopes. In EI-MS of **14**, the peak at  $m/z$  687 with 87% abundance corresponding to  $\text{WOL}^{\text{Se}}$  is observed as a result of fragmentation.



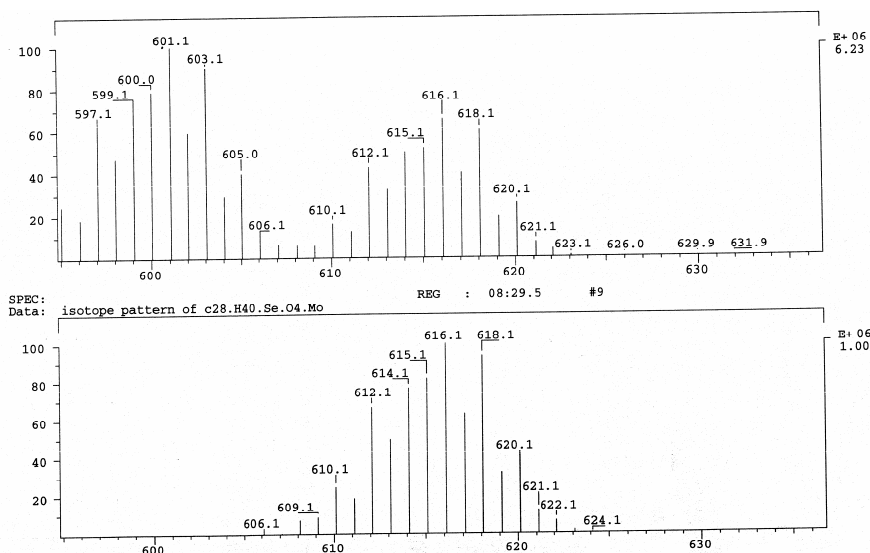


**Figure 21.** Molecular ion peaks in the EI mass spectra for complex **12** with experimental (upper) and calculated (lower) isotopic distributions.

The  $^1\text{H}$  and  $^{13}\text{C}$  NMR spectra of **11-14** characterized the ligands very well and all unexceptional. There is no OH resonance, indicating loss of hydroxyl protons. Complexes **12** and **14** were also characterized by  $^{77}\text{Se}$  NMR spectroscopy in  $\text{CDCl}_3$ . A singlet resonance at  $\delta$  268.7 ppm for **12** and  $\delta$  251.5 ppm for **14**, respectively, was observed. And the resonance of molybdenum compound **12** was shifted to lower field than that of tungsten compound **14**, which is in good agreement with the fact that tungsten donates more electron density to the coordinated selenium than molybdenum does. In addition, the resonance signals of  $^{77}\text{Se}$  NMR spectroscopies for both complexes **12** and **14** were shifted to higher frequencies/lower field than that for the free ligand  $\text{H}_2\text{L}^{\text{Se}}$  ( $\delta$  151.2 ppm), which indicates that metal-selenium bonds were indeed formed.<sup>[90]</sup>

Complexes **11** and **12** are intense purple and the UV-vis spectra of both show one band in the visible region,  $\lambda_{\text{max}}$  500 nm for **11** and  $\lambda_{\text{max}}$  538 nm for **12**, respectively.

The TG analyses of **11** and **12** were performed in the range of 0-500 °C as well. The TG curve

of **11** exhibits one step of weight losses. The weight loss is 58.01% in the temperature range 110-500 °C. The TG curve of **12** displays two steps of weight losses. The first step occurs in the temperature range 300-350 °C with 12.15% weight loss. The second one is 48.55% in the range of 350-500°C. The total weight loss is 61.06%. The weight losses of **11** and **12** are probably due to the losses of ligands.

Due to previous reports<sup>[111,112]</sup> that the reaction of a Mo(VI) starting material and excess thiolate ligand possibly leads to the formation of a  $\mu$ -oxo dimeric Mo(V) complex, magnetic susceptibility measurements were carried out for powdered samples of complexes **11** and **12** at 5000 G, in a temperature range from 295 to 395 K. Plots of the magnetic susceptibility  $\chi_M$  versus T for **11** and **12** are depicted in Figure 22. All the  $\chi_M$  values are negative for both complexes, which indicates that both **11** and **12** are diamagnetic and the valence of them should be VI.

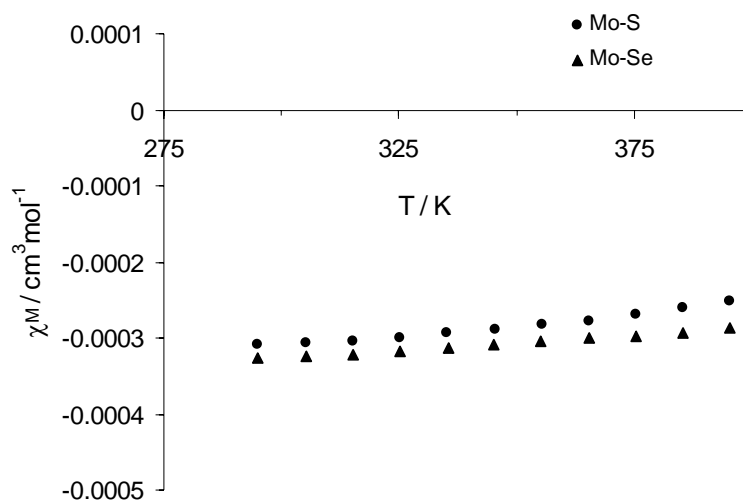


**Figure 22.** Plots of the magnetic susceptibility  $\chi_M$  versus T for **11** (●) and **12** (▲).

## 2.5. Molybdenum complexes with heterocyclic bidentate ligands (N,X) X = S, Se

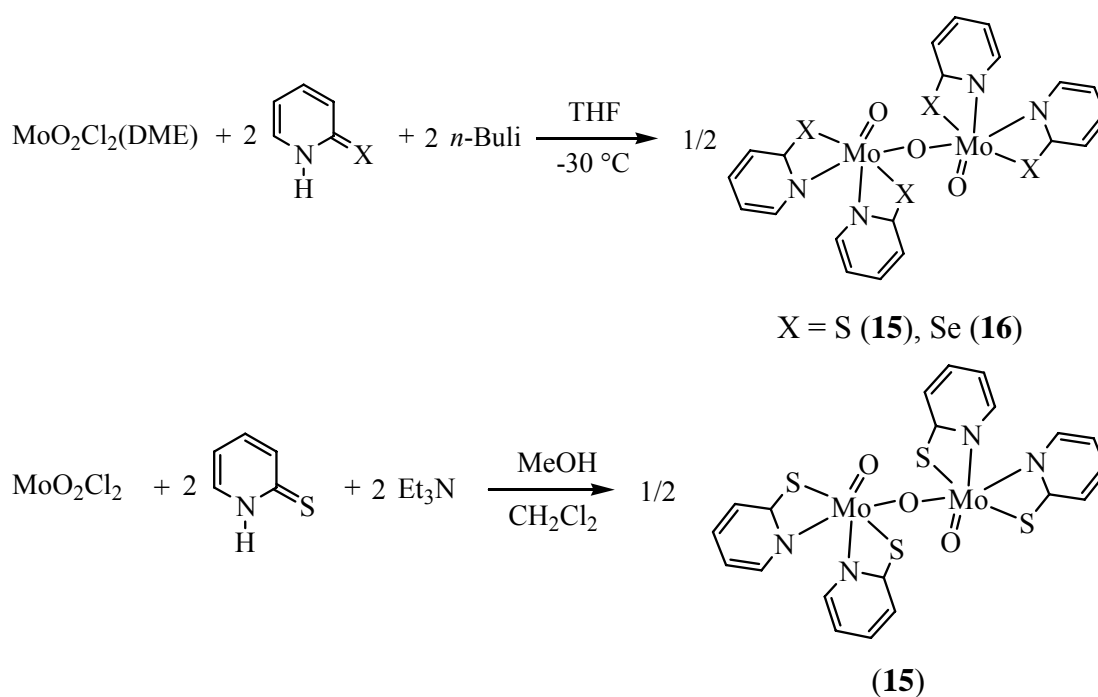
Interest in the chemistry of molybdenum thiolates arises in part from the presence of molybdenum-cysteine interactions in mononuclear molybdoenzymes. A class of thiols receiving particular attention at present is that of heterocyclic thiones, such as pyridine-2-thionato and pyrimidine-2-thionato and their derivatives, which are characterized by thione-thiol tautomerism. Thiones and thionates, the latter readily obtained by deprotonating the parent thiones, are electron-rich and polyfunctional ligands that lie on the borderline of stability between the +5 and +6 oxidation states of molybdenum.

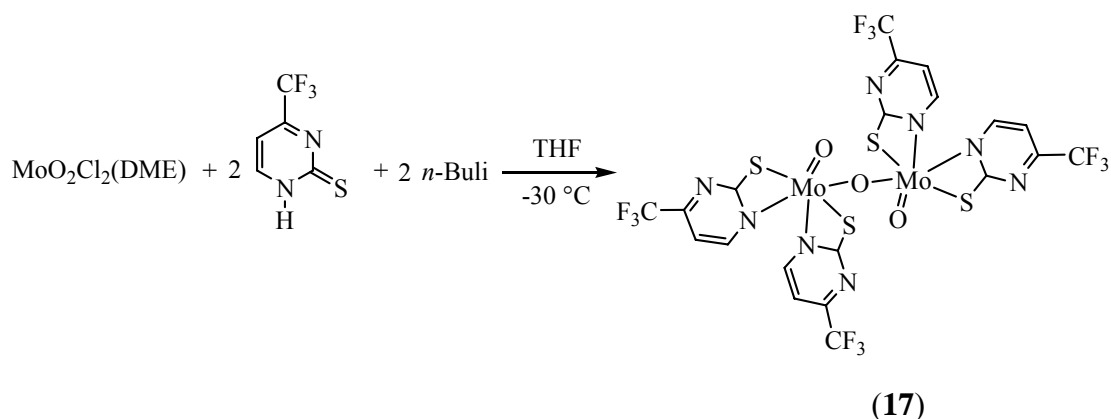
Furthermore, the comparison of coordination properties between the sulfur and selenium analogues is not only an intriguing subject but also a main objective of our research. Metal complexes with neutral or anionic ligands containing selenium and nitrogen donors have not been extensively studied,<sup>[113]</sup> although 2,2'-dipyridyl diselenide (Py<sub>2</sub>Se<sub>2</sub>) was first synthesized in 1962,<sup>[114]</sup> and its use in organic syntheses<sup>[115]</sup> and biochemistry<sup>[116]</sup> is well documented. This kind of ligand can provide insight into the competitive coordination behavior between the hard and soft Lewis bases nitrogen and selenium toward the same metal center. Metal complexes with heterocyclic thionato or selenolate ligands have the relevance to biological systems and these ligands also show a wide versatility in their coordination forms, acting as neutral monodentate systems,<sup>[117,118]</sup> bridging through S,<sup>[119]</sup> anionic S/Se-monodentate,<sup>[118,120]</sup> chelating<sup>[121]</sup> or bridging between two<sup>[122-125]</sup> or three metal atoms.<sup>[123,126]</sup> This versatility yields numerous complexes with unusual geometries, variable nuclearities and great structural diversity.<sup>[127]</sup> On the other hand, there is an experimental evidence that the nature and location of the substituent in the heterocyclic ring is important in determining the structure of the metal-pyridinethionate and selenolate complexes.<sup>[128-130]</sup>

Here, we employed pyridine-2-thionato (HPyS), 4-trifluormethyl-2-pyrimidinethiol (4-CF<sub>3</sub>-2-PymSH) and pyridine-2-selenolato (HPySe) as heterocyclic bidentate (N,X) ligands, X = S, Se.

### 2.5.1. Syntheses of [Mo<sub>2</sub>O<sub>3</sub>(PyS)<sub>4</sub>] (**15**), [Mo<sub>2</sub>O<sub>3</sub>(PySe)<sub>4</sub>] (**16**) and [Mo<sub>2</sub>O<sub>3</sub>(4-CF<sub>3</sub>-PymS)<sub>4</sub>] (**17**)

Molybdenum complexes with heterocyclic thiones and selenone were all obtained in different yields (68% for **15**, 28% for **16** and 45% for **17**) by the same methods. Firstly, the nucleophilic species, lithium thionates or lithium selenate, were obtained by the reaction of the corresponding pyridine-2-thionato, 2-pyrimidinethiol or selenolato with *n*-Butyllithium in THF at -30 °C. The mixture was allowed to be warmed to room temperature and stirred overnight. The product was subsequently reacted with the readily available molybdenum precursor [MoO<sub>2</sub>Cl<sub>2</sub>(DME)]<sup>[131]</sup> at -30 °C and the mixture was allowed to come to room temperature and stirred overnight again according to the following general process (Scheme 7):





### Scheme 7. Preparation of **15**, **16** and **17**

The purity methods were different for the three products. **15** was obtained through directly drying the extracted filtrate in  $\text{CH}_2\text{Cl}_2$ . Because the dried residue of the filtrate of **16** extracted by  $\text{CH}_2\text{Cl}_2$  was oily, **16** was precipitated by treatment with hexane and cooled at  $-30\text{ }^\circ\text{C}$  overnight. While **17** was obtained directly by crystallizing from the initial concentrated filtrate extracted with  $\text{CH}_2\text{Cl}_2$ . **15** can also be synthesized in 44% yield by adding a methanolic solution of the ligand and triethylamine to a stirred solution of precursor  $[\text{MoO}_2\text{Cl}_2]^{[132]}$  in dichloromethane (scheme 7). The three obtained compounds were all dinuclear  $\mu$ -oxomolybdenum(V) species which were not the expected mononuclear dioxomolybdenum(VI) species. Such behavior may be due to the corresponding ligands acting both as a reductant and as a ligand in the reaction and has been observed previously upon the reaction of thiol ligands with Mo(VI) starting materials.<sup>[111,112]</sup> All compounds are red brown (**15** and **16**) or dark purple (**17**). Compound **15** has been synthesized previously by different routes<sup>[133-135]</sup> and its structure has been determined<sup>[133]</sup>. One of the synthetic routes was that the mononuclear dioxomolybdenum(VI) thionate was quantitatively converted into the dinuclear oxomolybdenum(V) complex by oxygen atom abstraction with common

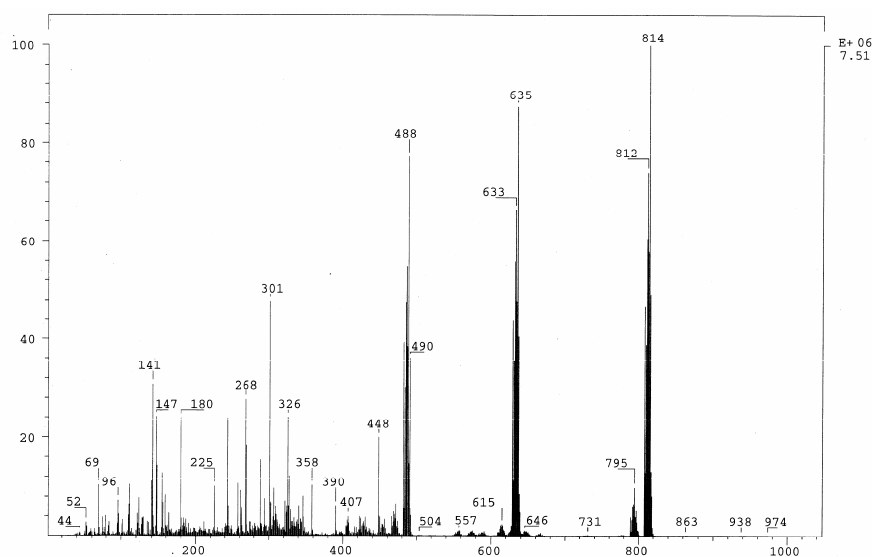
organophosphines and phosphates.<sup>[134,135]</sup> In the another route the formation of this molybdenum(V) compound from Na(PyS) and molybdenum(II) acetate was caused by atmospheric oxygen. In contrast, our preparation methods are different from these previous routes. To the best of our knowledges, **16** and **17** are unknown till now and furthermore **16** is the first oxomolybdenum complex containing pyridine-2-selenolato.<sup>[72]</sup>

Attempts to prepare dioxomolybdenum(VI) thionate and selenate by reacting MoO<sub>2</sub>(acac)<sub>2</sub> with the corresponding sulfur and selenium containing ligands were unsuccessful according to analytical data. The former may be due to the reason that important amounts of both oxomolybdenum(V) thionates and disulfides were simultaneously produced when the reaction were carried out in CH<sub>2</sub>Cl<sub>2</sub> or MeOH. This situation has occurred in previous reports.<sup>[134,136]</sup> For the latter, the reaction mixture in MeCN or MeOH gradually decomposed to black grey selenium powder from the initial red reaction solution.

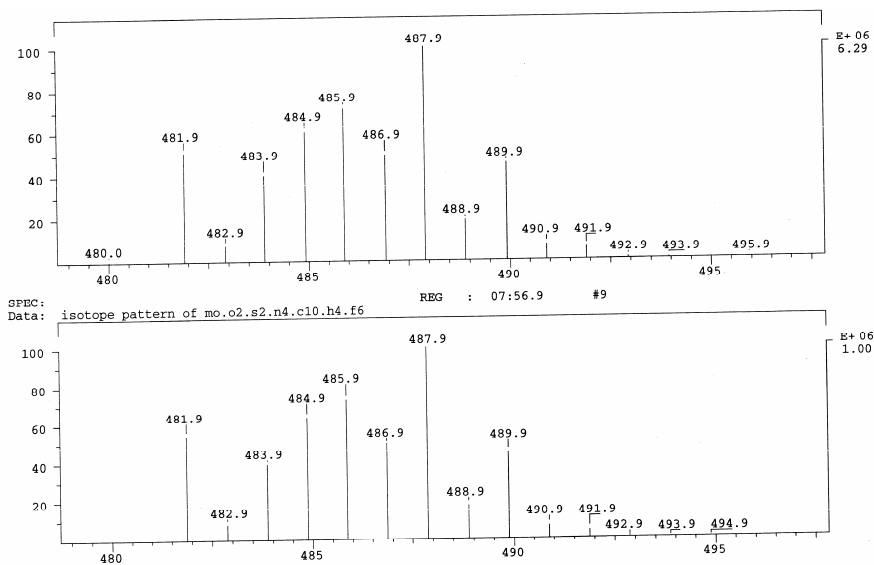
IR spectra of the complexes confirm the presence of the ligands coordinated to the metal. For example, the band attributable to the  $\nu(\text{N-H})$ , which appears at 3200–3100 cm<sup>-1</sup> in the free thione ligands, is absent and this indicates that the ligands are in the deprotonated form in the complexes. The strong ligand bands in the range 1640–1660 cm<sup>-1</sup> are due to the presence of  $\nu(\text{C=N})$  and  $\nu(\text{C=C})$  in a non-aromatic system. In the complexes, however, these bands appear in the region 1590–1545 cm<sup>-1</sup>, which is characteristic of stretching vibrations in an aromatic group<sup>[137]</sup>. These observations confirm that the ligand is present in the complexes in the thiolate form. The spectra of the complexes also show bands due to deformation of the aromatic ring, and these appear in the regions 1110–990 and 750–620 cm<sup>-1</sup> <sup>[138]</sup>. The IR spectrum also exhibits prominent absorptions in the 750-943 cm<sup>-1</sup> region consistent with the presence of both terminal and bridging oxo groups.

The  $^1\text{H}$  and  $^{13}\text{C}$  NMR spectra of **15-17** (except for  $^{13}\text{C}$  NMR spectra of **17** due to the poor solubility in  $\text{CDCl}_3$ ) are constant with their compositions and these signals are due to protons in the thiolate or selenolate ligands. And  $^1\text{H}$  and  $^{13}\text{C}$  NMR spectra of **15** are almost identical to those of **16**. A resonance signal from  $^{77}\text{Se}$  NMR spectroscopy of compound **16** ( $\delta = 428.0$  ppm) which shifted to lower field relative to that of the free ligand  $\text{PySeH}$  ( $\delta = 306.6$  ppm), was observed, hence indicating the formation of a metal-selenium bond.<sup>[90]</sup> The trend is consistent with the situations in chapters 2.2.1 and 2.4.1 discussed above.

In all cases the EI mass spectra of the compounds show peaks of the fragments ion of the molecular due to the loss of some parts, such as heterocyclic ligands or oxo ligand. The peak cluster has appropriate isotope distribution. One example is shown in Figure 23, which is corresponding to the ion formed by the loss of  $[(\text{MoO}(4\text{-CF}_3\text{-PymS})_2)]$  part for **17**.



(a)



(b)

**Figure 23.** (a) The EI mass spectra for complex **17**, (b) the fragments ion peak due to the loss of  $[(\text{MoO}(\text{4-CF}_3\text{-PymS})_2)]$  part.

In order to investigate the influence of the metal center on the properties of the complexes, we have already tried to prepare the tungsten analogues by the similar methods employing  $[\text{WO}_2\text{Cl}_2(\text{DME})]$  as a precursor. Compound  $[\text{WO}_2(\text{PyS})_2]$ ,  $[\text{WO}_2(\text{PySe})_2]$  and  $[\text{WO}_2(\text{PymS})_2]$  were all analyzed by EI mass spectroscopy and elemental analysis. In all cases the EI mass spectra of tungsten compounds show peaks due to the molecular ion which are exactly consistent with their isotope distributions (Figure 24).



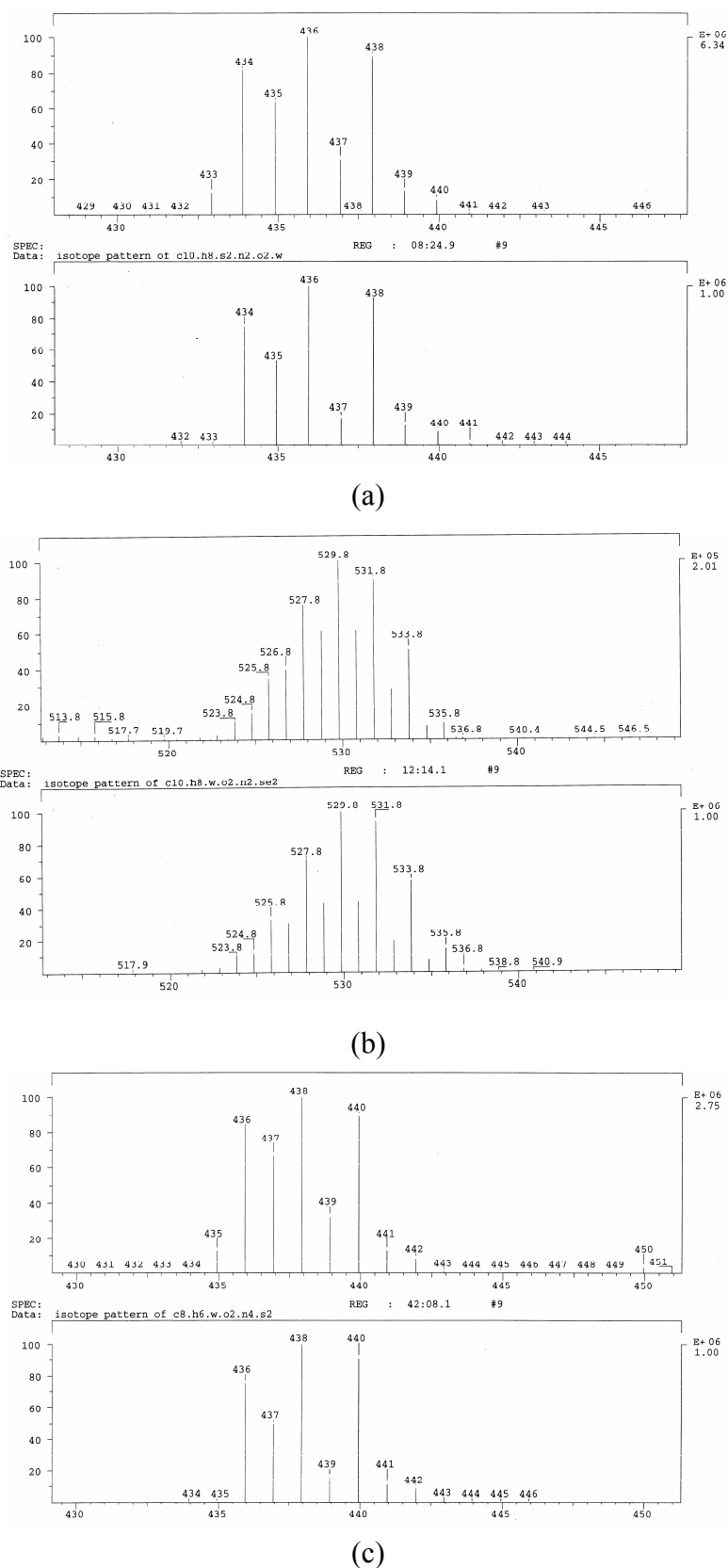


**Figure 24.** Molecular ion peaks in the EI mass spectra for complexes [WO<sub>2</sub>(PyS)<sub>2</sub>] (a), [WO<sub>2</sub>(PySe)<sub>2</sub>] (b) and [WO<sub>2</sub>(PymS)<sub>2</sub>] (c) with experimental (upper) and calculated (lower) isotopic distributions.

However, unfortunately the elemental analytical data (C, H, N) for the products were not in agreement with those for expected tungsten(VI) compounds. The found compositions were much higher than the calculated ones for all compounds. We also tried to extract  $[\text{WO}_2(\text{PyS})_2]$  with toluene and obtained some yellow crystals. Through single-crystal X-Ray diffraction analysis the obtained result was pyridine-2-thione. In combination with the elemental analysis data it can be concluded that the reactions were not accomplished completely. We tried different solvents and separation methods. Despite our efforts, we have been unable to obtain the pure products. It is very difficult to separate the mixture.

### 2.5.2. Crystal structures of **15**, **16** and **17**

The crystals of **15**, **16** and **17** suitable for X-ray studies were obtained by the recrystallization of the initial products from dichloromethane. The crystal structures of **15-17** are shown in Figure 25-27 along with the numbering schemes; solvent molecules of **17** are not shown. The selected bond lengths and angles are given in Table 9-11.

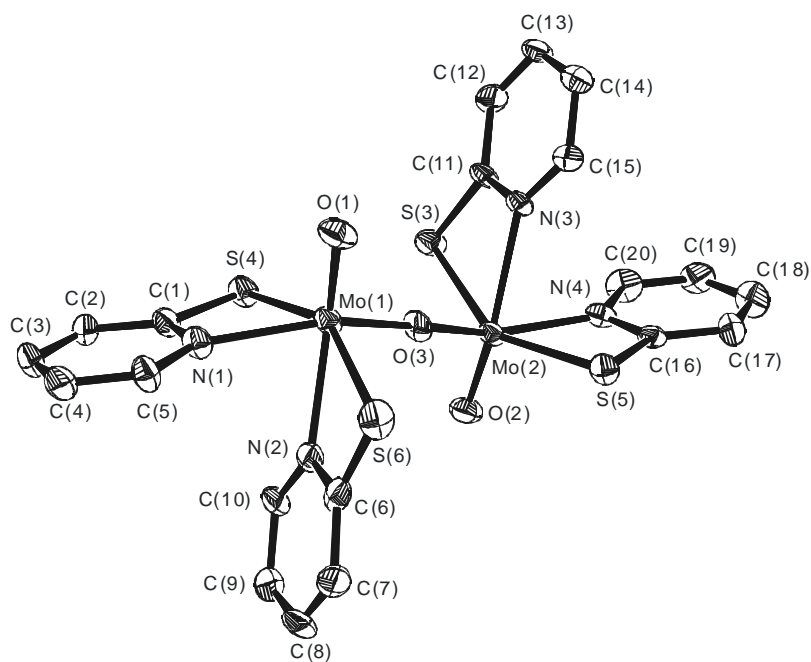


**Figure 25.** Molecular structure of [Mo<sub>2</sub>O<sub>3</sub>(PyS)<sub>4</sub>] (15).

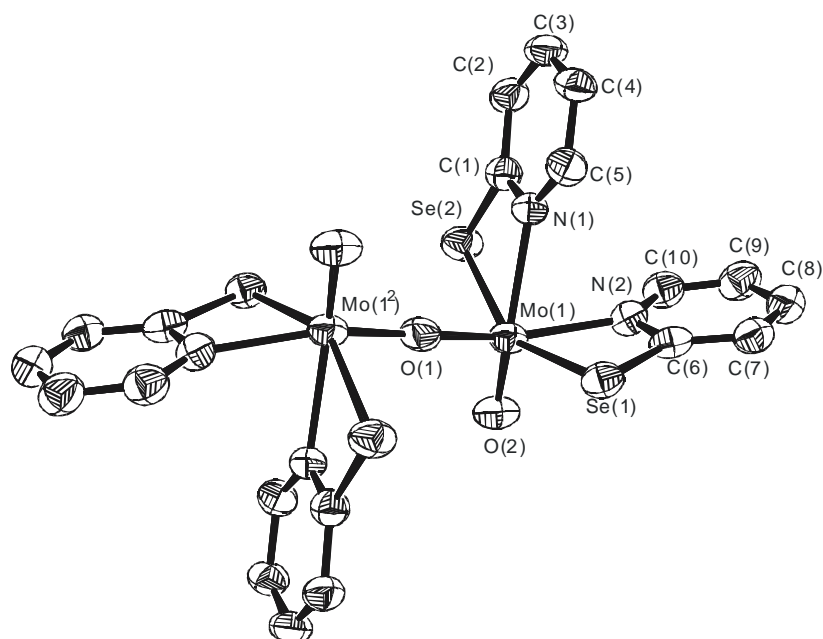


**Figure 26.** Molecular structure of [Mo<sub>2</sub>O<sub>3</sub>(PySe)<sub>4</sub>] (16).

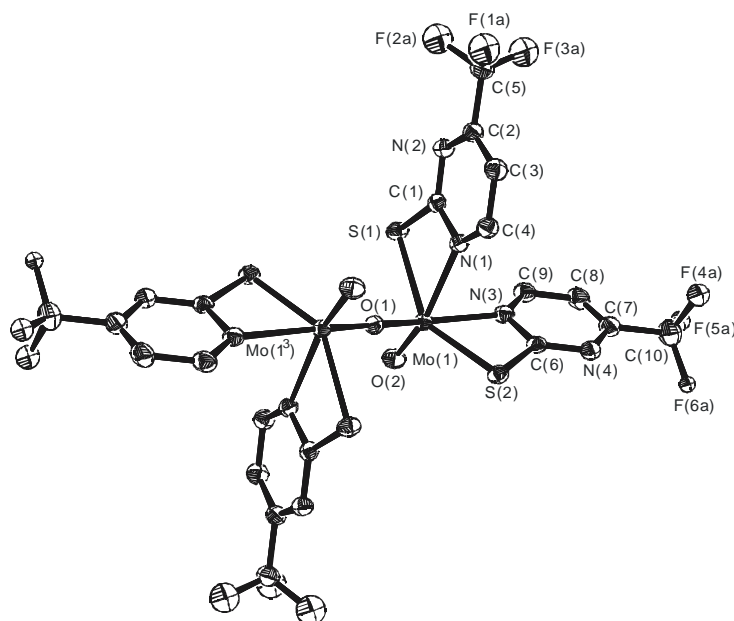


**Figure 27.** Molecular structure of  $[\text{Mo}_2\text{O}_3(4\text{-CF}_3\text{-PymS})_4]\cdot 2(\text{CH}_2\text{Cl}_2)$  (**17**).

**Table 9.** Selected bond lengths (Å) and angles (°) for **15**.

<i>Bond lengths</i>			
Mo(1)-O(1)	1.680(5)	Mo(1)-O(3)	1.863(5)
Mo(1)-N(1)	2.184(6)	Mo(1)-N(2)	2.308(6)
Mo(1)-S(4)	2.438(2)	Mo(1)-S(6)	2.496(2)
<i>Bond angles</i>			
O(1)-Mo(1)-O(3)	107.0(2)	N(1)-Mo(1)-S(4)	66.75(16)
O(1)-Mo(1)-N(1)	96.6(2)	N(2)-Mo(1)-S(4)	89.06(15)
O(3)-Mo(1)-N(1)	152.5(2)	O(1)-Mo(1)-S(6)	94.76(19)
O(1)-Mo(1)-N(2)	156.6(2)	O(3)-Mo(1)-S(6)	98.83(16)
O(3)-Mo(1)-N(2)	87.5(2)	N(1)-Mo(1)-S(6)	93.04(16)
N(1)-Mo(1)-N(2)	75.5(2)	N(2)-Mo(1)-S(6)	64.22(16)
O(1)-Mo(1)-S(4)	108.34(18)	S(4)-Mo(1)-S(6)	150.44(7)
O(3)-Mo(1)-S(4)	91.96(16)	Mo(1)-O(3)-Mo(2)	171.7(3)

**Table 10.** Selected bond lengths (Å) and angles (°) for **16**.

<i>Bond lengths</i>			
Mo(1)-O(1)	1.864(1)	Mo(1)-O(2)	1.683(4)
Mo(1)-N(1)	2.314(5)	Mo(1)-N(2)	2.215(5)
Mo(1)-Se(1)	2.557(1)	Mo(1)-Se(2)	2.624(1)
<i>Bond angles</i>			
O(2)-Mo(1)-O(1)	106.41(18)	N(2)-Mo(1)-Se(1)	68.10(13)
O(2)-Mo(1)-N(2)	96.1(2)	N(1)-Mo(1)-Se(1)	89.87(12)
O(1)-Mo(1)-N(2)	154.57(14)	O(2)-Mo(1)-Se(2)	93.72(15)
O(2)-Mo(1)-N(1)	156.19(19)	O(1)-Mo(1)-Se(2)	97.53(3)
O(1)-Mo(1)-N(1)	87.76(12)	N(2)-Mo(1)-Se(2)	92.57(13)
N(2)-Mo(1)-N(1)	75.46(17)	N(1)-Mo(1)-Se(2)	64.98(12)
O(2)-Mo(1)-Se(1)	107.86(15)	Se(1)-Mo(1)-Se(2)	152.01(3)
O(1)-Mo(1)-Se(1)	93.32(3)	Mo(1)-O(1)-Mo(1)#1	180.0

**15** and **16** crystallize in the same space group ( $P\bar{1}$ ) and crystal system (triclinic). They appear to be isomorphous. **17** crystallizes in the monoclinic space group  $P2_1/c$ . The structures of **15-17** are unexceptional for thiolate or selenide complexes with the common  $[\text{Mo}_2\text{O}_3]^{4+}$  core. Each molybdenum center exhibits distorted octahedral geometry coordinated by two chelating heterocyclic bidentate ligands, the terminal oxo group, and the bridging oxo group, which is located on a crystallographic inversion center (Figure 25-27). Thus, the  $[\text{Mo}_2\text{O}_3]^{4+}$  core exhibits a rigorously planar anti geometry. Furthermore, the three structures have a *trans* O=Mo-O-Mo=O chain with rigorous inversion symmetry, resembling previous reported compounds  $\text{Mo}_2\text{O}_3[\text{S}_2\text{P}(\text{OEt})_2]_4$  and  $\text{Mo}_2\text{O}_3(3\text{-SiMe-2-Spy})_4$ <sup>[139]</sup>, while a *cis* configuration is also found for example in  $\text{Mo}_2\text{O}_3[\text{S}_2\text{CNPr}_2]_4$  and  $\text{Mo}_2\text{O}_3(\text{Etxan})_4$ , where Etxan represents  $\text{EtOCS}_2$ <sup>[140,141]</sup>. This indicates that both the *cis* and *trans* arrangements may be of general

occurrence.

**Table 11.** Selected bond lengths (Å) and angles (°) for **17**.

<i>Bond lengths</i>			
Mo(1)-O(1)	1.856(1)	Mo(1)-O(2)	1.672(2)
Mo(1)-N(1)	2.349(3)	Mo(1)-N(3)	2.193(3)
Mo(1)-S(1)	2.500(1)	Mo(1)-S(2)	2.451(1)
C(2)-C(5)	1.507(4)	C(5)-F(1A)	1.327(9)
<i>Bond angles</i>			
O(2)-Mo(1)-O(1)	104.22(8)	N(1)-Mo(1)-S(2)	85.56(6)
O(2)-Mo(1)-N(3)	97.78(11)	O(2)-Mo(1)-S(1)	96.63(8)
O(1)-Mo(1)-N(3)	155.15(7)	O(1)-Mo(1)-S(1)	98.64(2)
O(2)-Mo(1)-N(1)	160.12(10)	N(3)-Mo(1)-S(1)	90.05(7)
O(1)-Mo(1)-N(1)	83.16(6)	N(1)-Mo(1)-S(1)	63.76(6)
N(3)-Mo(1)-N(1)	79.90(9)	S(2)-Mo(1)-S(1)	144.74(3)
O(2)-Mo(1)-S(2)	111.83(8)	Mo(1)#1-O(1)-Mo(1)	180.00(2)
O(1)-Mo(1)-S(2)	94.22(2)	F(3A)-C(5)-F(1A)	111.5(7)
N(3)-Mo(1)-S(2)	66.55(7)	F(1A)-C(5)-F(2A)	102.5(6)

In compound **16**, the distortions from the ideal octahedral geometry for each molybdenum center mainly arise from the disparate donor atom set and the restricted bite of the Py-Se ligand which subtend angles at the molybdenum center of 64.98(12)° and 68.10(13)°, respectively, considerably distorted from the octahedral limit of 90°. The Py-Se ligands are arranged so that the two selenium atoms are approximately *trans* to each other although with a grossly distorted angle of 152.01(3)°, which compels the nitrogen atoms to occupy approximate *cis*-positions (N-Mo-N, 75.46(17)°). The nitrogen donors occupy positions *trans*

to the strongly P-bonding oxo groups, thus minimizing competition between the oxo groups and the weakly  $\pi$ -interacting selenium donors for the Mo  $t_{2g}$  orbitals. The strong trans influence of the terminal oxo group is evident in the Mo(1)-N(1) distance of 2.314(5) Å, as compared to the Mo(1)-N(2) distance of 2.215(5) Å for the nitrogen *trans* to the less effective bridging oxo group. The Mo-N bond lengths lie in the ranges that are observed in molybdenum complexes with the pyridine-2-selenato ligand<sup>[72]</sup> (2.247(3) and 2.206(3) Å) and the analogous pyridine-2-thiolato ligand<sup>[112,139,142]</sup> (2.157(5)<sup>[142(a)]</sup> - 2.328(5) Å<sup>[139]</sup>). The two Mo-Se bond lengths (2.624(1) and 2.557(1) Å) which are in agreement with reported values (2.633(2) – 2.661(1) Å)<sup>[72,98(d)]</sup> are not equivalent. The four-membered rings derived from the chelating N,Se-coordination of the two 2-selenopyridines are coplanar with the adjacent pyridine rings. The distances of Mo to the terminal oxo ligand (1.683(4) Å), the bridging oxo group (1.864(1) Å) and the *cis*-O-Mo-O angle (106.41(18)°) are in the range of those reported for  $\mu$ -oxomolybdenum(V) complexes (1.680(4) Å, 1.863(1) Å and 105°, respectively)<sup>[139]</sup>.

Complex **15** is isomorphous to complex **16** and has been discussed previously<sup>[133]</sup>, so here we do not discuss it further but compare it with **16**. The geometrical parameters of both complexes are almost identical (see Table 9 and 10). The main differences for bond lengths derive from the bonds containing sulfur or selenium atom. The differences of the corresponding Mo-Se and Mo-S distances for **16** and **15** are 0.119 and 0.128 Å, and those distances of S and Se to a carbon atom of the pyridine ring are 0.133 and 0.157 Å, which can be ascribed to the different radii of both elements (van der Waals radii: 1.80 Å for S and 1.90 Å for Se). The biggest difference for the angles of **15** and **16** is within 3°. Overall both structures are similar maybe due to the fact that the nature of the donor atoms in the heterocyclic ligand does not markedly influence the structure of the complex.

Complex **17** has a similar structure as **15** except for pyrimidine rings instead of pyridine rings and additional substituents, CF<sub>3</sub> groups, in pyrimidine rings. The corresponding geometrical parameters for **17** and **15** are also almost identical. The 4-CF<sub>3</sub>-2-PymS ligands are as well arranged so that the two sulfur atoms are approximately *trans* to each other (S-Mo-S, 144.74(3)°) constraining the nitrogen atoms to occupy approximate *cis*-positions (N-Mo-N, 79.90°). Both N-donor atoms occupy positions *trans* to a terminal oxo and a bridging oxo functions, respectively. The *trans* influences of the two different oxo groups make the Mo-N distances different (2.193(3) and 2.349(3) Å), which leads to different Mo-S distances (2.451(1) and 2.500(1) Å). The configuration of **17** is very close to those of **15** and **16**. Through the analysis and discussion, we can conclude that the steric hindrance produced by the substituents on the heterocyclic ring of the ligands does not have significant influence on the structures of the complexes. These behaviors have been also been reported for ruthenium and osmium complexes.<sup>[143]</sup>

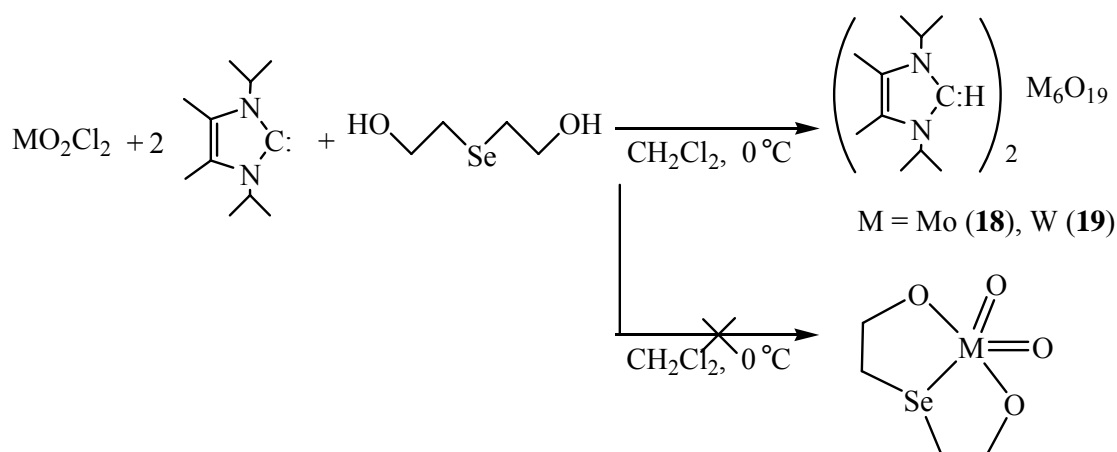


## 2.6. Additional experiments

### 2.6.1. Syntheses and structures of $[\text{H:C}]^+_2[\text{M}_6\text{O}_{19}]^{2-}$ (M = Mo (**18**), W (**19**))

In order to obtain crystals of the molybdenum and tungsten selenium compounds, **5** and **6**, we attempted to change synthetic method.

In general *N*-heterocyclic carbenes, a strong nucleophilic reagent, act as HCl scavengers.<sup>[144,145]</sup> This prompted us to employ the *N*-heterocyclic carbenes to scavenge protons of the selenoether ligand and chlorine atoms of the metal precursor,  $\text{MO}_2\text{Cl}_2$  (M = Mo, W), to achieve the coordination of alkoxylate functions and selenium of the selenoether ligand to the metal center. The reactions were performed in  $\text{CH}_2\text{Cl}_2$  at  $0^\circ\text{C}$ . However, we got polyoxometalates,  $[\text{M}_6\text{O}_{19}]^{2-}$  rather than the desired compounds (Scheme 8). Although the anions for both metals are known,<sup>[146-148]</sup> the whole molecules combined with cations  $[\text{H:C}]^+$  are both novel.



**Scheme 8.** Preparation of  $[\text{H:C}]^+_2[\text{M}_6\text{O}_{19}]^{2-}$  (M = Mo (**18**), W (**19**)).

The molecular structures of **18** and **19** have been determined by single-crystal X-ray diffraction and are shown in Figure 28 and 29.

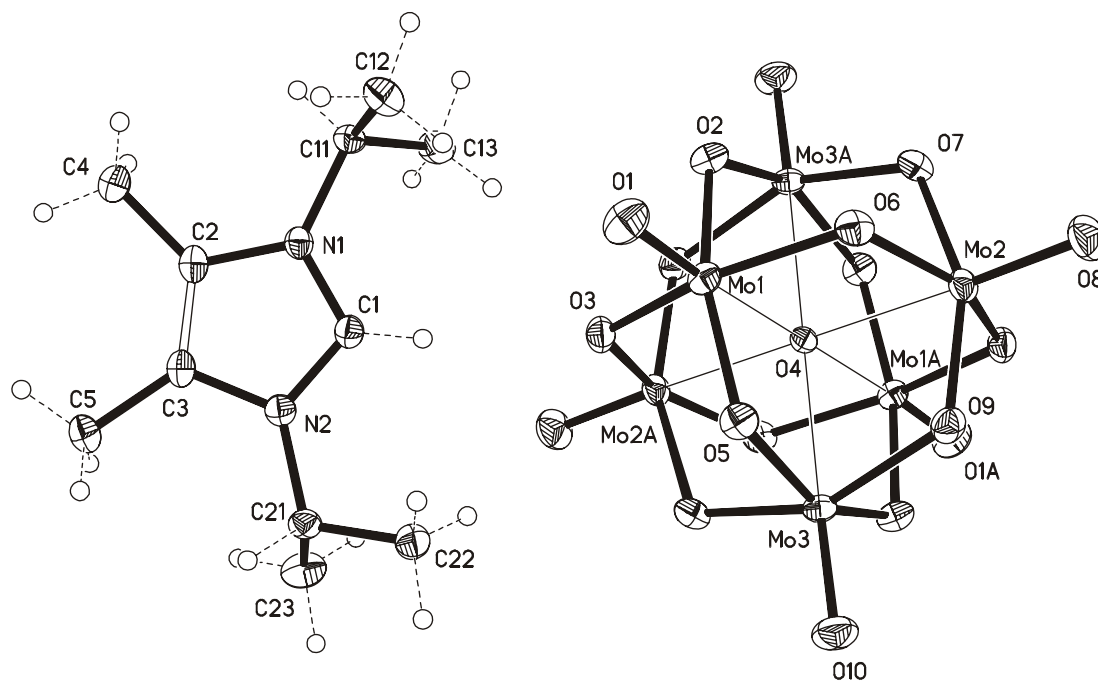


**Figure 28.** View of the structure of  $[\text{H:C}]_2[\text{Mo}_6\text{O}_{19}]^{2-}$  (18) compound with atom labeling scheme. One of cations is omitted for clarity.

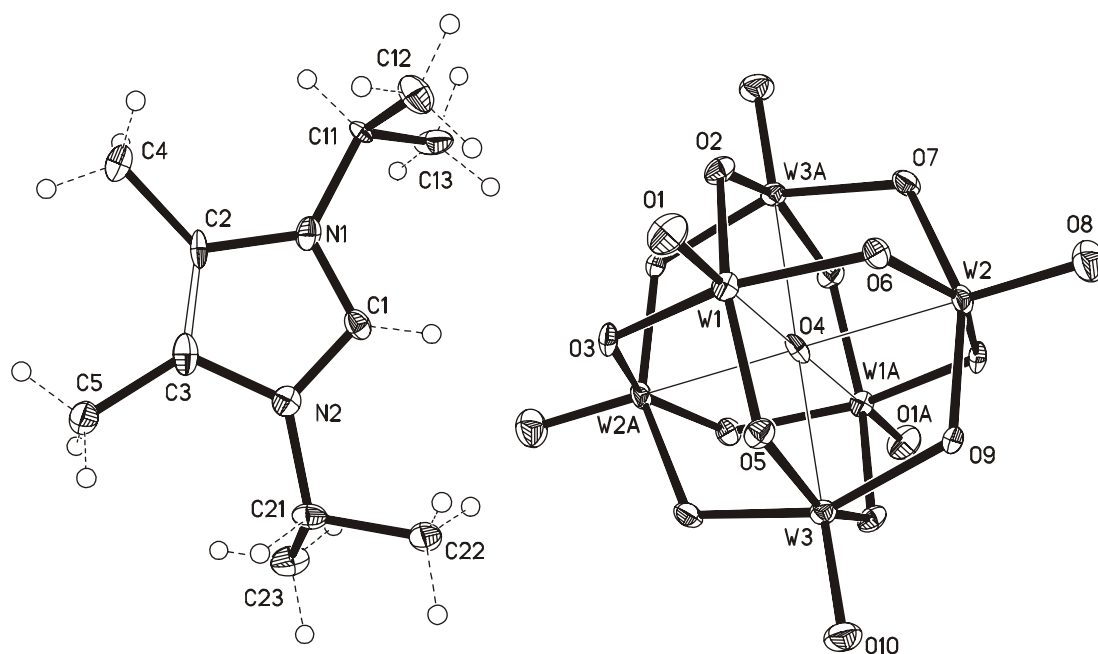


**Figure 29.** View of the structure of  $[\text{H:C}]_2[\text{W}_6\text{O}_{19}]^{2-}$  (19) compound with atom labeling scheme. One of cations is omitted for clarity.

The analytic results reveal that complexes **18** and **19** consist of two *N*-heterocyclic carbene cations and one isopolyanion  $[M_6O_{19}]^{2-}$  (M = Mo (**18**), W (**19**)). Both compounds crystallize in the monoclinic space group  $P2_1/n$ . In the case of **18** the  $[M_6O_{19}]^{2-}$  isopolyanion possessing the well-known Lindquist structure<sup>[149]</sup> is constructed by six  $MoO_6$  octahedra connected with each other through edge-sharing oxygen atoms and thus exhibits an approximate  $O_h$  symmetry. Six molybdenum atoms are located octahedrally around a central oxygen atom. Each molybdenum is then bonded peripherally to neighboring molybdenum atoms through oxygen bridges. One terminal oxygen atom is attached to each molybdenum atom. Selected bond lengths and angles are shown in Table 12.

The data in Table 12 illustrate that one feature of the  $[M_6O_{19}]^{2-}$  structure is a slight distortion of the octahedron that involves the bridging bonds on the surface of the cage. Three kinds of oxygen atoms exist in the cluster. These are the terminal oxygen  $O_a$ , double-bridging oxygen  $O_b$  and central oxygen  $O_c$ . Therefore, the Mo-O distances can be grouped into three sets: Mo- $O_a$  1.6802(18)-1.6837(17) Å, Mo- $O_b$  1.8421(17)-2.0148(17) Å and Mo- $O_c$  2.3132(2)-2.3298(2) Å. The *N*-heterocyclic carbene accepts one proton and forms a cation rather than acts as a HCl acceptor as usual. This result suggests the hexamolybdate dianion is easier to form than the mononuclear dioxo molybdenum complex coordinated with a tridentate selenoether ligand.

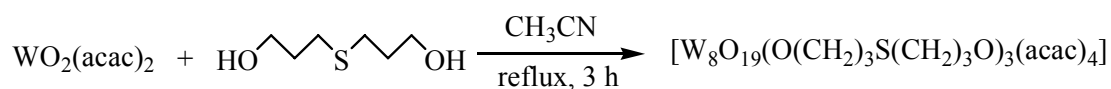
**Table 12.** Selected bond lengths (Å) and angles(°) for compound **18** and **19**.

<b>18</b>		<b>19</b>	
<i>Bond lengths</i>			
Terminal			
Mo(1)-O(1)	1.6810(17)	W(1)-O(1)	1.707(5)
Mo(2)-O(8)	1.6802(18)	W(2)-O(8)	1.701(6)
Mo(3)-O(10)	1.6837(17)	W(3)-O(10)	1.700(5)
Central			
Mo(1)-O(4)	2.3185(2)	W(1)-O(4)	2.3306(4)
Mo(2)-O(4)	2.3132(2)	W(2)-O(4)	2.3239(4)
Mo(3)-O(4)	2.3298(2)	W(3)-O(4)	2.3311(4)
Bridging			
Mo(1)-O(5)	1.8445(16)	W(1)-O(5)	1.906(5)
Mo(1)-O(3)	1.9257(17)	W(1)-O(6)	1.920(5)
Mo(1)-O(6)	1.9341(16)	W(1)-O(3)	1.933(5)
Mo(1)-O(2)	2.0136(17)	W(1)-O(2)	1.938(5)
Mo(2)-O(9)	1.8428(17)	W(2)-O(9)	1.910(5)
Mo(2)-O(6)	1.9174(17)	W(2)-O(6)	1.929(5)
Mo(2)-O(3A)	1.9376(17)	W(2)-O(3A)	1.932(5)
Mo(2)-O(7)	2.0132(17)	W(2)-O(7)	1.935(5)
Mo(3)-O(2A)	1.8422(17)	W(3)-O(2A)	1.909(5)
Mo(3)-O(7A)	1.8486(17)	W(3)-O(7A)	1.915(5)
Mo(3)-O(9)	2.0048(16)	W(3)-O(9)	1.930(5)
Mo(3)-O(5)	2.0148(17)	W(3)-O(5)	1.953(5)
<i>Bond angles</i>			
O(1)-Mo(1)-O(2)	101.68(8)	O(1)-W(1)-O(2)	103.7(2)
O(1)-Mo(1)-O(4)	176.49(7)	O(1)-W(1)-O(4)	179.2(2)
O(2)-Mo(1)-O(4)	74.89(5)	O(2)-W(1)-O(4)	75.71(15)
O(5)-Mo(1)-O(6)	90.55(7)	O(5)-W(1)-O(6)	88.3(2)
Mo(2)-O(6)-Mo(1)	115.95(8)	W(1)-O(6)-W(2)	117.2(3)
Mo(2)-O(4)-Mo(1)	89.664(8)	W(2)-O(4)-W(1)	89.797(12)

Complex **19** exhibits the analogous structure through the same synthetic method. This is not surprising because of the chemical similarity of the two metals. The W-O distances vary in the similar range as those of **18**: W-O<sub>a</sub> 1.700(5)-1.707(5) Å, W-O<sub>b</sub> 1.906(5)-1.953(5) Å and W-O<sub>c</sub> 2.3238(4)-2.3311(4) Å. The geometrical parameters for both complexes are almost identical with the exception that the average bond length of anion in **19** is slightly longer than in **18**. This difference can be ascribed to the different radii of both metals. The terminal oxygen atoms can be rendered as reactive sites. The hexamolybdate can serve as an octahedrally-directing template with which to build new types of interconnected extended polyoxometalate networks analogous to the beautiful and diverse examples of cascade molecules which are now the focus of intense activity in the field of supramolecular chemistry.<sup>[150]</sup>

### 2.6.2. Synthesis and crystal structure description of [W<sub>8</sub>O<sub>19</sub>(O(CH<sub>2</sub>)<sub>3</sub>S(CH<sub>2</sub>)<sub>3</sub>O)<sub>3</sub>(acac)<sub>4</sub>] (**20**)

The several attempts to prepare the thioether analogue of **9**, [ $\{WO_2[O(CH_2)_3S(CH_2)_3O]\}_n$ ], by the similar method as **9** in different solvents failed. There is no evidence for the tungsten thioether complex formation. This prompted us to use more intense reaction condition. WO<sub>2</sub>(acac)<sub>2</sub> reacted with bis(3-hydroxypropyl)sulfide in a molar ration of 1:1.2 in refluxing acetonitrile (Scheme 9). However, a polyoxotungstate **20** was obtain rather than the desired compound.



**Scheme 9.** Synthesis of the octatungstate cluster **20**.

Compound **20** was characterized by elemental analysis, IR spectroscopy, EI mass spectrometry and single-crystal X-Ray crystallography. The EI mass spectrometry exhibits regular increasing spectra in the interval of about 74 ( $m/z$ ) from 661 ( $m/z$ ) to 2577 ( $m/z$ ). The IR spectra of **20** exhibits the characteristic features of polyoxometalates: these are bands in the ranges of 900-1000  $\text{cm}^{-1}$  and 660-880  $\text{cm}^{-1}$ , respectively, assigned to  $\nu\text{W}=\text{O}_t$  and  $\nu\text{W-O-W}$  stretching modes involving terminal and bridging oxo ligands.

The X-ray structural analysis revealed that single crystals of **20**·2.5  $\text{CH}_3\text{CN}$  consist of centrosymmetric isometallic octanuclear clusters  $[\text{W}_8\text{O}_{19}(\text{O}(\text{CH}_2)_3\text{S}(\text{CH}_2)_3\text{O})_3(\text{acac})_4]$  and two and half cocrystallized acetonitrile solvent molecules (Figure 30 (a)). Compound **20** crystallizes in the triclinic space group  $\text{P}\bar{1}$ . The octatungstate cluster core in **20** has a novel unprecedented structure mode denoted  $\{\text{W}_8\text{O}_{33}\}$  composed of eight corner-sharing distorted  $\text{WO}_6$  octahedra. The whole W–O skeleton of the octatungstate looks like a shuttle (Figure 30 (b)). The selected bond lengths and angles are summarized in Table 13. The structural features of the  $\{\text{W}_8\text{O}_{33}\}$  unit in **20** can be compared with  $[\text{W}_{10}\text{O}_{32}]^{4-}$  in the cluster  $[\{\text{Cu}(\text{bpy})_2\}_2\text{W}_{10}\text{O}_{32}]^{[151]}$ . The differences between both are that there are four bottom  $\text{WO}_6$  octahedra linked to the top  $\text{WO}_6$  octahedron by edge sharing in the moiety of the  $[\text{W}_{10}\text{O}_{32}]^{4-}$  cluster. In addition, the structure of the  $\{\text{W}_8\text{O}_{33}\}$  core in **20** is also different from any one of eight molybdenum isomers  $[\text{Mo}_8\text{O}_{26}]^{4-}$  discovered so far<sup>[152-154]</sup>. They all have shared edges, while in the  $\{\text{W}_8\text{O}_{33}\}$  unit eight  $\text{WO}_6$  octahedra are arranged only by sharing corners (see Figure 31).

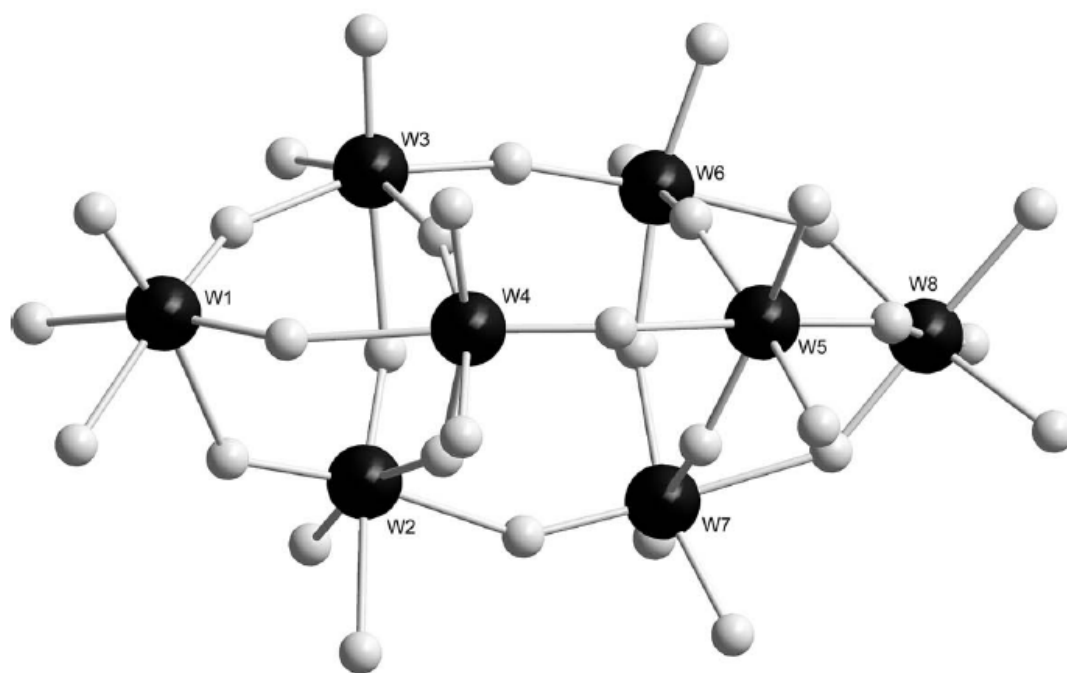
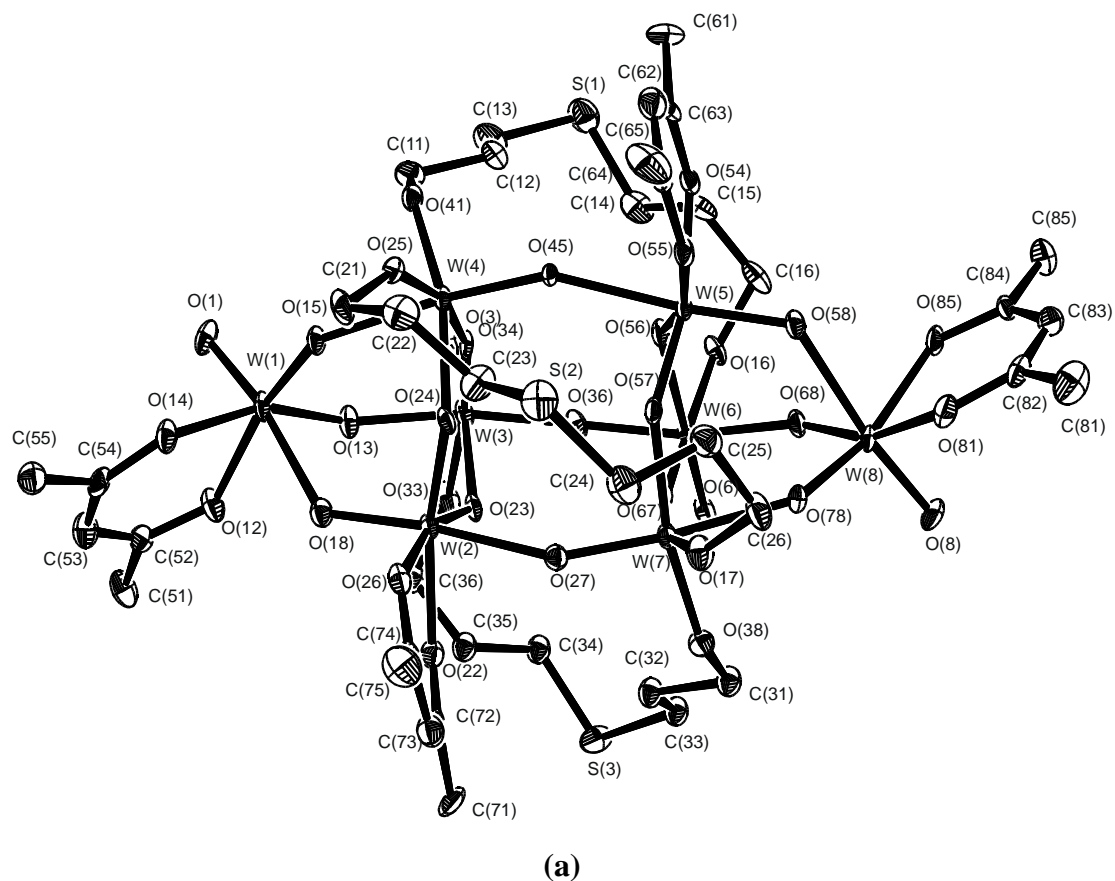


**Figure 30.** (a) Ortep plot of **20** in  $20 \cdot 2.5\text{CH}_3\text{CN}$  (thermal ellipsoids with 50% probability) and (b) Ball-and-stick representation of  $\{\text{W}_8\text{O}_{33}\}$  fragment.

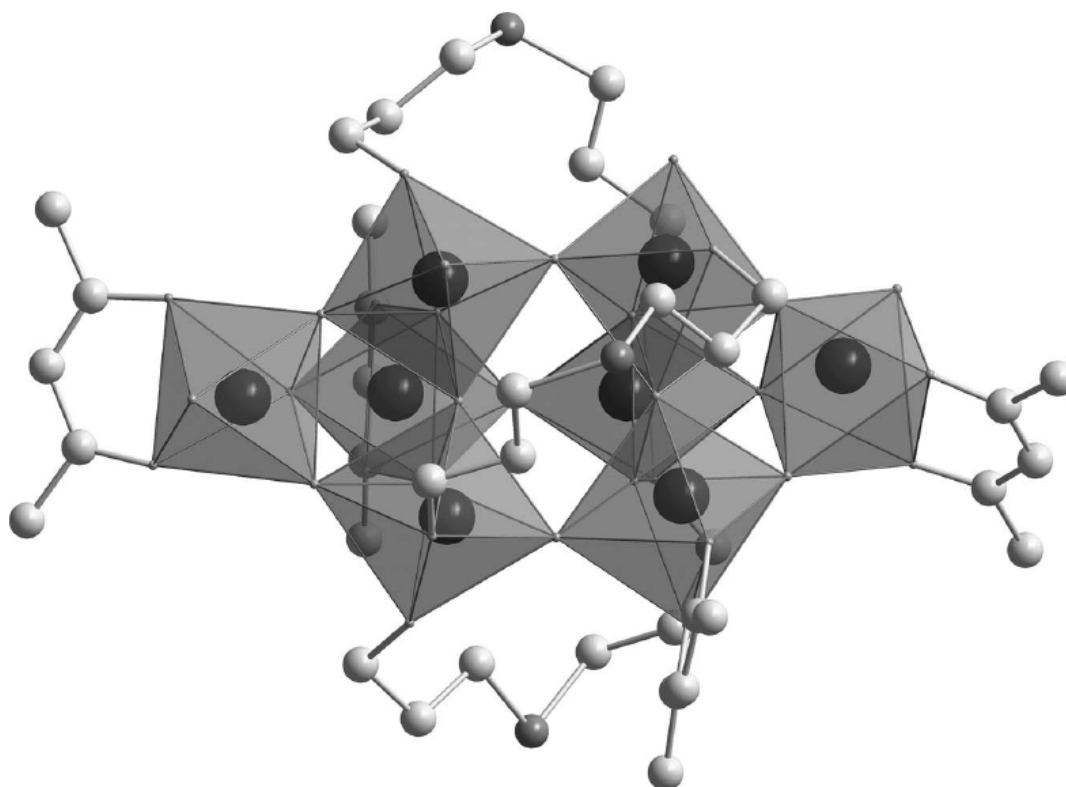


**Figure 31.** Combined polyhedral ball-and-stick representation of **20** in **20·2.5CH<sub>3</sub>CN**.

**Table 13.** Selected bond lengths (Å) and angles (°) for **20**.

*Bond lengths*

W(1)-O(1)	1.702(6)	W(1)-O(15)	1.782(5)
W(1)-O(13)	1.820(5)	W(1)-O(14)	2.034(5)
W(1)-O(12)	2.077(5)	W(1)-O(18)	2.256(6)
W(2)-O(23)	1.752(5)	W(2)-O(18)	1.763(5)
W(2)-O(24)	1.818(5)	W(2)-O(22)	2.059(5)
W(2)-O(26)	2.073(5)	W(2)-O(27)	2.152(5)
W(3)-O(3)	1.715(6)	W(3)-O(33)	1.844(5)
W(3)-O(36)	1.875(5)	W(3)-O(34)	1.945(5)
W(3)-O(13)	1.964(5)	W(3)-O(23)	2.228(5)
W(4)-O(45)	1.757(5)	W(4)-O(41)	1.849(5)
W(4)-O(25)	1.853(5)	W(4)-O(34)	1.858(5)
W(4)-O(24)	2.008(5)	W(4)-O(15)	2.158(5)



*Bond angles*

O(13)-W(1)-O(15)	96.6(2)	O(15)-W(1)-O(18)	83.8(2)
O(18)-W(1)-O(13)	84.3(2)	O(18)-W(2)-O(27)	171.4(2)
O(24)-W(2)-O(23)	98.7(2)	O(18)-W(2)-O(24)	97.6(2)
O(13)-W(3)-O(36)	163.0(2)	O(34)-W(3)-O(23)	77.7(2)
O(13)-W(3)-O(23)	81.1(2)	O(15)-W(4)-O(45)	174.2(2)
O(34)-W(4)-O(24)	85.3(2)	O(15)-W(4)-O(34)	82.1(2)
W(1)-O(18)-W(2)	129.1(3)	W(2)-O(27)-W(7)	147.9(3)
W(1)-O(13)-W(3)	149.5(3)	W(3)-O(36)-W(6)	166.2(3)
W(1)-O(15)-W(4)	142.8(3)	W(4)-O(45)-W(5)	149.2(3)
W(2)-O(23)-W(3)	137.0(3)	W(3)-O(34)-W(4)	162.4(3)
W(4)-O(24)-W(2)	138.2(3)		

The surface of the cluster core is decorated by two types of organic ligands, both of which originate from two reactants, three bis(3-hydroxypropyl)sulfide dianions and four acetylacetonate anions.

We can assume how this cluster has formed by comparing it with a structure we obtained from a very similar reaction<sup>[95]</sup>. The OSO ligand used there contained ethyl bridges instead of propyl bridges between O and S. These shorter bridges lead to the coordination of both alkoxyate functions to one tungsten atom and to a coordination of the thioether sulfur, though rather weak, to this same tungsten as well. In the now obtained octatungstate, sulfur is not coordinated at all. The structure with the shorter OSO ligand is a tungsten trimer. The tungsten atoms are bridged by  $\mu$ -oxo ligands that were former terminal oxo ligands from the starting material  $\text{WO}_2(\text{acac})_2$ . Two of this kind of tungsten trimers (W2, W3, W4 and W5, W6, W7) can be found as building blocks in the center of the new octatungstate cluster arranged as a perfect trigonal prism. The reason may be that the two trimers that are formed with the start

of the reaction, when acac ligands are replaced stepwise by coordination of the OSO ligands, are drawn together by the bridging coordination of the longer OSO ligand between two of these trimeric units. Due to the long alkyl bridges, a coordination of the terminal alkoxylate functions to different tungsten atoms is favoured over the coordination to one tungsten. Three of these bridging ligands enhance the stability of the resulting trigonal prismatic arrangement. Owing to the length of the OSO ligands, the bridging does not occur along the edges of that prism but across its tetragonal faces. To complete the octahedral coordination geometry of the tungsten atoms, both trigonal faces of the trigonal prism are capped by another tungsten (W1, W8). The former terminal oxo ligands of the capping tungsten atoms, are used to bind to the cluster. To complete the coordination sphere of these tungsten atoms one of their acac ligands remains bonded probably due to the fact that the coordination of readily available OSO ligand to one tungsten is clearly not favoured.

The three tungsten atoms of each trimeric unit are all differently coordinated. One tungsten (W4, W7) of the trimeric unit is bound to two alkoxylate oxygen atoms, while all other ligands are bridging  $\mu$ -oxos. One tungsten (W3, W6) is bound to one alkoxylate oxygen atom and four bridging  $\mu$ -oxos and one terminal oxo ligand is completing the octahedral coordination geometry. The last tungsten (W2, W5) of the trimeric unit is not bound to an alkoxylate function but is bound to an acac ligand and like the other two tungsten atoms is bound to four bridging  $\mu$ -oxos. The tungsten atom with no alkoxylate coordination is opposite from the tungsten of the other trimeric unit that is bound to two alkoxylate functions. The tungsten with only one alkoxylate coordination is opposite to the same kind of tungsten from the other trimeric unit. We can only assume that these different coordination modes occur because the formation of the trimeric unit is started only if at least at one tungsten the acac

ligand is replaced by two alkoxyate functions. Therefore, there is necessarily one tungsten from which two bridges lead to the other trimeric unit. If this really is a requirement for the formation of the building blocks, then no distribution of three OSO ligands between the two trimeric units is possible other than the one observed in the octatungstate structure of **20**.

Only one of the bis(3-hydroxypropyl)sulfide ligands is disordered. From both ends, the coordinated oxygen atoms (O33, O38) are at unique positions, while the rest of the chain (six carbon atoms and the sulfur S3) are found at two positions with occupancies of 56% and 44 %, respectively. In Figure 27 (a) only the position of higher occupancy is shown. The other two OSO ligands show no disorder.

All tungsten sites exhibit +6 oxidation state and are crystallographically independent, possessing octahedral coordination geometry with different distortion extents. Two kinds of oxo ligands exist in cluster **20**, that is, the terminal oxygen  $O_t$  and double-bridging oxygen  $O(\mu_2)$ . Therefore, the W–O bonds can be placed into two groups by different bond lengths: W– $O_t$  1.702(6)–1.715(6) Å, W– $O(\mu_2)$  1.752(5)–2.299(5) Å. Average W–O bond lengths in tungsten coordination octahedra are as follows: W(1)–O = 1.945 Å (av.), W(2)–O = 1.936 Å (av.), W(3)–O = 1.929 Å (av.), W(4)–O = 1.914 Å (av.), W(5)–O = 1.936 Å (av.), W(6)–O = 1.925 Å (av.), W(7)–O = 1.911 Å (av.), W(8)–O = 1.950 Å (av.). This is also evidence of the above-mentioned equality between W(1) and W(8), W(2) and W(5), W(3) and W(6), and W(4) and W(7), respectively. The angles of W– $O(\mu_2)$ –W are in the range of 129.1(3)–166.2(3)°. The +6 oxidation state is also confirmed by bond valence sum calculations<sup>[155]</sup> on every W atom. The results give the values of 6.306 for W(1), 6.252 for W(2), 6.304 for W(3), 6.408 for W(4), 6.275 for W(5), 6.350 for W(6), 6.393 for W(7) and 6.287 for W(8), respectively. Furthermore, the average value is 6.322, consistent with the formula of the title compound

given by X-ray structure determination.

Especially interesting is the presence of the four acac ligands, which can be rendered as leaving groups. Thus, cluster **20** has the potential for building new types of interconnected polyoxometalate networks by the incorporation of polyfunctional bridging ligands that are relevant with respect to the intense activity in the field of supramolecular chemistry. This possibility is well illustrated by the previous report on  $[\{\text{Mo}_6\text{O}_{18}\}(\text{N}-\text{Z}-\text{N})\{\text{Mo}_6\text{O}_{18}\}]^{4-}$  ( $\text{Z} = 1,4\text{-cyclo-C}_6\text{H}_{10}$ ), which consists of two terminally substituted imidohexamolybdate cages bridged by a *trans*-1,4-disubstituted cyclohexane ring<sup>[156]</sup>.

In conclusion, the reaction of  $\text{WO}_2(\text{acac})_2$  with bis(3-hydroxypropyl)sulfide in refluxing acetonitrile leads to a cluster with two types of original organic ligands in both reactants. The core unit  $\{\text{W}_8\text{O}_{33}\}$  of the cluster displays the first octatungstate complex and structure and exhibits corner sharing only of the  $\text{WO}_6$  octahedrals.

### 2.6.3. Synthesis and crystal structure of $\text{MoO}_2(\text{dipic})$ (**21**)

In addition, a biologically important and chemically interesting ONO tridentate ligand pyridine-2,6-dicarboxylic acid (dipicolinic acid, dipic) are used here as well. It is a versatile N–O donor capable of forming stable chelates<sup>[157]</sup> with various metal ions and can exhibit diverse coordination modes such as bidentate,<sup>[158]</sup> tridentate, meridian<sup>[159]</sup> or bridging.<sup>[160]</sup> It can stabilize unusual oxidation states<sup>[161]</sup> and has proved to be useful in analytical chemistry,<sup>[162]</sup> in corrosion inhibition<sup>[163]</sup> and decontamination of nuclear reactors.<sup>[164]</sup> Another interesting property of this ligand is its diverse biological activity.<sup>[165]</sup> Along with its 2,4- and 2,5-isomers, pyridine-2,6-dicarboxylic acid acts as an inhibitor of the enzyme GA 2b-hydroxylase and is also found to inhibit the mechanistically related enzyme proline

4-hydroxylase.<sup>[166]</sup> Herein, we will investigate the coordinated form of this ligand towards molybdenum(VI).

Relevant molybdenum(VI) pyridine-2,6-dicarboxylate complexes have been reported previously.<sup>[166(c),167]</sup> The complexes all adopt a six-<sup>[167]</sup> or seven-<sup>[168]</sup> coordination pattern with an additional ligand, such as DMF, DMSO, HMPA and OPPh<sub>3</sub>. To the best of our knowledge, the five-coordination complex of dioxomolybdenum(VI) pyridine-2,6-dicarboxylate without other coordinated ligands is still unknown.

Herein, MoO<sub>2</sub>(dipic) **21** was prepared by reacting MoO<sub>2</sub>(acac)<sub>2</sub> with dipicolinic acid in methanol at room temperature with stirring overnight. The compound is partly soluble in CH<sub>2</sub>Cl<sub>2</sub>, so it can be obtained by addition of CH<sub>2</sub>Cl<sub>2</sub> to the dried residue of the reaction, followed by precipitation, crystallization and collection.

The compound **21** was characterized by elemental analysis IR and EI mass spectroscopy. From the IR spectra of **21** it is indicated that the dipicolinic anion (dipic) acts as a tridentate chelating ligand being bonded to the Mo(VI) acceptor centre *via* the two deprotonated oxygen atoms of the carboxylate moieties ( $\nu$  (C=O) 1706 (vs), 1742 (vs) cm<sup>-1</sup>;  $\nu$  (C-O) 1307 (vs) cm<sup>-1</sup>) and the heterocyclic nitrogen. The  $\nu$  (C=O) of the free carboxylic acid<sup>[169]</sup> is found to be lowered by 30-40 cm<sup>-1</sup> due to coordination in the complex. The presence of two strong bands, 918 and 943 cm<sup>-1</sup> indicates that the complex contains the *cis*-MoO<sub>2</sub> moiety as usual for dioxomolybdenum (VI) species<sup>[170,171]</sup>. The EI-MS for **21** does not provide much useful and easily interpretable information.

Attempts to prepare the tungsten analogue by the reaction of WO<sub>2</sub>(acac)<sub>2</sub> with dipicolinic acid or WO<sub>2</sub>Cl<sub>2</sub>(DME) with Na<sub>2</sub>dipic failed. No evidence provided the formation of the tungsten complex.

The blue crystals of **21** were grown from a dichloromethane solution. The molecular structure is shown in Figure 32. The selected bond lengths and angles are list in Table 14.

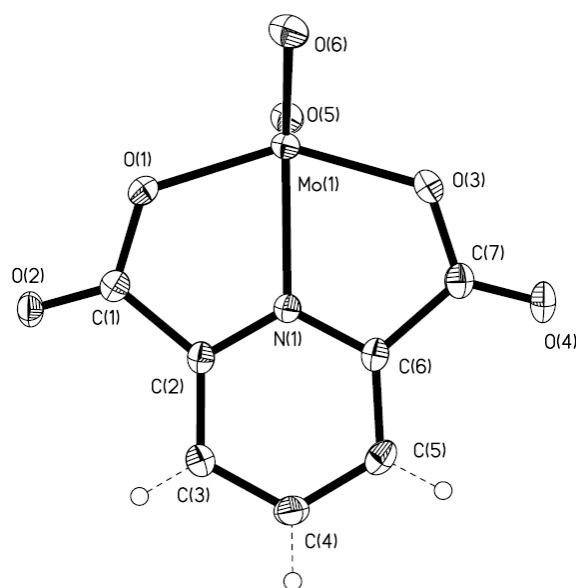


**Figure 32.** Molecular structure and atom-labeling for **21**; the hydrogen atoms are shown with small arbitrary radii.

**Table 14.** Selected bond lengths (Å) and angles (°) for **21**.

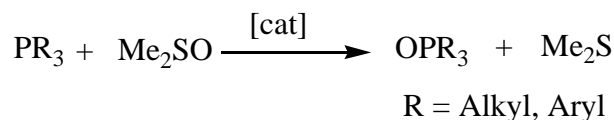
<i>Bond lengths</i>			
Mo(1)-O(5)	1.6830(17)	Mo(1)-O(6)	1.6943(17)
Mo(1)-O(1)	1.9960(16)	Mo(1)-O(3)	1.9879(18)
Mo(1)-N(1)	2.1716(18)	O(1)-C(1)	1.333(3)
O(3)-C(7)	1.332(3)		
<i>Bond angles</i>			
O(5)-Mo(1)-O(6)	107.08(8)	O(5)-Mo(1)-O(3)	98.76(8)
O(6)-Mo(1)-O(3)	98.92(8)	O(5)-Mo(1)-O(1)	100.56(8)
O(6)-Mo(1)-O(1)	103.09(8)	O(3)-Mo(1)-O(1)	144.81(7)
O(5)-Mo(1)-N(1)	110.02(7)	O(6)-Mo(1)-N(1)	142.81(7)
O(3)-Mo(1)-N(1)	73.07(7)	O(1)-Mo(1)-N(1)	72.77(7)

The molybdenum atom is coordinated by the tridentate ligand dipic in the doubly deprotonated pyridine-2,6-dicarboxylate form. In contrast to the molybdenum(VI) compounds discussed above the molybdenum atom in **21** is only five-coordinated with one terminal oxo groups O(5) or O(6) in the apical position of a distorted square pyramidal conformation. The bite angles around C(1), C(2), N(1), C(6) or C(7) atoms in the dipicolinate ligand sum up to be 360°. This shows the high planarity of the ligand. The bond lengths for two terminal oxo groups, Mo-O(5) and Mo-O(6), are not exactly identical, the former being 0.01 Å shorter. This is caused due to no *trans* ligand for O (5) and can be also explained by the difference of the two angles: O(5)-Mo(1)-N(1) 110.02(7)° and O(6)-Mo(1)-N(1) 142.81(7)°. Of the two Mo-O bonds generated by the coordinated carboxylated oxygen O(1) and O(3) of the dipicolinate moiety, Mo-O(1) is slightly longer. The angles for the *cis*-MoO<sub>2</sub> group, O(5)-Mo-O(6), are 107.08(8)°, which is good agreement with those found for analogous complexes with N- and O-coordinated ligands<sup>[170(b),172,173]</sup>. The bond length of Mo-N(1) (2.1716(18) Å) is close to those in analogous complexes.<sup>[167]</sup>

## 2.7. Catalytic oxygen atom transfer reaction

### 2.7.1. Oxygen atom transfer properties of **7** and **8**

In presence of a catalyst the oxygen atom of the DMSO molecule can be transferred to a phosphine ( $\text{PR}_3$ ) see Scheme 10.

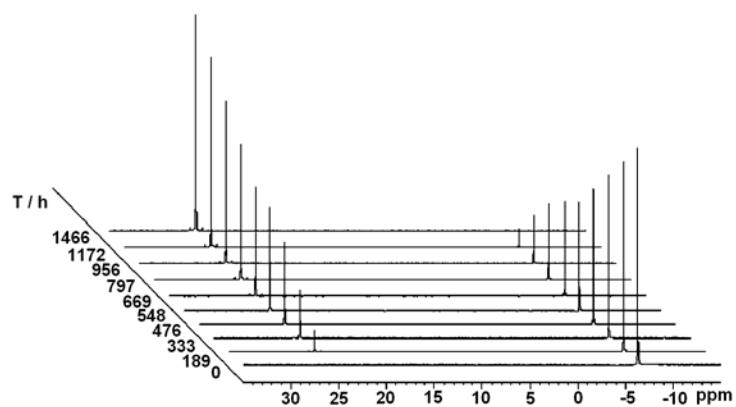


**Scheme 10.** The catalysed oxygen atom transfer from DMSO to phosphine.

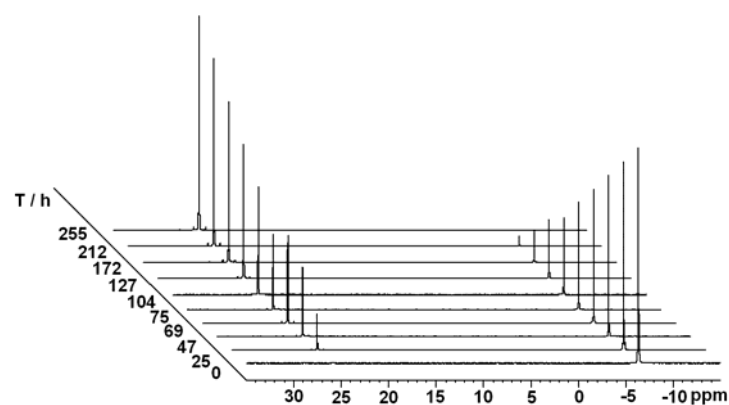
The catalytic oxygen atom transfer properties for this reaction were investigated for compound **7** as well as for compound **8** under the same conditions. The experiments were performed at room temperature in DMSO by mixing the catalyst and  $\text{PPh}_3$  in different ratios. Without catalyst no reaction occurs under these conditions.

The reactions were monitored with  $^{31}\text{P}$ -NMR spectroscopy. During the reactions only two phosphorous signals were observed: one for  $\text{PPh}_3$  and one for  $\text{OPPh}_3$  (see Figure 33). During catalysis for  $[\{\text{MoO}_2(\text{O}(\text{CH}_2)_3\text{S}(\text{CH}_2)_3\text{O})\}_2]$  **7** as catalyst the colour of the solution initially changes from colourless to light blue and back to colourless. For  $[\{\text{MoO}_2(\text{O}(\text{CH}_2)_3\text{Se}(\text{CH}_2)_3\text{O})\}_2]$  **8** as catalyst no colour change was observed at all. For all catalysed reactions a conversion of 100 % was reached.





(a)



(b)

**Figure 33.** The  $^{31}\text{P}$  NMR spectroscopy studies of oxo-transfer reactions of  $[\{\text{MoO}_2(\text{O}(\text{CH}_2)_3\text{S}(\text{CH}_2)_3\text{O})\}_2]$  (**7**, a) and  $[\{\text{MoO}_2(\text{O}(\text{CH}_2)_3\text{Se}(\text{CH}_2)_3\text{O})\}_2]$  (**8**, b) with  $\text{PPh}_3$  in DMSO in a ratio of 1:20 cat: $\text{PPh}_3$ . For clarity only ten spectra are displayed for each compound.

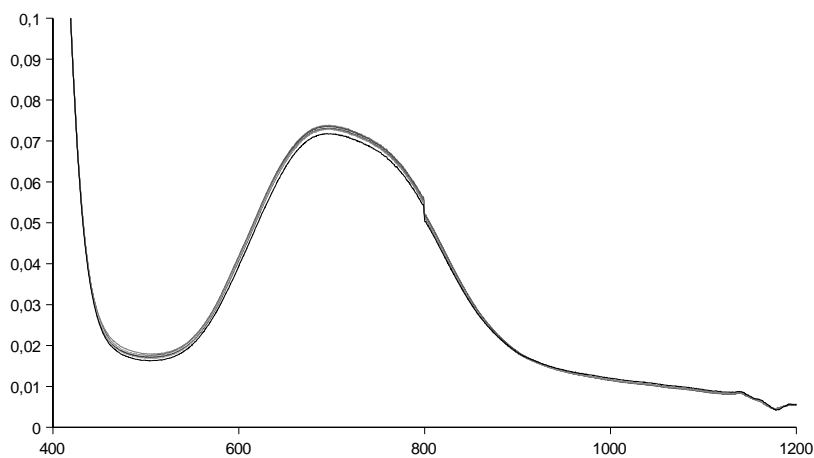


**Figure 34.** UV-Vis spectra of **8** in DMSO with  $\text{PPh}_3$  (Mo: $\text{PPh}_3$  1:7.5) monitored 3 h.

The catalysis with the selenium containing compound **8** which is UV-Vis active was monitored with this method in one experiment but no significant change of the spectrum was observed (see Figure 34). An intermediate with the phosphorous compound attached to the catalyst was detected with neither method indicating that the lifetime of such an intermediate is too short for observation by NMR and UV-Vis. The development of  $\text{OPPh}_3$  for both catalysts over time with different catalyst: $\text{PPh}_3$  ratios is shown in Figure 35.

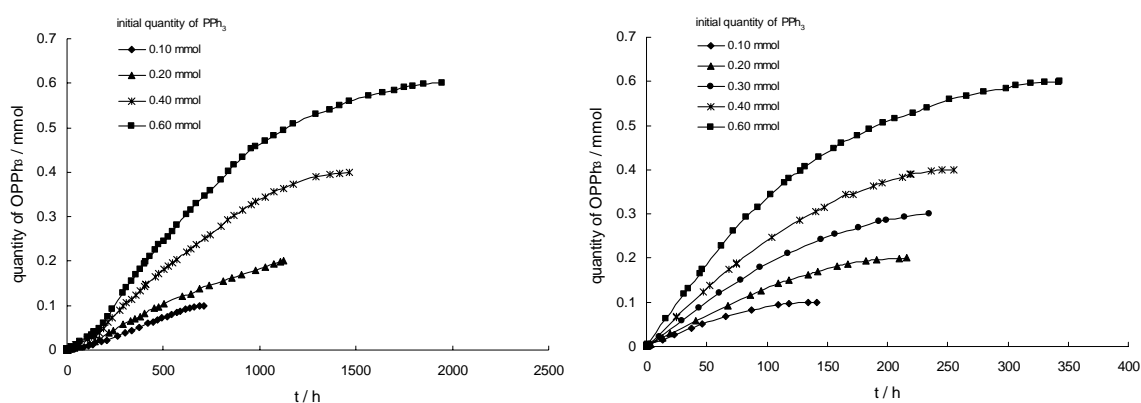
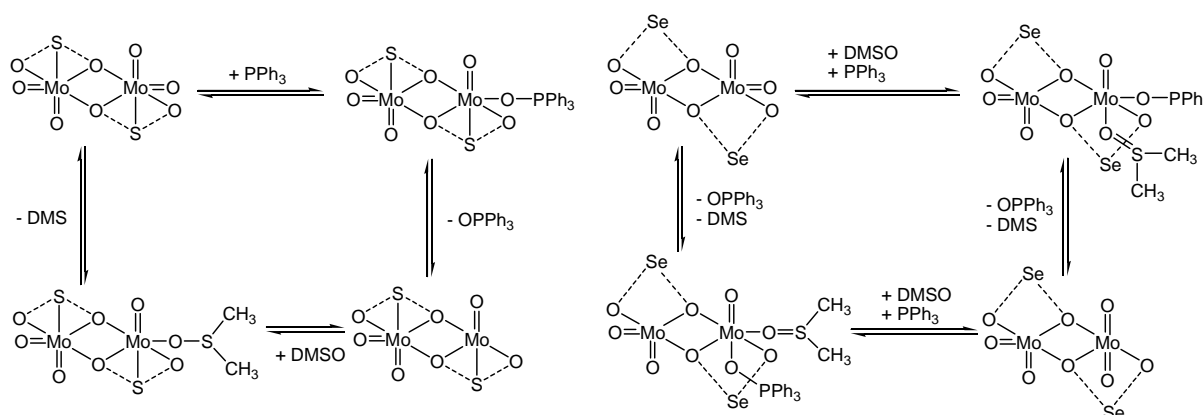


**Figure 35.** Development of  $\text{OPPh}_3$  with time for catalyst **7** (left) and catalyst **8** (right) with different quantities of substrate ( $\text{Mo}:\text{PPh}_3$ ; 1:2.5, 1: 5; 1:10, 1:15 and 1:7.5 only for **8**) in DMSO as solvent and second substrate.

The graphs for the reactions with compound **7** as catalyst are slightly sigmoidal (Figure 35). No such behaviour was observed for the reaction with compound **8** as catalyst. In addition, due to the similarity of resonance signal of  $^{77}\text{Se}$ -NMR spectra for the free ligand (149.82 ppm) and for the selenium complex **8** (150.18 ppm), we can deduce that at least the molybdenum selenium bond of complex **8** in solution is no longer intact. The bond length of Mo-S in **7** is

shorter than Mo-Se in **8**, so the bond of the former may be stronger than the latter. We assume that the bond of Mo-S in **7** is still intact in the solution. Based on the above mentioned, complexes **7** and **8** may adopt two different catalytical mechanisms. In the catalyzed reaction by **8**, PPh<sub>3</sub> is bound to one of oxo ligands of compound and at the meantime DMSO molecules may coordinate to the vacant position of the former Mo-Se bond. Then the formed OPPh<sub>3</sub> and DMS leave together. Subsequently DMSO molecules continue occupying the vacant coordination sites which are formed due to the OPPh<sub>3</sub> leaving and PPh<sub>3</sub> continues coordinating to one oxo ligand. Finally with their leaving catalytic cycle is accomplished and compound **8** is recovered. The catalyzed cycle by compound **7** is carried out as usual. Such the overall reaction rate catalyzed by **8** is enhanced by a concerted mechanism in comparison to the molybdenum sulfur catalyst **7** by a consecutive mechanism. We therefore suggest a consecutive mechanism for **7** and a concerted mechanism for **8** (see Scheme 11). The observation that the fragility of the molybdenum selenium bond plays a vital role for the catalytical mechanism correlates with the fact that the formate dehydrogenase from *E. coli* also employs a mechanism where the molybdenum selenium bond is broken.<sup>[174]</sup>



**Scheme 11.** Consecutive (left; probably effective for  $[\{\text{MoO}_2(\text{O}(\text{CH}_2)_3\text{S}(\text{CH}_2)_3\text{O})\}_2]$  (**7**)) vs. concerted mechanism (right; probably effective for  $[\{\text{MoO}_2(\text{O}(\text{CH}_2)_3\text{Se}(\text{CH}_2)_3\text{O})\}_2]$  (**8**)). The concerted mechanism shows two conversions, the consecutive mechanism only one.

**Table 15.** Kinetic data for the oxo transfer catalysis from DMSO to PPh<sub>3</sub> with  $[\{\text{MoO}_2(\text{O}(\text{CH}_2)_3\text{S}(\text{CH}_2)_3\text{O})\}_2]$  (**7**) and  $[\{\text{MoO}_2(\text{O}(\text{CH}_2)_3\text{Se}(\text{CH}_2)_3\text{O})\}_2]$  (**8**) as catalysts.

compound	[PPh <sub>3</sub> ] [mol L <sup>-1</sup> ]	k <sub>obs</sub> [h <sup>-1</sup> ]	v [mol L <sup>-1</sup> h <sup>-1</sup> ]	1/[PPh <sub>3</sub> ] [L mol <sup>-1</sup> ]	1/v [L h mol <sup>-1</sup> ]
<b>7</b>	0.1667	0.0021	0.0002	6.00	6250.00
	0.3333	0.0014	0.0003	3.00	3802.28
	0.6667	0.0012	0.0004	1.50	2631.58
	1.0000	0.0011	0.0005	1.00	2192.98
<b>8</b>	0.1667	0.0177	0.0019	6.00	540.54
	0.3333	0.0124	0.0040	3.00	253.16
	0.5000	0.0107	0.0033	2.00	306.09
	0.6667	0.0096	0.0042	1.50	238.10
	1.0000	0.0091	0.0063	1.00	160.00

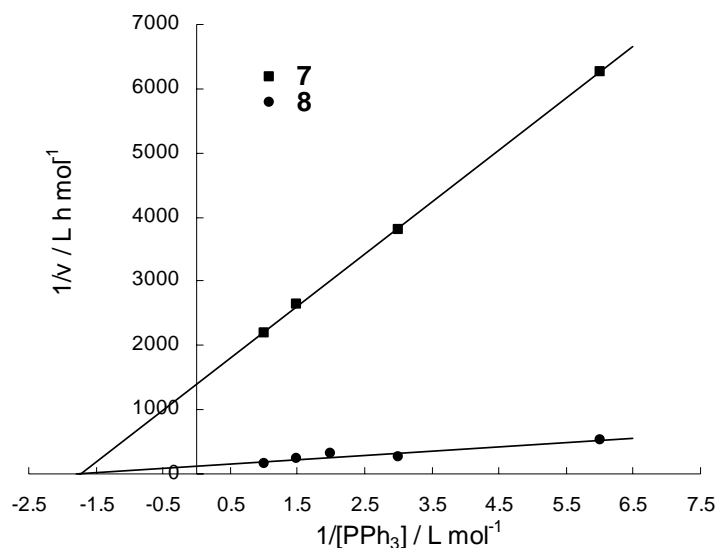
  

compound	t <sub>on</sub> [mol mol <sup>-1</sup> h <sup>-1</sup> ]	time to 100% conversion[h]	1/k <sub>obs</sub> [h]	K <sub>max</sub> [mol L <sup>-1</sup> ]	V <sub>max</sub> [mol L <sup>-1</sup> h <sup>-1</sup> ]
<b>7</b>	0.0070	709.27	476.19	0.5796	0.0007
	0.0089	1122.75	714.29		
	0.0136	1466.48	833.33		
	0.0154	1947.45	909.09		
<b>8</b>	0.0350	141.53	56.50	0.6058	0.0088
	0.0450	215.65	80.65		
	0.0640	235.10	93.46		
	0.0780	255.48	104.17		
	0.0875	342.78	109.89		

The sigmoidal behaviour of the catalysis with compound **7** can now be explained by the assumption that first the transfer of one oxo group to PPh<sub>3</sub> in comparison with compound **8** as

catalyst occurs relatively fast. Then the retardation is caused by an equilibrium that is reached and the reduced molybdenum molecules have to be re-oxidized by DMSO to push the reaction further. After that the whole process reaches an equilibrium again with permanent oxidation by DMSO and reduction by  $\text{PPh}_3$ . The obtained data for all catalytical experiments are summarized in Table 15.

For both compounds the initial velocity of the reactions referring to the  $\text{PPh}_3$  substrate concentrations is showing Michaelis-Menten type kinetics.  $K_{\text{max}}$  and  $V_{\text{max}}$  were determined by Lineweaver-Burk diagrams (see Figure 36).



**Figure 36.** Lineweaver-Burk diagrams for  $[\{\text{MoO}_2(\text{O}(\text{CH}_2)_3\text{S}(\text{CH}_2)_3\text{O})_2\}]$  **7** and  $[\{\text{MoO}_2(\text{O}(\text{CH}_2)_3\text{Se}(\text{CH}_2)_3\text{O})_2\}]$  **8** as catalysts dependent on the concentration of  $\text{PPh}_3$ .

The turnover numbers ( $\text{ton} [(\text{mol substrate}) \cdot (\text{mol catalyst})^{-1} \cdot \text{time}^{-1}]$ ) are increasing with the substrate concentration as well. Interestingly the  $k_{\text{obs}}$  determined from exponential fits ( $[\text{OPPh}_3]_t/[\text{PPh}_3]_0 = 1 - \exp(-k_{\text{obs}} \cdot t)$ ) show a reverse behaviour and are decreasing with the substrate concentration (Figure 37). This is unusual and an indication that with high  $\text{PPh}_3$  concentrations there is a stronger competition between  $\text{PPh}_3$  (and/or DMS) and DMSO for

binding to the molybdenum center even though an intermediate like  $[\text{Mo}_2\text{O}_3(\text{OPPh}_3)(\text{O}(\text{CH}_2)_3\text{X}(\text{CH}_2)_3\text{O})_2]$  ( $\text{X} = \text{S}, \text{Se}$ ) was not observed with  $^{31}\text{P}$  NMR nor with UV-VIS spectroscopy.

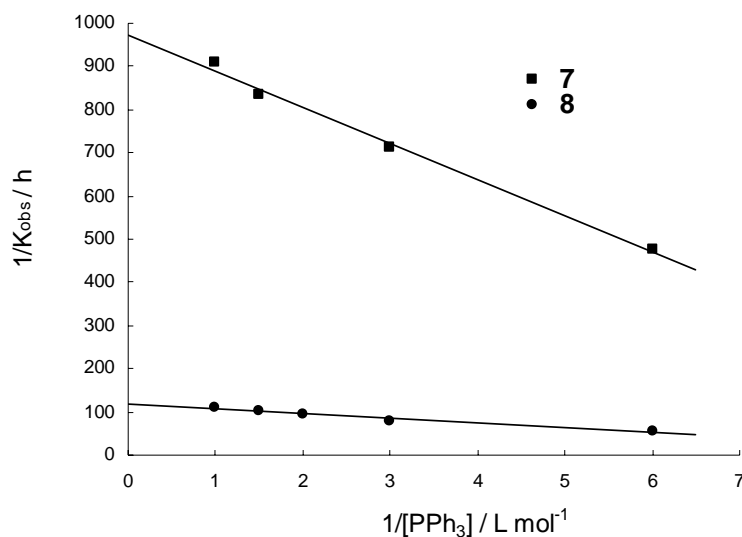


**Figure 37.** Graphs for the  $1/k_{\text{obs}}$  dependency on  $1/[\text{PPh}_3]$  for  $[\{\text{MoO}_2(\text{O}(\text{CH}_2)_3\text{S}(\text{CH}_2)_3\text{O})\}_2]$  **7** and  $[\{\text{MoO}_2(\text{O}(\text{CH}_2)_3\text{Se}(\text{CH}_2)_3\text{O})\}_2]$  **8** as catalysts.

The overall long reaction times as well as the large Michaelis constants suggest that the stability of the catalyst- $\text{PPh}_3$  complex is rather low and therefore only a very small amount of these complexes present during catalysis. This is supported by the fact that the UV-Vis-spectra of compound **8** obtained at various intervals during the catalysis show no significant changes and only a variation of the extension by some 2 to 3 percent (Figure 34). The more or less identical Michaelis constants for both catalysts further show that the catalyst- $\text{PPh}_3$  complexes are of almost the same stability for **7** and **8** even though the performance of both catalysts is very different. This is another indication that two different mechanisms may be effective.

Both catalysts perform rather poorly in comparison with other oxygen atom transfer catalysts

based on molybdenum.<sup>[167,175,176]</sup> But the important observation here is that the selenium containing molybdenum compound **8** is a better catalyst for the oxygen atom transfer than the sulfur containing compound **7** under identical conditions probably due to the fact that the bond between molybdenum and selenium is more fragile. Interestingly no DMSO reductase with selenocysteine coordinated to the metal center was found so far.

The obtained data suggests that the catalytical performance and mechanism of both compounds are strongly influenced by an exchange of ligand atoms sulfur versus selenium even though no strong influence on other investigated properties could be observed.

### 2.7.2. Catalytic oxo-transfer reactivity of **10**

The mononuclear dioxo molybdenum complexes as models of the active sites of molybdopterin-containing OATs usually have good oxo transfer catalytic abilities.<sup>[107,108,174]</sup> It is very interesting to investigate what would be the effect of the formation of mononuclear complex and the introduction of a siloxy group upon the capacity to transfer an oxygen atom to a substrate. Herein, the catalytic properties of compound **3** and **10** for the oxygen atom transfer reaction from DMSO to PPh<sub>3</sub> were investigated according to Scheme 10 under the exact same conditions. The experiments were performed at room temperature in dry deoxygenated DMSO-*d*<sub>6</sub> solutions containing  $2 \times 10^{-4}$  mol PPh<sub>3</sub> and  $2 \times 10^{-5}$  mol **10** or  $1 \times 10^{-5}$  mol **3** (due to **3** is a dimer). The reactions were monitored by <sup>31</sup>P NMR spectroscopy. Catalyst **10** oxidized 100% of PPh<sub>3</sub> within about 4 days, whereas catalyst **3** only catalyzed 24% oxidation of PPh<sub>3</sub> within 20 days. The development of conversion of PPh<sub>3</sub> to OPPh<sub>3</sub> for **10** over time is shown in Figure 38. The mononuclear compound with silyloxy **10** shows much higher catalytic activity than its dimeric precursor **3**, which indicates that the formation of

mononuclear molybdenum and the introduction of a siloxy group enhance the catalytic ability of the compound. No reaction occurs without catalyst under these conditions. In both cases, the color of the solution remained unchanged, indicating the equilibrium on the side of the dioxo molybdenum species. The obtained data suggests that the catalytic performance of both compounds is strongly influenced by mononuclear versus binuclear compound even though no strong influence on the structures in one molybdenum atom could be observed. Usual formation of a dimeric product is avoided by sterically demanding ligands.

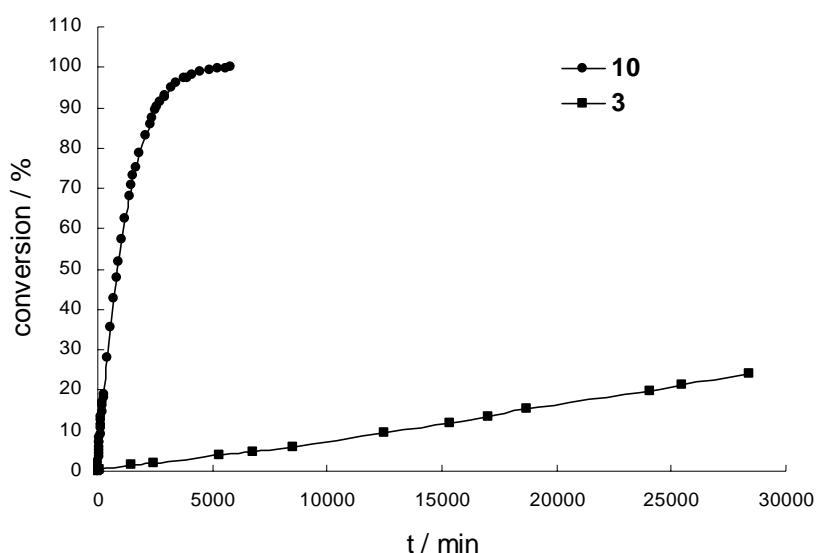


**Figure 38.** Conversion of  $\text{PPh}_3$  to  $\text{OPPh}_3$  with time for catalyst **10** and **3**.

Furthermore, the kinetics of oxo-transfer reaction from DMSO to  $\text{PPh}_3$  catalyzed by **10** with 2.5–15 equiv of  $\text{PPh}_3$  in 0.6 mL  $\text{DMSO-}d_6$  solution were investigated. The conversions for the oxidation of  $\text{PPh}_3$  to  $\text{OPPh}_3$  by DMSO for catalyst **10** with different catalyst: $\text{PPh}_3$  ratios are shown in Figure 39. 100% conversions were accomplished almost at the same time for the four different ratios of the catalyst **10** and  $\text{PPh}_3$ . No colour changes were observed during the whole catalytic reactions under the different ratios of **10** and  $\text{PPh}_3$ . The observed rate



constants ( $k_{\text{obs}}$ ) were obtained from the exponential fit ( $[\text{OPPh}_3]_t/[\text{PPh}_3]_0=1-\exp(-k_{\text{obs}}\cdot t)$ ). They are  $0.0013 \text{ min}^{-1}$ ,  $0.0010 \text{ min}^{-1}$ ,  $0.0010 \text{ min}^{-1}$  and  $0.0012 \text{ min}^{-1}$  for the ratios of **10**:PPh<sub>3</sub>, 1:2.5, 1:5, 1:10 and 1:15, respectively. The  $k_{\text{obs}}$  for the four ratios are approximately the same and irregular with the concentrations of the substrate PPh<sub>3</sub>. The increases in the concentration of PPh<sub>3</sub> have no significant effect on the reaction rate. This result at least is an indication that the catalytic activity of **10** is independent from the concentration of PPh<sub>3</sub> in the investigated range.

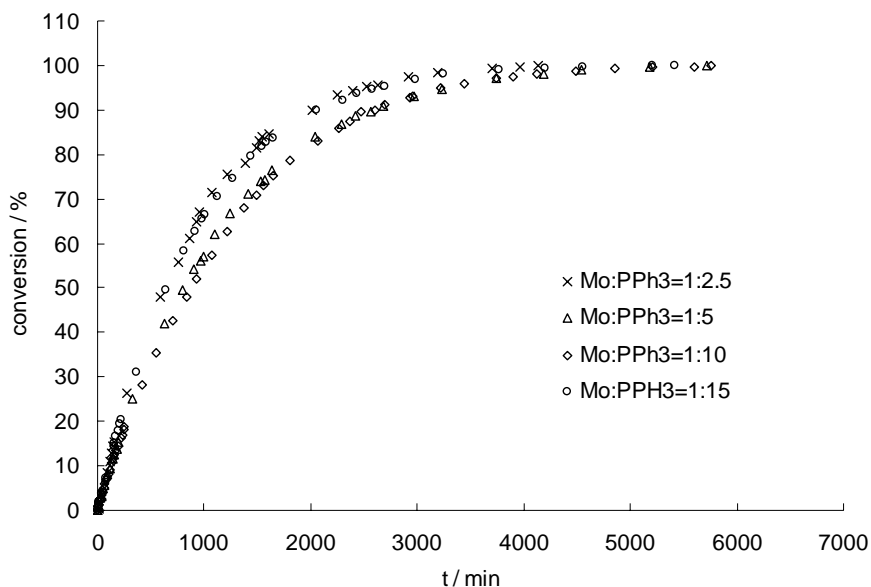
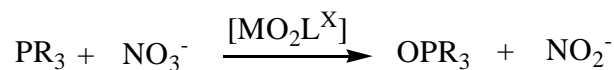


**Figure 39.** Oxidation of PPh<sub>3</sub> to OPPh<sub>3</sub> by DMSO-*d*<sub>6</sub> at r. t. with time for catalyst **10** with different quantities of substrate (Mo:PPh<sub>3</sub> = 1:2.5, 1:5, 1:10 and 1:15).

### 2.7.3. Catalytic oxo-transfer reactivity of **11-14**

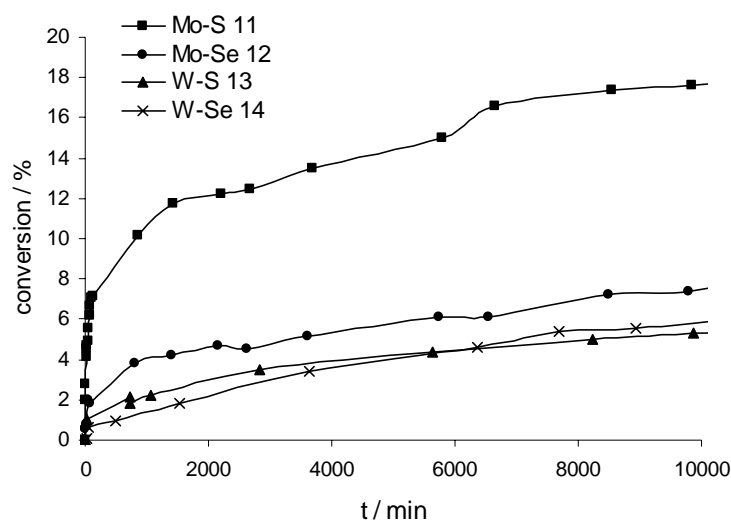
In order to assess the oxo transfer behavior of the complexes with phenol containing ligands a series of reactions were carried out with **11-14**. Herein we used two biological substrates, nitrate and dimethyl sulfoxide (DMSO), as oxidizer, and phosphines (PPh<sub>3</sub>) as reducing substrate.

First of all, the catalytic properties for the oxygen atom transfer reaction from  $\text{NO}_3^-$  to  $\text{PPh}_3$  were investigated for compounds **11-14** under the exact same conditions according to Scheme 12.

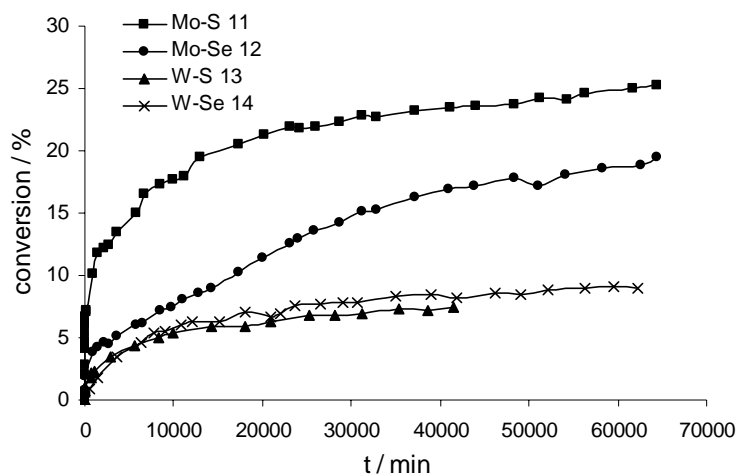


**Scheme 12.**

Nitrate reduction by  $\text{PPh}_3$  in the presence of molybdenum complexes as catalysts is well known.<sup>[167]</sup> In our investigation, the catalytic system involved complex (**11-14**),  $\text{PPh}_3$  and  $(\text{Bu}_4\text{N})(\text{NO}_3)$  with a ratio 1:10:20 in  $\text{CDCl}_3$  at room temperature.  $\text{PPh}_3$  consumption and  $\text{OPPh}_3$  production were confirmed by  $^{31}\text{P}$  NMR spectroscopy. Without catalyst no nitrite is produced under these conditions. At the initial stage 0-5795 min (Figure 40 (a)) catalytic reactions were carried out without colour change for all solutions, which demonstrate that the catalytic cycles were performed corresponding to the reactions 1 and 2.



(a)



(b)

**Figure 40.** Conversion of  $\text{PPh}_3$  oxidized by  $\text{NO}_3^-$  with time for complexes **11-14**. (a) the initial stage; (b) the whole process.

In this stage, the conversion of  $\text{PPh}_3$  to  $\text{OPPh}_3$  reached 15% for catalyst **11**, while the conversions catalyzed by **12**, **13** and **14** were lower and only reach 6% for **12**, 4% for **13** and **14**. At ca. 5795 min, the curves of **13** and **14** intersect. The conversions decreased according to this sequence:  $[\text{MoO}_2\text{L}^{\text{S}}]$  (**11**) >  $[\text{MoO}_2\text{L}^{\text{Se}}]$  (**12**) >  $[\text{WO}_2\text{L}^{\text{S}}]$  (**13**) >  $[\text{WO}_2\text{L}^{\text{Se}}]$  (**14**). This maybe is an indication that molybdenum compounds have much better catalytic activity than their tungsten analogues and sulfur containing compounds are better catalysts than their selenium containing analogues at least for this kind of compounds. Hereafter all reactions were accompanied by a gradual color change. The solution for **11** changes from dark purple finally to yellow-red, for **12** from dark purple to yellow and for both **13** and **14** from deep red to light red. The overall development of the conversion of  $\text{PPh}_3$  to  $\text{OPPh}_3$  with time is shown in Figure 40 (b). The increases of conversion of  $\text{PPh}_3$  to  $\text{OPPh}_3$  for the four compounds are very slow, especially for tungsten compounds **13** and **14** (lower than 10%), and almost tend to level. The developing trend combined with the color change is probably caused by the

formation of  $\mu$ -oxo dimers in reaction 3.



Due to the presence of an equilibrium in reaction 3,  $\text{PPh}_3$  will be oxidized slowly. When the equilibrium of the whole process is reached, the conversion of  $\text{PPh}_3$  will be maintained at a constant level.

As a further example of the reactivity complexes **11-14** were treated with 2.5-15 equiv  $\text{PPh}_3$  in degassed, dry  $\text{DMSO-}d_6$  solution, respectively. The developments of the  $\text{PPh}_3$  to  $\text{OPPh}_3$  for catalysts **11-14** over time with different catalyst: $\text{PPh}_3$  ratios are shown in Figure 41. In this case, compounds **11** and **13** catalyzed completely the reaction of  $\text{PPh}_3$  to  $\text{OPPh}_3$  considerably fast with different quantities of substrate except for the ratio of **11**: $\text{PPh}_3 = 1:15$  (Figure 41 (a) and (c)). They were all accomplished within 25 min and no colour changes were observed. Exceptively, the catalytic reaction of **11** with 15 equiv  $\text{PPh}_3$  exhibited different behavior. The solution started with a colour change from dark purple to brown at about 50% conversion (Figure 41 (b)), which can be likely attributed to the formation of a  $\mu$ -oxo dimer. A conversion of 100% was reached for all catalyzed reactions by **14** in which  $\text{PPh}_3$  was completely oxidized with in 27 h (Figure 41 (d)). They show no colour change, either. However, both oxo-transfer reactions catalyzed by **12** with two different ratios of catalyst and  $\text{PPh}_3$  exhibited the same behavior. First the conversion of  $\text{OPPh}_3$  developed relatively fast within 10% conversion. After that the colour of solutions changed gradually from dark purple to red-yellow and the conversion increased very slowly, which can also be explained by the formation of a  $\mu$ -oxo dimer as well.

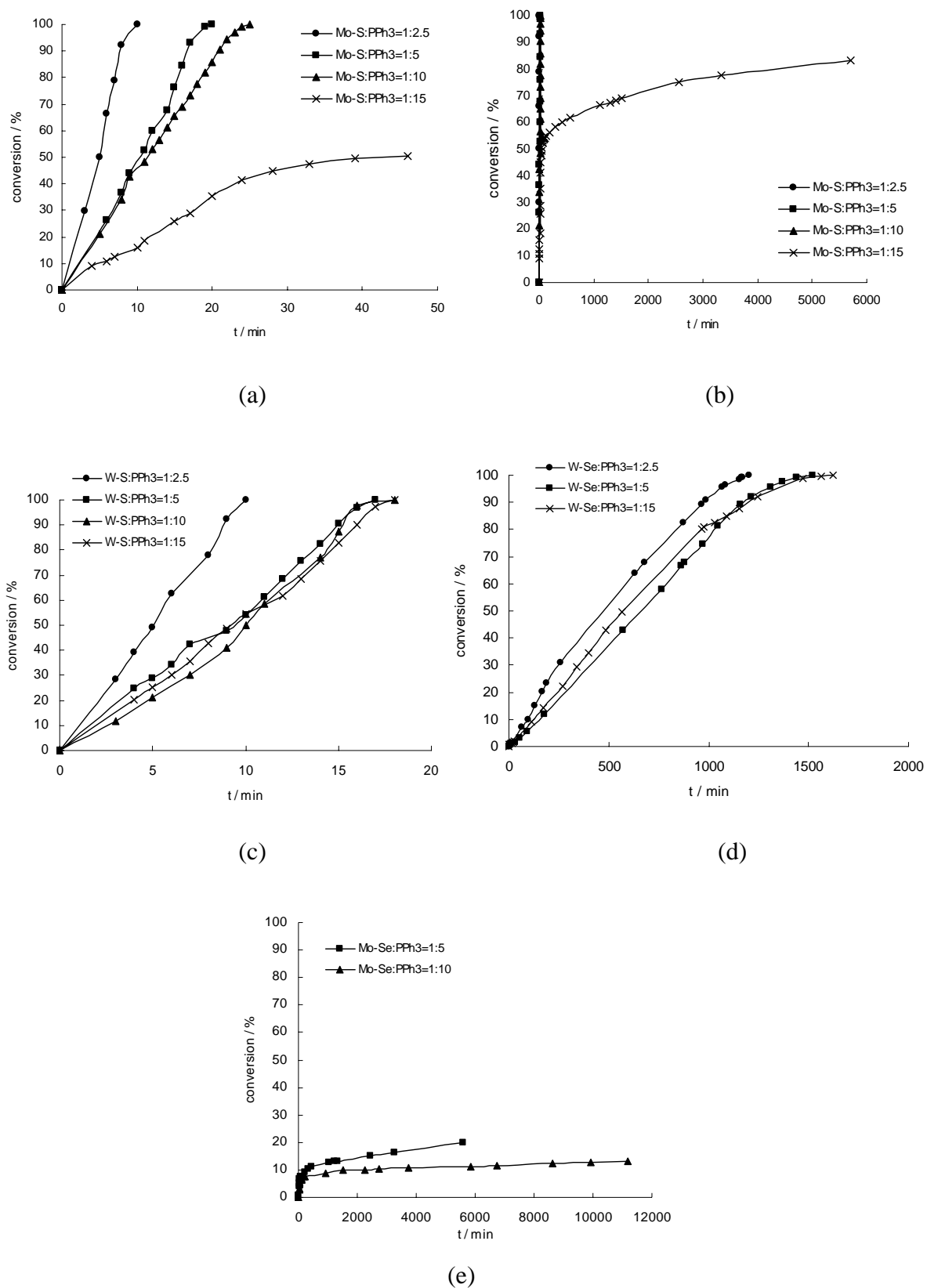


**Figure 41.** Conversion of  $\text{PPh}_3$  oxidized by DMSO with time with different catalyst: $\text{PPh}_3$  ratios (a) and (b) for complex **11**, (c) for complex **13**, (d) for complex **14** and (e) for complex

## 12.

The  $k_{\text{obs}}$  values determined from exponential fits ( $[\text{OPPh}_3]_t/[\text{PPh}_3]_0=1-\exp(-k_{\text{obs}}\cdot t)$ ) were calculated for all reactions catalyzed by **11-14** (for the reactions in which  $\mu$ -oxo dimers were formed the  $k_{\text{obs}}$  was calculated at the initial stage). In Figure 42,  $k_{\text{obs}}$  values are represented vs.  $\text{PPh}_3$  concentration. The trace in Figure 42 indicates that the reaction rate decreases as the  $\text{PPh}_3$  concentration increases, attaining a constant value. Further increases in the concentration of  $\text{PPh}_3$  have no effect on the reaction rate.

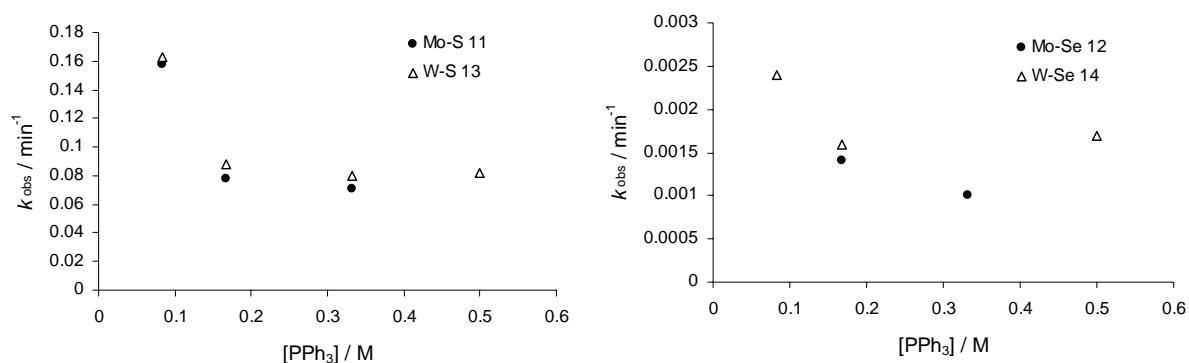


**Figure 42.** Dependence of the  $k_{\text{obs}}$  on the concentration of  $\text{PPh}_3$  in DMSO for **11-14**.

Through the comparison with the  $k_{\text{obs}}$  values under the same ratio of catalyst and  $\text{PPh}_3$  in DMSO for **11-14**, we can conclude that in this kind of catalytic reactions, tungsten compounds show better catalytic behavior than molybdenum analogues, and sulfur containing compounds have higher catalytic ability than selenium analogues.

Interestingly, the exchange of metals (Mo and W) causes a different influence on the catalytic abilities of compounds for  $\text{NO}_3^-$  and DMSO as the oxidizing substrates. The replacement of sulfur by selenium in ligands makes the compounds have accordant catalytic behaviors for the

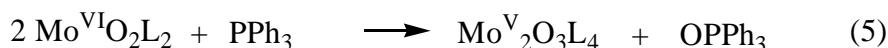
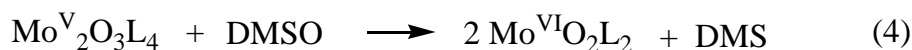
two substrates. The catalytic properties of molybdenum **11** and **12** for the oxygen atom transfer reaction from DMSO to PPh<sub>3</sub> are reverse to those of complexes **7** and **8**, which may be due to the influences of two phenolate groups in ligands on the coordinations of S or Se to molybdenum atom. In general, the four compounds catalyze the oxygen atom transfer reaction from DMSO to PPh<sub>3</sub> much more effective than from NO<sub>3</sub><sup>-</sup> to PPh<sub>3</sub>.

#### 2.7.4. Catalytic oxo-transfer activities of **15** and **16**

Generally speaking, dioxomolybdenum(VI) complexes are extensively employed as excellent catalysts for oxo transfer reactions as introduced above. A frequently used model reaction is the oxidation of triphenylphosphine by DMSO. The formation of  $\mu$ -oxo-dimers during the reduction of MoO<sub>2</sub> complexes is normally considered to be capable of breaking any catalytic cycle unless there is an equilibrium between the dimer of the M<sup>VI</sup>O<sub>2</sub> complexes and a M<sup>IV</sup>O species. However, the formation of  $\mu$ -oxo-bridged dimers does not necessarily exclude reversible oxo-transfer reactions. The reactivity itself to oxygen atom transfer in some cases<sup>[177,178]</sup> has been considered. The molybdenum(V) compounds may be oxidized by a common oxidizing agent, such as DMSO, Ph<sub>2</sub>SO and pyridine N-oxide. The reversibility of the oxo-transfer reactions involving dinuclear oxomolybdenum(V) complexes sometimes strongly depends on electronic features of the ligands rather than steric effects.<sup>[112]</sup>

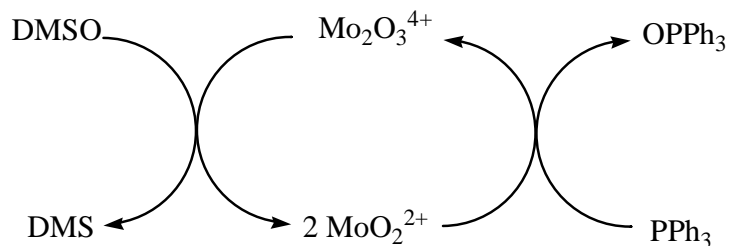
In order to assess the oxo transfer behavior of such complexes, oxo-transfer reactions of the molybdenum(V) compounds **15** and **16** were studied by the use of PPh<sub>3</sub> in DMSO under the exact same conditions. The experiments were performed at room temperature in dry deoxygenated DMSO-*d*<sub>6</sub> by treating the catalyst **15** or **16** with 10 equivalents of PPh<sub>3</sub> (2×10<sup>-4</sup> mol) in NMR tube. The reaction was monitored with <sup>31</sup>P-NMR spectroscopy. During the

reactions only two phosphorous signals were observed: one for  $\text{PPh}_3$  and one for  $\text{OPPh}_3$ . During the catalytic process for **15** as catalyst the reaction solution changed rapidly its colour from deep red to yellow at the beginning of the reaction (about 7 min). Thereafter the colour of the solution remained yellow and unchanged. For **16** as catalyst the colour change from deep red to green yellow finally to light brown was observed as well, but the change was slower in comparison to that for **15**. When the reaction carried out to about 6677 min, the colour change stopped and the colour light brown was kept to the end of the reaction. The colour change for both reactions can be probably elucidated by the following assumptions (reactions (4) and (5)):



First, oxidations of the oxomolybdenum(V) complexes occur according to reaction (4). The possibility was well illustrated by previous reports.<sup>[112,177,178]</sup> Another useful information can be provided by the observation that the colors of the solutions for **15** and **16** in DMSO also change from deep red to yellow and light brown, respectively. Subsequently, the reduction of the mononuclear dioxomolybdenum(VI) compounds, achieved by the reaction with  $\text{PPh}_3$ , leads to dinuclear  $\mu$ -oxomolybdenum(V) complexes (reaction (5)). This process has been conformed for **15**<sup>[134,135]</sup> and some dinuclear molybdenum(V) complexes<sup>[177]</sup>. Due to a large excess of DMSO in contrast with  $\text{PPh}_3$ , the dinuclear  $\mu$ -oxomolybdenum(V) complexes and  $\text{PPh}_3$  thoroughly converted to mononuclear dioxomolybdenum(VI) complexes and  $\text{OPPh}_3$ , respectively. The similarity of the colour change between the catalytic reaction mixtures and the solutions of only complexes in DMSO also provides the favourable evidence for the above assumption. The entire process can be summarized in Scheme 13.





**Scheme 13.**

The development of the conversion of  $\text{PPh}_3$  to  $\text{OPPh}_3$  for both complexes **15** and **16** over time is shown in Figure 43.

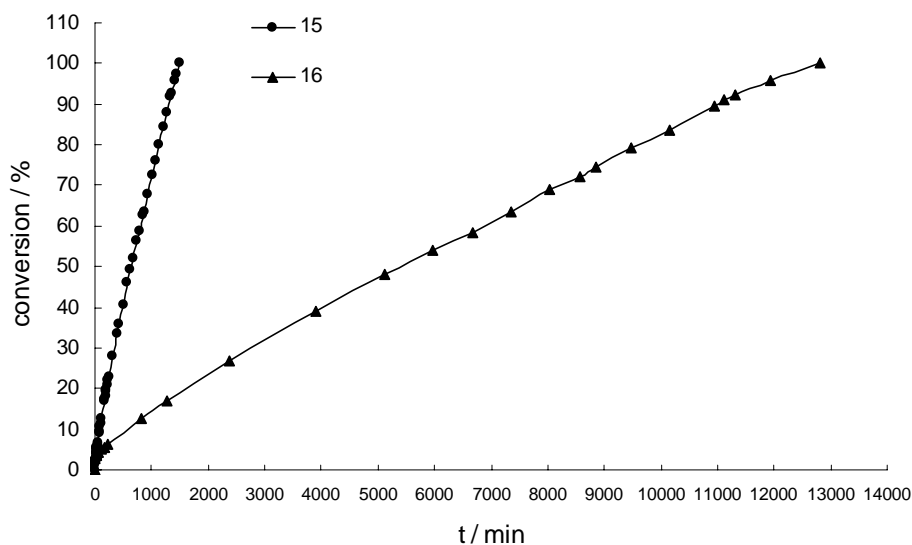


**Figure 43.** Oxidation of  $\text{PPh}_3$  to  $\text{OPPh}_3$  by  $\text{DMSO-}d_6$  at r. t. as a function of time for **15** and **16**.

The  $\text{PPh}_3$  was completely oxidized in only 1497 min (about 1 day) for **15**, whereas it took 12801 min (nearly 9 days) for **16**. The thionato containing complex **15** shows considerably higher catalytic activity than its selenolato containing analogue **16**. The function of the reactions for **15** and **16** is almost linear. These suggest that the catalytical performance of both compounds is strongly influenced by an exchanged of ligand atoms sulfur and selenium even

---

though no strong influence on the structures could be observed. This catalytic behavior of **15** and **16** is disparate from that of **7** and **8** shown above. This can possibly be attributed to the following reasons. On the one hand, the two ligand systems are different although they contain sulfur or selenium atoms. On the other hand, the reaction mechanisms are different due to the disparity of oxidation states of the molybdenum center even though they are all dinuclear complexes.

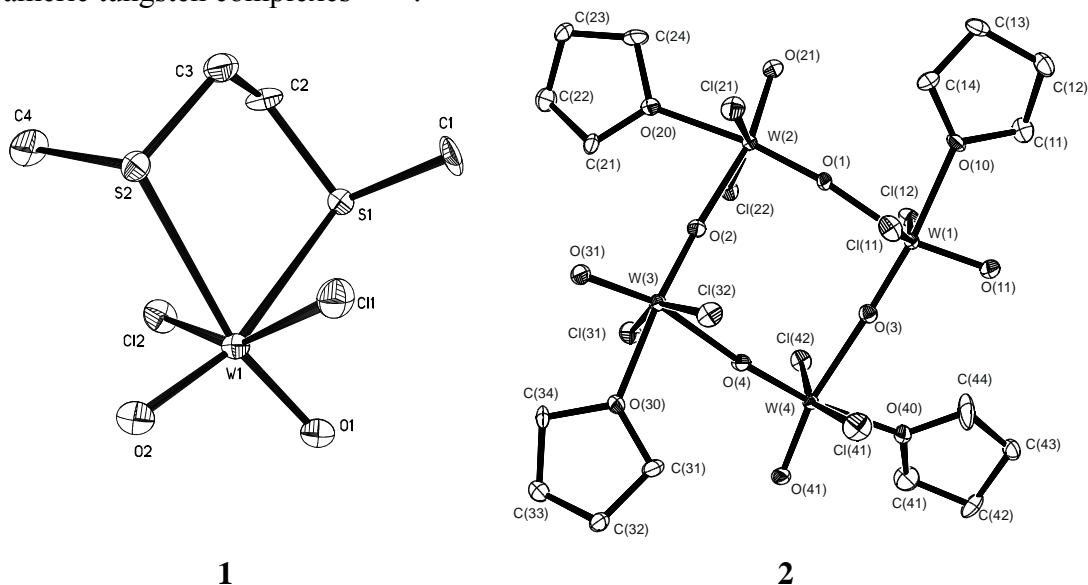
### 3. Summary and Outlook

#### 3.1. Summary

Molybdenum and tungsten can be found at the active sites of the molybdopterin-containing oxygen-atom-transfer enzymes (OATs)<sup>[28]</sup>. The distribution of the metals is quite interesting; molybdenum is found mainly in mesophilic organisms while tungsten is found mainly in thermophilic and hyperthermophilic microorganisms. Another interesting diversity of these enzymes is that in the DMSO reductase family<sup>[7]</sup> (molybdenum enzymes with two molybdopterin ligands) the metal is bound to the peptide moiety through either serine (O)<sup>[32]</sup>, cysteine (S)<sup>[33]</sup>, selenocysteine (Se)<sup>[34]</sup> or aspartate (O, mono- or bidentate)<sup>[35]</sup>. However, until today the reasons for the distribution of the two metals and the selectivity of the different types of amino acid ligands in these enzymes are unknown. In order to obtain more insight into these questions we have synthesized and characterized corresponding molybdenum and tungsten complexes as functional models by replacing molybdenum by tungsten, varying the ligand atoms (O/S/Se) and investigated their structural, electrochemical and oxygen atom transfer properties.

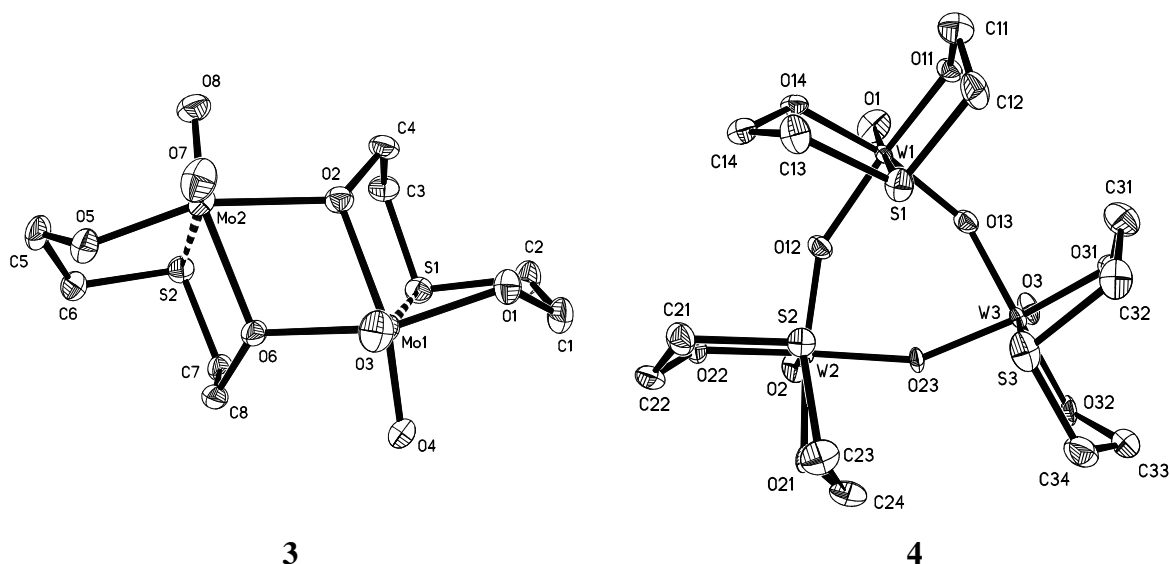
First of all we investigated tungsten complexes with neutral sulfur and oxygen donor ligands.  $\text{WO}_2\text{Cl}_2[\text{MeS}(\text{CH}_2)_2\text{SMe}]$  (**1**) and  $[\text{WO}_2\text{Cl}_2(\text{THF})]_4$  (**2**) were obtained by an analogous method to the preparation of  $\text{WO}_2\text{Cl}_2(\text{DME})$ <sup>[76]</sup>. A structural and electrochemical comparison of **1** with the recently published analogous molybdenum compound and the DME analogs of molybdenum and tungsten was undertaken. Their structures are almost identical. The molybdenum compounds have potentials that are higher than their tungsten analogs and the complexes with sulfur ligand atoms have potentials that are higher than their counterparts

with oxygen ligand atoms. Changing the metal atoms has a much more significant influence on the redox potentials than changing the ligand atoms. However, these differences of the redox potentials are all small. The obtained crystal structure of **2** confirmed a previous deduction<sup>[76]</sup> and exhibited a novel tetrameric structure, which is different from two published tetrameric tungsten complexes<sup>[81,82]</sup>.



The second part of this work mainly focused on the molybdenum and tungsten complexes with tridentate bis anionic thioether and selenoether ligands. The simple replacement of acetylacetonate ligands in precursors  $\text{MO}_2(\text{acac})_2$  ( $\text{M} = \text{Mo}, \text{W}$ ) by alkali salts of alkoxylates containing a thio- or selenoether function resulted in the formation of compounds  $[\{\text{MoO}_2[\text{O}(\text{CH}_2)_2\text{S}(\text{CH}_2)_2\text{O}]\}_2]$  (**3**),  $[\{\text{WO}_2[\text{O}(\text{CH}_2)_2\text{S}(\text{CH}_2)_2\text{O}]\}_3]$  (**4**) and  $[\{\text{MO}_2[\text{O}(\text{CH}_2)_2\text{Se}(\text{CH}_2)_2\text{O}]\}_n]$  ( $\text{M} = \text{W}$  (**5**),  $\text{Mo}$  (**6**)). Crystal structures of **3** and **4** were obtained. Interestingly the former gave a dimeric and the latter a trimeric complex. For **3** and **4** as well as for the virtual molybdenum trimer and the tungsten dimer, DFT calculations were performed in order to better understand the formation of two significantly different complexes for molybdenum and tungsten with the same ligand and by the same preparation method. A result can be made that molybdenum forms the dimeric structure, because it is able

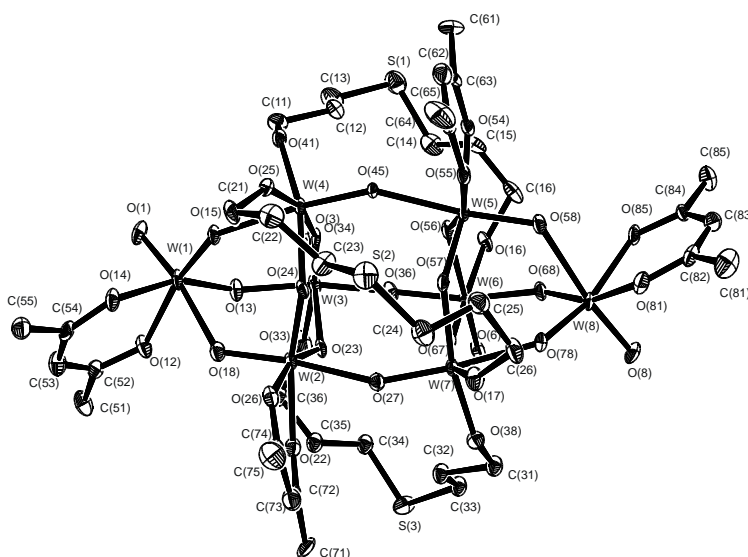
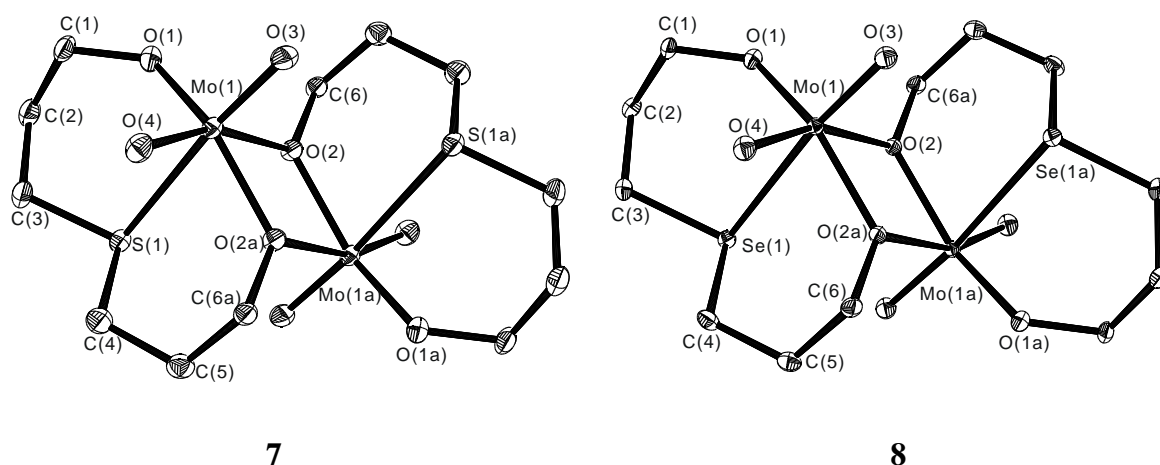
to keep both of the doubly bonded oxo ligands, and that tungsten forms the trimeric structure because it is able to form a stronger metal–sulfur interaction. In order to evaluate the influence of the metal and of the ligand atoms (S versus Se) on the redox properties, compounds **3**, **4**, and **5** were investigated by differential pulse voltammetry (DPV). The redox processes  $M^{VI} \leftrightarrow M^V$  and  $M^V \leftrightarrow M^{IV}$  for the molybdenum compound are at a higher voltage than those for the respective tungsten compound, and those for the tungsten–selenium compound are at a higher voltage than those for the tungsten–sulfur compound. An irreversible third redox process is caused by a structural reorganization of the molecule which takes place at ligand atoms.



Furthermore, by introduction of another  $\text{CH}_2$  group into the ligands backbones, bis(3-hydroxypropyl)sulfide and selenide were used as ligands to obtain a more flexible ligand system able to form stronger Mo-S and Mo-Se bonds. Molybdenum selenoether complex  $[\{\text{MoO}_2[\text{O}(\text{CH}_2)_3\text{Se}(\text{CH}_2)_3\text{O}]\}_2]$  (**8**) and its thioether analogue  $[\{\text{MoO}_2[\text{O}(\text{CH}_2)_3\text{S}(\text{CH}_2)_3\text{O}]\}_2]$  (**7**) as well as its tungsten analogue  $[\{\text{WO}_2[\text{O}(\text{CH}_2)_3\text{Se}(\text{CH}_2)_3\text{O}]\}_n]$  (**9**) were synthesized by similar synthetic methods. Crystals of **7** and **8** appear to be isomorphous and their electrochemical properties were compared. The

metal centered redox process ( $\text{Mo}^V \leftrightarrow \text{Mo}^VI$ ) is at lower voltage for **7** than **8**. The several attempts to prepare the thioether analogue of **9** failed. The reaction of  $\text{WO}_2(\text{acac})_2$  with bis(3-hydroxypropyl)sulfide in a molar ratio of 1:1.2 in refluxing acetonitrile led to the formation of  $[\text{W}_8\text{O}_{19}(\text{O}(\text{CH}_2)_3\text{S}(\text{CH}_2)_3\text{O})_3(\text{acac})_4]$  (**20**), an unprecedented polyoxotungstate.

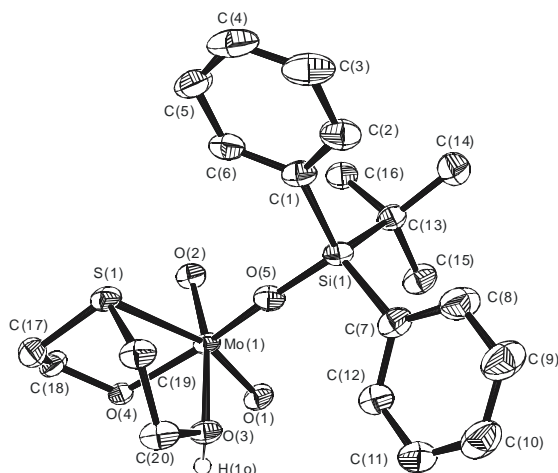
The molecular structure of **20** was analysed.



**20**

The monomerization of the dinuclear molybdenum(VI) dioxo complex **3** was achieved by a silylation reaction and generated the mononuclear molybdenum(VI) dioxo complex,  $[\text{MoO}_2(\text{O}(\text{CH}_2)_2\text{S}(\text{CH}_2)_2\text{OH})(\text{OSi}^t\text{Bu}^t\text{Ph}_2)]$  (**10**). The X-ray crystallographic study of **10** revealed that the structure of **10** has the same ligand positions as in the moiety of **3** and the

silyloxy is in place of one of the former bridging oxygen atoms.

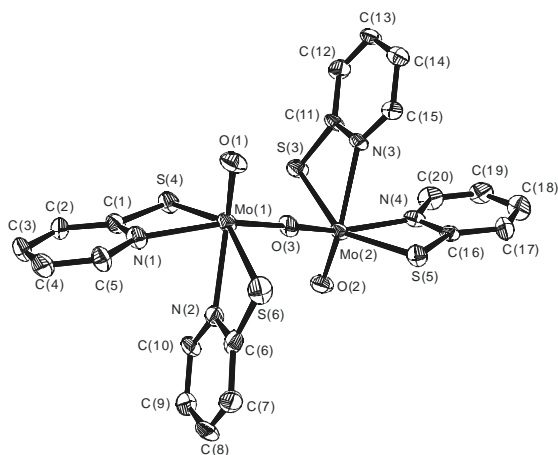


**10**

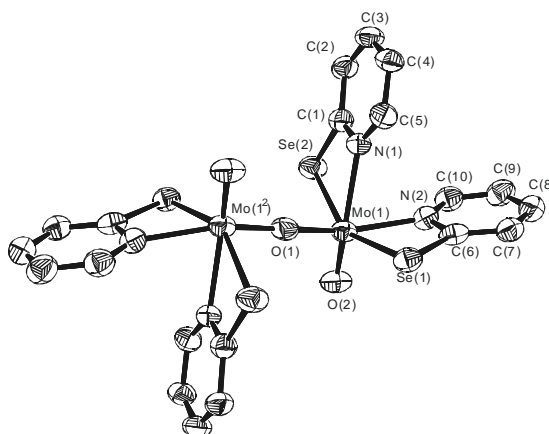
In the third part tridentate bisphenol ligands containing [O,X,O] donor atoms (X = S or Se) were used to generate novel molybdenum and tungsten complexes. The reaction of  $\text{MO}_2(\text{acac})_2$  with the ligands 2,2'-thio(or seleno)bis(4,6-di-*tert*-butylphenol) afforded complexes  $[\text{MoO}_2\text{L}^{\text{S}}]$  (**11**),  $[\text{MoO}_2\text{L}^{\text{Se}}]$  (**12**),  $[\text{WO}_2\text{L}^{\text{S}}]$  (**13**) and  $[\text{WO}_2\text{L}^{\text{Se}}]$  (**14**). Crystals suitable for X-ray diffraction could not be obtained. All analysis data characterized well the desired complexes **11–14**.

The fourth part of this work was focused on studies of molybdenum complexes with ligands containing S, Se and N donor atoms. Molybdenum complexes with bidentate heterocyclic thiones and selenones,  $[\text{Mo}_2\text{O}_3(\text{PyS})_4]$  (**15**),  $[\text{Mo}_2\text{O}_3(\text{PySe})_4]$  (**16**) and  $[\text{Mo}_2\text{O}_3(4\text{-CF}_3\text{-PymS})_4]$  (**17**), were all obtained by the similar reactions of the corresponding lithium thionates or selenatos with the molybdenum precursor  $[\text{MoO}_2\text{Cl}_2(\text{DME})]$  at  $-30\text{ }^\circ\text{C}$ . They all formed dinuclear  $\mu$ -oxomolybdenum(V) species maybe due to the corresponding ligands acting both as a reductant and as a ligand in the reactions. The crystal structures of **15**, **16** and **17** include the common  $[\text{Mo}_2\text{O}_3]^{4+}$  core. **15** and **16** are isomorphous. Their tungsten analogues  $[\text{WO}_2(\text{PyS})_2]$ ,  $[\text{WO}_2(\text{PySe})_2]$  and  $[\text{WO}_2(\text{PymS})_2]$  were also synthesized and evidenced by EI

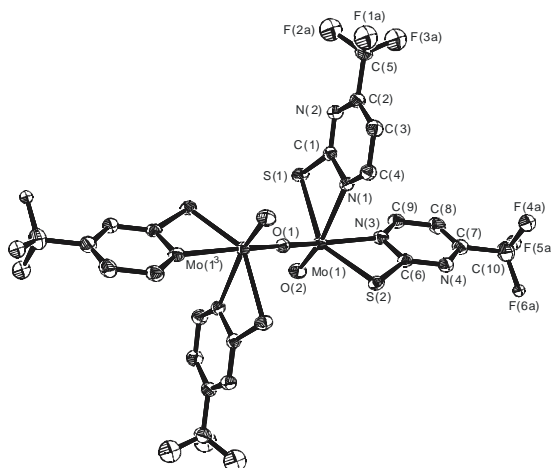
mass spectra, however the pure products can not be obtained.



15



16



17

All substances **1-21** have been fully characterized by analytical and spectroscopic techniques.

The solid state structures of the following compounds have been determined by means of

X-ray diffraction studies:  $\text{WO}_2\text{Cl}_2[\text{MeS}(\text{CH}_2)_2\text{SMe}]$  (**1**),  $[\text{WO}_2\text{Cl}_2(\text{THF})]_4$  (**2**),

$[\{\text{MoO}_2[\text{O}(\text{CH}_2)_2\text{S}(\text{CH}_2)_2\text{O}]\}_2]$  (**3**),  $[\{\text{WO}_2[\text{O}(\text{CH}_2)_2\text{S}(\text{CH}_2)_2\text{O}]\}_3]$  (**4**),

$[\{\text{MoO}_2[\text{O}(\text{CH}_2)_3\text{S}(\text{CH}_2)_3\text{O}]\}_2]$  (**7**),  $[\{\text{MoO}_2[\text{O}(\text{CH}_2)_3\text{Se}(\text{CH}_2)_3\text{O}]\}_2]$  (**8**),

$[\text{MoO}_2(\text{O}(\text{CH}_2)_2\text{S}(\text{CH}_2)_2\text{OH})(\text{OSiBu}^t\text{Ph}_2)]$  (**10**),  $[\text{Mo}_2\text{O}_3(\text{PyS})_4]$  (**15**),  $[\text{Mo}_2\text{O}_3(\text{PySe})_4]$  (**16**),

$[\text{Mo}_2\text{O}_3(4\text{-CF}_3\text{-PymS})_4]$  (**17**),  $[\text{H}:\text{C}]_2[\text{Mo}_6\text{O}_{19}]$  (**18**),  $[\text{H}:\text{C}]_2[\text{W}_6\text{O}_{19}]$  (**19**),

$[\text{W}_8\text{O}_{19}(\text{O}(\text{CH}_2)_3\text{S}(\text{CH}_2)_3\text{O})_3(\text{acac})_4]$  (**20**) and  $\text{MoO}_2(\text{dipic})$  (**21**).



Catalytical properties for oxygen atom transfer reaction were investigated in the last part. The oxygen atom transfer properties of **7** and **8** (though rather poor) are surprisingly different. At least for the transfer of one oxygen atom from DMSO to PPh<sub>3</sub> the selenium containing compound **8** is a better catalyst than the sulfur containing compound **7**. They probably employ different mechanisms, a consecutive mechanism for **7** and a concerted mechanism for **8**. The mononuclear compound with silyloxy **10** exhibits much higher catalytic activity than its dimeric precursor **3**. The kinetics of oxo-transfer reaction from DMSO to PPh<sub>3</sub> catalyzed by **10** with different catalyst:PPh<sub>3</sub> ratios were investigated. The results indicate that the catalytic oxo-transfer reactivity of **10** is not influenced by the concentration of PPh<sub>3</sub> in the investigated range. The catalytic oxo-transfer properties of **11–14** were investigated by oxo-transfer reactions from nitrate to PPh<sub>3</sub> with a ratio of complex (**11–14**):PPh<sub>3</sub>:(Bu<sub>4</sub>N)(NO<sub>3</sub>) = 1:10:20 and from DMSO to PPh<sub>3</sub> with different catalyst:PPh<sub>3</sub> ratios. For the catalytic reaction from nitrate to PPh<sub>3</sub> molybdenum compounds have much better catalytic activity than their tungsten analogues and sulfur containing compounds are better catalysts than their selenium containing analogues at least for this kind of compounds with phenol containing ligands. For the catalytic reaction from DMSO to PPh<sub>3</sub> tungsten compounds show better catalytic behavior than molybdenum analogues, and sulfur containing compounds have higher catalytic ability than selenium analogues. In comparison, the four compounds catalyze the oxygen atom transfer reaction from DMSO to PPh<sub>3</sub> much more effectively than from NO<sub>3</sub><sup>-</sup> to PPh<sub>3</sub> and the influence of the concentration of PPh<sub>3</sub> on the reaction rate at high concentration range is not very significant. The catalytic oxo-transfer abilities of the molybdenum(V) compounds **15** and **16** were studied by the use of PPh<sub>3</sub> in DMSO. The thionato containing complex **15** shows considerably higher catalytic activity than its selenolato containing analogue **16**. All the

catalytical studies for oxo-transfer reactions indicate that an exchange of ligand atoms sulfur versus selenium of the same ligand system can cause different mechanisms and certainly different activities even though no strong influence on other investigated properties could be observed.

### **3.2. Outlook**

This thesis concentrates on investigating synthesis, characterization, redox potential and catalytic oxo-transfer properties of molybdenum and tungsten complexes with sulfur and selenium containing ligands as functional models of the molybdopterin- containing OAT enzymes. These results lead to a general extension of this work as follows:

- (1) A novel way for the formation of a mononuclear molybdenum(VI) dioxo complex from a dinuclear complex by an uncommon silylation reaction provides the possibility for the monomerization of other dimeric and trimeric compounds presented in this thesis.
- (2) The terminal oxo ligands or the silyloxy group of mononuclear complexes could be rendered as reactive sites which may be substituted by other ligand systems to generate novel complexes.

## 4. Experimental Section

### 4.1. General Procedures

All manipulations were carried out under a purified dry nitrogen atmosphere using standard Schlenk techniques<sup>[179]</sup>. All glassware used in all the manipulations was oven-dried at 150 °C for at least 24 h, assembled hot and cooled under high vacuum prior to use. All solvents were distilled prior to use under nitrogen using conventional drying agents<sup>[180]</sup> (dichloromethane over CaH<sub>2</sub>, toluene over sodium/benzophenone ketyl and diphenylether, hexane over potassium/sodium/benzophenone ketyl and diphenylether, diethylether over sodium/benzophenone ketyl, tetrahydrofuran over potassium /benzophenone ketyl, methanol over Mg(OMe)<sub>2</sub> and DMSO distilled) and were stored over 4-Å molecular sieves.

### 4.2. Physical Measurements

Melting points were measured in sealed glass capillaries on a Büchi B-540 melting point apparatus and are not corrected.

Elemental analyses were performed by the Analytisches Chemisches Laboratorium des Instituts für Anorganische Chemie der Universität Göttingen.

IR spectra were recorded as KBr pellets on a Bio-Rad Digilab FTS-7 spectrometer from 4000 to 300 cm<sup>-1</sup>. In most cases all the absorption (weak to very strong) are listed.

NMR spectra were recorded on Bruker Avance 200, Bruker Avance 300 and Bruker Avance 500 NMR spectrometers. Chemical shifts are reported in ppm with referenc to external standards, SiMe<sub>4</sub> for <sup>1</sup>H, <sup>13</sup>C and <sup>29</sup>Si nuclei, SeMe<sub>2</sub> for <sup>77</sup>Se nuclei and 85% H<sub>3</sub>PO<sub>4</sub> for <sup>31</sup>P nuclei. Downfield shifts from the reference are quoted positive, upfield shifts are assigned

negative values. Heteroatom NMR spectra were recorded  $^1\text{H}$  decoupled. All NMR-grade solvents were dried prior to use. If not otherwise stated, the operation temperature was in the range from 293 to 300 K. The symbols are assigned as follows: s = singlet, d = doublet, t = triplet, q = quartet, sept = septet and m = multiplet.

Mass spectra were obtained with a Finnigan MAT system 8230 or Varian MAT CH5 instrument (70 eV) by EI-MS methods.

UV/Vis samples were prepared in a well-maintained glove-box with dry solvents and measured on a Varian Cary 5000 spectrophotometer.

The susceptibility measurements were carried out with a Quantum-Design MPMS-5S SQUID magnetometer in the range from 295 to 395 K at 5000 G. The powdered samples were contained in a gel bucket and fixed in a nonmagnetic sample holder. Each raw data file for the measured magnetic moment was corrected for the diamagnetic contributions of the sample holder and the gel bucket.

X-ray crystal structure determinations and refinements. Crystallographic data for compounds **1**, **3**, **4**, **7**, **10**, **15**, **16** and **17** were collected on a STOE IPDS II array detector system with four-circle instrument and the diffraction data for the compounds **2**, **8**, **18**, **19**, **20** and **21** were measured on a Bruker AXS instrument using graphite-monochromated Mo-K $\alpha$  ( $\lambda = 0.71073$  Å) radiation. The data for all the compounds were collected at low temperature except for **1** (for exact values see Tables in section 6). The data reduction and space group determination were carried out using Siemens SHELXTL program.<sup>[181]</sup> All structures were solved by direct methods (SHELXS-97)<sup>[182]</sup> and refined with all data by full-matrix least-squares methods on  $F^2$  using SHELXL-97.<sup>[183]</sup> All non-hydrogen atoms were refined anisotropically, and hydrogen atoms were attached at idealized positions on carbon atoms with  $U_{\text{iso}}$  related to the

$U_{\text{iso}}$  of the parent atoms and were refined with the riding model, or by difference Fourier synthesis and refined with isotropically. The various advanced features (e.g. restraints and constraints) of SHELXL programs were used to treat the disordered groups, lattice solvents such as THF, and the hydrogen atoms. The crystal data for all compounds along with the final residuals and other pertaining details are tabulated in Section 6.

### 4.3. DFT calculations

All calculations for compounds **3** and **4** have been carried out with the Gaussian G03<sup>[184]</sup> program package using the implemented DFT variant B3LYP<sup>[185,186]</sup> (Becke three-parameter exchange functional B3 and the Lee-Yang-Parr correlation functional LYP). A basis consisting of the well established small core ECP<sup>[187]</sup> (for Mo and W), 3-21g<sup>[188]</sup> (for carbon and hydrogen) and following a proposal by K. Peterson,<sup>[189,190]</sup> a modified 6-31G basis including double diffuse functions [6-31G(d', p')] to give a suitable description of the lone pairs on oxygen and sulfur was used.

All structures were fully optimized without employing any symmetry constraints. The starting geometries were taken from experimental data. Analytical frequency calculations were performed to verify these structures as local minima.

### 4.4. Electrochemistry

Electrochemical measurements were performed with an AUTOLAB PGSTAT12 potentiostat/galvanostat with a glassy carbon working electrode, a platinum wire reference electrode, and a platinum wire auxiliary electrode, in acetonitrile solutions within a glove box under argon. The supporting electrolyte was Bu<sub>4</sub>NPF<sub>6</sub> (0.1 M) used as received from Fluka.

Acetonitrile used for the electrochemistry was predried with  $\text{CaCl}_2$ , dried by reflux over  $\text{CaH}_2$  for 2 d, and distilled onto freshly regenerated molecular sieves 3 Å. Referencing was done internally using the ferrocene/ferrocenium couple. The temperature during the measurements was controlled with a Julabo refrigerated/heating circulator FP50-MV at 25 °C. The solutions were prepared within a glove box by dissolving the  $\text{Bu}_4\text{NPF}_6$  electrolyte ( $10^{-3}$  mol) and the compounds ( $10^{-6}$  mol for **1**,  $[\text{MoO}_2\text{Cl}_2(\text{MeS}(\text{CH}_2)_2\text{SMe})]$ ,  $[\text{MoO}_2\text{Cl}_2(\text{DME})]$ ,  $[\text{WO}_2\text{Cl}_2(\text{DME})]$ , **3**, **4** and **5**; approximately  $10^{-7}$  to  $10^{-8}$  mol for **7** and **8**) in acetonitrile (10 mL) to give solutions ( $10^{-4}$  M for **1**,  $[\text{MoO}_2\text{Cl}_2(\text{MeS}(\text{CH}_2)_2\text{SMe})]^{[78]}$ ,  $[\text{MoO}_2\text{Cl}_2(\text{DME})]^{[75]}$ ,  $[\text{WO}_2\text{Cl}_2(\text{DME})]^{[76]}$ , **3** and **4**;  $10^{-5}$  to  $10^{-6}$  M for **7** and **8**). For reasons of poor solubility, compound **5** could only be prepared as an approximately  $0.5 \times 10^{-5}$  M solution.

#### 4.5. Catalytic oxo-transfer reactions

In sealed NMR tubes a catalyst (0.02 mmol for **7**, **8**, and **10-14**) and  $\text{PPh}_3$  in different quantities (0.10, 0.20, 0.40, 0.60 mmol for **7**; 0.10, 0.20, 0.30, 0.40, 0.60 mmol for **8** and 0.05, 0.10, 0.20, 0.30 mmol for **10-14**) were mixed in degassed, dry  $\text{DMSO}-d_6$  (0.6 mL) solution, respectively. The reactions were monitored by  $^{31}\text{P}$  NMR spectroscopy.

The oxygen atom transfer reactions of compounds **7** and **8** of 0.02 mmol with 0.04 mmol  $\text{PPh}_3$  (Mo: $\text{PPh}_3$  ratio of 1:1) in 0.6 mL  $\text{CDCl}_3$  as solvent were carried out in sealed NMR tubes and were monitored by  $^{31}\text{P}$  NMR spectroscopy.

A 1:10 (1:20 for **3**) mixture of catalyst (0.02 mmol for compounds **15** and **16**, 0.01 mmol for **3**) and  $\text{PPh}_3$  (0.20 mmol) in degassed, dry  $\text{DMSO}-d_6$  (0.6 mL) in a sealed NMR tube was monitored by  $^{31}\text{P}$  NMR spectroscopy. The same procedure was applied to **11-14** with the difference that  $\text{DMSO}-d_6$  was replaced by 0.40 mmol  $(\text{Bu}_4\text{N})(\text{NO}_3)$  and 0.6 mL  $\text{CDCl}_3$ .

#### 4.6. Starting materials

Commerically available chemicals were purchased from Fluka or Aldrich and used as received.  $(\text{Me}_3\text{Si})_2\text{O}$  and  $\text{Bu}^t\text{Ph}_2\text{SiCl}$  were freshly distilled prior to use. The other compounds used in this thesis were prepared according to published procedures:  $[\text{MoO}_2\text{Cl}_2(\text{DME})]^{[131]}$ ,  $[\text{WO}_2\text{Cl}_2(\text{DME})]^{[76]}$ ,  $[\text{MoO}_2\text{Cl}_2(\text{MeS}(\text{CH}_2)_2\text{SMe})]^{[78]}$ ,  $\text{WOCl}_4^{[191]}$ ,  $\text{MeSCH}_2\text{CH}_2\text{SMe}^{[192]}$ ,  $[\text{WO}_2(\text{acac})_2]^{[64]}$ , bis(2-hydroxyethyl)selenide<sup>[193]</sup>,  $[\text{MoO}_2(\text{acac})_2]^{[194]}$ , bis(3-hydroxypropyl)selenide<sup>[193]</sup>, 3,4-dimethyl-N,N'-bis-isopropylimidazolyl carbene  $([\text{CN}(i\text{Pr})\text{C}_2\text{Me}_2\text{N}(i\text{Pr})])^{[195]}$ ,  $[\text{MoO}_2\text{Cl}_2]^{[132]}$ ,  $[\text{WO}_2\text{Cl}_2]^{[191]}$ ,  $\text{H}_2\text{L}^{\text{S}}$  (2,2'-Thiobis(4,6-di-*tert*-butylphenol))<sup>[110]</sup>,  $\text{H}_2\text{L}^{\text{Se}}$  (2,2'-Selenobis(4,6-di-*tert*-butylphenol))<sup>[71]</sup>,  $\text{PySeH}^{[72]}$ .

#### 4.7. Syntheses of compounds 1-21

##### 4.7.1. synthesis of $\text{WO}_2\text{Cl}_2(\text{MeSCH}_2\text{CH}_2\text{SMe})$ (**1**)

Liquid  $(\text{Me}_3\text{Si})_2\text{O}$  (0.341 g, 2.10 mmol) was added to a suspension of freshly sublimed  $\text{WOCl}_4$  (0.68 g, 2.00 mmol) in  $\text{CH}_2\text{Cl}_2$  (20 mL). The orange crystals were slowly consumed to give a yellow solution. After stirring for approximately 1.5 h at room temperature, a light yellow solid precipitate was obtained. A solution of  $\text{MeSCH}_2\text{CH}_2\text{SMe}$  (0.366 g, 3.00 mmol) in  $\text{CH}_2\text{Cl}_2$  (10 mL) was added, and the reaction mixture was stirred overnight and filtered to remove the brownish precipitate. The clear yellow filtrate was concentrated at room temperature in vacuo until the solid began to precipitate. After keeping this solution at 4 °C overnight colorless crystals were obtained. The crystals were collected on a filter, washed once with diethyl ether (5 mL), and dried in vacuo. Yield: 0.53 g, 65%. M.p. 128–130 °C.

$C_4H_{10}Cl_2S_2O_2W$  (407.90): calcd. C 11.75, H 2.46; found C 11.95, H 2.54. IR (KBr):  $\tilde{\nu}$  = 3013 (m), 2966 (m), 2933 (m), 1868 (w), 1618 (w), 1424 (m), 1326 (w), 1259 (s), 1179 (w), 1145 (w), 1099 (m), 1028 (m), 956 (vs), 917 (vs), 883 (s), 841 (s), 803 (s), 646 (s), 444 (w), 363 (m), 344 (vs)  $cm^{-1}$ . EI-MS (70 eV):  $m/z$  (%) = 409 (1)  $[M^+]$ , 288 (100)  $[WO_2Cl_2]^+$ , 251 (49)  $[WO_2Cl]^+$ , 255 (12)  $[WCl_2]^+$ .

#### 4.7.2. synthesis of $[WO_2Cl_2(THF)]_4$ (**2**)

The compound was prepared using the same procedure described for **1**,  $WOCl_4$  (0.343 g, 1.00 mmol) in  $CH_2Cl_2$  (25 mL),  $(Me_3Si)_2O$  (0.174 g, 1.00 mmol) and THF (0.216 g, 0.264 mL, 3.00 mmol). The reaction mixture was stirred overnight and filtered to remove the pale blue precipitates. The clear blue filtrate was concentrated at room temperature in vacuo to about 10 mL, 5 mL diethyl ether was added. After keeping this solution at  $-30\text{ }^\circ C$  overnight colorless crystals formed. The crystals were collected on a filter, washed once with diethyl ether (5 mL) and dried in vacuo. Yield: 0.19 g, 53%. Mp:  $185\text{ }^\circ C$  dec. Elemental analysis: calcd. for  $C_{16}H_{32}Cl_8O_{12}W_4$  (1435.45): C 13.39, H 2.25, Cl 19.76; found: C 13.50, H 2.45, Cl 20.08; IR (KBr):  $\tilde{\nu}$  = 2962 (s), 1614 (m), 1446 (w), 1345 (w), 1297(w), 1261 (m), 1176 (w), 1088 (m), 988 (s), 802 (s), 639 (vs)  $cm^{-1}$ ; EI-MS (70 eV):  $m/z$  (%) = 288 (100)  $[WO_2Cl_2]^+$ , 251 (50)  $[WO_2Cl]^+$ , 200 (10)  $[WO_2]^+$ .

#### 4.7.3. synthesis of $[MoO_2\{O(CH_2)_2S(CH_2)_2O\}]_2$ (**3**)

Bis(2-hydroxyethyl)sulfide (0.25 g, 2.05 mmol) was added to a stirred solution of  $MoO_2(acac)_2$  (0.65 g, 2.00 mmol) in  $CH_2Cl_2$  (20 mL) at room temperature. The reaction mixture was stirred for 24 h. A small amount of white precipitate was filtered off, and the



solvent was removed in vacuo. The residue was extracted with *n*-hexane (20 mL) and stored at room temperature for several days to yield colorless crystals. Yield: 0.10 g, 41%. M.p. 190 °C. C<sub>8</sub>H<sub>16</sub>O<sub>8</sub>S<sub>2</sub>Mo<sub>2</sub> (499.84): calcd. C 19.36, H 3.25; found C 19.61, H 3.26. IR (KBr):  $\tilde{\nu}$  = 1460 (m) 1415 (m), 1403 (m), 1368 (s), 1305 (w), 1277 (m), 1263 (m), 1218 (w), 1181 (w), 1069 (s), 1041 (s), 1025 (s), 997 (m), 936 (m), 910 (m), 802 (s), 723 (m), 694 (w), 651 (w), 571 (m), 530 (m), 475 (m), 396 (m), 360 (s) cm<sup>-1</sup>. <sup>1</sup>H NMR (CDCl<sub>3</sub>, 200 MHz):  $\delta$  = 2.31 (t), 3.36 (t) ppm. EI-MS (70 eV): *m/z* (%) = 248 (11) [ $\{\text{MoO}_2[\text{O}(\text{CH}_2)_2\text{S}(\text{CH}_2)_2\text{O}]\}^+$ ], 216 (40) [ $\{\text{Mo}[\text{O}(\text{CH}_2)_2\text{S}(\text{CH}_2)_2\text{O}]\}^+$ ].

#### 4.7.4. synthesis of [ $\{\text{WO}_2[\text{O}(\text{CH}_2)_2\text{S}(\text{CH}_2)_2\text{O}]\}_3$ ] (4)

Bis(2-hydroxyethyl)sulfide (0.12 g, 1.00 mmol) was added to a stirred solution of WO<sub>2</sub>(acac)<sub>2</sub> (0.41 g, 1.00 mmol) in CH<sub>2</sub>Cl<sub>2</sub> (20 mL) at room temperature. The reaction mixture was stirred for 24 h. The white precipitate was filtered off, and the clear filtrate was concentrated under reduced pressure until the solution was saturated. The solution was stored overnight at room temperature to yield colorless crystals. Yield: 0.11 g, 32%. M.p. 240 °C (dec.). C<sub>12</sub>H<sub>24</sub>O<sub>12</sub>S<sub>3</sub>W<sub>3</sub> (1007.90): calcd. C 14.30, H 2.40; found C 14.51, H 2.50. IR (KBr):  $\tilde{\nu}$  = 1464 (vs), 1378 (vs), 1306 (w), 1262 (w), 1261 (w), 1170 (w), 1153 (w), 1091 (m), 1066 (m), 1033 (m), 962 (w), 935 (w), 858 (w), 838 (w), 801 (m), 722 (m), 657 (w) cm<sup>-1</sup>. EI-MS (70 eV): *m/z* (%) = 352 (33) [ $\{\text{WO}_3[\text{O}(\text{CH}_2)_2\text{S}(\text{CH}_2)_2\text{O}]\}^+$ ], 337 (100) [ $\{\text{WO}_2[\text{O}(\text{CH}_2)_2\text{S}(\text{CH}_2)_2\text{O}]\}^+$ ].

#### 4.7.5. synthesis of [ $\{\text{WO}_2[\text{O}(\text{CH}_2)_2\text{Se}(\text{CH}_2)_2\text{O}]\}_n$ ] (5)

A solution of bis(2-hydroxyethyl)selenide (0.17 g, 1.00 mmol) in CH<sub>2</sub>Cl<sub>2</sub> (5 mL) was added

to a stirred solution of  $\text{WO}_2(\text{acac})_2$  (0.41 g, 1.00 mmol) in  $\text{CH}_2\text{Cl}_2$  (20 mL) at room temperature. The reaction mixture was stirred for 2 d. The green solution turned yellow, and a small amount of yellow precipitate formed. The precipitate was filtered off, and ether was added to the filtrate to precipitate the product. The yellow product was collected by filtration and washed with diethyl ether twice. The compound was dried in vacuo. Yield: 0.23 g, 60%. M.p. 210 °C.  $\text{C}_4\text{H}_8\text{O}_4\text{SeW}$  (383.91): calcd. C 12.55, H 2.11; found C 12.63, H 2.18. IR (KBr):  $\tilde{\nu} = 1527$  (w), 1459 (m), 1400 (m), 1377 (m), 1261 (vs), 1094 (vs), 1020 (vs), 962 (w), 939 (w), 863 (w), 800 (vs), 722 (w), 703 (w), 668 (w), 583 (w), 533 (w), 472 (w)  $\text{cm}^{-1}$ .  $^1\text{H}$  NMR (DMSO- $d_6$ , 300 MHz):  $\delta = 2.60$  (t), 3.56 (t) ppm.  $^{13}\text{C}$  NMR (DMSO- $d_6$ , 300 MHz):  $\delta = 26.14$  (s), 61.62 (s) ppm.  $^{77}\text{Se}$  NMR ([DMSO- $d_6$ , 500 MHz):  $\delta = 100.22$  (s) ppm. EI-MS (70 eV):  $m/z$  (%) = 355 (50) [ $\text{M}^+ - \text{CH}_2\text{CH}_2$ ].

#### 4.7.6. synthesis of [ $\{\text{MoO}_2[\text{O}(\text{CH}_2)_2\text{Se}(\text{CH}_2)_2\text{O}]\}_n$ ] (6)

A solution of bis(2-hydroxyethyl)selenide (0.55 g, 3.25 mmol) in  $\text{CH}_3\text{OH}$  (10 mL) was added to a stirred solution of  $\text{MoO}_2(\text{acac})_2$  (0.83 g, 2.54 mmol) in  $\text{CH}_3\text{OH}$  (10 mL) at room temperature. After stirring for one week the solvent was removed in vacuo.  $\text{CH}_2\text{Cl}_2$  (10 mL) was added to the oily residue and the mixture was stirred for 1 h and filtered. The precipitate was collected and dried in vacuo. Yield: 0.236 g, 31%. Mp: 130 °C dec. Elemental analysis: calcd. for  $\text{C}_4\text{H}_8\text{O}_4\text{SeMo}$  (295.01): C 16.29, H 2.73; found: C 16.04, H 2.81; IR (KBr):  $\tilde{\nu} = 2998$  (m), 2935 (m), 2857 (m), 1577 (w), 1527 (w), 1458 (w), 1409 (w), 1358 (w), 1264 (w), 1182 (w), 1103 (m), 1066 (w), 954 (s), 911 (s), 872 (s), 798 (vs), 666 (s), 564 (s), 450 (w), 375 (w)  $\text{cm}^{-1}$ ; EI-MS (70 eV):  $m/z$  (%) = 328 (39), 295 (3) [ $\text{MoO}_2[\text{O}(\text{CH}_2)_2\text{Se}(\text{CH}_2)_2\text{O}]^+$ ], 279 (92) [ $\text{MoO}[\text{O}(\text{CH}_2)_2\text{Se}(\text{CH}_2)_2\text{O}]^+$ ], 224 (100) [ $\text{Mo}_2\text{O}_2^+$ ].

**4.7.7.** synthesis of [ $\{\text{MoO}_2(\text{O}(\text{CH}_2)_3\text{S}(\text{CH}_2)_3\text{O})\}_2$ ] (**7**)

A solution of bis(3-hydroxypropyl)sulfide (0.30 g, 2.00 mmol) in  $\text{CH}_2\text{Cl}_2$  (10 mL) was added to a stirred solution of  $\text{MoO}_2(\text{acac})_2$  (0.65 g, 2.00 mmol) in  $\text{CH}_2\text{Cl}_2$  (20 mL) at room temperature. The reaction mixture was stirred for 24 h. A small amount of white precipitate was filtered off and the solvent was removed in vacuo. The residue was extracted with toluene (20 mL) and stored at room temperature for two weeks to yield colorless crystals suitable for X-ray diffraction measurements. Yield: 0.23 g, 42%. Mp: 170 °C dec. Elemental analysis: calcd. for  $\text{C}_{12}\text{H}_{24}\text{O}_8\text{S}_2\text{Mo}_2$  (552.32): C 26.10, H 4.38; found: C 26.22, H 4.58; IR (KBr):  $\tilde{\nu}$  = 3435 (br, m), 2967 (m), 2949 (s), 2918 (s), 2866 (s), 2838 (m), 2721 (m), 1820 (w), 1636 (w), 1577 (w), 1454 (s), 1433 (s), 1424 (s), 1375 (m), 1345 (w), 1298 (w), 1268 (s), 1218 (w), 1196 (s), 1182 (w), 1067 (vs), 1043 (s), 1013 (vs), 983 (vs), 927 (vs), 906 (vs), 890 (vs), 865 (vs), 842 (s), 826 (s), 738 (w), 686 (m), 671 (w), 571 (vs), 538 (vs), 501 (s), 477 (s), 379 (s), 363 (s), 338 (w), 310 (m)  $\text{cm}^{-1}$ ; EI-MS (70 eV):  $m/z$  (%) = 276 (38)  $1/2 \text{ M}^+$ , 260 (54)  $[[\text{MoO}(\text{O}(\text{CH}_2)_3\text{S}(\text{CH}_2)_3\text{O})]^+]$ , 128 (21)  $[[\text{MoO}_2]^+]$ .

**4.7.8.** synthesis of [ $\{\text{MoO}_2(\text{O}(\text{CH}_2)_3\text{Se}(\text{CH}_2)_3\text{O})\}_2$ ] (**8**)

A solution of bis(3-hydroxypropyl)selenide (0.24 g, 1.20 mmol) in  $\text{CH}_3\text{OH}$  (10 mL) was added to a stirred solution of  $\text{MoO}_2(\text{acac})_2$  (0.33 g, 1.00 mmol) in  $\text{CH}_3\text{OH}$  (10 mL) at room temperature. After stirring for one week the solvent was removed in vacuo.  $\text{CH}_2\text{Cl}_2$  (10 mL) was added to the oily residue and the mixture was stirred for 1 h and filtered. The filtrate was stored at room temperature for one week to yield light green crystals suitable for X-ray diffraction measurements. Yield: 0.06 g, 20%. Mp: 160 °C dec. Elemental analysis: calcd. for

$C_{12}H_{24}O_8Se_2Mo_2$  (646.12): C 22.31, H 3.74; found: C 21.96, H 3.75; IR (KBr):  $\tilde{\nu}$  = 2962 (m), 2933 (m), 1585 (s), 1529 (s), 1422 (w), 1359 (m), 1263 (m), 1191 (w), 1029 (s), 941 (s), 907 (vs), 875 (s), 799 (vs), 669 (s), 568 (s), 450 (w), 375 (w)  $cm^{-1}$ ;  $^1H$  NMR ( $CDCl_3$ , 500 MHz):  $\delta$  = 3.73 (t), 2.66 (t), 1.91 (q) ppm;  $^{13}C$  NMR ( $CDCl_3$ , 500 MHz):  $\delta$  = 62.42 (s), 32.80 (s), 20.28 (s) ppm;  $^{77}Se$  NMR ( $CDCl_3$ , 500 MHz):  $\delta$  = 150.18 (s) ppm; EI-MS (70 eV):  $m/z$  (%) = 323 (80)  $1/2 M^+$ .

#### 4.7.9. synthesis of [ $\{WO_2(O(CH_2)_3Se(CH_2)_3O)\}_n$ ] (**9**)

A solution of bis(3-hydroxypropyl)selenide (0.20 g, 1.00 mmol) in  $CH_2Cl_2$  (5 mL) was added to a stirred solution of  $WO_2(acac)_2$  (0.41 g, 1.00 mmol) in  $CH_2Cl_2$  (20 mL) at room temperature. The solution changed in colour from brown to yellow after half hour. The reaction mixture was stirred for 2 days. A yellow powder precipitated out of the solution and was collected by filtration and washed with diethyl ether twice. The compound was dried in vacuo. Yield: 0.26 g, 63%. Mp: 224 - 226 °C. Elemental analysis: calcd. for  $C_6H_{12}O_4SeW$  (410.97): C 17.54, H 2.94; found: C 17.52, H 2.89; IR (KBr):  $\tilde{\nu}$  = 2926 (s), 2863 (s), 1573 (s), 1535 (s), 1457 (w), 1425 (m), 1360 (s), 1285(m), 1259 (w), 1192 (w), 1156 (w), 1079 (s), 1051 (s), 972 (s), 878 (br, vs), 804 (br, vs), 667 (br, vs), 447 (m), 352 (s)  $cm^{-1}$ ;  $^1H$  NMR ( $DMSO-d_6$ , 500 MHz):  $\delta$  = 3.44 (t), 2.55 (t), 1.72 (q) ppm;  $^{13}C$  NMR ( $DMSO-d_6$ , 500 MHz):  $\delta$  = 60.21 (s), 33.35 (s), 19.63 (s) ppm;  $^{77}Se$  NMR ( $DMSO-d_6$ , 500 MHz):  $\delta$  = 149.30 (s) ppm.

#### 4.7.10. synthesis of [ $MoO_2(O(CH_2)_2S(CH_2)_2OH)(OSiBu^tPh_2)$ ] (**10**)

To a suspension of **3** (0.248 g, 0.5 mmol) in 20 mL of  $CH_2Cl_2$  was added  $Bu^tPh_2SiCl$  (0.260 mL, 0.275 g, 1.0 mmol) and 3 mL methanol. The white suspension changed gradually to a

clear colorless solution within 5 min. The mixture was stirred for 1 h at room temperature. Evaporation of the solvent gave a crystalline solid in nearly quantitative yield. This material was recrystallized from acetonitrile/methanol and colorless prisms were obtained. Yield: 0.45 g, 89%. Mp: 150 °C. Elemental analysis: calcd. for  $C_{20}H_{28}O_5SSiMo$  ( $504.52 \text{ g}\cdot\text{mol}^{-1}$ ): C 47.61, H 5.59; found: C 47.75, H: 5.88; IR (KBr):  $\tilde{\nu} = 3440(\text{m, br}), 2854\text{-}3070 (\text{m}), 1473 (\text{w}), 1428 (\text{w}), 1419 (\text{w}), 1388 (\text{w}), 1357 (\text{w}), 1262 (\text{w}), 1177 (\text{w}), 1108 (\text{m}), 1070 (\text{m}), 1038 (\text{w}), 1006 (\text{w}), 968 (\text{m}), 915 (\text{s}), 904 (\text{s}), 819 (\text{m}), 742 (\text{w}), 701 (\text{m}), 689 (\text{w}), 615 (\text{w}), 554 (\text{w}), 503 (\text{m}), 491 (\text{m}), 412 (\text{w}), 376 (\text{w}), 348 (\text{w}), 318 (\text{w}) \text{ cm}^{-1}$ ;  $^1\text{H NMR}$  ( $\text{CD}_3\text{OD}$ , 500 MHz):  $\delta$  7.63 (m, 4 H,  $\text{C}_5\text{H}_6$ ), 7.36 (m, 6 H,  $\text{C}_5\text{H}_6$ ), 3.66 (t, 4 H,  $\text{OCH}_2$ ), 3.49 (s, 1 H, OH), 2.65 (t, 4 H,  $\text{SCH}_2$ ), 0.99 (s, 9 H,  $\text{C}(\text{CH}_3)_3$ ) ppm;  $^{13}\text{C NMR}$  ( $\text{CD}_3\text{OD}$ , 500 MHz):  $\delta$  136.5, 134.6, 130.8, 128.8 ( $\text{C}_5\text{H}_6$ ), 62.5 ( $\text{OCH}_2$ ), 35.5 ( $\text{SCH}_2$ ), 27.1 ( $\text{C}(\text{CH}_3)_3$ ), 19.9 ( $\text{C}(\text{CH}_3)_3$ ) ppm;  $^{29}\text{Si NMR}$  ( $\text{CD}_3\text{OD}$ , 500 MHz):  $\delta$  -2.37 ppm; MS (EI):  $m/z = 505 \text{ M}^+, 448 [\text{M}^+\text{-Bu}^t], 384 [\text{M}^+\text{-(O}(\text{CH}_2)_2\text{S}(\text{CH}_2)_2\text{OH})], 327 [\text{M}^+\text{-(O}(\text{CH}_2)_2\text{S}(\text{CH}_2)_2\text{OH)- Bu}^t], 249 [\text{M}^+\text{-(OSiBu}^t\text{Ph}_2)]$ .

#### 4.7.11. synthesis of $[\text{MoO}_2\text{L}^{\text{S}}]$ (**11**)

A solution of  $\text{H}_2\text{L}^{\text{S}}$  (0.91 g, 2.05 mmol) in  $\text{CH}_2\text{Cl}_2$  (10 mL) was added to a stirred solution of  $\text{MoO}_2(\text{acac})_2$  (0.67 g, 2.05 mmol) in  $\text{CH}_2\text{Cl}_2$  (10 mL) at room temperature. The reaction mixture became immediately intense purple and was stirred overnight. The solvent was removed in vacuo and the residue was extracted with MeCN. The resulting solution was dried in vacuo. Yield: 0.91 g, 78%. Mp: 260 °C dec. Elemental analysis: calcd. for  $\text{C}_{28}\text{H}_{40}\text{O}_4\text{SMo}$  ( $568.62 \text{ g}\cdot\text{mol}^{-1}$ ): C 59.14, H 7.09; found: C 58.52, H 7.17; IR (KBr):  $\tilde{\nu} = 2959\text{-}2870 (\text{s}), 1586 (\text{s}), 1506 (\text{s}), 1427 (\text{m}), 1400 (\text{m}), 1362 (\text{s}), 1263 (\text{s}), 1202 (\text{w}), 1183 (\text{w}), 1137 (\text{w}), 1101 (\text{m}), 1023 (\text{m}), 964 (\text{s}), 935 (\text{s}), 906 (\text{s}), 883 (\text{w}), 867 (\text{w}), 845 (\text{m}), 799 (\text{m}), 761 (\text{w}),$

664 (s), 633 (m), 603 (m), 574 (w), 553 (s), 489 (m), 452 (m), 407 (w), 375 (w), 314 (m)  $\text{cm}^{-1}$ ;  
 $^1\text{H}$  NMR ( $\text{C}_6\text{D}_6$ , 300 MHz):  $\delta$  1.18 (s,  $\text{C}(\text{CH}_3)_3$ , 18H), 1.42 (s,  $\text{C}(\text{CH}_3)_3$ , 18H), 7.32 (m, ArH, 4H) ppm;  $^{13}\text{C}$  NMR ( $\text{C}_6\text{D}_6$ , 500 MHz):  $\delta$  30.0 (s, *tert*-butyl), 31.5 (s, *tert*-butyl), 34.8 (s, *tert*-butyl), 35.7 (s, *tert*-butyl), 125.7 (s), 128.3 (s), 129.1 (s), 138.8 (s), 146.7 (s), 162.4 (s) ppm; UV-vis spectrum ( $2 \times 10^{-5}$  M  $\text{CH}_2\text{Cl}_2$  solution):  $\lambda_{\text{max}}$  ( $\epsilon_{\text{M}}$ ) 500 nm ( $5650 \text{ dm}^3 \text{ mol}^{-1} \text{ cm}^{-1}$ ); MS (EI):  $m/z$  (%) = 569 (14) [ $\text{M}^+$ ], 554 (24) [ $\text{M}^+ - \text{Me}$ ].

#### 4.7.12. synthesis of [ $\text{MoO}_2\text{L}^{\text{Se}}$ ] (**12**)

The preparation of **12** followed an analogous procedure as for compound **11** employing 0.98 g (2.00 mmol) of  $\text{H}_2\text{L}^{\text{Se}}$  and 0.65 g (2.00 mmol) of  $\text{MoO}_2(\text{acac})_2$ . The product was extracted with toluene. Yield: 0.98 g, 80%. Mp: 172 °C. Elemental analysis: calcd. for  $\text{C}_{28}\text{H}_{40}\text{O}_4\text{SeMo}$  ( $615.52 \text{ g} \cdot \text{mol}^{-1}$ ): C 54.64, H 6.55; found: C 54.75, H 6.86; IR (KBr):  $\tilde{\nu} = 2965\text{-}2868$  (s), 1587 (m), 1550 (w), 1536 (w), 1477 (m), 1462 (m), 1428 (s), 1398 (m), 1362 (s), 1284 (s), 1259 (s), 1201 (m), 1136 (m), 1094 (s), 1017 (m), 962 (s), 933 (w), 916 (m), 875 (m), 856 (m), 838 (m), 790 (s), 755 (s), 741 (s), 662 (m), 629 (s), 580 (w), 554 (s), 482 (m), 456 (m), 401 (m), 316 (m)  $\text{cm}^{-1}$ ;  $^1\text{H}$  NMR ( $\text{CDCl}_3$ , 500 MHz):  $\delta$  1.16 (s,  $\text{C}(\text{CH}_3)_3$ , 18H), 1.30 (s,  $\text{C}(\text{CH}_3)_3$ , 18H), 7.32 (m, ArH, 4H) ppm;  $^{13}\text{C}$  NMR ( $\text{CDCl}_3$ , 500 MHz):  $\delta$  29.7 (s, *tert*-butyl), 31.4 (s, *tert*-butyl), 34.8 (s, *tert*-butyl), 35.4 (s, *tert*-butyl), 125.1 (s), 127.8 (s), 129.7 (s), 138.8 (s), 146.2 (s), 161.7 (s) ppm;  $^{77}\text{Se}$  NMR ( $\text{CDCl}_3$ , 500 MHz):  $\delta$  268.7 (s) ppm; UV-vis spectrum ( $2 \times 10^{-5}$  M  $\text{CH}_2\text{Cl}_2$  solution):  $\lambda_{\text{max}}$  ( $\epsilon_{\text{M}}$ ) 538 nm ( $10550 \text{ dm}^3 \text{ mol}^{-1} \text{ cm}^{-1}$ ); MS (EI):  $m/z$  (%) = 616 (67) [ $\text{M}^+$ ], 601 (100) [ $\text{M}^+ - \text{Me}$ ].

#### 4.7.13. synthesis of [ $\text{WO}_2\text{L}^{\text{S}}$ ] (**13**)

A solution of  $\text{H}_2\text{L}^{\text{S}}$  (0.44 g, 1.00 mmol) in MeOH (10 mL) was added to a stirred solution of  $\text{WO}_2(\text{acac})_2$  (0.41 g, 1.00 mmol) in MeOH (10 mL) at room temperature. The reaction mixture became immediately deep red and was stirred overnight. The precipitate was filtered off and the filtrate was concentrated in vacuo. The resulting solution was stored at room temperature overnight. The formed red microcrystalline solid which was not suitable for X-ray diffraction was collected by filtration and dried in vacuo. Yield: 0.35 g, 53%. Mp: 168 °C. Elemental analysis: calcd. for  $\text{C}_{28}\text{H}_{40}\text{O}_4\text{SW}$  ( $656.53 \text{ g}\cdot\text{mol}^{-1}$ ): C 51.22, H 6.14; found: C 50.85, H 6.55; IR (KBr):  $\tilde{\nu} = 2962\text{-}2871$  (s), 1598 (m), 1527 (m), 1464 (m), 1436 (s), 1399 (m), 1362 (s), 1287 (s), 1258 (s), 1239 (m), 1203 (w), 1162 (w), 1139 (w), 1099 (m), 1030 (w), 981 (s), 949 (w), 917 (w), 881 (s), 858 (s), 817 (s), 773 (m), 750 (s), 668 (w), 639 (m), 604 (w), 555 (s), 490 (m), 443 (w), 400 (m)  $\text{cm}^{-1}$ ;  $^1\text{H}$  NMR ( $\text{CDCl}_3$ , 300 MHz):  $\delta$  1.25 (s,  $\text{C}(\text{CH}_3)_3$ , 18H), 1.39 (s,  $\text{C}(\text{CH}_3)_3$ , 18H), 7.37 (m, ArH, 4H) ppm;  $^{13}\text{C}$  NMR ( $\text{CDCl}_3$ , 500 MHz):  $\delta$  29.6 (s, *tert*-butyl), 31.5 (s, *tert*-butyl), 34.6 (s, *tert*-butyl), 35.4 (s, *tert*-butyl), 124.6 (s), 125.7 (s), 128.0 (s), 140.1 (s), 145.0 (s), 160.8 (s) ppm; MS (EI):  $m/z$  (%) = 657 (29) [ $\text{M}^+$ ], 625 (4) [ $\text{M}^+ - 2\text{O}$ ].

#### 4.7.14. synthesis of $[\text{WO}_2\text{L}^{\text{Se}}]$ (**14**)

The preparation of **14** followed an analogous procedure as for compound **13** employing 0.49 g (1.00 mmol) of  $\text{H}_2\text{L}^{\text{Se}}$  and 0.41 g (1.00 mmol) of  $\text{WO}_2(\text{acac})_2$ . Yield: 0.32 g, 46%. Mp: 255 °C. Elemental analysis: calcd. for  $\text{C}_{28}\text{H}_{40}\text{O}_4\text{SeW}$  ( $703.43 \text{ g}\cdot\text{mol}^{-1}$ ): C 47.81, H 5.73; found: C 49.43, H 6.24; IR (KBr):  $\tilde{\nu} = 2962\text{-}2870$  (s), 1591 (w), 1559 (w), 1540 (w), 1477 (m), 1463 (m), 1435 (s), 1399 (m), 1363 (s), 1336 (w), 1286 (s), 1257 (s), 1240 (m), 1202 (m), 1180 (w), 1137 (w), 1094 (m), 1023 (w), 978 (s), 917 (m), 881 (m), 859 (m), 839 (m), 809 (s), 756 (s),

744 (s), 645 (w), 632 (m), 579 (w), 559 (s), 485 (m), 468 (w), 443 (w), 404 (m), 312 (m)  $\text{cm}^{-1}$ ;  $^1\text{H}$  NMR ( $\text{CDCl}_3$ , 500 MHz):  $\delta$  1.20 (s,  $\text{C}(\text{CH}_3)_3$ , 18H), 1.30 (s,  $\text{C}(\text{CH}_3)_3$ , 18H), 7.30 (m, ArH, 4H) ppm;  $^{13}\text{C}$  NMR ( $\text{CDCl}_3$ , 500 MHz):  $\delta$  29.7 (s, *tert*-butyl), 31.5 (s, *tert*-butyl), 34.7 (s, *tert*-butyl), 35.2 (s, *tert*-butyl), 125.6 (s), 126.3 (s), 129.3 (s), 140.5 (s), 146.0 (s), 160.5 (s) ppm;  $^{77}\text{Se}$  NMR ( $\text{CDCl}_3$ , 500 MHz):  $\delta$  251.5 (s) ppm; MS (EI):  $m/z$  (%) = 703 (46) [ $\text{M}^+$ ], 687 (87) [ $\text{M}^+ - \text{O}$ ].

#### 4.7.15. synthesis of $[\text{Mo}_2\text{O}_3(\text{PyS})_4]$ (**15**)

**Method 1.** To a  $-30$  °C precooled solution of PySH (0.222 g, 2 mmol) in 10 mL THF, *n*-BuLi (0.8 mL of a 2.5 M solution in hexanes, 2 mmol) was added dropwise *via* syringe. The mixture was warmed to room temperature, stirred for 7 h, then cooled to  $-30$  °C. A colourless solution of  $[\text{MoO}_2\text{Cl}_2(\text{DME})]$  (0.289 g, 1 mmol) in 10 mL THF was added dropwise to this solution. The mixture was allowed to come to room temperature and stirred overnight. The solvent was removed *in vacuo* and the obtained solid was extracted with  $\text{CH}_2\text{Cl}_2$ . The red brown solution was filtered and dried under vacuum. The red brown microcrystalline solid was obtained. Yield: 0.23 g, 68%.

**Method 2.**  $\text{Et}_3\text{N}$  (0.30 mL, 2 mmol) was added to a methanolic solution of PySH (0.222 g, 2 mmol). The resulting solution was stirred for 1 h and a solution of  $[\text{MoO}_2\text{Cl}_2]$  (0.199 g, 1 mmol) in dichloromethane was added. The reaction mixture was stirred overnight and the resulting suspension was dried under vacuum and the obtained solid was extracted with  $\text{CH}_3\text{CN}$ . The filtrate was concentrated to approx. 5 mL and left at room temperature for several days. The red brown crystals appeared that were filtered from the solution, washed thoroughly with ether and dried *in vacuo* giving 0.15 g (44 %) product.



Crystals of **15** suitable for X-ray studies were obtained by crystallization of the initial product from dichloromethane.

Mp: 215 °C. Elemental analysis: calcd. for  $C_{20}H_{16}N_4O_3S_4Mo_2$  ( $680.49 \text{ g}\cdot\text{mol}^{-1}$ ): C 35.30, H 2.37, N 8.23; found: C 35.12, H 3.00, N 7.66; IR (KBr):  $\tilde{\nu} = 3059$  (m), 1615 (w), 1583 (s), 1558 (s), 1447 (s), 1425 (s), 1367 (m), 1267 (s), 1182 (w), 1151 (m), 1136 (s), 1086 (s), 1037 (s), 1017 (s), 985 (w), 963 (w), 929 (s), 897 (s), 872 (m), 801 (m), 763 (s), 754 (s), 727 (s); 645 (m), 616 (w), 484 (m), 456 (m), 446 (w), 418 (w), 405 (m), 371 (s), 329 (w), 294 (s)  $\text{cm}^{-1}$ ;  $^1\text{H}$  NMR ( $\text{CDCl}_3$ , 500 MHz):  $\delta$  8.46 (m,  $H_6$ , 4 H), 7.58 (m,  $H_4$ , 4 H), 7.16 (m,  $H_3$ , 4 H), 6.95 (m,  $H_5$ , 4 H) ppm;  $^{13}\text{C}$  NMR ( $\text{CDCl}_3$ , 500 MHz):  $\delta$  167.0 (s,  $C_2$ ), 125.6 (s,  $C_3$ ), 139.9 (s,  $C_4$ ), 119.6 (s,  $C_5$ ), 145.2 (s,  $C_6$ ) ppm; MS (EI):  $m/z$  (%) = 492 (15) [ $M^+$ -PyS-Py], 475 (11) [ $M^+$ -PyS-Py-O], 348 (100) [ $M^+$ -( $\text{MoO}(\text{PyS})_2$ )], 332 (55) [ $M^+$ -( $\text{MoO}_2(\text{PyS})_2$ )], 239 (39) [ $M^+$ -( $\text{MoO}(\text{PyS})_2$ )-PyS].

#### 4.7.16. synthesis of $[\text{Mo}_2\text{O}_3(\text{PySe})_4]$ (**16**)

To a  $-30$  °C precooled solution of PySeH (0.316 g, 2 mmol) in 10 mL THF, *n*-BuLi (0.8 mL of a 2.5 M solution in hexanes, 2 mmol) was added dropwise *via* syringe. The mixture was warmed to room temperature, stirred for 7 h, then cooled to  $-30$  °C. A colourless solution of  $[\text{MoO}_2\text{Cl}_2(\text{DME})]$  (0.289 g, 1 mmol) in 10 mL THF was added dropwise to this solution. The mixture was allowed to come to room temperature and stirred overnight. The solvent was removed *in vacuo* and the obtained solid was extracted with  $\text{CH}_2\text{Cl}_2$ . The red brown solution was filtered and dried *in vacuo*. 5 mL  $\text{CH}_2\text{Cl}_2$  and 30 mL hexane was added to the obtained oily residue. The product was precipitated and the mixture was stored in the freezer at  $-30$  °C overnight. The product was collected by the filtration and dried under vacuum. Yield: 0.12 g,

28%.

Crystals of **16** suitable for X-ray studies were obtained by crystallization of the initial product from dichloromethane.

Mp: 240 °C. Elemental analysis: calcd. for  $C_{20}H_{16}N_4O_3Se_4Mo_2$  (868.09  $g \cdot mol^{-1}$ ): C 27.67, H 1.86, N 6.45; found: C 27.07, H 1.94, N 5.86; IR (KBr):  $\tilde{\nu}$  = 1581 (vs), 1552 (m), 1444 (s), 1421 (s), 1265 (s), 1149 (m), 1122 (s), 1079 (m), 1039 (m), 1014 (w), 939 (w), 926 (s), 892 (s), 873 (m), 804 (w), 763 (s), 753 (s), 728 (w); 701 (m), 642 (w), 468 (w), 435 (w), 418 (w), 406 (w), 364 (w), 336 (w), 296 (w), 269 (s)  $cm^{-1}$ ;  $^1H$  NMR ( $CDCl_3$ , 500 MHz):  $\delta$  8.72 (m,  $H_6$ , 4 H), 7.51 (m,  $H_4$ , 4 H), 7.32 (m,  $H_3$ , 4 H), 6.99 (m,  $H_5$ , 4 H) ppm;  $^{13}C$  NMR ( $CDCl_3$ , 500 MHz):  $\delta$  159.8 (s,  $C_2$ ), 129.1 (s,  $C_3$ ), 139.3 (s,  $C_4$ ), 120.4 (s,  $C_5$ ), 147.4 (s,  $C_6$ ) ppm;  $^{77}Se$  NMR ( $CDCl_3$ , 500 MHz):  $\delta$  428.0 (s) ppm; MS (EI):  $m/z$  (%) = 695 (3) [ $M^+$ -PySe-O], 632 (27) [ $M^+$ -PySe-Se], 442 (70) [ $M^+$ -(MoO(PySe) $_2$ )], 426 (48) [ $M^+$ -(MoO $_2$ (PySe) $_2$ )], 285 (100)[ $M^+$ -(MoO (PySe) $_2$ )-PySe].

#### 4.7.17. synthesis of $[Mo_2O_3(4-CF_3-PymS)_4]$ (**17**)

To a -30 °C precooled solution of 4- $CF_3$ -PymSH (0.324 g, 1.8 mmol) in 10 mL THF, *n*-BuLi (0.72 mL of a 2.5 M solution in hexanes, 1.8 mmol) was added dropwise *via* syringe. The mixture was warmed to room temperature, stirred overnight, then cooled to -30 °C. A colourless solution of  $[MoO_2Cl_2(DME)]$  (0.260 g, 0.9 mmol) in 10 mL THF was added dropwise to this solution. The mixture was allowed to come to room temperature and stirred overnight. The solvent was removed *in vacuo* and the obtained solid was extracted with  $CH_2Cl_2$ . The red brown solution was filtered, concentrated and kept at room temperature for several days. The black-purple prismatic crystals were collected by the filtration and dried *in*

*vacuo*. Yield: 0.19 g, 45%. Mp: 315 °C dec. Elemental analysis: calcd. for  $C_{20}H_8F_{12}N_8O_3S_4Mo_2$  (956.44  $g \cdot mol^{-1}$ ): C 25.12, H 0.84, N 11.72; found: C 25.63, H 0.95, N 11.90; IR (KBr):  $\tilde{\nu} = 3080$  (w), 1579 (m), 1558 (m), 1429 (m), 1361 (s), 1332 (vs), 1265 (w), 1207 (m), 1193 (m), 1149 (m), 1116 (s), 968 (m), 842 (m), 789 (w), 735 (m), 702 (w), 680 (m); 476 (w), 441 (w)  $cm^{-1}$ ;  $^1H$  NMR ( $CDCl_3$ , 300 MHz):  $\delta$  8.79 (d, 4 H), 7.38 (t, 4 H) ppm; MS (EI):  $m/z$  (%) = 818 (100) [ $M^+ - 2 CF_3$ ], 638 (89) [ $M^+ - 2 CF_3 - (4-CF_3-PymS)$ ], 488 (78) [ $M^+ - (MoO(4-CF_3-PymS)_2)$ ].

#### 4.7.18. synthesis of $[H:C]_2[Mo_6O_{19}]$ (**18**)

A solution of bis(2-hydroxyethyl)selenide (0.17 g, 1.00 mmol) in  $CH_2Cl_2$  (10 mL) was added to a stirred mixture of  $[CN(iPr)C_2Me_2N(iPr)]$  (0.36 g, 2.00 mmol) and  $MoO_2Cl_2$  (0.20 g, 1.00 mmol) in  $CH_2Cl_2$  (10 mL) at 0 °C. The mixture of the reaction was allowed to come to room temperature and stirred overnight. The resulting suspension was filtered. The filtrate was concentrated to ca. 10 mL in *vacuo* and diethyl ether (5 mL) was added. The solution was stored overnight at room temperature to yield yellow crystals. The crystals were collected on a filter, washed once with diethyl ether (5 mL) and dried in *vacuo*. Yield: 0.12 g. 58% based on Mo. Mp: 200 °C dec. Elemental analysis: calcd. for  $C_{22}H_{42}N_4O_{19}Mo_6$  (1242.23): C 21.27, H 3.41, N 4.51; found: C 22.84, H 3.72, N 4.62; IR (KBr):  $\tilde{\nu} = 3136$  (s), 3067 (s), 2984 (s), 2939 (s), 1940 (w), 1909 (w), 1663 (w), 1631 (m), 1554 (s), 1466 (s), 1443 (s), 1391 (m), 1376 (m), 1340 (m), 1291 (w), 1262 (w), 1230 (s), 1195 (s), 1141 (s), 1114 (s), 1083 (w), 1043 (w), 956 (vs), 800 (vs), 653 (s), 592 (s), 539 (s), 418 (s), 352 (s)  $cm^{-1}$ .

#### 4.7.19. synthesis of $[H:C]_2[W_6O_{19}]$ (**19**)

The compound was prepared using the same procedure described for **18**, bis(2-hydroxyethyl)selenide (0.17 g, 1.00 mmol) in CH<sub>2</sub>Cl<sub>2</sub> (10 mL) and a mixture of [CN(*i*Pr)C<sub>2</sub>Me<sub>2</sub>N(*i*Pr)] (0.36 g, 2.00 mmol) and WO<sub>2</sub>Cl<sub>2</sub> (0.29 g, 1.00 mmol) in CH<sub>2</sub>Cl<sub>2</sub> (10 mL). The filtrate was stored overnight at room temperature to yield yellow crystals. The crystals were collected on a filter, washed once with diethyl ether (5 mL) and dried in vacuo. Yield: 0.15 g. 51% based on W. Mp: 200 °C dec. Elemental analysis: calcd. for C<sub>22</sub>H<sub>42</sub>N<sub>4</sub>O<sub>19</sub>W<sub>6</sub> (1769.69): C 14.93, H 2.39, N 3.17; found: C 14.20, H 2.06, N 3.07; IR (KBr):  $\tilde{\nu}$  = 3353 (br, s), 3142 (s), 3073 (s), 2977 (s), 2939 (s), 2874 (m), 1976 (w), 1951 (w), 1653 (w), 1630 (m), 1555 (s), 1465 (s), 1443 (s), 1393 (m), 1377 (m), 1341 (m), 1262 (s), 1231 (s), 1194 (s), 1141 (s), 1113 (s), 1072 (s), 1043 (s), 1020 (s), 978 (s), 806 (vs), 665 (m), 587 (m), 539 (w), 443 (s), 440 (m), 366 (m) cm<sup>-1</sup>.

#### 4.7.20. synthesis of [W<sub>8</sub>O<sub>19</sub>(O(CH<sub>2</sub>)<sub>3</sub>S(CH<sub>2</sub>)<sub>3</sub>O)<sub>3</sub>(acac)<sub>4</sub>] (**20**)

A solution of bis(3-hydroxypropyl)sulfide (0.180 g, 1.20 mmol) in CH<sub>3</sub>CN (10 ml) was added to a stirred solution of WO<sub>2</sub>(acac)<sub>2</sub> (0.414 g, 1.00 mmol) in CH<sub>3</sub>CN (10 ml). The resultant mixture was refluxed for 3 h during which time the clear green solution developed to a pale green precipitate and yellow solution. The suspension was stirred continuously overnight. The precipitate was removed by filtration and the limpid filtrate was then concentrated. Ether (5 mL) was added to this concentrated solution. A small amount of yellow crystals was obtained by keeping the solution at room temperature for one month. Yield: 33 mg, 10% based on W. Elemental analysis: calcd. For C<sub>38</sub>H<sub>64</sub>O<sub>33</sub>S<sub>3</sub>W<sub>8</sub> (2615.89): C 17.45, H 2.47; found: C 17.24, H 2.89. IR (KBr):  $\tilde{\nu}$  = 2927(m), 2867(w), 1701(w), 1574(s), 1538(s), 1425(m), 1360(m), 1288(w), 1263(w), 1211(w), 1167(w), 1083(m), 1022(m), 973(s), 931(s), 877(vs), 804(vs),

668(s), 607(s), 448(w), 352(m)  $\text{cm}^{-1}$ . EI-MS (70 eV):  $m/z = 43, 73, 113, 147, 207, 221, 281, 341, 355, 415, 429, 489, 503, 513, 577, 661, 735, 809, 883, 957, 1033, 1096, 1171, 1245, 1319, 1393, 1467, 1542, 1615, 1690, 1764, 1838, 1911, 1988, 2059, 2134, 2207, 2284, 2357, 2431, 2505, 2577$ .

#### 4.7.21. synthesis of $\text{MoO}_2(\text{dipic})$ (**21**)

To a stirred solution of  $\text{MoO}_2(\text{acac})_2$  (0.326 g, 1.00 mmol) in  $\text{CH}_3\text{OH}$  (20 mL) a solution of pyridine-2,6-dicarboxylic acid (0.225 g, 1.00 mmol) in 10 mL  $\text{CH}_3\text{OH}$  was added at room temperature. The reaction mixture was stirred overnight. The solvent was removed in vacuo.  $\text{CH}_2\text{Cl}_2$  (10 mL) was added to the residue and yellow solution and pale green precipitate formed. The mixture was stored at room temperature for several days to yield blue crystals. The precipitate and crystal were collected on a filter and dried in vacuo. Yield: 0.18 g, 61%. Mp: 230 °C. Elemental analysis: calcd. for  $\text{C}_7\text{H}_3\text{NO}_6\text{Mo}$ (293.04): C 28.69, H 1.03, N 4.78; found: C 29.75, H 1.31, N: 4.75; IR (KBr):  $\tilde{\nu} = 3109$  (m) 3061 (m), 1742 (vs), 1706 (vs), 1603 (m), 1577 (m), 1479 (m), 1455 (w), 1433 (w), 1418 (w), 1351 (m), 1307 (vs), 1268 (m), 1203 (w), 1138 (s), 1111 (s), 1082 (s), 1038 (w), 1025 (w), 997 (w), 975 (s), 943 (s), 918 (s), 848 (w), 833 (w), 807 (w), 785 (w), 765 (s), 753 (s), 703 (w), 683 (m), 670 (m), 648 (w), 596 (w), 470 (m), 455 (s), 356 (m), 311 (m)  $\text{cm}^{-1}$ ; EI-MS (70 eV):  $m/z$  (%) = 341 (20), 326 (100), 284 (9), 218 (24).

## 5. Handling and Disposal of Solvents and Residual Waste

1. The recovered solvents were distilled or condensed into cold-traps under vacuum, collected in halogen-free or halogen-containing solvent containers, and stored for disposal.
2. Used NMR solvents were classified into halogen-free or halogen-containing solvents and were disposed as heavy metal-containing wastes and halogen-containing wastes, respectively.
3. The heavy metal residues were dissolved in nitric acid and after neutralization stored in the container for heavy metal wastes.
4. Drying agents such as KOH, CaCl<sub>2</sub>, MgCl<sub>2</sub>, MgSO<sub>4</sub>, and P<sub>4</sub>O<sub>10</sub> were hydrolyzed and disposed as acid or base wastes.
5. Wherever possible, sodium metal used for drying solvents was collected for recycling.<sup>[196]</sup> The non-reusable sodium metal was carefully hydrolyzed in cold ethanol and potassium in cold isopropanol and collected into the base-bath cleaning glassware.
6. Ethanol and acetone used for cooling baths (with solid CO<sub>2</sub> or liquid N<sub>2</sub>) were subsequently used for cleaning glassware.
7. The acid bath for cleaning glassware was neutralized with Na<sub>2</sub>CO<sub>3</sub> and the resulting NaCl solution was washed off in the water drainage system.
8. The residual of the base bath for cleaning glassware was poured into the container for base wastes.

Amount of various types of disposable wastes generated during the work.

Metal containing wastes	5 L
Halogen-containing wastes	6 L
Halogen-free solvent wastes	40 L
Acid wastes	10 L
Base wastes	15 L

## 6. Crystal Data and Refinement Details

**Table CD1.** Crystal Data and Structure Refinement Details for  $\text{WO}_2\text{Cl}_2(\text{MeSCH}_2\text{CH}_2\text{SMe})$  (1).

Empirical formula	$\text{C}_4\text{H}_{10}\text{Cl}_2\text{O}_2\text{S}_2\text{W}$
Formula weight	408.99
Temperature	293(2) K
Wavelength	0.71073 Å
Crystal system	Hexagonal
Space group	$P6_5$
Unit cell dimensions	$a = 7.3222(3)$ Å, $\alpha = 90^\circ$ $b = 7.3222(3)$ Å, $\beta = 90^\circ$ $c = 33.3889(17)$ Å, $\gamma = 120^\circ$
Volume	1550.30(12) Å <sup>3</sup>
<i>Z</i>	6
Density (calculated)	2.628 Mg/m <sup>3</sup>
Absorption coefficient	12.051 mm <sup>-1</sup>
<i>F</i> (000)	1140
Crystal size	0.1 x 0.2 x 0.1 mm <sup>3</sup>
$\theta$ range for data collection	3.21 to 24.80°
Index ranges	$-8 \leq h \leq 8$ , $-7 \leq k \leq 8$ , $-39 \leq l \leq 39$
Reflections collected	15469
Independent reflections	1757 [ $R_{\text{int}} = 0.0473$ ]
Completeness to $\theta = 24.80^\circ$	99.4%
Refinement method	Full-matrix least-squares on $F^2$
Data / restraints / parameters	1757 / 1 / 102
Goodness-of-fit on $F^2$	1.111
Final <i>R</i> indices [ $I > 2\sigma(I)$ ]	$R1 = 0.0247$ , $wR2 = 0.0535$
<i>R</i> indices (all data)	$R1 = 0.0260$ , $wR2 = 0.0538$
Largest diff. peak and hole	0.710 and -0.759 e·Å <sup>-3</sup>



**Table CD2.** Crystal Data and Structure Refinement Details for [WO<sub>2</sub>Cl<sub>2</sub>(THF)]<sub>4</sub> (2).

Empirical formula	C <sub>17</sub> H <sub>34</sub> Cl <sub>10</sub> O <sub>12</sub> W <sub>4</sub>
Formula weight	1520.34
Temperature	103(2) K
Wavelength	0.71073 Å
Crystal system	Monoclinic
Space group	<i>P</i> 2 <sub>1</sub> / <i>n</i>
Unit cell dimensions	<i>a</i> = 19.7426(10) Å, $\alpha$ = 90° <i>b</i> = 16.9644(9) Å, $\beta$ = 93.8000(10)° <i>c</i> = 22.5364(12) Å, $\gamma$ = 90°
Volume	7531.3(7) Å <sup>3</sup>
<i>Z</i>	8
Density (calculated)	2.682 Mg/m <sup>3</sup>
Absorption coefficient	12.937 mm <sup>-1</sup>
<i>F</i> (000)	5584
Crystal size	0.20 x 0.20 x 0.20 mm <sup>3</sup>
$\theta$ range for data collection	1.42 to 26.40°
Index ranges	-24 <i>h</i> ≤ 24, 0 <i>k</i> ≤ 1, 0 ≤ <i>l</i> ≤ 28
Reflections collected	15443
Independent reflections	15443 [ <i>R</i> <sub>int</sub> = 0.0000]
Completeness to $\theta$ = 26.40°	99.9%
Refinement method	Full-matrix least-squares on <i>F</i> <sup>2</sup>
Data / restraints / parameters	15443 / 0 / 775
Goodness-of-fit on <i>F</i> <sup>2</sup>	1.085
Final <i>R</i> indices [ <i>I</i> > 2σ( <i>I</i> )]	<i>R</i> 1 = 0.0318, <i>wR</i> 2 = 0.0649
<i>R</i> indices (all data)	<i>R</i> 1 = 0.0424, <i>wR</i> 2 = 0.0686
Largest diff. peak and hole	2.165 and -1.242 e·Å <sup>-3</sup>

**Table CD3.** Crystal Data and Structure Refinement Details for [ $\{\text{MoO}_2[\text{O}(\text{CH}_2)_2\text{S}(\text{CH}_2)_2\text{O}]\}_2$ ]  
(3).

Empirical formula	$\text{C}_8\text{H}_{16}\text{Mo}_2\text{O}_8\text{S}_2$
Formula weight	496.21
Temperature	133(2) K
Wavelength	0.71073 Å
Crystal system	Monoclinic
Space group	$P2_1/n$
Unit cell dimensions	$a = 9.4839(5)$ Å, $\alpha = 90^\circ$ $b = 12.4405(7)$ Å, $\beta = 101.567(4)^\circ$ $c = 12.8003(7)$ Å, $\gamma = 90^\circ$
Volume	1479.56(14) Å <sup>3</sup>
<i>Z</i>	4
Density (calculated)	2.228 Mg/m <sup>3</sup>
Absorption coefficient	2.008 mm <sup>-1</sup>
<i>F</i> (000)	976
Crystal size	0.20 x 0.20 x 0.10 mm <sup>3</sup>
$\theta$ range for data collection	2.31 to 24.84°
Index ranges	$-11 \leq h \leq 11$ , $-14 \leq k \leq 14$ , $-15 \leq l \leq 15$
Reflections collected	22121
Independent reflections	2554 [ $R_{\text{int}} = 0.0458$ ]
Completeness to $\theta = 24.84^\circ$	99.7%
Refinement method	Full-matrix least-squares on $F^2$
Data / restraints / parameters	2554 / 0 / 181
Goodness-of-fit on $F^2$	1.004
Final <i>R</i> indices [ $I > 2\sigma(I)$ ]	$R1 = 0.0108$ , $wR2 = 0.0442$
<i>R</i> indices (all data)	$R1 = 0.0228$ , $wR2 = 0.0451$
Largest diff. peak and hole	0.308 and -0.481 e·Å <sup>-3</sup>

**Table CD4.** Crystal Data and Structure Refinement Details for  $[\{\text{WO}_2[\text{O}(\text{CH}_2)_2\text{S}(\text{CH}_2)_2\text{O}\}]_3\} \cdot \text{CH}_2\text{Cl}_2$  (4).

Empirical formula	$\text{C}_{13}\text{H}_{25}\text{Cl}_2\text{O}_{12}\text{S}_3\text{W}_3$
Formula weight	1091.96
Temperature	133(2) K
Wavelength	0.71073 Å
Crystal system	Monoclinic
Space group	$P2_1$
Unit cell dimensions	$a = 11.615(2)$ Å, $\alpha = 90^\circ$ $b = 7.8739(16)$ Å, $\beta = 111.81(3)^\circ$ $c = 14.462(3)$ Å, $\gamma = 90^\circ$
Volume	1228.0(4) Å <sup>3</sup>
<i>Z</i>	2
Density (calculated)	2.953 Mg/m <sup>3</sup>
Absorption coefficient	14.545 mm <sup>-1</sup>
<i>F</i> (000)	1006
Crystal size	0.20 x 0.20 x 0.10 mm <sup>3</sup>
$\theta$ range for data collection	1.52 to 24.94°
Index ranges	$-13 \leq h \leq 13$ , $-9 \leq k \leq 9$ , $-16 \leq l \leq 16$
Reflections collected	12796
Independent reflections	4153 [ $R_{\text{int}} = 0.0377$ ]
Completeness to $\theta = 24.94^\circ$	97.6%
Refinement method	Full-matrix least-squares on $F^2$
Data / restraints / parameters	4153 / 391 / 287
Goodness-of-fit on $F^2$	1.051
Final <i>R</i> indices [ $I > 2\sigma(I)$ ]	$R1 = 0.0350$ , $wR2 = 0.0904$
<i>R</i> indices (all data)	$R1 = 0.0403$ , $wR2 = 0.0957$
Largest diff. peak and hole	2.802 and -1.684 e·Å <sup>-3</sup>

**Table CD5.** Crystal Data and Structure Refinement Details for [ $\{\text{MoO}_2(\text{O}(\text{CH}_2)_3\text{S}(\text{CH}_2)_3\text{O})\}_2$ ] (7).

Empirical formula	$\text{C}_{12}\text{H}_{24}\text{Mo}_2\text{O}_8\text{S}_2$
Formula weight	552.31
Temperature	133(2) K
Wavelength	0.71073 Å
Crystal system	Monoclinic
Space group	$P2_1/n$
Unit cell dimensions	$a = 9.4886(7)$ Å, $\alpha = 90^\circ$ $b = 8.7913(5)$ Å, $\beta = 109.044(6)^\circ$ $c = 11.1434(9)$ Å, $\gamma = 90^\circ$
Volume	878.67(11) Å <sup>3</sup>
$Z$	2
Density (calculated)	2.088 Mg/m <sup>3</sup>
Absorption coefficient	1.702 mm <sup>-1</sup>
$F(000)$	552
Crystal size	0.20 x 0.20 x 0.10 mm <sup>3</sup>
$\theta$ range for data collection	2.46 to 24.77°
Index ranges	$-11 \leq h \leq 9$ , $-10 \leq k \leq 10$ , $-13 \leq l \leq 13$
Reflections collected	12108
Independent reflections	1507 [ $R_{\text{int}} = 0.0483$ ]
Completeness to $\theta = 24.77^\circ$	99.7%
Refinement method	Full-matrix least-squares on $F^2$
Data / restraints / parameters	1507 / 0 / 109
Goodness-of-fit on $F^2$	1.290
Final $R$ indices [ $I > 2\sigma(I)$ ]	$R1 = 0.0278$ , $wR2 = 0.0773$
$R$ indices (all data)	$R1 = 0.0310$ , $wR2 = 0.0783$
Largest diff. peak and hole	0.710 and -0.759 e·Å <sup>-3</sup>

**Table CD6.** Crystal Data and Structure Refinement Details for  $[\{\text{MoO}_2(\text{O}(\text{CH}_2)_3\text{Se}(\text{CH}_2)_3\text{O})\}_2]$  (**8**).

Empirical formula	$\text{C}_{12}\text{H}_{24}\text{Mo}_2\text{O}_8\text{Se}_2$
Formula weight	646.11
Temperature	103(2) K
Wavelength	0.71073 Å
Crystal system	Monoclinic
Space group	$P2_1/n$
Unit cell dimensions	$a = 9.5298(14)$ Å, $\alpha = 90^\circ$ $b = 8.8814(14)$ Å, $\beta = 108.874(2)^\circ$ $c = 11.2161(17)$ Å, $\gamma = 90^\circ$
Volume	898.3(2) Å <sup>3</sup>
<i>Z</i>	2
Density (calculated)	2.389 Mg/m <sup>3</sup>
Absorption coefficient	5.485 mm <sup>-1</sup>
<i>F</i> (000)	624
Crystal size	0.20 x 0.20 x 0.05 mm <sup>3</sup>
$\theta$ range for data collection	2.99 to 26.14°
Index ranges	$-11 \leq h \leq 11$ , $-11 \leq k \leq 11$ , $-13 \leq l \leq 13$
Reflections collected	17947
Independent reflections	1783 [ $R_{\text{int}} = 0.0255$ ]
Completeness to $\theta = 26.14^\circ$	99.9%
Refinement method	Full-matrix least-squares on $F^2$
Data / restraints / parameters	1783 / 0 / 109
Goodness-of-fit on $F^2$	1.197
Final <i>R</i> indices [ $I > 2\sigma(I)$ ]	$R1 = 0.0179$ , $wR2 = 0.0431$
<i>R</i> indices (all data)	$R1 = 0.0180$ , $wR2 = 0.0431$
Largest diff. peak and hole	0.661 and -0.267 e·Å <sup>-3</sup>

**Table CD7.** Crystal Data and Structure Refinement Details for [MoO<sub>2</sub>(O(CH<sub>2</sub>)<sub>2</sub>S(CH<sub>2</sub>)<sub>2</sub>OH)(OSiBu<sup>t</sup>Ph<sub>2</sub>)] (**10**).

Empirical formula	C <sub>20</sub> H <sub>28</sub> MoO <sub>5</sub> SSi
Formula weight	504.51
Temperature	133(2) K
Wavelength	0.71073 Å
Crystal system	Triclinic
Space group	$P\bar{1}$
Unit cell dimensions	a = 7.4823(8) Å, $\alpha$ = 87.721(9)° b = 7.3222(3) Å, $\beta$ = 87.463(9)° c = 16.2001(19) Å, $\gamma$ = 75.743(9)°
Volume	1108.1(2) Å <sup>3</sup>
Z	2
Density (calculated)	1.512 Mg/m <sup>3</sup>
Absorption coefficient	0.767 mm <sup>-1</sup>
F(000)	520
Crystal size	mm <sup>3</sup>
$\theta$ range for data collection	2.23 to 24.75°
Index ranges	-7 ≤ h ≤ 8, -11 ≤ k ≤ 11, -18 ≤ l ≤ 19
Reflections collected	10987
Independent reflections	3752 [ $R_{\text{int}} = 0.0707$ ]
Completeness to $\theta = 24.75^\circ$	98.8%
Refinement method	Full-matrix least-squares on $F^2$
Data / restraints / parameters	3752 / 0 / 259
Goodness-of-fit on $F^2$	0.987
Final R indices [ $I > 2\sigma(I)$ ]	R1 = 0.0356, wR2 = 0.0816
R indices (all data)	R1 = 0.0476, wR2 = 0.0854
Largest diff. peak and hole	0.433 and -1.021 e·Å <sup>-3</sup>

**Table CD8.** Crystal Data and Structure Refinement Details for [Mo<sub>2</sub>O<sub>3</sub>(PyS)<sub>4</sub>] (**15**).

Empirical formula	C <sub>20</sub> H <sub>16</sub> Mo <sub>2</sub> N <sub>4</sub> O <sub>3</sub> S <sub>4</sub>
Formula weight	680.49
Temperature	133(2) K
Wavelength	0.71073 Å
Crystal system	Triclinic
Space group	$P\bar{1}$
Unit cell dimensions	a = 8.9399(10) Å, $\alpha$ = 100.055(10)° b = 11.3934(13) Å, $\beta$ = 107.432(9)° c = 13.1679(16) Å, $\gamma$ = 96.812(9)°
Volume	1238.9(2) Å <sup>3</sup>
Z	2
Density (calculated)	1.824 Mg/m <sup>3</sup>
Absorption coefficient	1.379 mm <sup>-1</sup>
F(000)	672
Crystal size	mm <sup>3</sup>
$\theta$ range for data collection	1.66 to 24.77°
Index ranges	-10 ≤ h ≤ 10, -13 ≤ k ≤ 13, -15 ≤ l ≤ 15
Reflections collected	13145
Independent reflections	4229 [ $R_{\text{int}}$ = 0.1128]
Completeness to $\theta$ = 24.77°	99.4%
Refinement method	Full-matrix least-squares on $F^2$
Data / restraints / parameters	4229 / 0 / 298
Goodness-of-fit on $F^2$	0.943
Final R indices [ $I > 2\sigma(I)$ ]	R1 = 0.0450, wR2 = 0.0944
R indices (all data)	R1 = 0.0810, wR2 = 0.1016
Largest diff. peak and hole	0.606 and -0.752 e·Å <sup>-3</sup>

**Table CD9.** Crystal Data and Structure Refinement Details for [Mo<sub>2</sub>O<sub>3</sub>(PySe)<sub>4</sub>] (**16**).

Empirical formula	C <sub>20</sub> H <sub>16</sub> Mo <sub>2</sub> N <sub>4</sub> O <sub>3</sub> Se <sub>4</sub>
Formula weight	868.09
Temperature	133(2) K
Wavelength	0.71073 Å
Crystal system	Triclinic
Space group	$P\bar{1}$
Unit cell dimensions	a = 7.2195(8) Å, $\alpha$ = 73.637(8)° b = 9.0239(10) Å, $\beta$ = 77.288(8)° c = 10.6741(11) Å, $\gamma$ = 77.726(8)°
Volume	642.40(12) Å <sup>3</sup>
Z	1
Density (calculated)	2.244 Mg/m <sup>3</sup>
Absorption coefficient	6.671 mm <sup>-1</sup>
F(000)	408
Crystal size	mm <sup>3</sup>
$\theta$ range for data collection	2.02 to 24.83°
Index ranges	-8 ≤ h ≤ 7, -10 ≤ k ≤ 10, -12 ≤ l ≤ 12
Reflections collected	8007
Independent reflections	1893 [ $R_{\text{int}} = 0.1004$ ]
Completeness to $\theta = 24.83^\circ$	84.8%
Refinement method	Full-matrix least-squares on $F^2$
Data / restraints / parameters	1893 / 0 / 152
Goodness-of-fit on $F^2$	1.085
Final R indices [ $I > 2\sigma(I)$ ]	R1 = 0.0505, wR2 = 0.1448
R indices (all data)	R1 = 0.0521, wR2 = 0.1474
Largest diff. peak and hole	0.915 and -1.192 e·Å <sup>-3</sup>



**Table CD10.** Crystal Data and Structure Refinement Details for  $[\text{Mo}_2\text{O}_3(4\text{-CF}_3\text{-PymS})_4]\cdot 2\text{CH}_2\text{Cl}_2$  (**17**· $2\text{CH}_2\text{Cl}_2$ ).

Empirical formula	$\text{C}_{22}\text{H}_{12}\text{F}_{12}\text{Mo}_2\text{N}_8\text{O}_3\text{S}_4$
Formula weight	1126.32
Temperature	133(2) K
Wavelength	0.71073 Å
Crystal system	Monoclinic
Space group	$P2_1/c$
Unit cell dimensions	$a = 14.9773(8)$ Å, $\alpha = 90^\circ$ $b = 10.5230(5)$ Å, $\beta = 106.832(4)^\circ$ $c = 12.3575(7)$ Å, $\gamma = 90^\circ$
Volume	1864.18(17) Å <sup>3</sup>
<i>Z</i>	2
Density (calculated)	2.007 Mg/m <sup>3</sup>
Absorption coefficient	1.285 mm <sup>-1</sup>
<i>F</i> (000)	1096
Crystal size	mm <sup>3</sup>
$\theta$ range for data collection	2.40 to 24.77°
Index ranges	$-17 \leq h \leq 17$ , $-12 \leq k \leq 12$ , $-14 \leq l \leq 14$
Reflections collected	26766
Independent reflections	3189 [ $R_{\text{int}} = 0.0351$ ]
Completeness to $\theta = 24.77^\circ$	99.6%
Refinement method	Full-matrix least-squares on $F^2$
Data / restraints / parameters	3189 / 0 / 268
Goodness-of-fit on $F^2$	1.042
Final <i>R</i> indices [ $I > 2\sigma(I)$ ]	$R1 = 0.0289$ , $wR2 = 0.0697$
<i>R</i> indices (all data)	$R1 = 0.0332$ , $wR2 = 0.0716$
Largest diff. peak and hole	0.971 and -0.479 e·Å <sup>-3</sup>

**Table CD11.** Crystal Data and Structure Refinement Details for [H:C]<sub>2</sub>[Mo<sub>6</sub>O<sub>19</sub>] (**18**).

Empirical formula	C <sub>22</sub> H <sub>42</sub> Mo <sub>6</sub> N <sub>4</sub> O <sub>19</sub>
Formula weight	1242.24
Temperature	133(2) K
Wavelength	0.71073 Å
Crystal system	Monoclinic
Space group	<i>P</i> 2 <sub>1</sub> / <i>n</i>
Unit cell dimensions	<i>a</i> = 11.0840(5) Å, $\alpha$ = 90° <i>b</i> = 12.7449(8) Å, $\beta$ = 95.941(3)° <i>c</i> = 13.0142(6) Å, $\gamma$ = 90°
Volume	1828.57(16) Å <sup>3</sup>
<i>Z</i>	2
Density (calculated)	2.256 Mg/m <sup>3</sup>
Absorption coefficient	2.075 mm <sup>-1</sup>
<i>F</i> (000)	1212
Crystal size	0.30 x 0.20 x 0.20 mm <sup>3</sup>
$\theta$ range for data collection	2.30 to 24.73°
Index ranges	-13 ≤ <i>h</i> ≤ 13, -14 ≤ <i>k</i> ≤ 14, -13 ≤ <i>l</i> ≤ 15
Reflections collected	26164
Independent reflections	3106 [ <i>R</i> <sub>int</sub> = 0.0471]
Completeness to $\theta$ = 24.73°	99.6%
Refinement method	Full-matrix least-squares on <i>F</i> <sup>2</sup>
Data / restraints / parameters	3106 / 0 / 238
Goodness-of-fit on <i>F</i> <sup>2</sup>	0.985
Final <i>R</i> indices [ <i>I</i> > 2σ( <i>I</i> )]	<i>R</i> 1 = 0.0172, <i>wR</i> 2 = 0.0427
<i>R</i> indices (all data)	<i>R</i> 1 = 0.0199, <i>wR</i> 2 = 0.0437
Largest diff. peak and hole	0.390 and -0.455 e·Å <sup>-3</sup>

**Table CD12.** Crystal Data and Structure Refinement Details for [H:C]<sub>2</sub>[W<sub>6</sub>O<sub>19</sub>] (19).

Empirical formula	C <sub>22</sub> H <sub>42</sub> N <sub>4</sub> O <sub>19</sub> W <sub>6</sub>
Formula weight	1769.70
Temperature	103(2) K
Wavelength	0.71073 Å
Crystal system	Monoclinic
Space group	<i>P</i> 2 <sub>1</sub> / <i>n</i>
Unit cell dimensions	a = 11.1284(14) Å, α = 90° b = 12.8384(17) Å, β = 96.410(2)° c = 12.9328(17) Å, γ = 90°
Volume	1836.2(4) Å <sup>3</sup>
<i>Z</i>	2
Density (calculated)	3.201 Mg/m <sup>3</sup>
Absorption coefficient	18.797 mm <sup>-1</sup>
<i>F</i> (000)	1596
Crystal size	0.20 x 0.20 x 0.20 mm <sup>3</sup>
θ range for data collection	2.43 to 26.40°
Index ranges	-13 ≤ <i>h</i> ≤ 13, 0 ≤ <i>k</i> ≤ 16, 0 ≤ <i>l</i> ≤ 16
Reflections collected	21419
Independent reflections	3752 [ <i>R</i> <sub>int</sub> = 0.0431]
Completeness to θ = 26.40°	99.8%
Refinement method	Full-matrix least-squares on <i>F</i> <sup>2</sup>
Data / restraints / parameters	3752 / 0 / 238
Goodness-of-fit on <i>F</i> <sup>2</sup>	1.453
Final <i>R</i> indices [ <i>I</i> > 2σ( <i>I</i> )]	<i>R</i> 1 = 0.0313, <i>wR</i> 2 = 0.0598
<i>R</i> indices (all data)	<i>R</i> 1 = 0.0318, <i>wR</i> 2 = 0.0599
Largest diff. peak and hole	1.270 and -1.218 e·Å <sup>-3</sup>

**Table CD13.** Crystal Data and Structure Refinement Details for  $[\text{W}_8\text{O}_{19}(\text{O}(\text{CH}_2)_3\text{S}(\text{CH}_2)_3\text{O})_3(\text{acac})_4] \cdot 2.5\text{CH}_3\text{CN}$  (**20**·2.5CH<sub>3</sub>CN).

Empirical formula	$\text{C}_{43}\text{H}_{71.5}\text{N}_{2.5}\text{O}_{33}\text{S}_3\text{W}_8$
Formula weight	2718.51
Temperature	100(2) K
Wavelength	0.71073 Å
Crystal system	Triclinic
Space group	$P\bar{1}$
Unit cell dimensions	$a = 12.963(3)$ Å, $\alpha = 92.80(3)^\circ$ $b = 15.438(3)$ Å, $\beta = 110.20(3)^\circ$ $c = 18.062(4)$ Å, $\gamma = 100.75(3)^\circ$
Volume	3307.5(11) Å <sup>3</sup>
<i>Z</i>	2
Density (calculated)	2.730 Mg/m <sup>3</sup>
Absorption coefficient	14.032 mm <sup>-1</sup>
<i>F</i> (000)	2502
Crystal size	0.20 x 0.20 x 0.20 mm <sup>3</sup>
$\theta$ range for data collection	1.94 to 26.43°
Index ranges	$-16 \leq h \leq 14$ , $-19 \leq k \leq 19$ , $0 \leq l \leq 22$
Reflections collected	69247
Independent reflections	13499 [ $R_{\text{int}} = 0.0550$ ]
Completeness to $\theta = 26.43^\circ$	99.1%
Refinement method	Full-matrix least-squares on $F^2$
Data / restraints / parameters	13499 / 750 / 829
Goodness-of-fit on $F^2$	1.062
Final <i>R</i> indices [ $I > 2\sigma(I)$ ]	$R1 = 0.0376$ , $wR2 = 0.0942$
<i>R</i> indices (all data)	$R1 = 0.0440$ , $wR2 = 0.0983$
Largest diff. peak and hole	3.317 and -3.591 e·Å <sup>-3</sup>

**Table CD14.** Crystal Data and Structure Refinement Details for MoO<sub>2</sub>(dipic) (**21**).

Empirical formula	C <sub>7</sub> H <sub>3</sub> MoNO <sub>6</sub>
Formula weight	293.04
Temperature	133(2) K
Wavelength	0.71073 Å
Crystal system	Monoclinic
Space group	<i>P2<sub>1</sub>/n</i>
Unit cell dimensions	a = 6.7916(14) Å, α = 90° b = 8.3655(17) Å, β = 94.96(3)° c = 14.504(3) Å, γ = 120°
Volume	821.0(3) Å <sup>3</sup>
Z	4
Density (calculated)	2.371 Mg/m <sup>3</sup>
Absorption coefficient	1.606 mm <sup>-1</sup>
<i>F</i> (000)	568
Crystal size	0.20 x 0.20 x 0.20 mm <sup>3</sup>
θ range for data collection	2.81 to 24.76°
Index ranges	-8 ≤ <i>h</i> ≤ 7, -9 ≤ <i>k</i> ≤ 9, -17 ≤ <i>l</i> ≤ 17
Reflections collected	8902
Independent reflections	1395 [ <i>R</i> <sub>int</sub> = 0.0492]
Completeness to θ = 24.76°	99.4%
Refinement method	Full-matrix least-squares on <i>F</i> <sup>2</sup>
Data / restraints / parameters	1395 / 0 / 136
Goodness-of-fit on <i>F</i> <sup>2</sup>	1.037
Final <i>R</i> indices [ <i>I</i> > 2σ( <i>I</i> )]	<i>R</i> 1 = 0.0178, <i>wR</i> 2 = 0.0483
<i>R</i> indices (all data)	<i>R</i> 1 = 0.0202, <i>wR</i> 2 = 0.0490
Largest diff. peak and hole	0.321 and -0.292 e·Å <sup>-3</sup>

## 7. References

- [1] A. Heydeman, in: K. H. Wedepohl (Eds.), *Handbook of Geochemistry*, Springer Verlag, New York, 1969.
- [2] M. T. Pope, in: G. Wilkinson (Eds.), *Comprehensive Coordination Chemistry*, Pergamon, New York, 1987.
- [3] J. A. McCleverty, in: R. B. King (Eds.), *Encyclopedia of Inorganic Chemistry*, John Wiley, New York, 1994.
- [4] J. J. R. Fraústo da Silva, R. J. P. Williams, *The Inorganic Chemistry of Life*, Clarendon Press, Oxford, 1991.
- [5] P. J. Peterson, *Sci. Prog. (Oxford)* **1971**, *59*, 505-526.
- [6] C. D. Garner, L. J. Stewart, in: A. Sigel, H. Sigel (Eds.), *Metal Ions in Biological Systems (Vol 39) – Molybdenum and Tungsten: their Roles in Biological Processes*, Marcel Dekker, New York, 2002.
- [7] R. Hille, *Chem. Rev.* **1996**, *96*, 2757-2816.
- [8] R. Hille, *Trends Biochem. Sci.* **2002**, *27*, 360-367.
- [9] R. Hille, J. Rétey, U. Bartlewski-Hof, W. Reichenbecher, B. Schink, *FEMS Microbiol. Rev.* **1999**, *22*, 489-501.
- [10] R. S. Pilato, E. I. Stiefel, in: J. Reedijk (Eds.), *Bioinorganic catalysis*, Marcel Dekker, New York, 1993.
- [11] R. H. Holm, J. M. Berg, *Acc. Chem. Res.* **1986**, *19*, 363-370.
- [12] R. H. Holm, *Coor. Chem. Rev.* **1990**, *110*, 183-221.
- [13] D. Collison, C. D. Garner, J. A. Joule, *Chem. Soc. Rev.* **1996**, *25*, 25-32.

- [14] J. E. Enemark, C. D. Garner, *J. Biol. Inorg. Chem.* **1997**, *2*, 817-822.
- [15] (a) K. V. Rajagopalan, J. L. Johnson, *J. Biol. Chem.* **1992**, *267*, 10199-10202. (b) K. V. Rajagopalan, *Adv. Enzymol. Relat. Areas Mol. Biol.* **1991**, *64*, 215-290.
- [16] (a) C. Kisker, H. Schindelin, D. Baas, J. Rétey, R. U. Meckenstock, P. M. H. Kroneck, *FEMS Microbiol. Rev.* **1999**, *22*, 503-521. (b) M. J. Romão, J. Knäblein, R. Huber, J. J. G. Moura, *Prog. Biophys. Mol. Biol.* **1997**, *68*, 121-144. (c) R. Hille, *J. Biol. Inorg. Chem.* **1996**, *1*, 397-404. (d) C. Kisker, H. Schindelin, D. C. Rees, *Annu. Rev. Biochem.* **1997**, *66*, 233-267. (e) D. C. Rees, Y. Hu, C. Kisker, H. Schindelin, *J. Chem. Soc., Dalton Trans.* **1997**, 3909-3914. (f) C. G. Young, A. G. Wedd, in: R. B. King (Eds.), *Encyclopedia of inorganic chemistry*, vol 5, Wiley, New York, 1994.
- [17] C. D. Garner, R. Banham, S. J. Cooper, E. S. Davies, L. J. Stewart, in: I. Bertini, A. Sigel and H. Sigel (Eds.), *Handbook on Metalloproteins*, Marcel Dekker, New York, 2001.
- [18] B. K. Burgess, D. J. Lowe, *Chem. Rev.* **1996**, *96*, 2983-3011.
- [19] J. B. Howard, D. C. Rees, *Chem. Rev.* **1996**, *96*, 2965-2982.
- [20] R. Hille, *Biochim. Biophys. Acta* **1994**, *1184*, 143-169.
- [21] M. K. Chan, S. Mukund, A. Kletzin, M. W. W. Adams, D. C. Rees, *Science*, **1995**, *267*, 1463-1469.
- [22] M. K. Johnson, D. C. Rees, M. W. W. Adams, *Chem. Rev.* **1996**, *96*, 2817-2840.
- [23] A. Kletzin, M. W. W. Adams, *FEMS Microbiol. Rev.* **1996**, *18*, 4-63.
- [24] A. Kletzin, S. Mukund, T. L. Kelley-Crouse, M. K. Chan, D. C. Rees, M. W. W. Adams, *J. Bacteriol.* **1995**, *177*, 4817-4819.
- [25] S. Mukund, M. W. W. Adams, *J. Biol. Chem.* **1991**, *266*, 14208-14216.

- [26] I. Yamamoto, T. Saiki, S.-M. Liu, L. G. Ljungdahl, *J. Biol. Chem.* **1983**, *258*, 1826-1832.
- [27] B. Rosner, B. Schink, *J. Bacteriol.* **1995**, *177*, 5767-5772.
- [28] J. H. Enemark, J. J. A. Cooney, J.-J. Wang, R. H. Holm, *Chem. Rev.* **2004**, *104*, 1175-1200.
- [29] S. K. Das, D. Biswas, R. Maiti, S. Sarkar, *J. Am. Chem. Soc.* **1996**, *118*(6), 1387-1397.
- [30] J. Bernholc, E. I. Stiefel, *Inorg. Chem.* **1985**, *24*(9), 1323-1330.
- [31] H. Oku, N. Ueyama, A. Nakamura, *Chem. Lett.*, **1996**, 1131-1132.
- [32] (a) H. Schindelin, C. Kisker, J. Hilton, K. V. Rajagopalan, D. C. Rees, *Science* **1996**, *272*, 1615-1621; (b) G. N. George, J. Hilton, K. V. Rajagopalan, *J. Am. Chem. Soc.* **1996**, *118*, 1113-1117; (c) G. N. George, J. Hilton, C. Temple, R. C. Prince, K. V. Rajagopalan, *J. Am. Chem. Soc.* **1999**, *121*, 1256-1266.
- [33] J. M. Dias, M. E. Than, A. Humm, R. Huber, G. P. Bourenkov, H. D. Bartunik, S. Bursakov, J. Calvete, J. Caldeira, C. Carveiro, J. J. G. Moura, I. Moura, M. J. Romão, *Structure* **1999**, *7*, 65-79.
- [34] J. C. Boyington, V. N. Gladyshev, S. V. Khangulov, T. C. Stadtman, P. D. Sun, *Science* **1997**, *275*, 1305-1308.
- [35] M. G. Bertero, R. A. Rothery, M. Palak, C. Hou, D. Lim, F. Blasco, J. H. Weiner, N. C. J. Strynadka, *Nature Struct. Biol.* **2003**, *10*, 681-687.
- [36] Y. Hu, S. Faham, R. Roy, M. W. W. Adams, D. C. Rees, *J. Mol. Biol.* **1999**, *286*, 899-914.
- [37] (a) H. Raaijmakers, S. Macieria, J. M. Dias, S. Texeira, S. Bursakov, R. Huber, J. J. G. Moura, I. Moura, M. J. Romão, *Structure* **2002**, *10*, 1261-1272. (b) H. Raaijmakers, S.



- Texeira, J. M. Dias, M. J. Almendra, C. D. Brondino, I. Moura, J. J. G. Moura, M. J. Romão, *J. Biol. Inorg. Chem.* **2001**, *6*, 398-404.
- [38] C. G. Young, A. G. Wedd, *Chem. Commun.* **1997**, 1251-1257.
- [39] A. G. Wedd, *Coord. Chem. Rev.* **1996**, *154*, 5-11.
- [40] J. H. Enemark, C. G. Young, *Adv. Inorg. Chem.* **1993**, *40*, 1-88.
- [41] D. Sellmann, *Bioinorganic chemistry: transition metals in biology and their coordination chemistry*, Wiley-VCH, New York, 1997.
- [42] R. Singh, J. T. Spence, G. N. George, S. P. Cramer, *Inorg. Chem.* **1989**, *28*, 8-10.
- [43] J. M. Berg, R. H. Holm, *J. Am. Chem. Soc.* **1985**, *107*, 925-932.
- [44] J. M. Berg, R. H. Holm, *J. Am. Chem. Soc.* **1985**, *107*, 917-925.
- [45] S. F. Gheller, B. E. Schultz, M. J. Scott, R. H. Holm, *J. Am. Chem. Soc.* **1992**, *114*, 6934-6935.
- [46] B. E. Schultz, S. F. Gheller, m. C. Muetterties, M. J. Scott, R. H. Holm, *J. Am. Chem. Soc.* **1993**, *115*, 2714-2722.
- [47] P. Palanca, T. Picher, V. Sanz, P. Gómez-Romero, E. Llopis, A. Domenech, A. Cervilla, *J. Chem. Soc., Chem. Commun.* **1990**, 531-533.
- [48] R. C. Bray, *Polyhedron* **1986**, *5*, 591-595.
- [49] S. R. Davie, N. D. Rubie, B. S. Hammes, C. J. Carrano, M. L. Kirk, P. Basu, *Inorg. Chem.* **2001**, *40*, 2632-2633.
- [50] K. R. Barnard, R. W. Gable, A. G. Wedd, *J. Biol. Inorg. Chem.* **1997**, *2*, 623-633.
- [51] A. Cervilla, E. Llopis, A. Ribera, A. Dome'nech, E. Sinn, *J. Chem. Soc., Dalton Trans.* **1994**, *23*, 3511-3513.
- [52] A. A. Eagle, S. M. Harben, E. R. T. Tiekink, C. G. Young, *J. Am. Chem. Soc.* **1994**,

- 116, 9749-9750.
- [53] A. A. Eagle, E. R. T. Tiekink, C. G. Young, *J. Chem. Soc., Chem. Commun.* **1991**, 1746-1748.
- [54] J. A. McCleverty, *prog. Inorg. Chem.* **1968**, 10, 49-221.
- [55] B. S. Lim, M. W. Willer, M. Miao, R. H. Holm, *J. Am. Chem. Soc.* **2001**, 123, 8343-8349.
- [56] S. Sarkar, S. K. Das, *Proc. Indian Acad. Sci. (Chem. Sci.)* **1992**, 104, 533-534.
- [57] N. Ueyama, H. Oku, A. Nakamura, *J. Am. Chem. Soc.* **1992**, 114, 7310-7311.
- [58] H. Oku, N. Ueyama, A. Nakamura, *Bull. Chem. Soc. Jpn.* **1996**, 69, 3139-3150.
- [59] E. S. Davies, G. M. Aston, R. L. Beddoes, D. Collison, A. Dinsmore, Docrat, A.; J. A. Joule, C. R. Wilson, C. D. Garner, *J. Chem. Soc., Dalton Trans.* **1998**, 3647-3656.
- [60] L. E. Mortenson, R. N. F. Thorneley, *Annu. Rev. Biochem.* **1979**, 48, 387-418.
- [61] G. C. Tucci, J. P. Donahue, R. H. Holm, *Inorg. Chem.* **1998**, 37, 1602-1608.
- [62] K.-M. Sung, R. H. Holm, *Inorg. Chem.* **2001**, 40, 4518-4525.
- [63] Y.-L. Wang, O. Yang, Z.-Y. Zhou, H. K. Lee, T. C. Mak, D. K. P. Mg, *New J. Chem.* **2001**, 25, 353-357.
- [64] S.-B. Yu, R. H. Holm, *Inorg. Chem.* **1989**, 28, 4385-4391.
- [65] K. Most, J. Hoßbach, D. Vidović, J. Magull, N. C. Mösch-Zanetti, *Adv. Synth. Catal.* **2005**, 347, 463-472.
- [66] C. Lorber, M. R. Plutino, L. I. Elding, E. Mordlander, *J. Chem, Soc., Dalton Trans.* **1997**, 3997-4003.
- [67] B. E. Schultz, R. H. Holm, R. Hille, *J. Am. Chem. Soc.* **1995**, 117, 827-828.
- [68] B. S. Lim, R. H. Holm, *J. Am. Chem. Soc.* **2001**, 123, 1920-1930.

- [69] B. S. Lim, K.-M. Sung, R. H. Holm, *J. Am. Chem. Soc.* **2000**, *122*, 7410-7411.
- [70] R. Hart, W. Levason, B. Patel, G. Reid, *J. Chem. Soc., Dalton Trans.* **2002**, 3153-3159.
- [71] T. K. Paine, T. Weyhermüller, E. Bothe, K. Wieghardt, P. Chaudhuri, *J. Chem. Soc., Dalton Trans.* **2003**, 3136-3144.
- [72] C. O. Kienitz, C. Thöne, P. G. Jones, *Inorg. Chem.* **1996**, *35*, 3990-3997.
- [73] M. Chatterjee, M. Maji, S. Ghosh, T. C. W. Mak, *J. Chem. Soc., Dalton Trans.* **1998**, 3641-3645.
- [74] W. Levason and G. Reid, *J. Chem. Res.* **2002**, 467-472.
- [75] B. Kamenar, M. Penavić, B. Kopar-Ć Olig, B. Marković, *Inorg. Chim. Acta* **1982**, *65*, L245-L247.
- [76] K. Dreisch, C. Andersson, C. Stålhandske, *Polyhedron* **1991**, *10*, 2417-2421.
- [77] P. C. Crouch, G. W. A. Fowles, P. R. Marshall, R. A. Walton, *J. Chem. Soc. A* **1968**, 1634-1638.
- [78] M. D. Brown, M. B. Hursthouse, W. Levason, R. Ratnani, G. Reid, *J. Chem. Soc., Dalton Trans.* **2004**, 2487-2491.
- [79] K. Tatsumi, R. Hoffman, *Inorg. Chem.* **1980**, *19*, 2656-2658.
- [80] J. M. Mayer, *Inorg. Chem.* **1988**, *27*, 3899-3903.
- [81] Y. Jeannin, J.-P. Launay, J. Livage, A. Nel, *Inorg. Chem.* **1978**, *17*, 374-378.
- [82] J. P. Launay, Y. Jeannin, A. Nel, *Inorg. Chem.* **1983**, *22*, 277-281.
- [83] F. E. Kühn, E. Herdtweck, J. J. Haider, W. A. Herrmann, I. S. Gonçalves, A. D. Lopes, C. C. Romão, *J. Organomet. Chem.* **1999**, *583*, 3-10.
- [84] D. Sevdic, L. Fekete, *Inorg. Chim. Acta* **1982**, *57*, 111-117.

- [85] P. M. Boorman, M. Islip, M. M. Reimer, K. J. Reimer, *J. Chem. Soc., Dalton Trans.* **1972**, 890–893.
- [86] P. Berges, W. Hinrichs, A. Holzmann, J. Wiese, G. Klar, *J. Chem. Research (S)* **1986**, 10–11.
- [87] (a) C. A. McAuliffe, A. Werfalli, *Inorg. Chim. Acta* **1982**, *64*, L19-L20; (b) A. J. Barton, J. Connolly, W. Levason, A. M. Jalon, S. D. Orchard, G. Reid, *Polyhedron* **2000**, *19*, 1373-1379.
- [88] (a) H. Fischer, U. Gerbing, J. Riede, *J. Organomet. Chem.* **1989**, *364*, 155-167; (b) M. K. Davies, M. C. Durrant, W. Levason, G. Reid, R. L. Richards, *Dalton Trans.* **1999**, 1077-1084; (c) G. Thaler, W. Fimml, K. Wurst, F. Sladky, *Inorg. Chim. Acta* **2003**, *349*, 45-57; (d) E. W. Abel, N. L. Long, K. G. Orrell, A. G. Osborne, V. Šik, P. A. Bates, M. B. Hursthouse, *J. Organomet. Chem.* **1989**, *367*, 275-289; (e) H. Fischer, U. Gerbing, K. Treier, J. Hofmann, *Chem. Ber.* **1990**, *123*, 725-732; (f) H. Fischer, K. Treier, C. Troll, R. Stumpf, *Chem. Commun.* **1995**, 2461-2463; (g) M. G. Choi, R. J. Angelici, *J. Am. Chem. Soc.* **1990**, *112*, 7811-7812.
- [89] B. S. Lim, J.P. Donahue, R. H. Holm, *Inorg. Chem.* **2000**, *39*, 263-273.
- [90] E. G. Hope, W. Levason, *Coord. Chem. Rev.* **1993**, *122*, 109–170.
- [91] S. G. Murray, F. H. Hartley, *Chem. Rev.* **1981**, *81*, 365–414.
- [92] A. J. Wilson, B. R. Penfold, C. J. Wilkins, *Acta Crystallogr. C: Cryst. Struct. Commun.* **1983**, *39*, 329–330.
- [93] P. Berges, W. Hinrichs, A. Holzmann, J. Wiese, G. Klar, *J. Chem. Research (S)* **1986**, 10–11.
- [94] V. McKee, C. J. Wilkins, *J. Chem. Soc., Dalton Trans.* **1987**, 523–528.

- [95] X. Ma, K. Starke, C. Schulzke, H.-G. Schmidt, M. Noltemeyer, *Eur. J. Inorg. Chem.* **2006**, 628-637.
- [96] A. Bondi, *J. Phys. Chem.* **1964**, *68*, 441-451.
- [97] (a) P. M. Boorman, H.-B. Kraatz, M. Parvez, *Polyhedron* **1993**, *12*, 601-606; (b) M. Hong, R. Cao, H. Kawaguchi, K. Tatsumi, *Inorg. Chem.* **2002**, *41*, 4824-4833; (c) M. Formigué, B. Domercq, I. V. Jourdain, P. Molinié, F. Guyon, J. Amandrut, *Chem. Eur. J.* **1998**, *4*, 1714-1723; (d) B. Domercq, C. Coulon, M. Formigué, *Inorg. Chem.* **2001**, *40*, 371-378; (e) J. H. Shin, W. Savage, V. J. Murphy, J. B. Bonanno, D. G. Churchill, G. Parkin, *Dalton Trans.* **2001**, 1732-1753; (f) C. G. Pierpont, R. Eisenberg, *J. Chem. Soc. A* **1971**, 2285-2289; (g) M. H. Chisholm, J. C. Huffman, I. P. Parkin, W. E. Streib, *Polyhedron* **1990**, *9*, 2941-2952; (h) M. H. Chisholm, I. P. Parkin, J. C. Huffman, W. E. Streib, *Chem. Commun.* **1990**, 920-921.
- [98] (a) A. Rettenmeier, K. Weidenhammer, M. L. Ziegler, *Zeitschr. Angew. Allg. Chem.* **1981**, *473*, 91-100; (b) L.-C. Song, Y.-C. Shi, W.-F. Zhu, Q.-M. Ha, L.-H. Weng, *J. Organomet. Chem.* **2000**, *613*, 42-49; (c) P. G. Jones, J. Laube, C. Thöne, *Inorg. Chem.* **1997**, *36*, 2097-2102; (d) H. Rakoczy, M. Schollenberger, B. Nuber, M. L. Ziegler, *J. Organomet. Chem.* **1994**, *467*, 217-222; (e) D. Miguel, J. A. Perez, V. Riera, S. Garcia-Granda, *Organometallics* **1994**, *13*, 4667-4669.
- [99] (a) T. Adachi, M. D. Durrant, D. L. Hughes, C. J. Pickett, R. L. Richards, J. Talarmin, T. Yoshida, *Chem. Commun.* **1992**, 1464-1467; (b) B. B. Kaul, J. H. Enemark, S. L. Merbs, J. T. Spence, *J. Am. Chem. Soc.* **1985**, *107*, 2885-2891; (c) A. Bruce, J. L. Corbin, P. L. Dahlstrom, J. R. Hyde, M. Minelli, E. I. Stiefel, J. T. Spence, J. Zubieta, *Inorg. Chem.* **1982**, *21*, 917-920; (d) J. M. Berg, K. O. Hodgson, S. P. Cramer, J. L.

- Corbin, A. Elsberry, N. Pariyadath, E. I. Stiefel, *J. Am. Chem. Soc.* **1979**, *101*, 2774-2776; (e) J. M. Berg, K. O. Hodgson, A. E. Bruce, J. L. Corbin, N. Pariyadath, E. I. Stiefel, *Inorg. Chim. Acta* **1984**, *90*, 25-33; (f) G. Lyashenko, V. Jancik, A. Pal, R. Herbst-Irmer, N. C. Mösch-Zanetti, *Dalton Trans.* **2006**, 1294-1301.
- [100] (a) H. K. Lee, Y.-L. Wong, Z.-Y. Zhon, Z.-Y. Zhang, D. Ng, T. Mak, *Dalton Trans.* **2000**, 539-544; (b) H. Lam, G. Wilkinson, B. Hussain-Bates, M. B. Hursthouse, *Dalton Trans.* **1993**, 1477-1482; (c) A. G. Orpen, C. Brammer, F. H. Allen, O. Kennard, D. G. Watson, R. Taylor, *J. Chem. Soc., Dalton Trans.* **1989**, S1-S83.
- [101] J. R. Bradbury, A. F. Masters, A. C. McDonell, A. A. Brunette, A. M. Bond, A. G. Wedd, *J. Am. Chem. Soc.* **1981**, *103*, 1959-1964.
- [102] (a) D. V. Fomitchev, B. S. Lim, R. H. Holm, *Inorg. Chem.*, **2001**, *40*, 645-654; (b) E. S. Davies, R. L. Beddoes, D. Collison, A. Dinsmore, A. Docrat, J. A. Joule, C. R. Wilson, C. D. Garner, *J. Chem. Soc., Dalton Trans.*, **1997**, 3985-3996.
- [103] C. Schulzke, *Dalton Trans.* **2005**, 713-720.
- [104] L. M. Thomson and M. B. Hall, *J. Am. Chem. Soc.*, **2001**, *123*, 3995-4002.
- [105] J. P. Donahue, C. Lorber, E. Nordlander and R. H. Holm, *J. Am. Chem. Soc.*, **1998**, *120*, 3259-3260.
- [106] J. P. Donahue, C. R. Goldsmith, U. Nadiminti and R. H. Holm, *J. Am. Chem. Soc.*, **1998**, *120*, 12869-12881.
- [107] C. Lorber, J. P. Donahue, C. A. Goddard, E. Nordlander and R. H. Holm, *J. Am. Chem. Soc.*, **1998**, *120*, 8102-8112.
- [108] H. Arzoumanian, C. Corao, H. Krentzien, R. Lopez and H. Teruel, *J. Chem. Soc., Chem. Commun.*, **1992**, 856-858.

- [109] A. E. Pierce, *Silylation of Organic Compounds*, Pierce Chemical Company, Rockford, Illinois, 1968.
- [110] S. D. Pastor, J. D. Spivack, L. P. Steinhuebel, *J. Heterocycl. Chem.* **1984**, *21*, 1285-1287.
- [111] C. Pickett, S. Kumar, P. Vella, J. Zubieta, *Inorg. Chem.* **1982**, *21*, 908-916.
- [112] L. Stelzig, S. Kötte and B. Krebs, *J. Chem. Soc., Dalton Trans.* **1998**, 2921-2926.
- [113] S. Patai, Z. Rappoport (Eds.), *The chemistry of organic selenium and tellurium compounds*, J. Wiley & Sons, New York, 1986.
- [114] H. G. Mautner, S.-H. Chu, C. M. Lee, *J. Org. Chem.* **1962**, *27*, 3671-3673.
- [115] (a) A. Toshimitsu, H. Owada, S. Uemura, M. Okano, *Tetrahedron Lett.* **1982**, *23*, 2105-2108; (b) A. Toshimitsu, H. Owada, K. Terao, S. Uemura, M. Okano, *J. Org. Chem.* **1984**, *49*, 3796-3800; (c) A. Toshimitsu, H. Owada, K. Terao, S. Uemura, M. Okano, *J. Chem. Soc., Perkin Trans. 1* **1985**, 373-378; (d) D. H. R. Barton, D. Crich, *Tetrahedron* **1985**, *41*, 4359-4364; (e) A. Toshimitsu, G. Hayashi, K. Terao, S. Uemura, *J. Chem. Soc., Perkin Trans. 1* **1988**, 2113-2117.
- [116] (a) H. Takadu, Y. Shimida, Y. Nakajima, T. Hata, *Nucleic Acids Res.* **1976**, *3*, 1233-1248; (b) H. Takadu, T. Konishi, T. Hata, *Chem. Lett.* **1977**, *6*, 655-658; (c) H. Takadu, T. Yamazaki, *Nucleic Acid Chem.* **1978**, *2*, 869; (d) H. Takadu, M. Kato, M. Yoshida, R. Yamaguchi, *J. Org. Chem.* **1980**, *45*, 3347-3350.
- [117] (a) A. J. Deeming, M. N. Meah, H. M. Dawes, M. B. Hursthouse, *J. Organomet. Chem.* **1986**, *299*, C25-C26; (b) G. Valle, R. Ettore, U. Vettori, V. Peruzzo, G. Plazzogna, *J. Chem. Soc., Dalton Trans.* **1987**, 815-817; (c) T. S. Lobana, P. K. Bathia, E. R. T. Tiekink, *J. Chem. Soc., Dalton Trans.* **1989**, 749-751; (d) E. C. Constable, A.

- C. King, C. A. Palmer, P. R. Raithby, *Inorg. Chim. Acta* **1991**, *184*, 43–45; (e) K. Umakoshi, A. Ichimura, I. Kinoshita, S. Ooi, *Inorg. Chem.* **1990**, *29*, 4005–4010.
- [118] J. Laube, S. Jäger, C. Thöne, *Eur. J. Inorg. Chem.* **2001**, 1983–1992.
- [119] (a) E. C. Constable, P. R. Raithby, *J. Chem. Soc., Dalton Trans.* **1987**, 2281–2283; (b) P. Karagiannidis, P. Aslanidis, D. P. Kessissoglou, B. Krebs, M. Dartmann, *Inorg. Chim. Acta* **1989**, *156*, 47–56; (c) P. Aslanidis, S. K. Hadjikakou, P. Karagiannidis, B. Kojic-Prodic, M. Luic, *Polyhedron* **1994**, *13*, 3119–3125.
- [120] (a) P. Mura, B. G. Olby, S. D. Robinson, *J. Chem. Soc., Dalton Trans.* **1985**, 2101–2112; (b) P. Mura, B. G. Olby, S. D. Robinson, *Inorg. Chim. Acta* **1985**, *98*, L21–22; (c) P. D. Cookson, E. R. T. Tiekink, *J. Chem. Soc., Dalton Trans.* **1993**, 259–263.
- [121] (a) M. A. Ciriano, F. Viguri, J. J. Pérez-Torrente, F. J. Lahoz, L. A. Oro, A. Tiripicchio, M. Tiripicchio-Camellini, *J. Chem. Soc., Dalton Trans.* **1989**, 25–32; (b) Y. Nakatsu, Y. Nakamura, K. Matsumoto, S. Ooi, *Inorg. Chim. Acta* **1992**, *196*, 81–88; (c) R. Schmiedgen, F. Huber, H. Preud, G. Ruisi, R. Barbieri, *Appl. Organomet. Chem.* **1994**, *8*, 397–407; (d) M. Gupta, R. E. Cramer, K. Ho, C. Pettersen, S. Mishina, J. Belli, C. M. Jensen, *Inorg. Chem.* **1995**, *34*, 60–65.
- [122] (a) H. Yamamoto, W. Yoshida, C. M. Jensen, *Inorg. Chem.* **1991**, *30*, 1353–1357; (b) J. G. Reynolds, S. C. Sendlinger, A. M. Murray, J. C. Huffman, G. Christou, *Angew. Chem., Int. Ed. Engl.* **1992**, *31*, 1253–1255; (c) H. Engelking, S. Karentzopoulos, G. Reusmannand, B. Krebs, *Chem Ber.* **1994**, *127*, 2355–2361; (d) R. M. Tylicki, W. Wu, P. E. Fanwick, R. A. Walton, *Inorg. Chem.* **1995**, *34*, 988–991.
- [123] A. Sousa-Pedrares, J. Romero, J. A. García-Vázquez, M. L. Durán, I. Casanova, A.



- Sousa, *J. Chem. Soc., Dalton Trans.* **2003**, 1379–1388.
- [124] Y. Cheng, T. J. Emge, J. G. Brennan, *Inorg. Chem.* **1994**, *33*, 3711–3714.
- [125] Y. Cheng, T. J. Emge, J. G. Brennan, *Inorg. Chem.* **1996**, *35*, 342–346.
- [126] E. Block, G. Ofori-Okai, H. Kang, J. Wu, J. Zubieta, *Inorg. Chim. Acta* **1991**, *190*, 5–6.
- [127] (a) E. S. Raper, *Coord. Chem. Rev.* **1985**, *61*, 115–184; (b) E. S. Raper, *Coord. Chem. Rev.* **1996**, *153*, 199–255; (c) E. S. Raper, *Coord. Chem. Rev.* **1997**, *165*, 475–567.
- [128] R. Castro, M. L. Durán, J. A. García-Vázquez, J. Romero, A. Sousa, A. Castiñeiras, W. Hiller, J. Strahle, *Z. Naturforsch., Teil B* **1992**, *47*, 1067–1074.
- [129] R. Castro, J. A. García-Vázquez, J. Romero, A. Sousa, A. Castiñeiras, W. Hiller, J. Strähle, *Inorg. Chim. Acta* **1993**, *211*, 47–53.
- [130] (a) N. Zhang, S. R. Wilson, P. A. Shapley, *Organometallics* **1988**, *7*, 1126–1131; (b) A. J. Deeming, M. N. Meah, P. A. Bates, M. B. Hursthouse, *J. Chem. Soc., Dalton Trans.* **1988**, 235–238; (c) A. J. Deeming, M. N. Meah, P. A. Bates, M. B. Hursthouse, *J. Chem. Soc., Dalton Trans.* **1988**, 2193–2199; (d) M. A. Ciriano, J. J. Pérez-Torrente, F. Viguri, F. J. Lahoz, L. A. Oro, A. Tiripicchio, M. Tiripicchio-Camellini, *J. Chem. Soc., Dalton Trans.* **1990**, 1493–1502; (e) O. F. Z. Khan, M. Mazid, M. Motevalli, P. O'Brien, *Polyhedron* **1990**, *9*, 541–544; (f) P. Yu, L. Huang, B. Zhuang, *Acta Crystallogr., Sect. C* **1994**, *50*, 1191–1193; (g) B. R. Cockerton, A. J. Deeming, *Polyhedron* **1994**, *13*, 2085–2088.
- [131] T. Robin, F. Montilla, A. Galindo, C. Ruiz, J. Hartmann, *Polyhedron* **1999**, *18*, 1485–1490.
- [132] V. C. Gibson, T. P. Kee, A. Shaw, *Polyhedron* **1988**, *7*, 579–580.

- [133] F. A. Cotton, P. E. Fanwick, J. W. Fitch, *Inorg. Chem.* **1978**, *17*, 3254-3257.
- [134] F. J. Arnáiz, R. Aguado, M. R. Pedrosa, M. A. Maestro, *Polyhedron* **2004**, *23*, 537-543.
- [135] P. R. Traill, A. G. Wedd, E. R. T. Tiekink, *Aust. J. Chem.* **1992**, *45*, 1933-1937.
- [136] M. Cindrić, N. Strukan, T. Kajfež, Gerald Giester, B. Kamenar, *Z. Anorg. Allg. Chem.* **2001**, *627*, 2604-2608.
- [137] E. Spinner, *J. Chem. Soc.* **1960**, 1237-1242.
- [138] (a) C. Paul, H. S. Makhni, P. Singh, S. L. Chadha, *Z. Anorg. Allg. Chem.* **1970**, *337*, 108-112; (b) R. D. Kross, V. A. Fassel, M. Hargoshes, *J. Am. Chem. Soc.* **1956**, *78*, 1332-1335.
- [139] E. Block, M. Gernon, H. Kang, G. Ofori-Okai, J. Zubieta, *Inorg. Chem.* **1991**, *30*, 1736-1747.
- [140] E. I. Stiefel, *Prog. Inorg. Chem.* **1977**, *22*, 1-223.
- [141] J. Hyde, K. Venkatasubramanian, J. Zubieta, *Inorg. Chem.* **1978**, *17*, 414-426.
- [142] (a) M. A. A. F. De C. T. Carrondo, A. R. Dias, M. H. Garcia, A. Mirpuri, M. F. M. Piedade, M. S. Salema, *Polyhedron* **1989**, *8*, 2439-2447; (b) P. E. Fanwick, J.-S. Qi, Y.-P. Wu, R. A. Walton, *Inorg. Chim. Acta* **1990**, *168*, 159-161; (c) E. Block, H. Kang, J. Zubieta, *Inorg. Chim. Acta* **1991**, *181*, 227-231; (d) E. Block, G. Ofori-Okai, H. Kang, J. Zubieta, *Inorg. Chim. Acta* **1991**, *190*, 179-184; (e) E. Block, G. Ofori-Okai, *J. Am. Chem. Soc.* **1992**, *114*, 758-759.
- [143] A. Sousa-Pedrares, M. L. Durán, J. Romero, J. A. García-Vázquez, J. C. Monteagudo, A. Sousa, J. R. Dilworth, *Inorg. Chim. Acta* **2006**, *359*, 863-876.
- [144] Z. Yang, H. P. Zhu, X. L. Ma, J. F. Chai, H. W. Roesky, C. He, J. Magull, H. G.

- Schmidt, M. Noltemeyer, *Inorg. Chem.* **2006**, *45*, 1823-1827.
- [145] H. P. Zhu, J. F. Chai, C. He, G. C. Bai, H. W. Roesky, V. Jancik, H. G. Schmidt, M. Noltemeyer, *Organometallics* **2005**, *24*, 380-384.
- [146] H. R. Allcock, E. C. Bissell, E. T. Shawl, *Inorg. Chem.* **1973**, *12*, 2963-2968.
- [147] J. Fuchs, W. Freiwald, H. Hartl, *Acta Cryst.* **1978**, *B34*, 1764-1770.
- [148] E. C. Alyea, D. Craig, I. Dance, K. Fisher, G. Willett, M. Scudder, *Cryst. Eng. Comm.* **2005**, *7*, 491-503.
- [149] M. T. Pope, *Heteropoly and Isopoly Oxometalates*, Springer, Berlin, 1983.
- [150] (a) J.-M. Lehn, *Angew. Chem., Znt. Ed. Engl.* **1990**, *29*, 1347-1362; (b) G. M. Whitesides, J. P. Mathias, C. T. Seto, *Science* **1991**, *254*, 1312-1319; (c) S. Denti, S. Campagna, M. Serroni, V. Ciano, V. Balzani, *J. Am. Chem. Soc.* **1992**, *114*, 2944-2950; (d) T. Bein (Eds.), *Supramoleculur Architecture*, ACS Symp. Ser. **1992**, 499; (e) F. Moulines, L. Djakovitch, R. Boese, B. Gloaguen, W. Theil, J.-L. Fillaut, M.-H. Delville, D. Astruc, *Angew. Chem., Znt. Ed. Engl.*, **1993**, *32*, 1075-1077.
- [151] R. N. Devi, E. Burkholder, J. Zubieta, *Inorg. Chim. Acta* **2003**, *348*, 150-156.
- [152] J.-Q. Xu, R.-Z. Wang, G.-Y. Yang, Y.-H. Xing, D.-M. Li, W.-M. Bu, L. Ye, Y.-G. Fan, G.-D. Yang, Y. Xing, Y.-H. Lin, H.-Q. Jia, *Chem. Commun.* **1999**, 983-984.
- [153] D. Xiao, Y. Hou, E. Wang, S. Wang, Y. Li, L. Xu, C. Hu, *Inorg. Chim. Acta* **2004**, *357*, 2525-2531.
- [154] D. G. Allis, E. Burkholder, J. Zubieta, *Polyhedron* **2004**, *23*, 1145-1152.
- [155] I. D. Brown, D. Altermatt, *Acta Crystallogr.* **1985**, *B41*, 244-247.
- [156] J. L. Stark, A. L. Rheingold, E. A. Maatta, *Chem. Commun.* **1995**, 1165-1166.
- [157] (a) T. E. Erikson, I. Grenthe, I. Puigdomenech, *Inorg. Chim. Acta* **1987**, *126*, 131-135;

- (b) Y. Ducommun, L. Helm, G. Laurenezy, A. Merbach, *Inorg. Chim. Acta* **1989**, *158*, 3-4.
- [158] (a) D. Ventur, K. Wieghardt, J. Weiss, *Z. Anorg. Allg. Chem.* **1985**, *524*, 40-50; (b) X. Y. Zhou, N. M. Kostic, *Inorg. Chem.* **1988**, *27*, 4402-4408; (c) A. M. Herring, L. Henling, J. A. Labinger, J. E. Bercaw, *Inorg. Chem.* **1991**, *30*, 851-853.
- [159] (a) M. G. B. Drew, G. W. A. Fowles, R. W. Matthews, R. A. Walton, *J. Am. Chem. Soc.* **1969**, *91*, 7769-7770; (b) M. G. B. Drew, R. W. Matthews, R. A. Walton, *J. Chem. Soc. A* **1970**, 1405-1410; (c) W. Fürst, P. Gouzerth, Y. Jeannin, *J. Coord. Chem.* **1979**, *8*, 237.
- [160] (a) G. Nardin, L. Randaccio, R. P. Bonomo, E. Rizzaretti, *J. Chem. Soc., Dalton Trans.* **1980**, 369-375; (b) S. K. Sengupta, S. K. Shani, R. W. Kapoor, *Polyhedron* **1983**, *2*, 317-322.
- [161] (a) D. L. Hoof, D. G. Tisley, R. A. Walton, *J. Chem. Soc., Dalton Trans.* **1973**, 200-204 and refs. therein; (b) S. Ghosh, P. K. Ray, T. K. Bandopadhyay, A. K. Deb, *Z. Naturforsch., Teil B* **1981**, *36*, 1270-1272.
- [162] (a) I. Morimoto, S. Tanaka, *Anal. Chem.* **1963**, *35*, 141-144; (b) Y. Kanay, *Analyst* **1990**, *115*, 809-812.
- [163] R. L. Every, O. L. Riggs, Jr., *Mater. Prot.* **1964**, *3*, 46.
- [164] C. G. Pope, E. Matijevic, R. C. Patel, *J. Colloid Interface Sci.* **1981**, *80*, 874-879.
- [165] (a) G. F. Bailey, S. Karp, T. E. Sacks, *J. Bacteriol.* **1965**, *89*, 984-989; (b) B. Setlow, P. Setlow, *Appl. Environ. Microbiol.* **1993**, *59*, 640-643; (c) L. D. Waterbury, C. Serrato, G. R. Martinez, *Proc. West. Pharmacol. Soc.* **1989**, *32*, 9-13.
- [166] D. L. Griggs, P. Heden, K. E. Temple Smith, W. Rademacher, *Phytochemistry* **1991**,

- 30, 2513-2517.
- [167] F. J. Arnáiz, R. Aguado, M. R. Pedrosa, A. De Cian, J. Fischer, *Polyhedron* **2000**, *19*, 2141-2147.
- [168] L. S. Liebeskind, K. B. Sharpless, R. D. Wilson, J. A. Ibers, *J. Am. Chem. Soc.* **1978**, *100*, 7061-7063.
- [169] J. C. Robles, Y. Matsuzaka, S. Inomata, M. Shimoi, W. Mori, H. Ogino, *Inorg. Chem.* **1993**, *32*, 13-17.
- [170] (a) P. C. H. Mitchell, *Quart. Rev.* **1966**, *20*, 103-118. (b) Y. L. Wong, J. F. Ma, W. F. Law, Y. Yan, W. T. Wong, Z. Y. Zhang, T. C. W. Mak, D. K. P. Ng, *Eur. J. Inorg. Chem.* **1999**, 313-321.
- [171] F. J. Arnáiz, R. Aguado, J. Sanz-Aparicio, M. Martinez-Ripoll, *Polyhedron* **1994**, *13*, 2745-2749.
- [172] R. H. Holm, *Chem. Rev.* **1987**, *87*, 1401-1449.
- [173] J. Stiefel, in: G. Wilkinson, J. A. McCleverty (Eds.), *Comprehensive Coordination Chemistry*, vol. 3, Pergamon Press, Oxford, 1987.
- [174] H. C. A. Raaijmakers, M. João Romão, *J. Biol. Inorg. Chem.* **2006**, *11*, 849-854.
- [175] K. Most, S. Köpke, F. Dall'Antonia, N. C. Mösch-Zanetti, *Chem. Commun.* **2002**, 1676-1677.
- [176] (a) A. Majumdar, K. Pal, S. Sarkar, *J. Am. Chem. Soc.* **2006**, *128*, 4196-4197; (b) J. T. Hoffman, S. Einwaechter, B. S. Chohan, P. Basu, C. J. Carrano, *Inorg. Chem.* **2004**, *43*, 7573-7575; (c) F. J. Arnáiz, R. Aguado, *Polyhedron* **1994**, *13*, 3257-3259.
- [177] J. A. Craig, E. W. Harlan, B. S. Snyder, M. A. Whitener, R. H. Holm, *Inorg. Chem.* **1989**, *28*, 2082-2091.

- [178] D. M. Baird, S. Falzone, J. E. Haky, *Inorg. Chem.* **1989**, 28, 4561-4562.
- [179] D. F. Shriver, M. A. Drezdon, *The manipulation of Air-Sensitive Compounds*, 2<sup>nd</sup> ed., McGraw-Hill, New York, USA, 1969.
- [180] D. D. Perrin, W. L. F. Armarego, *Purification of Laboratory Chemicals*, 3<sup>rd</sup> ed., Pergamon, London, 1988.
- [181] G. M. Sheldrick, SHELXTL-PLUS, Siemens X-ray Instruments, Madison, 1990.
- [182] G. M. Sheldrick, *SHELXS-97, Programs for Structure Solution, Acta Crystallogr., Sect. A* **1990**, 46, 467-473.
- [183] G. M. Sheldrick, *SHELXL-97, Programs for Crystal Structure Refinement*, University of Göttingen, Germany, 1997.
- [184] M. J. Frisch, G. W. Trucks, H. B. Schlegel, G. E. Scuseria, M. A. Robb, J. R. Cheeseman, J. A. Montgomery, Jr., T. Vreven, K. N. Kudin, J. C. Burant, J. M. Millam, S. S. Iyengar, J. Tomasi, V. Barone, B. Mennucci, M. Cossi, G. Scalmani, N. Rega, G. A. Petersson, H. Nakatsuji, M. Hada, M. Ehara, K. Toyota, R. Fukuda, J. Hasegawa, M. Ishida, T. Nakajima, Y. Honda, O. Kitao, H. Nakai, M. Klene, X. Li, J. E. Knox, H. P. Hratchian, J. B. Cross, C. Adamo, J. Jaramillo, R. Gomperts, R. E. Stratmann, O. Yazyev, A. J. Austin, R. Cammi, C. Pomelli, J. W. Ochterski, P. Y. Ayala, K. Morokuma, G. A. Voth, P. Salvador, J. J. Dannenberg, V. G. Zakrzewski, S. Dapprich, A. D. Daniels, M. C. Strain, O. Farkas, D. K. Malick, A. D. Rabuck, K. Raghavachari, J. B. Foresman, J. V. Ortiz, Q. Cui, A. G. Baboul, S. Clifford, J. Cioslowski, B. B. Stefanov, G. Liu, A. Liashenko, P. Piskorz, I. Komaromi, R. L. Martin, D. J. Fox, T. Keith, M. A. Al-Laham, C. Y. Peng, A. Nanayakkara, M. Challacombe, P. M. W. Gill, B. Johnson, W. Chen, M. W. Wong, C. Gonzalez, and J. A. Pople, *Gaussian 03*,

- Revision B.04*, Gaussian, Inc., Pittsburgh, PA, 2003.
- [185] C. Lee, W. Yang, R. G. Parr, *Phys. Rev.* **1988**, *B* 37, 785-789.
- [186] B. Miehlich, A. Savin, H. Stoll, H. Preuss, *Chem. Phys. Lett.* **1989**, 157, 200-206.
- [187] T. R. Cundari W. J. Stevens, *J. Chem. Phys.* **1993**, 98, 5555-5565.
- [188] K. D. Dobbs, W. J. Hehre, *J. Comp. Chem.* **1987**, 8, 880-893.
- [189] G. A. Petersson, M. A. Al-Laham, *J. Chem. Phys.* **1991**, 94, 6081-6090.
- [190] G. A. Petersson, A. Bennett, T. G. Tensfeldt, M. A. Al-Laham, W. A. Shirley, J. Mantzaris, *J. Chem. Phys.* **1988**, 89, 2193-2218.
- [191] V. C. Gibson, T. P. Kee, A. Shaw, *Polyhedron* **1990**, 9, 2293-2298.
- [192] O. V. Alekminskaya, N. V. Russavskaya, N. A. Korchevin, E. N. Deryagina, *Russian Journal of General Chemistry* **2002**, 72, 75-78.
- [193] X. Hu, Z. Tian, Y. Chen, X. Lu, *Synthetic Commun.* **2000**, 30, 523-529.
- [194] G. J.-J. Chen, J. W. McDonald, W. E. Newton, *Inorg. Chem.* **1976**, 15, 2612-2615.
- [195] N. Kuhn, T. Kratz, *Synthesis*, **1993**, 561-562.
- [196] B. Hübler-Blank, M. Witt, H. W. Roesky, *J. Chem. Educ.* **1993**, 70, 408-409.

## Lebenslauf

Name: Xiaoli Ma  
Geboren: Datong, Shanxi, P. R. China, am 07. 03. 1978  
Staatsangehörigkeit: Chinesisch  
Eltern: Jiye Ma, Ingenieur  
Dongyan Song, Arbeiterin  
Familienstand: verheiratet

### Schulbildung

09/1985 – 07/1991: Primary school in Datong, Shanxi, China  
09/1991 – 07/1997: Middle school and high school in Datong, Shanxi, China

### Hochschulausbildung

09/1997 - 06/2001: B. Sc. study in Department of Chemical Engineering, Tianjin  
University of Science & Technology, Tianjin, China  
06/2001: *Bachelor of Engineering*  
09/2001 – 03/2004: M. Sc. study in School of Chemical Engineering and Environmental  
Science, Beijing Institute of Technology, Beijing, China  
03/2004: *Master of Engineering*  
05/2004 – 06/2004: Äquivalenzprüfung zum Diplomexamen – Fach Chemie  
10/2004 – 01/2007: Anfertigung der Dissertation unter Anleitung von Jun.-Prof. Dr. rer.  
nat. C. Schulzke am Institut für Anorganische Chemie der Georg-  
August-Universität zu Göttingen